PHOTOCATALYTIC APPLICATIONS OF NANO-STRUCTURED Ag or Au/TiO_2 THIN FILMS IN THE EFFICIENT REMOVAL OF MICRO-POLLUTANTS FROM AQUEOUS SOLUTIONS

LALLIANSANGA

DEPARTMENT OF CHEMISTRY
MIZORAM UNIVERSITY

PHOTOCATALYTIC APPLICATIONS OF NANO-STRUCTURED Ag or Au/TiO_2 THIN FILMS IN THE EFFICIENT REMOVAL OF MICRO-POLLUTANTS FROM AQUEOUS SOLUTIONS

By

Lalliansanga

Department of Chemistry

Submitted

in partial fulfillment of the requirement of the Degree of Doctor of Philosophy in Chemistry of Mizoram University, Aizawl.

MIZORAM UNIVERSITY
(A central University under the Act of Parliament)
Department of Chemistry
School of Physical Sciences

CERTIFICATE

This is to certify that the thesis entitled *'Photocatalytic applications of nano-structured Ag or Au/TiO_2 thin films in the efficient removal of micro-pollutants from aqueous solutions'* submitted by ***Mr. Lalliansanga,*** for the degree of ***Doctor of Philosophy*** in the Mizoram University, Aizawl, Mizoram, embodies the record of original investigations carried out by him under my supervision. He has been duly registered and the thesis presented is worthy of being considered for the award of the Ph.D degree. This work has not been submitted for any degree in any other university.

Dated: 20th December, 2019

(Prof. Diwakar Tiwari)
Supervisor

MIZORAM UNIVERSITY

December, 2019

DECLARATION OF THE CANDIDATE

I, **Lalliansanga**, hereby declare that the subject matter of this thesis is the record of work done by me, that the contents of this thesis did not form basis of the award of any previous degree to me or to do the best of my knowledge to anybody else, and that the thesis has not been submitted by me for any research degree in any other University/Institute.

This is being submitted to the Mizoram University for the degree of Doctor of Philosophy in Chemistry.

Dated: 20th December, 2019

(Lalliansanga)

Candidate

(Prof. Diwakar Tiwari)

Head

(Prof. Diwakar Tiwari)

Supervisor

Acknowledgements

It is a great pleasure to express my deepest gratitude to my Research Supervisor, *Professor Diwakar Tiwari*, Department of Chemistry, Mizoram University for his continuous and ardent support for my research work. I am greatly indebted to him for his keen interest in my work and guidance which has nurtured me to complete my research with success. He has been a guiding light, a friend and a great teacher to me. I would also like to thank him for his continuous support and equipping me with all the necessary facilities required to carry out experiments in the department.

I extend my thanks to *Professor Seung-Mok Lee* and his department, Department of Environmental Engineering, Catholic Kwandong University, Gangneung, Korea for supporting my work with the instrumental facilities. Their valuable input helps to the success of my research.

I wish to express my heartiest gratitude to *Professor Zaithanzauva Pachuau*, Dean, School of Physical Sciences, Mizoram University for his kind co-operation and encouragement during the entire course of my research.

I also convey my deepest gratitude to all the faculty members, *viz*., *Dr. Zodinpuia Pachuau, Dr. N. Mohandas Singh, Prof. Muthukumaran R., Dr. Ved Prakash Singh, Dr. Ayekpam Bimolini Devi*, Department of Chemistry, Mizoram University for their continuous inspiration, support and innovative suggestions while carrying out my research work.

I would like to convey my heartiest thanks to my fellow research scholars, *viz*., *Ms. J. Lalmalsawmi, Ms. Ngainunsiami, Mr. R. Malsawmdawngzela, Mr. Himangshu Dihingia, Mr. Sarikokba, Mr. C.V.L. Hmingmawia, Mr. Levia Lalthazuala, Mr. Ricky Lalawmpuia* and others for their valuable co-operation throughout the course of this research work. I am

forever indebted to all the non-teaching staff of Chemistry Department for their support and helping hand while carrying out my research work.

I will remain thankful to my family for their constant support, endless love and help during my entire work.

Last but not least, I thank the Almighty God for all the blessings showered upon me during my research work.

LALLIANSANGA

Regd. No.: MZU/Ph.D/731 of 11.05.2015

CONTENTS

Inner cover page title of the thesis i

Certificate ii

Declaration of the Candidate iii

Acknowledgements iv

Contents vi

List of Figures x

List of Tables xx

CHAPTER-1

1. INTRODUCTION 1

1.1. Background 1

1.2. Micropollutants and dyes in Aquatic Environment 5

1.2.1. Micropollutants 5

1.2.1.1. Tetracycline (TC) 5

1.2.1.2. Triclosan (TCS) 7

1.2.1.3. Amoxicillin (AMX) 9

1.2.2. Dyes in aquatic environment 11

1.2.2.1. Alizarin yellow (AY) 14

1.3. Removal of Micropollutants in Wastewater Treatment Plants (WWTPs) 16

1.4. Alternative Treatments for Micropollutants Removal 20

1.4.1. Removal by Physical Adsorption Processes 20

1.4.1.1 Activated carbon (ACs) 20

1.4.1.2. Graphene and graphene oxide 21

1.4.1.3. Carbon nanotubes 22

1.4.2. Removal by Advanced Oxidation Processes (AOPs) 23

1.4.2.1. Ozonation 24

1.4.2.2. Fenton oxidation 24

1.4.2.3. Photocatalysis (UV and UV/H_2O_2) 25

1.4.2.4. Sonolysis 26

1.4.2.5. Electrochemical oxidation 27

1.4.2.6. Heterogeneous photocatalysis (TiO_2/UV) 28

1.5. Heterogeneous Photocatalysis (TiO_2/UV) with Nanoparticles of Silver (Ag), Gold (Au) and Cerium (Ce) 30

1.5.1. Factors Affecting Heterogeneous TiO_2 Photocatalysis 33
1.5.1.1. Light intensity 33
1.5.1.2. Nature and concentration of the pollutant 34
1.5.1.3. Nature of photocatalyst 35
1.5.1.4. pH of the solution 35
1.5.1.5. Reaction temperature 36
1.6. Review of Literature 37
1.7. Scope of the Present Investigation 50

CHAPTER-2

2. METHODOLOGY 53
2.1. Materials 53
2.1.1. Chemicals and Apparatus 53
2.2.2. Reagents 54
2.1.3. Ultra violet−Visible (UV−Vis) Spectroscopy 54
2.1.4. Total Organic Carbon Analyser (TOCA) 56
2.2. Methods 59
2.2.1. Preparation of Silver Nanoparticles 59
2.2.2. Preparation of Gold Nanoparticles 59
2.2.3. Preparation of Ag^0(NP)/Titania Sol Solutions 60
2.2.4. Preparation of Au^0(NP)/Titania Sol Solutions 60
2.2.5. Fabrication of Ag^0/Au^0(NP)/TiO_2 Thin Films 61
2.2.6. Synthesis of Ce-Nanocomposite Materials 61
2.2.7. Fabrication of Ce^{3+}(NP)/TiO_2 thin films 62
2.2.8. Preparation of Nanostructured TiO_2 and Nanocomposite Powders 62
2.2.9. Characterization of Thin Films 63
2.2.10. Morphological Study of Thin Films 64
2.2.11. Batch Reactor Studies 65
2.2.11.1. Photo–catalytic degradation experiment 65
2.2.11.2. Effect of pH 66
2.2.11.3. Effect of pollutant concentration 67
2.2.11.4. Degradation kinetics 67
2.2.11.5. Effect of interfering ions 68

2.2.11.6. Mineralization study 68

2.2.12. Reusability test of the thin films 69

CHAPTER-3

3. RESULTS AND DISCUSSIONS 70

3.1 Characterization of Samples 70

3.1.1. X-ray Diffraction (XRD) Analysis 70

3.1.2. BET Analysis 77

3.1.3. Diffuse Reflectance Spectroscopic Analysis 80

3.1.4. SEM Analysis 83

3.1.5. Transmission Electron Microscopic (TEM) Analysis 85

3.1.6. Atomic Force Microscopic (AFM) Analysis 92

3.2. Heterogeneous Photocatalytic Degradation of Triclosan and Alizarin Yellow using Meso-porous Thin Films (Triclosan by Ag^0(NP)/TiO_2 and Alizarin Yellow by Ag^0(NP)/TiO_2, Au^0(NP)/TiO_2 thin films). 95

3.2.1. Batch reactor studies 95

3.2.1.1. Effect of pH in the degradation of Triclosan (TCS) 95

3.2.1.2. Effect of pH in the degradation of Alizarin Yellow (AY) 98

3.2.1.3. Effect of concentration in the degradation of Triclosan (TCS) 106

3.2.1.4. Effect of concentration in the degradation of Alizarin Yellow (AY) 108

3.2.1.5. Degradation Kinetics of Triclosan (TCS) 111

3.2.1.6. Degradation Kinetics of Alizarin Yellow (AY) 115

3.2.1.7. Effect of Interfering Ions on Triclosan Removal 122

3.2.1.7.1. Mechanism of Degradation 124

3.2.1.8. Effect of Interfering Ions on Alizarin Yellow (AY) Removal 126

3.2.1.8.1. Degradation Mechanism 126

3.2.1.9. Mineralization of Triclosan 132

3.2.1.10. Mineralization of Alizarin Yellow (AY) 134

3.2.2. Stability of thin film photocatalyst 138

3.3. Photocatalytic Degradation using Ce^{3+}/TiO_2 Thin Films (Removal of Amoxicillin, Tetracycline and Alizarin Yellow) 142

3.3.1. Batch Reactor Studies 142

3.3.1.1. Effect of pH 142

3.3.1.2. Effect of Pollutant Concentration 149
3.3.1.3. Degradation Kinetics 153
3.3.1.4. Effect of Co-existing ions on Tetracycline and Amoxicillin degradation 162
3.3.1.5 Mechanism of antibiotic removal 165
3.3.1.6. Effect of Co-existing ions on Alizarin Yellow degradation 167
3.3.1.7. Mineralization Study 169
3.3.2. Stability of thin film photocatalyst 176

CHAPTER-4

4. CONCLUSIONS 178
4.1. Future Scope of Present Work 182
REFERENCES 184
LIST OF PULBICATIONS 233
APPENDIX: Candidate details, published journal papers and biodata 235

List of Figures

Figure	Page No.
1.2.1. Structure of micropollutants.	15
1.6(a). Schematic diagram illustrating the principle of TiO_2 photocatalysis.	39
1.6(b). Conceptual diagram for the primary processes involved in photo-mineralization of organic compounds.	43
3.1.1(a). X-ray diffraction pattern of thin film materials A1: Ag^0(NP)/TiO_2(A1) and A2: Ag^0(NP)/TiO_2(A2).	71
3.1.1(b). X-ray diffraction pattern of Ag^0(NP)/TiO_2(A1) and Ag^0(NP)/TiO_2(A2) nanocomposite materials annealed at 800 ^{0}C. [Inset: nanocomposite Ag^0(NP)/TiO_2(A1)].	72
3.1.1(c). X-ray diffraction spectra of thin film samples B1: Au^0(NP)/TiO_2(B1) and B2: Au^0(NP)/TiO_2(B2).	73
3.1.1(d). X-ray diffraction pattern of Au^0(NP)/TiO_2(B1) and Au^0(NP)/TiO_2(B2) nanocomposite materials annealed at 800 ^{0}C. [Inset: nanocomposite Au^0(NP)/TiO_2(B1)]	73
3.1.1(e). X-ray diffraction pattern of thin film samples Ce^{3+}/TiO_2(C1) and Ce^{3+}/TiO_2(C2).	74
3.1.1(f). X-ray photoelectron spectra of (i) Ce^{3+}/TiO_2(C2) powder (ii) Ti2p (iii) O1s and (iv) Ce3d.	76
3.1.2(a). BET adsorption/desorption isotherms for the A1: Ag^0(NP)/TiO_2(A1) and A2: Ag^0(NP)/TiO_2(A2) solid samples.	78
3.1.2(b). Nitrogen adsorption-desorption isotherms (i) Au^0(NP)/TiO_2(B1) and (ii) Au^0(NP)/TiO_2(B2) solids.	80

3.1.3(a). Diffuse reflectance spectra of bare TiO_2, $Ag^0(NP)/TiO_2(A1)$ and $Ag^0(NP)/TiO_2(A2)$ solids. [Inset: The intermediate E_g determination of bare TiO_2, $Ag^0(NP)/TiO_2(A1)$ and $Ag^0(NP)/TiO_2(A2)$ solids]. 81

3.1.3(b). Diffuse reflectance spectra of bare TiO_2, $Au^0(NP)/TiO_2(B1)$ and $Au^0(NP)/TiO_2(B2)$ solids. [Inset: The intermediate E_g determination of TiO_2, $Au^0(NP)/TiO_2(B1)$ and $Au^0(NP)/TiO_2(B2)$ solids]. 82

3.1.4(i). Scanning electron microscopic images of (a) $Ag^0(NP)/TiO_2(A1)$ and (b) $Ag^0(NPs)/TiO_2(A2)$ thin films. 83

3.1.4(ii). Scanning electron microscopic images of (a) $Au^0(NP)/TiO_2(B1)$ and $Au^0(NPs)/TiO_2(B2)$ thin films. 84

3.1.4(iii). FE-SEM images of (a) $Ce^{3+}/TiO_2(C1)$ and (b) $Ce^{3+}/TiO_2(C2)$ thin film materials. 85

3.1.5(i). Transmission electron microscopic images of (a) $Ag^0(NP)/TiO_2(A1)$ and (b) $Ag^0(NP)/TiO_2(A2)$ thin films. 86

3.1.5(ii). TEM/EDX mapping of nanocomposite materials (a) $Ag^0(NP)/TiO_2(A1)$ and (b) $Ag^0(NP)/TiO_2(A2)$. 87

3.1.5(iii). Transmission electron microscopic images of (a) $Au^0(NP)/TiO_2(B1)$ and (b) $Au^0(NP)/TiO_2(B2)$ nanocomposite materials. 88

3.1.5(iv). TEM/EDX mapping of nanocomposite materials (a) $Au^0(NP)/TiO_2(B1)$ and (b) $Au^0(NP)/TiO_2(B2)$. 89

3.1.5(v). TEM images of the (a) $Ce^{3+}/TiO_2(C1)$, (b) $Ce^{3+}/TiO_2(C2)$ and interplanar distance of Ce in (c) $Ce^{3+}/TiO_2(C1)$ and (d) $Ce^{3+}/TiO_2(C2)$ powders. 90

3.1.5(vi). Elemental mapping of the (a) Ce^{3+}/TiO_2(C1) and (b) Ce^{3+}/TiO_2(C2) powders in TEM/EDX analysis. 91

3.1.6(i). Atomic force microscopic images of (a) Ag^0(NP)/TiO_2(A1) (Scale 35 nm) and (b) Ag^0(NP)/TiO_2(A2) (Scale 250 nm). 92

3.1.6(ii). Atomic force microscopic images of (a) Au^0(NP)/TiO_2(B1) (Scale 50 nm) and (b) Au^0(NP)/TiO_2(B2) (Scale 600 nm). 93

3.1.6(iii). 3D atomic force microscopic images of (a) Ce^{3+}/TiO_2(C1) and (b) Ce^{3+}/TiO_2(C2) thin films. 94

3.2.1.1. Percentage distribution of species of triclosan as a function of pH (Smooth line) and percentage removal of triclosan as a function of pH (scattered points) under the photolytic and photocatalytic operations [Initial concentration of triclosan: 1.0 mg/L; Thin Film(A): bare TiO_2 thin film; Thin Film (B): Ag^0(NP)/TiO_2(A1) and Thin Film (C): Ag^0(NP)/TiO_2(A2); Temperature: 25±1 ^{0}C]. 98

3.2.1.2(a). Percentage distribution of alizarin yellow species at different pH values (Smooth Line) and percentage oxidative removal of alizarin yellow at different pH values (Scattered Points) for photolytic and photocatalytic operations using the Ag(NPs)TiO_2: Ag^0(NP)TiO_2(A1) and Ag(NPs)TiO_2(T): Ag^0(NP)TiO_2(A2) thin films [Initial concentration of Alizarin Yellow: 1.0 mg/L; Temperature 25±1 ^{0}C]. 102

3.2.1.2(i). pH dependence dissociation of alizarin yellow in aqueous solution. 104

3.2.1.2(b). Percentage distribution of alizarin yellow species as a function of pH (Smooth Line) and percentage removal of alizarin yellow at various pH values (Scattered Points) for catalytic and photolytic treatments. Au^0(NPs)/TiO_2: Au^0(NP)/TiO_2(B1) and Au^0(NPs)/TiO_2(T): Au^0(NP)/TiO_2(B2) thin films [Initial concentration of alizarin yellow: 1.0 mg/L; Temperature 25±1 ^{0}C]. 105

3.2.1.3. Percentage removal of triclosan (dotted lines) as a function of triclosan initial concentrations and the C/C_0 values (smooth line) against the triclosan concentration under the photolytic and photocatalytic processes [pH: 6.0; F1: Ag^0(NP)/TiO_2(A1) thin film; F2: Ag^0(NP)/TiO_2(A2) thin film; Temperature 25±1 ^{0}C]. 107

3.2.1.4(a). Effect of concentration in the photocatalytic degradation of alizarin yellow (AY) by using UV-A only, Ag^0(NP)/TiO_2(A1) and Ag^0(NP)/TiO_2(A2) thin films [pH: 6.0; Irradiation time: 2 hours; Temperature 25±1 ^{0}C]. 109

3.2.1.4(b). Effect of concentration in the photocatalytic degradation of alizarin yellow by using UV-A only, Au^0(NP)/TiO_2(B1) and Au^0(NP)/TiO_2(B2) thin films [pH: 6.0; Irradiation time: 2 hours; Temperature 25±1 ^{0}C]. 111

3.2.1.5(a). The pseudo-first-order rate constant as a function of initial concentration of triclosan under the photolytic and photocatalytic processes [Insets Linear and Non-linear fitting of data for the pseudo-first-order rate kinetics; Initial concentration of triclosan: 1.0 mg/L at pH: 6.0; Temperature: 25±1 ^{0}C; F1: Ag^0(NP)/TiO_2(A1) and F2: Ag^0(NP)/TiO_2(A2)]. 113

3.2.1.5(b). Langmuir-Hinshelwood plot for the photocatalytic degradation of triclosan using A1: Ag^0(NP)/TiO_2(A1) and A2: Ag^0(NP)/TiO_2(A2) photocatalytic thin films and UV-A only photolysis [TCS concentration: 0.5 – 15.0 mg/L; pH: 6.0 at temperature: 25±1 ^{0}C]. 115

3.2.1.6(a). Kinetics of photocatalytic degradation of alizarin yellow as a function of time using Ag^0(NPs)/TiO_2: Ag^0(NP)/TiO_2(A1) and Ag^0(NPs)/TiO_2(T): Ag^0(NP)/TiO_2(A2) thin film photocatalysts along with simple photolysis [AY concentration: 1.0 mg/L; pH: 6.0; Temperature: 25±1 ^{0}C]. 117

3.2.1.6(b). Langmuir-Hinshelwood plot for the photocatalytic degradation of alizarin yellow using A1: Ag^0(NP)/TiO_2(A1) and A2: Ag^0(NP)/TiO_2(A2) photocatalytic thin films and UV-A only photolysis [AY concentration: 0.5 – 15.0 mg/L; pH: 6.0; Temperature: 25±1 ^{0}C]. 119

3.2.1.6(c). The pseudo-first order rate constant values for various concentrations of alizarin yellow for photolytic and photocatalytic operations [Insets Linear and Non-linear fitting of time dependence results for the pseudo-first order rate kinetics [Initial concentration of alizarin yellow: 1.0 mg/L at pH: 6.0; Temperature: 25±1 ^{0}C]. Au^0(NPs)/TiO_2: Au^0(NP)/TiO_2(B1) and Au^0(NPs)/TiO_2(T): Au^0(NP)TiO_2(B2) photocatalytic thin films. 120

3.2.1.6(d). Langmuir-Hinshelwood plot for the photocatalytic degradation of alizarin yellow using B1: Au^0(NP)/TiO_2(B1) and B2: Au^0(NP)/TiO_2(B2) photocatalytic thin films and UV-A only photolysis [AY concentration: 0.5 – 15.0 mg/L; pH: 6.0; Temperature: 25±1 ^{0}C]. 122

3.2.1.7(a). Photocatalytic degradation of triclosan in presence of interfering ions using Ag^0(NP)/TiO_2(A2) thin film [TCS concentration 5.0 mg/L; Ion concentration: 50.0 mg/L; pH: 6.0; Temperature: 25±1 ^{0}C]. 125

3.2.1.7(b). Effect of scavengers in the photocatalytic degradation of triclosan using the Ag^0(NP)/TiO_2(A2) thin film [TCS concentration: 5.0 mg/L; Scavenger concentration: 1000.0 mg/L; pH: 6.0; Temperature: 25±1 ^{0}C]. 125

3.2.1.8(a). Photocatalytic degradation of AY in presence of interfering ions using Ag^0(NP)/TiO_2(A2) thin film catalyst [AY concentration: 5.0 mg/L; Co-existing ion concentration: 50.0 mg/L; pH: 6.0; Temperature: 25±1 ^{0}C]. 128

3.2.1.8(b). Effect of scavengers in the photocatalytic degradation of AY using the Ag^0(NP)/TiO_2(A2) thin film catalyst [AY concentration: 5.0mg/L; Scavenger concentration: 1000.0 mg/L; pH: 6.0; Temperature: 25±1 ^{0}C]. 129

3.2.1.8(c). Photocatalytic degradation of alizarin yellow in presence of interfering ions using Au^0(NP)/TiO_2(B2) thin film catalyst [AY concentration: 5.0 mg/L; Co-existing ion concentration: 50.0 mg/L; pH: 6.0; Temperature: 25±1 ^{0}C]. 131

3.2.1.8(d): Effect of scavengers in the photocatalytic degradation of alizarin yellow using the Au^0(NP)/TiO_2(B2) thin film catalyst [AY concentration: 5.0 mg/L; Scavenger concentration: 1000.0 mg/L; pH: 6.0; Temperature: 25±1 ^{0}C]. 131

3.2.1.9. Percent mineralization of triclosan (a) as a function of initial triclosan concentration and (b) as a function of pH in the photolytic and photocatalytic degradations of triclosan [A1: Ag^0(NP)TiO_2(A1) and A2: Ag^0(NP)TiO_2(A2)]. 134

3.2.1.10. Percentage mineralization of alizarin yellow (a) as a function of initial AY concentration and (b) as a function of pH in the photolytic and photocatalytic degradations of AY [A1: Ag^0(NP)/TiO_2(A1); and A2: Ag^0(NP)/TiO_2(A2)]. 136

3.2.1.10. Percent mineralization of alizarin yellow (c) as a function of initial alizarin yellow concentration and (d) as a function of pH in the photolytic and photocatalytic degradations of alizarin yellow [B1: Au^0(NP)/TiO_2(B1) and B2: Au^0(NP)/TiO_2(B2)]. 138

3.2.2(a). Repeated use of nanocomposite Ag^0(NP)/TiO_2(A2) photocatalyst in the photocatalytic elimination of triclosan and Alizarin Yellow using the UV-A illumination [Initial concentration of TCS or AY: 5.0 mg/L; pH: 6.0]. 139

3.2.2(b). Repeated use of nanocomposite Au^0(NP)/TiO_2(B2) photocatalyst in the photocatalytic removal of alizarin yellow using the UV-A illumination [Initial concentration of AY: 5.0 mg/L; pH: 6.0]. 141

3.3.1.1(a). Effect of pH in the photocatalytic degradation of amoxicillin (AMX) using Ce^{3+}/TiO_2(C1) and Ce^{3+}/TiO_2(C2) thin films. AMX (1.0 mg/L); Irradiation time: 2 hours; Temperature 25±1 ^{0}C. 146

3.3.1.1(b). Effect of pH in the photocatalytic degradation of tetracycline (TC) using Ce^{3+}/TiO_2(C1) and Ce^{3+}/TiO_2(C2) thin films: TC (1.0 mg/L); Irradiation time: 2 hours; Temperature 25±1 ^{0}C. 146

3.3.1.1(c). Effect of pH in the photocatalytic degradation of alizarin yellow (AY): (C1: Ce^{3+}/TiO_2(C1); C2: Ce^{3+}/TiO_2(C2)); [AY]: 1.0 mg/L; Irradiation time: 2 hours; Temperature 25±1 ^{0}C). 149

3.3.1.2(a). Removal efficiency of amoxicillin (Primary axis) and tetracycline (Secondary axis) at different concentration of antibiotics for blank and photocatalytic operations using the Ce^{3+}/TiO_2(C1) and Ce^{3+}/TiO_2(C2) photocatalysts [pH: 6.0; Temperature 25±1 ^{0}C]. 151

3.3.1.2(b). Effect of concentration in the photocatalytic degradation of alizarin yellow [C1: Ce^{3+}/TiO_2(C1); C2: Ce^{3+}/TiO_2(C;); pH: 6.0; Irradiation time: 2 hours; Temperature 25±1 ^{0}C]. 153

3.3.1.3(a). Photocatalytic degradation of tetracycline as a function of time using C1 (Ce^{3+}/TiO_2(C1)) and C2 (Ce^{3+}/TiO_2(C1)) thin film photocatalysts along with simple photolysis [TC concentration: 1.0 mg/L; pH: 6.0; Temperature: 25±1 ^{0}C]. 154

3.3.1.3(b). Photocatalytic degradation of amoxicillin as a function of time using C1 (Ce^{3+}/TiO_2(C1)) and C2 (Ce^{3+}/TiO_2(C1)) thin film photocatalysts along with simple photolysis [AMX concentration: 1.0 mg/L; pH: 6.0 at Temperature: 25±1 ^{0}C]. 155

3.3.1.3(c). The pseudo-first order rate constant values for various concentrations of antibiotics (amoxicillin (Primary axis) and tetracycline (Secondary axis)) for photocatalytic degradation of antibiotics using the Ce^{3+}/TiO_2(C1) and Ce^{3+}/TiO_2(C2) photocatalysts. [Inset: Linear fitting of time dependence results or the pseudo-first-order rate kinetics; Initial concentration of antibiotic: 1.0 mg/L at pH: 6.0]. 156

3.3.1.3(d). Langmuir-Hinshelwood plot for the photocatalytic degradation of amoxicillin using C1: Ce^{3+}/TiO_2(C1) and C2: (Ce^{3+}/TiO_2(C2) thin film photocatalysts and UV-A only photolysis [AMX concentration: 0.5 – 15.0 mg/L; pH: 6.0 at temperature: 25±1 ^{0}C]. 158

3.3.1.3(e). Langmuir-Hinselwood plot for the photocatalytic degradation of tetracycline using using C1: Ce^{3+}/TiO_2(C1) and C2: Ce^{3+}/TiO_2(C2) thin film photocatalysts and UV-A only photolysis [TC concentration: 0.5 – 15.0 mg/L; pH: 6.0: Temperature: 25±1 ^{0}C]. 159

3.3.1.3(f). Photocatalytic degradation of alizarin yellow as a function of time using C1: Ce^{3+}/TiO_2(C1) and C2: Ce^{3+}/TiO_2(C2) thin film photocatalysts along with simple photolysis [AY concentration: 1.0 mg/L; pH: 6.0; Temperature: 25±1 ^{0}C]. 161

3.3.1.3(g). Langmuir-Hinshelwood plots for the photocatalytic degradation of alizarin yellow using C1: Ce^{3+}/TiO_2(C1) and C2: Ce^{3+}/TiO_2(C1) photocatalytic thin films and UV-A only photolysis [AY concentration: 0.5 – 15.0 mg/L; pH: 6.0: Temperature: 25±1 ^{0}C]. 162

3.3.1.4(a). Photocatalytic degradation of tetracycline in presence of co-existing ions using Ce^{3+}/TiO_2(C2) thin film catalyst [TC concentration: 5.0 mg/L; Co-existing ion concentration: 50.0 mg/L; pH: 6.0; Temperature: 25±1 ^{0}C]. 164

3.3.1.4(b). Photocatalytic degradation of amoxicillin in presence of several co-exiting ions using Ce^{3+}/TiO_2(C2) thin film catalyst [AMX concentration: 5.0 mg/L; Co-existing ion concentration: 50.0 mg/L; pH: 6.0; Temperature: 25±1 ^{0}C]. 164

3.3.1.5. Photocatalytic removal of amoxicillin and tetracycline in presence of several scavengers using the Ce^{3+}/TiO_2(C2) thin film catalyst [TC/AMX concentration: 5.0mg/L; Scavenger concentration: 1000.0 mg/L; pH: 6.0; Temperature: 25±1 ^{0}C]. 167

3.3.1.6(a). Photocatalytic degradation of alizarin yellow in presence of interfering ions using Ce^{3+}/TiO_2(C2) thin film catalyst [AY concentration: 5.0mg/L; Co-existing ion concentration: 50.0 mg/L; pH: 6.0; Temperature: 25±1 ^{0}C]. 168

3.3.1.6(b). Effect of scavengers in the photocatalytic degradation of alizarin yellow using the Ce^{3+}/TiO_2(C2) thin film catalyst [AY concentration: 5.0mg/L; Scavenger concentration: 1000.0 mg/L; pH: 6.0; Temperature: 25±1 ^{0}C]. 169

3.3.1.7. Percent mineralization of tetracycline (a) as a function of initial tetracycline concentration and (b) as a function of pH in the photolytic and photocatalytic degradations of tetracycline [C1: Ce^{3+}/TiO_2(C1); C2: Ce^{3+}/TiO_2(C2)]. 171

3.3.1.7. Percent mineralization of AMX (c) as a function of initial AMX concentration and (d) as a function of pH in the photolytic and photocatalytic degradations of AMX [C1: Ce^{3+}/TiO_2(C1); C2: Ce^{3+}/TiO_2(C2)]. 173

3.3.1.7. Percent mineralization of alizarin yellow (e) as a function of initial alizarin yellow concentration and (f) as a function of pH in the photolytic and photocatalytic degradations of alizarin yellow [C1: Ce^{3+}/TiO_2(C1); C2: Ce^{3+}/TiO_2(C2)]. 175

3.3.2(a). Cycling runs for photocatalytic degradation of amoxicillin and tetracycline using the Ce^{3+}/TiO_2(C2) thin film photocatalyst ([AMX and TC] = 5.0 mg/L, pH: 6). 177

3.3.2(b). Cycling runs for photocatalytic degradation of alizarin yellow using the Ce^{3+}/TiO_2(C2) thin film photocatalyst. ([Alizarin Yellow] = 5.0 mg/L, pH: 6). 177

List of Tables

Table	Page No.
1.6. Primary processes and time domains in TiO_2 catalyzed mineralization of organic pollutants.	41
3.1.2(a). Pore size, pore volume and BET specific surface area of the Ag^0(NP)/TiO_2(A1) and Ag^0(NP)/TiO_2(A2) solid samples.	78
3.1.2(b). Pore size, pore volume and BET specific surface area of the Au^0(NP)/TiO_2(B1) and Au^0(NP)/TiO_2(B2) solid samples.	79
3.2.1.1. Effect of pH in the photocatalytic degradation of triclosan by using UV-A only, Ag^0(NPs)/TiO_2(A1) and Ag^0(NPs)/TiO_2(A2) thin films.	97
3.2.1.2(a). Effect of pH in the photocatalytic degradation of alizarin yellow by using UV-A only, Ag^0(NPs)/TiO_2(A1) and Ag^0(NPs)/TiO_2(A2) thin films.	101
3.2.1.2(b). Effect of pH in the photocatalytic degradation of alizarin yellow by using UV-A only, Au^0(NPs)/TiO_2(B1) and Au^0(NPs)/TiO_2(B2) thin films.	105
3.2.1.3. Effect of concentration in the photocatalytic degradation of triclosan (TCS) using UV-A, Ag^0(NPs)/TiO_2(A1) and Ag^0(NPs)/TiO_2(A2).	107
3.2.1.4(a). Effect of concentration in the photocatalytic degradation of alizarin yellow.	109
3.2.1.4(b). Effect of pH in the photocatalytic degradation of alizarin yellow by using UV-A only, Au^0(NP)TiO_2(B1) and Au^0(NP)TiO_2(B2) thin films.	110

3.2.1.5. Kinetic data obtained for the degradation of triclosan using $Ag^0(NP)/TiO_2(A1)$ and $Ag^0(NP)/TiO_2(A2)$ thin film photocatalysts along with UV-A only photolysis at different initial triclosan concentrations. 114

3.2.1.6(a). Kinetic data obtained for the degradation of alizarin yellow using $Ag^0(NP)/TiO_2(A1)$ and $Ag^0(NP)/TiO_2(A2)$ thin film photocatalysts along with UV-A only photolysis at different initial AY concentrations. 118

3.2.1.6(b). Kinetic data obtained for the degradation of alizarin yellow using $Au^0(NP)/TiO_2(B1)$ and $Au^0(NP)/TiO_2(B2)$ thin film photocatalysts along with UV-A only photolysis at different initial AY concentrations. 121

3.2.1.9. Percentage removal of NPOC for triclosan as a function of **(a)** concentration; and **(b)** pH [A1: $Ag^0(NP)/TiO_2(A1)$ and A2: $Ag^0(NP)/TiO_2(A2)$]. 133

3.2.1.10. Percentage removal of NPOC for alizarin yellow as a function of **(a)** concentration: **(b)** pH [A1: $Ag^0(NP)/TiO_2(A1)$ and A2: $Ag^0(NP)/TiO_2(A2)$]. 135

3.2.1.10. Percentage removal of NPOC for alizarin yellow as a function of (**c)** concentration; and **(d)** pH [B1: $Au^0(NP)/TiO_2(B1)$ and B2: $Au^0(NP)/TiO_2(B2)$]. 137

3.3.1.1(a). Effect of pH in the photocatalytic degradation of amoxicillin (AMX). ([AMX]:1.0 mg/L; Irradiation time: 2 hours; Temperature 25±1 ^{0}C). 147

3.3.1.1(b). Effect of pH in the photocatalytic degradation of tetracycline (TC). ([TC]:1.0 mg/L; Irradiation time: 2 hours; Temperature 25±1 ^{0}C). 147

3.3.1.1(c). Effect of pH in the photocatalytic degradation of alizarin yellow (AY). ([AY]: 1.0 mg/L; Irradiation time: 2 hours; Temperature 25±1 ^{0}C). 149

3.3.1.2(a). Effect of concentration in the photocatalytic degradation of amoxicillin (AMX). [pH: 6.0; Temperature 25±1 ^{0}C]. 150

3.3.1.2(b). Effect of concentration in the photocatalytic degradation of tetracycline (TC). [pH: 6.0; Temperature 25±1 ^{0}C]. 151

3.3.1.2(c). Effect of concentration in the photocatalytic degradation of alizarin yellow (AY). [pH: 6.0; Temperature 25±1 ^{0}C]. 153

3.3.1.3(a). Kinetic data obtained for the degradation of tetracycline using the thin film photocatalysts Ce^{3+}/TiO_2(C1) and Ce^{3+}/TiO_2(C2) and UV-A only irradiations. 157

3.3.1.3(b). Kinetic data obtained for the degradation of amoxicillin using the thin film photocatalysts Ce^{3+}/TiO_2(C1), Ce^{3+}/TiO_2(C2) and UV-A only irradiations. 157

3.3.1.3(c). Kinetic data obtained for the degradation of alizarin yellow using the thin film photocatalysts Ce^{3+}/TiO_2(C1), Ce^{3+}/TiO_2(C2) and UV-A only irradiations. 161

3.3.1.7. Percent removal of NPOC for tetracycline as a function of **(a)** concentration: **(b)** pH [C1: Ce^{3+}/TiO_2(C1); C2: Ce^{3+}/TiO_2(C2)]. 170

3.3.1.7. Percent removal of NPOC for amoxicillin as a function of **(c)** concentration: **(d)** pH [C1: Ce^{3+}/TiO_2(C1); C2: Ce^{3+}/TiO_2(C2)]. 173

3.3.1.7. Percent removal of NPOC for alizarin yellow as a function of **(e)** concentration **(f)** pH [C1: Ce^{3+}/TiO_2(C1); C2: Ce^{3+}/TiO_2(C2)]. 175

1. INTRODUCTION

1.1. Background

Water is essential for life and it is abundantly available in nature. It is used by the living beings on this earth more than any other resources for the nourishment of life. Fresh water is essential for the sustainable growth of human and wild life around the globe. Moreover, the clean drinking water is important to maintain healthier life. It is well known fact that only 2.5% of total stock water is available as fresh water with the hydrosphere. Similarly, within the available fresh water, a large fraction (68.7%) is in the form of ice and permanent snow covered in and around the antartic and arctic regions. Fresh water in lakes and rivers, which are essentially the main sources of water for human consumptions is just of 0.26% of the total global fresh water resources (Gleick, 1993). However, if the rivers, lakes, and wetlands are polluted with emerging pollutants may result in greater and global environmental concerns. It may lead even to the serious health concerns for the living beings dependent or bound to take such contaminated water resources.

The contamination of aquatic environment by variety of micropollutants is pervasive and found serious global concern. This is, perhaps, due to the large-scale use of personal care products (PCPs) (e.g., shampoos, soaps, toothpastes, creams, cosmetics, medical skin care products, deodorants, etc.) that primarily contained with preservatives, biocides, musks or UV-filters. These micropollutants are found to be emerging water pollutants that need to be addressed adequately for its efficient removal/treatment in aquatic environment (Dai *et al*., 2011; Heberer, 2002) since these are found to be relatively persistent and often escaped through the existing conventional wastewater or sewage water treatment plants (Li *et al*., 2010; Hirsch *et al*., 1999; Sassman *et al*., 2005; Miao *et al*., 2004). Therefore, these micropollutants contained with its metabolites readily enter into the water bodies primarily

through the wastewater treatment plants. Effluents of wastewater treatment plants (WWTPs) are the main source of pharmaceuticals in the aquatic environment (Bartelt-Hunt *et al*., 2009; da Silva *et al*., 2011). With the advancement of the detection technologies at low level, these micropollutants has attracted greater attention in recent time since these compounds are efficiently detected in the aquatic environment and shown the potential hazard to the ecosystems (Kolpin *et al*., 2002; Fent *et al*., 2006; Jjemba, 2006). It is reported that variety of pharmaceuticals are readily detected in the rivers or lakes (Huerta-Fontela *et al*., 2011). The global production/use of antibiotics was exceeded to 70 billions of standard units (i.e., tablets) in 2010 (Gelband *et al*., 2015), and over 63,000 tonnes were administered for livestock production (Van Boeckel *et al*., 2015). It is known fact that *Ca*. 60 – 90% of the consumed antibiotic was excreted through the urine/or faeces hence, these compounds along with the metabolites are found in the wastewater system (Hirsch *et al*., 1999; Sarmah *et al*., 2006). Antibiotics are widely used in aquaculture farms in order to prevent from various infectious diseases. Therefore, these are major sources of pharmaceuticals that enter into the water bodies through the wastewater treatment plants (Asha *et al*., 2007). Antibiotics eventually promotes the spread of antibiotic resistant genes among bacterial populations (Chee-Sanford *et al*., 2001). This also induces biological responses in non-target organisms (Daughton and Ternes, 1999). Once these resistance genes are transferred to pathogenic bacteria, the potency of threat to human health could be increased. The antibiotics are possessed of toxic effects towards algae or several organisms that impacted indirectly the long-term ecological sustainability (Putra *et al*., 2009). Similarly, the antibiotics causes for several chronic toxicity (Michael *et al*., 2013). Therefore, the presence of these micropollutants, even at low level concentrations, impacted adversely and showed potential risk towards human and animal health (Zhang *et al*., 2015). Hence, these pollutants are, in recent time, known to be emerging water pollutants which need to be eliminated completely

from the water bodies.

Various conventional methods for wastewater treatment is described since ancient times (Narmadha *et al*., 2012; Avinash Shivajirao, 2012). It was observed that the conventional wastewater treatment plants were inefficient towards the effective removal of these persistent pollutants. Therefore, the pollutants are often detected in several aquatic matrices and poses a serious and widespread threat to the aquatic life or even to the human (Rodriguez-Mozaz *et al*., 2015). Moreover, as mentioned, the detection of several pharmaceuticals and personal care products (PCPs) in water bodies is ubiquitous and widespread (Mompelat *et al*., 2009; da Silva *et al*., 2011; Wu *et al*., 2012) since these are persistent and found difficult to eliminate completely in the existing biological or physico-chemical wastewater treatment plants. These contaminants are eventually escaped through the wastewater treatment plants, at low level, and subsequently enter into the fresh water system, contaminating the water bodies, *viz*., drinking water, surface water, or even the river/lake waters. Based on its toxicity or prevalence to drug resistance in the environment and human commensal microbes or due to persistence in nature, these compounds are known as emerging water pollutants (Constantin *et al*., 2018; Han *et al*., 2017). Although the regulatory bodies have not prescribed the permissible limit of these emerging pollutants in the water bodies, however, based on its potential risk towards the human beings, animals or aquatic life, it is important to eliminate effectively from aqueous solutions (Kosera *et al*., 2017).

The existing urban WWTPs are seemingly reported the main source of releasing the antibiotics in the terrestrial environment since these plants are not adequately designed to eliminate completely the antibiotics from aqueous wastes. The widespread and ubiquitous presence of these emerging water contaminants poses a serious environmental challenge to

tune better the existing wastewater treatment technologies to eliminate these contaminants effectively. Hence, there is an emergent concern to upgrade the existing treatment plants in order to eliminate completely the emerging and important class of water pollutants in a cost-effective and environmental benign way. Efforts are made and suggested to couple the existing wastewater treatment plants with advanced oxidation processes (AOPs) (De la Cruz *et al*., 2013; Liu *et al*., 2014; Sousa *et al*., 2012). Advanced oxidation process integrated with TiO_2 photocatalyst is an effective method to degrade the stable and potentially emerging micropollutants. The process includes with *in situ* generation of highly reactive radical species that are predominantly responsible for the degradation/or even mineralization of micropollutants from wastewaters. The treatment is based on the 'no-waste' concept and the nonreactive and chemically stable TiO_2 catalyst enhances the useful applications in the area of high catalytic activity and wastewater treatment strategies (Babic *et al*., 2017).

1.2. Micropollutants and Dyes in Aquatic Environment

1.2.1. Micropollutants

1.2.1.1. Tetracycline (TC)

Tetracycline (TC) is one of the commonly used antibiotics which enters into the aquatic environment through various sources (Tolls, 2001). It is relatively cheaper antibiotic, hence, widely used in developing countries having with limited health care budgets. The drug is sometimes abused due to the self–prescription, which is rife in this part of the world (Farombi *et al*., 2008). Tetracycline is the second most produced and consumed antibiotics in the world, while on top of the ranking is China (Xie *et al*., 2010; Cheng, 2005). Each year thousands tons of tetracyclines are produced worldwide (Michalova *et al*., 2004). Tetracycline exhibits antimicrobial activity against variety of bacteria and is often used in human therapy and livestock industry (Thrile-Bruhn, 2003). Tetracycline is employed in the treatment of leptospirosis, actinomycetes, rickettsial, mycoplasma, acne vulgaris, skin disorders, etc. Hence, it is known to be a broad-spectrum antibiotic (Moellering, 1979; Oka *et al*., 2000; Farombi *et al*., 2008). Tetracycline possessed relatively high aqueous solubility associated with long environmental half-life (Li *et al*., 2010).

It was reported that *Ca.* 5500 tons of tetracycline is consumed every year in the United States and Europe (Hirsch *et al*., 1999). Similarly, the Animal Health Institute reported that the usage of tetracyclines in China was estimated to be 6950 tons in the year 2013 (Zhang *et al*., 2015). Tetracycline is stable and biorefractory, and their removal by conventional water treatment methods is ineffective (Liu *et al*., 2013). Tetracycline is an important widely used as steatogenic drugs. The biochemical actions of tetracycline showed micro vesicular steatosis and broadly connected to: (i) impairing mitochondrial fatty acid-oxidation (Letteron *et al*., 1996); (ii) inhibiting hepatic VLDL secretion (Labbe *et al*., 1991)

due to the inhibition of microsomal triglyceride transfer protein activity (Letteron *et al*., 2003). Several biochemical dysfunctions are induced by the excessive intake of tetracycline, e.g., hepatotoxicity causes fatty infiltration of the liver (George and Crawford, 1996; Asha *et al*., 2007) and liver parenchymal cell damage due to the tetracycline toxicity (Navaro and Senior, 2006). This also induces the hyperglycemia (Storozhuk and Shamsutdinova, 1976) and injuries to the pancreas (Asha *et al*., 2007). In addition, other effects of tetracycline include superinfection, liver toxicity, tetracycline stained teeth, renal toxicity, gastrointestinal reactions and allergic reactions (Pico and Andreu, 2007; Kasik and Thompson, 1970). A small fraction of tetracycline is absorbed in metabolism process once administered, however, a greater fraction, i.e., *Ca.* 50 – 80% is released via feces and urine (Sarmah *et al*., 2006).

The mass production of tetracycline in pharmaceutical industry makes a large amount of residual tetracycline in the wastewater and the concentration of tetracycline in wastewater effluents greatly varied from 0.15 μg L^{-1} to 2.37 μg L^{-1} (Tao and Mai, 2002; Pena *et al*., 2010; Deblonde *et al*., 2011). Therefore, tetracycline is often detected in surface water, groundwater, and even drinking water, which causes harmfulness to environment and human health (Miao *et al*., 2004). Residues of tetracycline discharged from municipal wastewater treatment plants and agricultural runoff are often detected in municipal sewage (Liu *et al*., 2009a; Prado *et al*., 2009), surface water, ground water (Miao *et al*., 2004; Karthikeyan and Meyer, 2006), soils (Andreu *et al*., 2009) and sediments (Simon, 2005). Luo et al. (2011) reported that the average concentrations of tetracycline in the Haihe river (Tianjin, China) and its sediment is around 26 ng/L and 600 ng/kg, respectively (Luo *et al*., 2011). The agricultural application of livestock manures directly introducing it into the soil environment which greatly impacting the ecological safety (Halling-Sorensen *et al*., 1988).

Therefore, the fate and transport of tetracycline in the environment has received special attention in recent time.

Tetracycline showed serious concerns due to its toxic effects associated with enhanced antibiotic resistance of microorganisms (Hamscher, 2009; Thevenon *et al*., 2012). The escaped tetracycline residue through the existing wastewater treatment plants induces significantly the resistant microorganisms and poses severe threat to the human health. In addition, tetracycline residue in drinking water will directly harm the health of human body. So it has been considered to be a serious environmental pollutant (Locatelli *et al*., 2011; Liu *et al*., 2013a).

1.2.1.2. Triclosan (TCS)

Triclosan (TCS) is commonly employed antimicrobial and preservative chemical which is often used in wide range of consumer products such as toothpastes, antiseptic soaps, detergents, cosmetics, plastic kitchenware, socks, carpets, toys, etc., (Bedoux *et al*., 2012; Reiss *et al*., 2002; Singer *et al*., 2002). The global demand of triclosan is increased significantly and a rough estimate indicated that *Ca.* 350 tons of triclosan is consumed every year in Europe itself (Halden and Paull, 2005; Pintado-Herrera *et al*., 2014; Young *et al*., 2008). Further, global demand of triclosan as active ingredient of personal care products is approximately 1500 tons (Chen *et al*., 2011a). This was estimated further that *Ca.* 96% of triclosan is discharged into the sewerage system and eventually entered into the aquatic environment (Gao *et al*., 2014).

The widespread use of triclosan in variety of personal care products for last 5 decades has caused massive discharge of triclosan through the wastewater treatment plants (WWTPs) which eventually enters into the surface waters (Halden and Paull, 2005; Pintado-

Herrera *et al*., 2014). Triclosan is widely detected in wastewater (8.05 μg/L) (Lozano *et al*., 2013), sludge (1956 μg/kg) (Yang *et al*., 2016a), river (0.282 μg/L), groundwater (0.03 μg/L) (Sorensen *et al*., 2015) and sediments (41.7 μg/kg) (Peng *et al*., 2017). Because of its hydrophobic nature, with relatively high octanol-water partition coefficients (log K_{ow}) of 4.86, triclosan is likely to accumulate in aquatic and terrestrial organisms which ultimately threatens the safety of organisms. It is indeed detected even in human samples (e.g., urine, plasma and breast milk) (Dann and Hontela, 2011). Triclosan is partly removed (approximately 72 – 93%) by the conventional wastewater treatment plants (McAvoy *et al*., 2002; Heidler and Halden, 2007; Ying and Kookana, 2007). This causes the occurrence of triclosan in surface water and drinking water is inevitable and is found to be 4.9 ng/L in US to 5.16 μg/L in India (Kolpin *et al*., 2002; Singer *et al*., 2002; Morrall *et al*., 2004; Nishi *et al*., 2008; Fair *et al*., 2009; Zhao *et al*., 2010; Ramaswamy *et al*., 2011). Triclosan currently ranks among the important and emerging water contaminants showed greater concerns worldwide (Kolpin *et al*., 2002; Ohe *et al*., 2012).

Triclosan is a potential endocrine disrupting compound (Gee *et al*., 2008). Several studies showed the biochemical effects of triclosan. It causes to decrease the estrogen levels in the placenta during pregnancy. It changes the testosterone levels disordering the sperm production, endocrine modifications, decrease of viability and survival of neural stem cells and increase of body mass index (Marques *et al*., 2017). Triclosan is known to be highly toxic towards the aquatic species, *viz.*, green algae, the water flea *Daphnia magna*, and fish (*zebrafish, fathead minnows, bluegill sunfish*) (Chen *et al*., 2014; Dann and Hontela, 2011). It affects to the earth worms (*Eisenia fetida*) (Lin *et al*., 2010) or the Japanese medaka fish (Nassef *et al*., 2010). Triclosan causes the endocrine disruption towards rats and a prolonged exposure causes breast cancer cells in human (Zorilla *et al*., 2009; Gee *et al*., 2008).

Triclosan inhibits bacterial growth through blocking the lipid biosynthesis in bacteria (Adolfsson-Erici *et al*., 2002). Triclosan impaired muscle contraction in mice and swimming behavior of fish (Cherednichenko *et al*., 2012; Fritsch *et al*., 2013). Triclosan also induces the microbial resistance in human (Dhillon *et al*., 2015).

The other studies also indicated that triclosan had caused to bacterial resistance, skin irritation, endocrine disruption (Brausch and Rand, 2011; Dayan, 2007; Novo *et al*., 2013). Triclosan generates several carcinogenic byproducts which are found to be highly toxic and persistent. Some of these byproducts are 2,4-dichlorophenol (2,4-DCP) and 2,8-dichlorodibenzo-p-dioxin (Kanetoshi *et al*., 1992; Latch *et al*., 2003, 2005; Mezcua *et al*., 2004; Lores *et al*., 2005; Aranami and Readman, 2007). The toxicities of these byproducts are relatively higher than the precursor triclosan, and some of these are found to be potential carcinogen (Lores *et al*., 2005). Therefore, the European Union (EU) has eventually restricted the use of triclosan in biocidal products since 27th January 2016 (EU, 2016).

1.2.1.3. Amoxicillin (AMX)

Amoxicillin is another widely used semi-synthetic penicillin antibiotic. Amoxicillin is widely used antibiotic. It is phenolic type penicillin having the structure of β-lactam ring. This represents it for high bacterial resistance including the *Neisseria gonorrhoeae*, *Escherichia coli, Haemophilus influenza, Pneumococci, Streptococci*, and some strains of *Staphylococci* (Bebu *et al*., 2011; Fazelirad *et al*., 2015). Amoxicillin possesses relatively high oral absorption ability, compared to other members of the penicillin, has attracted its widespread consumption by human or in livestock (Berghe *et al*., 2011; Ball, 2007; Angadi *et al*., 2012; Chen *et al*., 2011). Amoxicillin is effective in treating the bacterial infections encountered in gastro-intestinal and systemic infections (Putra *et al*., 2009; Homem *et al*.,

2013; Aksu and Tunc, 2005). Amoxicillin was prescribed to treat various infections, *viz*., the middle ear, tonsils, throat, larynx, pharynx, bronchi, lungs, urinary tract, skin, gonorrhea, etc., (Kaur *et al*., 2011, Andreozzi *et al*., 2005).

Some of the physico-chemical properties of amoxicillin include, molecular weight of 365.40 g/mol, pK_a (acid dissociation constants) of 9.41 and Log K_{OW} (octanol/water partition coefficient) of 0.87 (Carless, 1996; Windholz *et al*., 1976). Due to its chemical structure, consumption rate, solubility, pharmacological characteristics and environmental toxicity, amoxicillin is considered as one of the primary contaminants of water and needs greater environmental attention (Homem and Santos, 2011; De Gusseme *et al*., 2011; Fent *et al*., 2006). Although amoxicillin is notably sensitive towards hydrolysis under a variety of pH conditions (Zia *et al*., 1977; Nagele and Moritz, 2005), it is difficult to degrade completely. This results that amoxicillin is found both in urine and faeces, along with its hydrolysed and metabolised byproducts (Putra *et al*., 2009). It was reported that the oral administration of 500 mg of amoxicillin in humans resulted the excretion of 86 ± 8% mg of amoxicillin through the urine after two hours of consumption (Kanakaraju *et al*., 2015). Amoxicillin poses serious threat to several aquatic organisms (Pan *et al*., 2008; Sun *et al*., 2012). Pan et al. (2008) reported the toxic effects of amoxicillin compounds towards algae *Synechocystis* sp., mainly by inhibiting its photosynthesis mechanism. Amoxicillin also causes chronic risk in the aquatic environment (Jones *et al*., 2002; Lee *et al*., 2008).

The presence of amoxicillin in domestic wastewater is ranged from ng/L to mg/L (Andreozzi *et al*., 2004; Zuccato *et al.*, 2010; Putra *et al*., 2009; Elmolla and Chaudhuri, 2010). Due to the persistence and bioaccumulation nature, the amoxicillin seemingly induces the toxic effects and alters the natural ecosystems (Homem *et al*., 2013). In Australia, amoxicillin is widely prescribed drug and detected in river water and hospital effluents at

ng/L levels (Watkinson *et al*., 2009). The presence of amoxicillin in wastewater/or effluent waters causes unpleasant odor, and microbial resistance among pathogen organisms or the death of microorganisms. Therefore, the resistant bacteria causes the disease which cannot be treated by the usual antibiotics (Kanakaraju *et al*., 2015). The amoxicillin causes the propagation of β-lactam resistant bacteria (Martinez, 2009). The conventional wastewater treatment plants enable to remove the antibiotics partially hence, it becomes important water pollutants (Michael *et al*., 2013). Because of the insufficient treatments of amoxicillin in conventional water and wastewater treatment plants, this compound enters both into the surface water and groundwater, that destroys the aquatic ecosystems. It also leads to bacterial resistance and consequently the inability to treat diseases using conventional antibiotics (Elmolla and Chaudhuri, 2009; Ding *et al*., 2012; Fatta *et al*., 2007). This enables to understand the frequent presence of resistance genes in surface or drinking waters (Vaz-Moreira *et al*., 2014). These studies, therefore, compel to remove completely the amoxicillin from the aquatic environment.

1.2.2. Dyes in aquatic environment

Dyes are water-soluble synthetic and natural organic compounds (Gurses *et al*., 2016). Roughly more than 10,000 dye compounds are known having worldwide annual production of 70,000 tons. Dyes are designed to give fabrics, papers, or any colorable materials a hue (Yagub *et al*., 2014; Zeng *et al*., 2017). Dyes are utilized by humans for over thousand years for various applications. Previously, dyes were usually produced on a small scale from naturally available material such as insects or plants and were known as natural dyes (Kant, 2012). However, natural dyes had drawbacks because of its limited variety as well as muted tones which fades when exposed to sunlight and washings (Solis *et al*., 2012).

Synthetic dyes were discovered and the rise in dyes demand commenced its production at large scales. The dye industries posing serious environmental problems by discharging huge amount of dye products into the aquatic environment. This presented a serious threat to the living organisms to the aquatic environment (Borujeni *et al*., 2011). The dyes contained effluents is undesirable to terrestrial environment (Pandey *et al*., 2007). It was assumed that the usage of natural dyes is a safe choice instead of using the synthetic dyes. However, it is not safe since the use of natural dyes requires mordant which bonds the dye with fabrics (Couto *et al*., 2009). Mordants are binders and found to be toxic and more dangerous than synthetic dyes (Kant, 2012). Currently, synthetic dyes are integral ingredient employed to give color to textiles, cosmetics, plastics, printings, etc., (Abdi *et al*., 2017; Nguyen and Juang, 2013). Synthetic dye molecules are complex and relatively recalcitrant because of the auxochrome (water soluble bonding compounds) and chromophores (color giving compound) in nature (Chacko and Subramaniam, 2011; Pan *et al*., 2017). Auxochromes (color helpers), *viz*., sulfonic acid, hydroxyl, carboxylic acids, and amino groups which helps in colour shifts provides the dye solubility (Abrahart, 1977), however, responsible for reduced degradation in conventional treatment methods (Santos *et al*., 2007). Dye compounds resist degradation in water, detergents or any other washing agents medium (Alwani *et al*., 2018) and it withstand even when exposed to extreme heat sources, oxidizing agents or strong light illumination (Forgacs *et al*., 2004; Peng *et al*., 2018).

The discharge of effluents contained with dye compounds received greater attention (Miranda *et al*., 2013) because of serious environmental concerns (Canizares *et al*., 2006; Mu *et al*., 2009). Therefore, the color-free discharge of effluents is a public demand (Hao *et al*., 2000). Dyes enter into the environment due to inefficient effluent treatment which subsequently discharged into water bodies. Dyes are hence; accumulated in water bodies and

have shown several adverse effects in terms of dissolved oxygen (DO), biological oxygen demand (BOD), chemical oxygen demand (COD), color, etc., (Solis *et al*., 2012). The potential threat of dyes are due to its toxic, non-biodegradable, carcinogenic, mutagenic, and even teratogenetic nature. This creates serious concerns to the human health and marine organisms (Denoncourt *et al*., 2014; Luna *et al*., 2014).

The textile, leather, food, cosmetic, paper, pharmaceutical industries are greatly utilizing the synthetic dyes and among these industries the textile industries are the main culprit of contaminating the aquatic environment (Couto *et al*., 2009). This industry alone produces *Ca.* 100 tons of effluents per year (Solis *et al*., 2012). It is interesting to note that maximum *Ca.* 80% of dye and chemical molecules from dye mixtures are able to be adsorbed by materials intended for coloring (Nguyen and Juang, 2013). Fabrics in particular, can only absorb a maximum 25% of dye mixture onto its surface due to its limited absorption capacity (Geundi *et al*., 1995). Therefore, a significant amount of the dye contained effluent (dye effluent) is discharged into the aquatic environment (Robinson *et al*., 2001). In addition to dyes, the industrial effluents also contained with variety of solvents, salts, detergents, etc., which makes it more complex (Damas *et al*., 2006). The presence of dyes in water bodies affects greatly the water quality and the photosynthesis in aquatic environments. The other chemical parameters of water, *viz*., pH, chemical oxygen demand (COD) are also affected in presence of dyes (Aksu and Balibek, 2010; Lade *et al*., 2012). Color removal, especially from textile wastewaters, is a challenging task for last several decades since there is no single and economically viable technology to be implemented for complete decolorization of dye from effluents (Robinson *et al*., 2001).

1.2.2.1. Alizarin Yellow (AY)

The organic dyes are broadly divided into three classes, *viz.*, azo, anthraquinone and triphenylmethane dyes (He *et al*., 2012). Azo dyes is a class of hydrophobic dyes known as disperse dyes. This constitutes *Ca.* 60 – 70% of worldwide dye production and poses several environmental problems (Bafana *et al*., 2011; Kostantinou and Albanis, 2004; Mansour *et al*., 2012). These compounds are eventually the visible indicator of water pollution (O'Neill *et al*., 1999). The release of these dyes into ecosystem is harmful, not only because of its color, but also due to the fact that many azo dyes and their breakdown products (colorless amines) are toxic and mutagenic to living organisms (Weisburger, 2002; Xu *et al*., 2007). Azo dyes are known to be electron deficient xenobiotic compounds since they possess electron withdrawing groups, generating electron deficiency in the molecule (dyes) making them persistent in nature (Singh *et al*., 2014).

Alizarin Yellow is an azo dye and widely employed in textile, food, paper and leather industries. Azo dyes are characterized by the presence of nitrogen double bonds (–N=N–) (Sen *et al*., 2016) and are found water soluble. Alizarin yellow is a hue for yellow and orange color. It is also employed as acid-base indicator. Its chromophore is azo bonds, which decreases significantly the water transmittance and affecting the aquatic life (You *et al*., 2010).

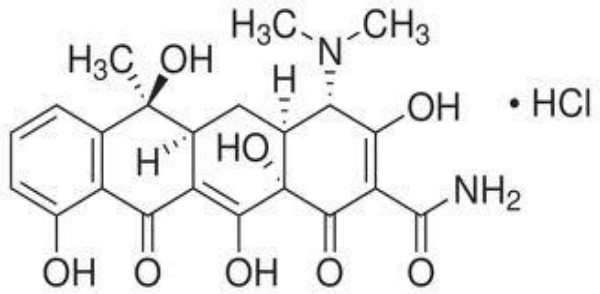

(1)

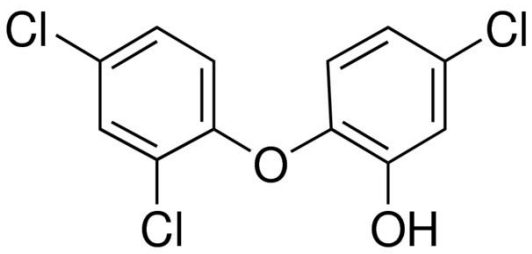

(2)

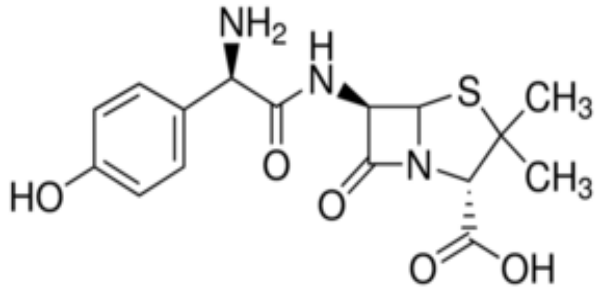

(3)

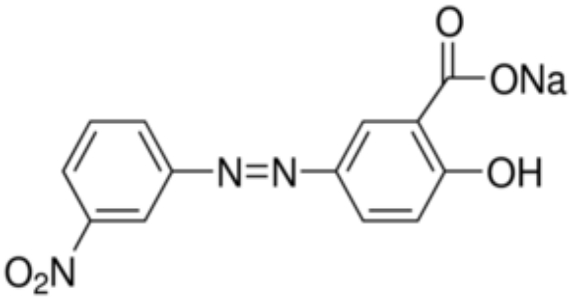

(4)

Figure 1.2.1: Structure of micropollutants: (1) Tetracycline (2) Triclosan (3) Amoxicillin (4) Alizarin Yellow

1.3. Removal of Micropollutants in Wastewater Treatment Plants (WWTPs)

WWTPs are, in general, developed by the public departments but several other organizations have their own WWTPs in order to treat the wastewaters coming from various sources, *viz*., domestic, laboratories, sanitation or sewage, etc., (Raghuvanshi *et al*., 2017). The conventional WWTPs are enabled to remove pathogens, coliforms and to reduce the load of carbon, nitrogen, and phosphorus from wastewaters. Moreover, the sludge obtained in the treatment able to remove several non-polar chemical compounds by the sorption process. The removal pathways of organic compounds in WWTPs are biotransformation/biodegradation and stripping by aeration (volatilization) (Radjenovic *et al*., 2007a). However, it was noted that several water contaminants and emerging micropollutants are not removed and escaped through the WWTPs effluents and enter into the receiving waters followed by entering into the surface waters (Reemtsma *et al*., 2006).

Further, these WWTPs possess limited capacities to eliminate the pharmaceutical compounds from urban wastewaters, since most of these chemicals are metabolized by microorganisms as source of carbon and may even inhibit the activity of the microorganisms or produce their bioaccumulation in the food chain (Rivera-Utrilla *et al*., 2013). The pharmaceutical concentrations is greatly fluctuate with the effluents of Sewage Treatment Plants (STPs), WWTPs and surface waters which is, possibly, due to varied load of pollutants at different regions and inconsistent efficiency of wastewater treatment plants (Pal *et al*., 2010). Wastewater treatment is a complicated process due to highly polluted wastewater characteristics. Wastewater must be thoroughly treated prior to discharge into receiving waters. The dilution of wastewater effluent upon discharge into water bodies results in a significant decrease in the concentration of endocrine disrupting compounds (EDCs) and pharmaceuticals and personal care products (PPCPs), either by degradation or

through binding to natural organic matter or soil along the riverbank which results in lower concentrations down the stream. The occurrence of these micropollutants ranged from μg/L to ng/L in drinking water system (Verstraeten *et al*., 2003; Bowman *et al*., 2002). On the other hand, no proper regulation is laid down by the regulatory bodies for these emerging pollutants in drinking water. None or very few precautions and monitoring units are enforced to ensure these unregulated or newer compounds and associated byproducts, specifically the micro-range pollutants. The quality of surface water in Europe has improved significantly since 1970 due to EU environmental directives. To protect the environment from the potential chemical pollution of urban wastewater discharges and emissions from the industry, a considerable progress has been made following the implementation of the Directive 91/271 (UWWD) (EC, 1991). EC, (1991) concerns the collection, treatment and discharge of urban wastewater and wastewater from certain industrial sectors. Further, the Member States of the European Union, the chemical quality of surface waters is controlled under the Water Framework Directive (WFD) 2000/60/EC (EC, 2000). Within this framework the key strategy adopted in the area of chemical pollution was the Decision 2455/2001/EC which established a list of 33 substances or groups of substances of priority concern due to their persistence, toxicity, bioaccumulation and widespread use and detection in rivers, lakes, transitional and coastal waters. The effective and efficient treatment of municipal wastewater in Europe during last couple of decades enabled significantly to improve the water quality of surface waters (EC, 2004; Reemtsma *et al*., 2006). Directive 2008/105/EC (EC, 2008) is a new step in the progress of regulation, establishing for the first time, quality standards (EQS) for priority substances and other pollutants of concern, to ensure adequate protection of the aquatic environment and human health. The emerging interest is being included in a review process for identification as possible "priority substances" or "hazardous substances". Actually, 13 new substances are under the review

process (EC, 2008), 7 are pharmaceuticals and 6 are personal care products. Further, the European Commission has developed strategies to deal urgently with endocrine disrupters as well (Bolong *et al*., 2009). Various studies have shown that treated municipal wastewater contributes significantly the micropollutants load in the water bodies (De la Cruz *et al*., 2012).

In primary treatment unit of WWTPS, some of the pharmaceuticals are removed by adsorption, however, other chemicals keep remain in the water, e.g., ibuprofen, naproxen, sulfamethoxazole, iopromide, etc., (Carballa *et al*., 2004). Furthermore, in the clarifier section, sludge and water is separated by decantation process. Sludge is then collected as solid waste which is air-dried and stored for further use. The semi-treated water then enters into the chlorination tank where disinfection takes place. The disinfected water then passes through the dual filter media, where the treated water is stored. The secondary treatment removes the PPCPs from the wastewater, but the removal efficiency of PPCPs changed greatly, and varied with the physico-chemical properties of compounds as well as environmental conditions such as the biological reactor configuration and operational parameters (hydraulic retention time, sludge retention time and pH) (Li *et al*., 2016; Roberts *et al*., 2016). The removal efficiency of PPCPs by biological treatment processes was extensively reviewed previously (Miege *et al*., 2009; Verlicchi *et al*., 2012). Secondary treatment in WWTPs removes 30 – 75% of anti-inflammatory and antibiotic compounds (Carballa *et al*., 2004). The other studies show that the carbamazepine is not appreciably removed by the WWTPs (Ternes, 1998; Heberer, 2002; Strenn *et al*., 2004; Clara *et al*., 2005). The WWTPs eliminates paracetamol, acetylsalicylic acid and ibuprofen but diclofenac is not removed by the WWTPs (Heberer, 2002). The penicillin readily hydrolyze in water and tetracycline precipitates with Ca^{2+} which is agglomerated with sludge

(Daughton and Ternes, 1999). Similarly, the estrogens, androgens or detergent components are not treated effectively in the conventional wastewater treatment plants because of their chemical and structural stability as well due to their low bioavailability. The municipal sewage sludge is repository of these emerging pollutants (Stamatelatou *et al*., 2011). Further, the biological micropollutants threaten public health and tempted for the development of newer and cost-effective technologies for disinfection of water. Therefore, the advanced treatment methods, *viz*., chemical degradation assisted with specific microorganisms, or UV light action is receiving greater attention in recent past. It was clearly demonstrated that the tertiary water treatments are required for the advanced and specific elimination of variety of contaminants from the aqueous wastes (Rivera-Utrilla *et al*., 2013).

Since the emerging micropollutants are not completely eliminated from the existing WWTPs, and remain in effluents at low levels. This, therefore, contaminates the receiving surface and ground waters, which are the main source of drinking water (Halling-Sorensen, 2001). Moreover, the development of newer resources with advanced technologies has produced more chemicals and compounds which are known to be potential environmental threats to the living beings. Several PPCPs, surfactants, various industrial additives and numerous chemicals purported to be endocrine disrupters are not metabolized and discharged into sewers and WWTPs which render greater challenges to the engineers for advancing the effective technologies (Bolong *et al*., 2009). In general, the occurrence of the new “unregulated” micro-contaminants such as EDCs, dyes and PPCPs requires advanced treatment technologies for efficient and effective elimination of these ever-growing micropollutants from aqueous wastes.

1.4. Alternative Treatments for Micropollutants Removal

1.4.1. Removal by Physical Adsorption Processes

Adsorption is the most common and widely utilized process in the removal of trace organic micropollutants in water. Adsorption may enable to remove PPCPs in the environment. In order to enhance the adsorption capacity for emerging water pollutants, different adsorbents are investigated and assessed specifically for wastewater treatment technologies (Wang and Wang, 2016).

1.4.1.1 Activated Carbon (AC)

Activated carbon having higher surface area and meso-porosity is widely employed in the treatment of water since it shows potential in the removal of several micropollutants from wastewater. Powdered activated carbon (PAC) and granular activated carbon (GAC) are commonly employed in treatment methods. The performance and application of activated carbon in the removal of EDCs is elaborately reviewed elsewhere (Liu *et al*., 2009). The use of activated carbon possessed with couple of problems which may underline as: (i) Relatively less adsorption capacity and (ii) the deterioration of activated carbon in the complex wastewater systems. Activated carbon is employed in the removal of PPCPs compounds, however, the adsorption capacity of activated carbon greatly depends on the hydrophobicity and charge of the PPCPs. Rodriguez et al. (2016) indicated that the adsorption capacity of activated carbon much depended on the PPCPs hydrophobicity studied for 3-methylindole, chloroprene and nortriptyline. In addition to the hydrophobicity and charge of PPCPs, it was observed that the water matrix had also affected the adsorption of PPCPs by activated carbon (Mailler *et al*., 2015; Rodriguez *et al*., 2016). In a pilot scale experiment using PAC as adsorbent, organic matter existing in the water was removed

completely (Mailler *et al*., 2015). Moreover, column studies showed that the higher PAC dose was required to achieve enhanced removal efficiency of PPCPs. Moreover, the removal efficiency of PPCPs by activated carbon is impacted by several parameters, *viz.*, the contact time, loading concentration of pollutant, co-existing ions, pH, morphology of activated carbon, etc., (Nam *et al*., 2014; Mestre *et al*., 2007). A pilot level experiments indicated that the lower dose of PAC is required for efficient removal of water contaminants compared to the GAC solids (Meinel *et al*., 2015). Aiming to achieve better performance of activated carbon in the removal of PPCPs, extensive experimentation is required which need to be conducted at pilot scale to investigate the optimum operational conditions, *viz*., the contact time, solid dose, structure of activated carbon, etc., (Wang and Wang, 2016).

1.4.1.2. Graphene and graphene oxide

Graphene is a newer carbon-based material having two-dimensional array of carbon atoms which are covalently bonded by the sp^2 hybridization forming honeycomb sheet. Graphene is a thinnest known material having very high specific surface area. Graphene oxide is a precursor of graphene and obtained by the oxidation of graphite. The graphene or graphene oxide showed potential in the remediation of aquatic environment contaminated with variety of contaminants including the PPCPs (Wang and Wang, 2016). Various physico-chemical properties affected the removal efficiency of graphene or graphene oxide for variety of PPCPs that includes the pH, contact time, background electrolytes, etc., (Kyzas *et al*., 2015; Yang and Tang, 2016). The adsorption studies for the removal of PPCPs using the graphene are conducted under batch reactor operations. Moreover, the studies conducted with the synthetic PPCPs contained wastewaters, which is obviously less complex than the real matrix samples. Therefore, the extensive studies need to be performed to

investigate the performance of graphene and its oxide for efficient removal of PPCPs in the real matrix samples (Wang and Wang, 2016).

1.4.1.3. Carbon nanotubes

Carbon nanotubes are having promising properties and enable it for several applications in energy storage and medical devices. Studies are conducted to assess the removal capacity of carbon nanotube in the removal of several PPCPs, *viz*., ketoprofen, carbamazepine (Liu *et al*., 2014a, 2014b), sulfamethoxazole (Ji *et al*., 2009) and triclosan (Cho *et al*., 2011). Removal capacities of carbon nanotubes for various pollutants varied with the surface structure of carbon nanotubes or the speciation of pollutant species. A review article summarizes the role of carbon nanotubes for variety of PPCPs (Jung *et al*., 2015). Multi-walled carbon nanotubes were efficiently employed for the removal of triclosan, ibuprofen, acetaminophen, carbamazepine, caffeine, prometryn, carbendazim, 4-acetylamino-antipyrine (Wang *et al*., 2016a). The removal of PPCPs was increased by decrease in initial sorptive concentration. Further, it was noted that larger the inner diameter of carbon nanotubes possesses better competitive adsorption in presence of fulvic acid (Wang and Wang, 2016).

Adsorption behavior of PPCPs onto the activated carbon, graphene, graphene oxide and carbon nanotubes showed several advantages but possessed with several problems which need to be addressed in real and large-scale implications of these materials (Wang and Wang, 2016).

(i) The removal capacity of graphene or activated carbon need to be enhanced at least for the macromolecular substances. The steric effect of micropore carbons of these materials has caused for lower adsorption capacity to the macromolecular substances.

(ii) The production cost of these materials needs to be economical. High cost of graphene restricts its large-scale use. Therefore, synthesis of low cost with high-surface-area graphene are in great demand.

(iii) It is further imperative to synthesize the carbon nanotubes by using the robust and simple methods.

Moreover, the attention is required for recycle and regeneration of these materials (i.e., activated carbon, graphene, graphene oxide and carbon nanotubes). Further, the co-existence of these solids along with the target PPCPs may induce toxic effects on the aquatic microorganism. A comprehensive and detailed studies further enable to understand the insight of the process (Wang and Wang, 2016).

1.4.2. Removal by Advanced Oxidation Processes (AOPs)

PPCPs or dye compounds are often detected in the effluents of WWTPs at low concentration this indicates that existing wastewater treatment plants are found inefficient to eliminate several micropollutants. This tempted to devise with some advanced treatment method which deals efficiently the elimination of these micropollutants including the dye compounds. The chemical oxidation processes, *viz.*, ozonation and advanced oxidation processes (AOPs), *viz*., O_3/UV, UV/ H_2O_2, Fenton and Fenton-like oxidation, sonolysis and electrochemical oxidation have shown potential in the oxidative removal of recalcitrant organic pollutants including dyes from aqueous wastes (Wang and Xu, 2012).

Free radicals are found strong oxidizing agent that initiates the AOPs in the degradation process. It is known that free radical species are atoms or molecules contained with at least one unpaired electron, e.g., the hydroxyl radical ($^{\bullet}OH$), superoxide anion radical ($O_2^{\bullet -}$), hydroperoxyl radical ($HO_2^{\bullet}$) or alkoxyl radical ($RO^{\bullet}$). The $^{\bullet}OH$ radical has attracted

greater attention in the area of advanced oxidation processes. The distinctive characters of $^{\bullet}OH$ radicals are their non-selective nature, high reactivity and strong oxidizing capacities (E^{o} = +2.80 V) (Andreozzi *et al*., 1999). It is able to attack a wide range of organic contaminants having the rate constants in the order of $10^{6} – 10^{9}$ $M^{-1}s^{-1}$ (Andreozzi *et al*., 1999; Legrini *et al*., 1993).

1.4.2.1. Ozonation

Ozonation is the widely employed oxidation process for several PPCPs. The ozonation depends on the *in situ* formation of $^{\bullet}OH$ radicals which eliminates the PPCPs (Bai *et al*., 2016a, 2016b). The content of hydroxyl radicals is related to the oxidation rate of micropollutants. The ozonation inhibited significantly in presence of scavengers of hydroxyl radicals. The real wastewater is a complex matrix contained with variety of pollutants. Therefore, to make ozonation process more effective, further studies need to be conducted in real wastewater matrices. In addition, attentions needed to study the fate of toxic byproducts in ozonation. Chemical oxidation processes, ozonation and combinations of O_3 with H_2O_2 (O_3/H_2O_2), and O_3 with UV (O_3/UV) was conducted to eliminate the pharmaceuticals from aqueous samples in a single or hybrid oxidation method (Andreozzi *et al*., 2005; Ikehata *et al*., 2006; Kidak and Dogan, 2018). The parametric studies, *viz*., pH, ozone dose and temperature had been studied extensively and an apparent mineralization of pharmaceuticals were also obtained. Ozone which is having short life time shows the method expensive and requires high-energy for real operation (Ikehata *et al*., 2006).

1.4.2.2. Fenton oxidation

Fenton oxidation is performed with iron salts and hydrogen peroxide in acidic medium. It is often used for the remediation of industrial wastewater contaminated with

variety of micropollutants. Similar to ozonation, Fenton oxidation is also relying on the $^{\bullet}OH$ radicals. Moreover, in addition to Fenton process, the Fenton-like processes, *viz*., electro-Fenton and photo-Fenton processes received greater attention in recent past (Wang and Wang, 2016). Several review articles demonstrated the Fenton or Fenton-like processes in the environmental remediation (Feng *et al*., 2013; Bokare and Choi, 2014). The Fenton-like system is useful and easily recyclable heterogeneous catalyst which is found to be environment-friendly as well (Xu and Wang, 2012). Fenton process for the elimination of PPCPs may result with the formation of toxic byproducts which need to be identified and the environmental fate of byproducts is equally important to be studied extensively (Wang and Wang, 2016).

The Fenton process is relatively less energy intensive which needs low pH (3 – 5) conditions (Malato *et al*., 2002; Perini *et al*., 2018). pH > 3, Fe^{3+} precipitates as $Fe(OH)_3$, however, at even higher pH values, the formation of Fe(II) complexes leads to significant decline of Fe^{2+} concentration. Several studies were conducted performing the Fenton or photo-Fenton processes at around neutral pH. This intended the viability of processes at large-scale operations or real wastewater operations (e.g., hospital wastewater) (Giraldo-Aguirre *et al*., 2017; Perini *et al*., 2018). Further, more rigorous studies are need to be conducted in order to optimize the suitable pH range using natural and real wastewater matrices (Kanakaraju *et al*., 2018).

1.4.2.3. Photocatalysis (UV and UV/H_2O_2)

UV-photolysis is introduced for photolytic degradation of pollutants. The UV-radiations facilitate the interaction of light radiations with the pollutant molecules and initiated with series of chemical reactions (Gjessing and Kallqvist, 1991; Frimmel, 1994).

UV-radiations also applied for the disinfectant of biological activity. The UV photolysis is used for the elimination of several PPCPs (Kim *et al*., 2009). The oxidation of pharmaceuticals greatly depends on the absorption of UV light (Kim *et al*., 2009). The mechanism of UV treatment is to study the cleavage of chemical bonds of pollutant molecules by direct absorption of UV-radiations. This is called as "photolysis". However, photolysis is not always effective (Vogna *et al*., 2004). Further, in order to enhance the efficiency of UV treatment in PPCPs removal, the researchers introduced the hybrid system of UV with hydrogen peroxide. This is called as "advanced oxidation process". This combined process is effective for degradation of several water pollutants (Yuan *et al*., 2011).

UV-photolysis depends largely on the irradiation intensity, the response of active pharmaceutical ingredients (APIs) and the quantum yield, the addition of peroxides to generate reactive radicals. UV/H_2O_2 reduces the intended UV-energy in the degradation of pharmaceuticals (Kim *et al*., 2009). The degradation is no longer dependent on direct absorption by the API. Therefore, the UV/H_2O_2 process is considered to be a promising technology for effective removal of PPCPs. However, this combination process showed different removal efficiency for different target compounds. In order to increase the applicability of this combination process, more studies are to be conducted to optimize various physico-chemical parameters (temperature, pH and dosage of H_2O_2) along with the selectivity of treatment.

1.4.2.4. Sonolysis

The sonolysis is based on the ultrasound irradiation and the oxidation process is proceeded through *in situ* generation of $^{\bullet}OH$ radicals. This is produced by the water pyrolysis using high intensity of acoustic cavity bubbles (Guyer and Ince, 2011). The power

and frequency of applied ultrasound greatly affected the efficiency of sonolysis in the oxidation of active pharmaceutical ingredients (APIs) (Ince, 2018; Kidak and Dogan, 2018). Similarly, the frequency of ultrasound was studied in the removal of ciprofloxacin (De Bel *et al*., 2011) and the results indicated that the lower frequency, i.e., 544 kHz resulted a high degradation of ciprofloxacin having the pseudo-first order rate constant 0.0067 min^{-1} at 15 mg/L of ciprofloxacin. The mineralization of pollutants was further enhanced with the aid of radical promoters (Naddeo *et al*., 2010; Liang *et al*., 2007; Rayaroth *et al*., 2016). Sonolysis requires high energy input and the low mineralization of pollutants limits its wider applications. However, the advanced oxidation process integrated with the sonolysis may enable it cost effective and also enhances apparent mineralization of pollutants (Kanakaraju *et al*., 2018).

1.4.2.5. Electrochemical oxidation

Electrochemical oxidation is one of attractive and efficient way of pharmaceuticals degradation. It operates by generation of reactive species via electricity. The operation is devoid with additional chemical use which creates further load on environment as secondary waste (Garcia-Segura *et al*., 2018). Electrodialysis and electrocoagulation separations along with the anodic oxidation of pollutants were reviewed extensively and demonstrated the usefulness of these electrochemical techniques (Sires and Brillas, 2012). The electro-oxidation is proceeded either by the direct oxidation at the anode or the indirect oxidation proceeds via *in situ* generation of reactive oxygen species by oxidants at the electrode surface (Feng *et al*., 2013).

The boron-doped diamond (BDD) anodes are often employed in the degradation of pharmaceuticals since BDD are found to be corrosion resistive, high oxygen-over potential

(to generate more $^{\bullet}OH$ radicals) and provides inert surfaces (Garcia-Espinoza *et al*., 2018; Svorc *et al*., 2017). It was reported that the electrochemical process using the BDD had more efficiency than Fenton oxidation in the degradation of real pharmaceutical wastewater samples (Perez *et al*., 2017).

1.4.2.6. Heterogeneous photocatalysis (TiO_2/UV)

The heterogeneous photocatalysts using different semiconductors (*viz*., TiO_2, ZnO, ZnS, WO_3, $SrTiO_3$) are studied for photocatalysis processes (Hoffmann *et al*., 1995). Among all the semiconductor catalysts in photoinduced processes, titanium dioxide (TiO_2) or titania is mostly used because it possesses several advantages over the other catalysts. The TiO_2 is chemically and biologically inert and found to be stable towards the catalytic operations which exaggerates the use of TiO_2 in various catalytic operations (Carp *et al*., 2004). In nature TiO_2 exists in three different mineral forms, *viz.*, anatase, rutile and brookite. Anatase usually exhibits highest photocatalytic activity. Anatase type possesses crystalline structure that resembles the tetragonal system (with dipyramidal type) and is used mainly as a photocatalyst under UV irradiation. The UV irradiation enables the excitation of electrons from the valence band to the conduction band which makes highly reactive oxidative holes on the valence band in TiO_2 solids. The hole takes part in generation of radical species in aqueous medium, *viz*., the formation of $^{\bullet}OH$ radicals. Therefore, the radical species are involved in the degradation of organic compounds onto the catalyst surface (Hoffmann *et al*., 1995; Carp *et al*., 2004).

Advanced oxidation process integrated with TiO_2 photocatalyst is an effective method to oxidize even the persistent and emerging micropollutants (Guillard *et al*., 1999). One of the important functions of heterogeneous photocatalysis is photocatalytic oxidation

(PCO) to effect partial or total mineralization of gas phase or liquid phase contaminants to benign substances (Zeltner and Tompkin, 2005). While degradation begins with a partial degradation, the term photocatalytic degradation usually refers to a complete photocatalytic oxidation or photo-mineralization, essentially to CO_2, H_2O, NO_3^- , PO_4^{3-} and halide ions (Carp *et al*., 2004). The treatment is based on the 'no-waste' concept and the nonreactive and chemically stable TiO_2 catalyst boosts the useful applications in the area of high catalytic activity and wastewater treatment strategies (Babic *et al*., 2017).

1.5. Heterogeneous Photocatalysis (TiO_2/UV) with Nanoparticles of Silver (Ag), Gold (Au) and Cerium (Ce)

In spite of several advantages, TiO_2 shows several limitations for its wider and enhanced applications, *viz*., it possesses a wide band gap (E_{gap}: *Ca* 3.2 eV) and having high number of e^-/h^+ pair recombination events that eventually restricts its efficiency in ultimate wastewater treatment technology (Soleymani *et al*., 2016; Guo *et al*., 2016). The lifespans of these species are very small and in the absence of suitable scavengers, it dispels the stored energy within a few nanoseconds by recombination. Further, the electronic excitation of TiO_2 requires a photon having the energy in the ultra violet (UV) region. However, a suitable modification enables its enhanced applicability for the implications in wastewater treatment. Many studies have been carried out to advance the photocatalytic activity by reducing the recombination reaction by the addition of noble metals (Choi *et al*., 1994; Cozzoli *et al*., 2004). It is found that doping with silver or gold nanoparticles has been of considerable relevance because of its potential functions. The TiO_2 photocatalyst modified or decorated with noble metal nanoparticles (NPs), *viz*., Silver (Ag), Gold (Au) and rare earth metal, *viz*., Cerium (Ce) had shown exciting and valuable photocatalytic properties. The Ag or Au nanoparticles decorated TiO_2 absorbs the light in the visible region and undergoes with the surface plasmon resonance that arouses the localized electric field in the vicinity of TiO_2 that results in facile production of e^-/h^+ pairs at the surface of TiO_2 (Ihara *et al*., 1997). Moreover, the nanoparticles on TiO_2 act as co-catalyst which helps the e^-/h^+ separations (Seery *et al*. 2007). Nevertheless, the plasmon resonance and the catalytic activity of catalyst mainly depends on the particle size, geometry and the noble metal nanoparticles doped to its sphere (El-Sayed, 2001; Feldstein *et al*., 1997). This naturally overcomes the limitations of TiO_2 and enables the use of solar visible light that constitutes

Ca. 40% in solar radiations. This eventually reduces the cost of operation and perhaps makes it further viable in the treatment technology (Tiwari *et al*., 2019b).

The importance in medical uses of silver nanoparticles as antibacterial agents is widely implied. It is combined with TiO_2 to fabricate the silver doped titania coated sanitary wares (Machida *et al*., 2004), medical devices, food preparation surfaces, air conditioning filters, etc. Silver can confine the excited electrons from TiO_2 and depart the holes for the degradation reaction of organic species (Ilisz *et al*., 1999; Stathatos *et al*.,2001). It also results in the delay of their wavelength response towards the visible region (Kamat, 2002). Besides, silver particles can support the electron excitation by creating a local electric field (Hermann *et al*., 1997), and plasmon resonance effect in metallic silver particles displays a reasonable improvement in this electric field (Zhao *et al*., 1996). The effect of Ag doping on titania and its photocatalytic activity by UV irradiation was studied by Chao et al. (Chao *et al*., 2003). They found that Ag doping helps the anatase to rutile conversion, which is credited to the increase in specific surface area which causes the improvement in photocatalytic activity and boosts the electron-hole pair separation.

The gold doped titania shows a strong absorption of visible light and possesses the surface resonance plasmon (SPR) of their free electrons (Wang *et al*., 2012; Ghosh and Pal, 2007). The plasmonic photocatalyst Au-TiO_2 shows high degradation efficiency of acetic acid and 2-propanol (Kowalska *et al*., 2010), thiocyanate (Dawson and Kamat, 2001) and alcohol oxidations using the visible light irradiation (Naya *et al*., 2010). The CO_2 reduction with either UV (245, 365 nm), or visible (532 nm) light was performed efficiently using the Au-TiO_2 (Hou *et al*., 2011). Similarly, water splitting for H_2 and O_2 production was conducted using the UV and visible light (Silva *et al*., 2011; Jovic *et al*., 2013).

An inexpensive and relatively non-toxic material cerium doped TiO_2 has been used to degrade organic pollutants (Chai *et al*., 2006) and the rare earth (RE) ions particularly the cerium is found to be an ideal dopant. This significantly modifies the crystal structure, electronic structure and optical properties of TiO_2 (Zhu *et al*., 2006; Koepke *et al*., 2006; Ranjit *et al*., 2001).

Moreover, the doping of cerium found greater attention during recent past owing to the reasons that cerium possesses redox couple Ce^{3+}/Ce^{4+} helps in converting the CeO_2 to Ce_2O_3 under the oxidizing and reducing conditions. Moreover, the variable electronic configurations Ce^{3+} ($4f^15d^0$) and Ce^{4+} ($4f^05d^0$) caused different optical and catalytic properties (Touati *et al*., 2016; Liu *et al*., 2008; Li *et al*., 2005). Literature reveals several studies conducted in the synthesis of metals doped hybrid materials (Chen *et al*., 2017; Patil *et al*., 2019). A simple sol-gel method was adopted using the titanium butoxide and cerium nitrate as precursor materials to obtain the Ce^{3+}-TiO_2 solid. The visible light driven photocatalyst was then used for the hydrogen production from sulphide wastewater (Bharatvaj *et al*., 2018). A novel hydrothermal method combined with wet-chemical deposition followed by the *in situ* solid-state chemical reduction was enabled to synthesize the composite Ti^{3+}-TiO_2/Ce^{3+}-CeO_2 nanosheet. The material has shown efficient degradation of dye compound due to doping of Ti^{3+} and Ce^{3+} and formation of surface oxygen vacancy and heterojunction (Xiu *et al*., 2018). Ce was doped *in situ* with the composite SiO_2-TiO_2 which enabled the material to inhibit the phase transformation from anatase to rutile even at higher annealing temperature and enhanced the thermal stability (Sun *et al*., 2014). The growth of the anatase TiO_2 crystallites was inhibited with the increased doping of cerium until the 3 mol.% Ce, however, the Ce loadings ($\geq$ 5 mol.%), showed that the anatase lattice was saturated by Ce^{4+} and the formation/separation of amorphous ceria and/or ceria (~1 nm)

nucleation was taken place. This resulted the increase of TiO_2 anatase crystallite-size (Matejova *et al*., 2014). It was reported previously that doping of cerium with TiO_2 was suitable for degradation of complex matrix compounds, e.g., polyvinylpyrrolidone (PVP) compared to the simple dye compound (methyl thymol blue) (Vieira *et al*., 2018). Similarly, the TiO_2-CeO_2 showed a macro-meso porosity and the degradation of Rhodamine B (Fiorenza *et al*., 2018) or bromophenol dye (Ameen *et al*., 2014) is studied under the visible light driven reactor (Fiorenza *et al*., 2018). The Ce and Mn were co-doped with the TiO_2 and the textural and optical results showed that manganese and cerium caused to reduce the gap energy and increased significantly the surface area as compared to the mono-doped or pristine TiO_2. Moreover, the co–doping enhances the lifetime of electron/hole pairs (Tbessi *et al*., 2019). Graphene oxide/magnetite/cerium-doped titania composite was synthesized by single step process and the efficient degradation of tetracycline was conducted. The material contained with Fe_2O_3 having superparamagnetic property hence, easily separable from the reactor (Cao *et al*., 2016). A synergistic effect was observed in the degradation of herbicide 2,4-dichlorophenoxyacetic acid by doping the Au nanoparticles with the TiO_2-CeO_2 photocatalysts under the visible light driven photocatalytic process. Further, it was reported that the Au (NPs) trap the electrons whereas cerium oxide behaves as oxidizing agent in the degradation mechanism (Guzmana *et al*., 2011).

1.5.1. Factors Affecting Heterogeneous TiO_2 Photocatalysis

1.5.1.1. Light intensity

Photocatalytic reaction rate depends largely on the radiation absorbed by the photocatalyst (Curco *et al*., 2002). Qamar et al. (2006) revealed that increased rate of degradation for some of the pollutants was increased with light intensity. The nature or form of the light does not affect the reaction pathway (Stylidi *et al*., 2004). In other words, the

band gap sensitization mechanism does not affect the photocatalytic degradation. The intensity of light greatly affects the rate of electron-hole formation in the photochemical reactions and eventually governs the overall efficiency of pollutant degradation (Cassano and Alfano, 2000; Pareek *et al*., 2008; Hermann, 1999; Ollis *et al*., 1991).

Unfortunately, only 5% of the total irradiated natural sunlight possesses adequate energy to enable the effective photosensitization (Wilk and Breuer, 1999) and a huge fraction of light energy is lost due to the reflection, transmission and heat energy (Yang and Liu, 2007). These limitations tempted researchers to carry further research in the application of TiO_2 in remediation of aquatic environment contaminated with variety of micropollutants.

1.5.1.2. Nature and concentration of pollutant

The substrate concentration and nature of pollutant species are important factors in the photocatalytic degradation of pollutant species (Ahmed *et al*., 2010). Similarly, the effective sorption of pollutant species onto the catalyst surface governs the catalytic degradation. However, the adsorption of pollutant is greatly depending on the initial pollutant concentration. Further, the percentage degradation decreases with increasing the amount of pollutant concentration, while keeping a fixed amount of catalyst.

The number of photons striking the catalyst surface determines the rate of the surface reactions and this correlates the surface coverage of TiO_2 photocatalyst by pollutant molecules (Kogo *et al*., 1980; Guillard *et al*., 2003). The photocatalytic degradation of aromatic compounds depends largely on the substituent group present. Nitrophenol adsorbs strongly on the catalyst surface than the phenol and therefore degrades faster than phenols (Bhatkhande *et al*., 2004). Similarly, mono-chlorinated phenol degrades faster than di- or tri-chlorinated member of chloro-aromatics (Hugul *et al*., 2002). Therefore, the molecules

having electron withdrawing group, *viz*., nitrobenzene and benzoic acid are reported to be adsorbed specifically than the electron donating groups (Palmisano *et al*., 2007).

1.5.1.3. Nature of photocatalyst

A very important parameter influencing the performance of photocatalyst in photocatalytic oxidation is the surface morphology, namely the particle size and agglomerate size (Ding *et al*., 2005). Numerous forms of TiO_2 have been synthesized by different methods to attain a photocatalyst exhibiting desirable physical properties, activity and stability for photocatalytic application (Gao and Liu, 2005). Evidently, there is a clear connection between the surface properties, the rational development of improved synthesis routes and the possible usefulness of the material prepared in application (Mohammadi *et al*., 2006; Diebold, 2003). For instance, smaller nanoparticle size is reported to give higher conversion in gaseous phase photo-mineralization of organic compounds over nano-sized titanium dioxide (Maira *et al*., 2001).

1.5.1.4. pH of the solution

Similarly, the pH of the solution is an important parameter which controls significantly the photocatalytic degradation processes since the pollutant species and catalyst surface change with change in solution pH (Singh *et al*., 2007; Haque *et al*., 2006). Pollutant molecule exists in positive, neutral or negatively charged species and depending on the catalysts charges the electrostatic interaction varies with pH. Therefore, it renders the change in photocatalytic degradation (Saien and Khezrianjoo, 2008). In the current update of the point of zero charge (PZC) (Kosmulski, 2006), the pH_{pzc} of Degussa P-25 TiO_2 was reported to be 6.9. This indicates that TiO_2 possesses net positive charge in acidic medium ($pH < 6.9$) and negative charge at $pH > 6.9$. In general, the catalytic activity of titanium dioxide is

favored at lower pH, however, it diminishes at very low pH conditions since the excess of H^+ suppresses the reaction rates (Sun *et al*., 2006). It is important to underline that the photocatalytic degradation of pollutants need to be optimized with solution pH (Mansilla *et al*., 2006).

1.5.1.5. Reaction temperature

It was pointed that the reaction rate of photocatalytic degradation of pollutants depend on temperature (Wang *et al*., 1999; Tunesi and Anderson, 1987; Evgenidou *et al*., 2005). In general, increase in temperature decrease the degradation due to the enhancement of recombination of charge carriers and desorption of adsorbed pollutant species. This was in a line to the Arrhenius equation, for which the apparent first order rate constant K_{app} increases linearly with $\exp(-1/T)$ (Gaya and Abdullah, 2008).

1.6. REVIEW OF LITERATURE

Titania photocatalysis also stated as the "Honda-Fujishima effect" is originally publicized by the pioneering work of Fujishima and Honda, (1972). Titanium dioxide (TiO_2) is a semiconductor material employed in science of photocatalysis (Lee *et al*., 2005; Ni *et al*., 2007). It was employed as a photocatalyst for splitting of water for H_2 production (Feng *et al*., 2011; Garcia *et al*., 2011). Honda and Fujishima (1972) initially utilized it for H_2 production on a titanium dioxide electrode, however, it received greater attention for catalytic and energy-related uses. Moreover, the nanostructured TiO_2, e.g., nanoparticles, nanowires, nanorods, nanosheets, etc., are possessed with enhanced applications in diverse area of science and technology (Gharagozlou and Bayati, 2014; Kilinc *et al*., 2014; Fujishima and Honda, 1972; O'Regan and Gratzel, 1991; Xu *et al*., 2009). Titanium dioxide is widely studied as an excellent photocatalyst in the oxidative elimination of organic pollutants from aqueous wastes (Chowdhury *et al*., 2015). Among the three crystalline forms of titanium dioxide, the anatase and rutile possesses considerable applications as potential photocatalysts. Anatase phase is relatively more effective than the rutile phase. The photocatalysis of several pesticide and herbicide derivatives dominant in storm water and wastewater effluents is treated using the titanium dioxide photocatalyst employing UV and solar radiations in the batch reactor operations (Ahmed *et al*., 2010).

Heterogeneous photocatalysis is an advanced oxidation process that applies a semiconductor to upsurge the construction of reactive species and degradation rates (Chong *et al*., 2010). Studies of heterogeneous photocatalysis started almost five decades back, after the finding of the photoinduced splitting of water on TiO_2 electrodes (Fujishima *et al*., 1969; Fujishima and Honda, 1972). During the last couple of decades, practical applications of TiO_2 photocatalysts was applied in both indoor and outdoor environments (Fujishima *et al*.,

1999; Fujishima and Zhang, 2006). Photocatalysis is widely studied in a range of research areas, *viz*., organic synthesis, water splitting, photo induced oxidation, hydrogen transfer, $O_2^{18} - O_2^{16}$ and deuterium-alkane isotopic exchange, metal deposition, disinfection and anti-cancer therapy, water detoxification, gaseous pollutant removal, etc., (Carp *et al*., 2004; Herrmann, 1999). The heterogeneous photocatalytic processes are efficient and effective methods for the purification of both air and water streams and titania is greatly applied as a catalyst which enables efficient charge carriers which helps in inducing reductive and oxidative processes (Kim *et al*., 2005).

The photocatalytic oxidation process is carried out with the energized light source along with an oxidizing agent, *viz*., oxygen or air. The photons having energies greater than the band-gap energy (ΔE), induces the excitation of electrons from valence band (VB) which then stimulates the oxidative reactions. Moreover, the absorption of photon energies less than ΔE (i.e., longer wavelengths) produces energy dissipation in the forms of heat. The absorption of light energy by the titanium dioxide catalyst creates positive hole (h^+) in the valence band and an electron (e^-) in the conduction band (CB). The positive hole oxidizes either pollutant directly or water to generate $^{\bullet}OH$ radicals, whereas the electron in the conduction band reduces the oxygen adsorbed on the catalyst surface (TiO_2) (Ahmed *et al*., 2010). The $^{\bullet}OH$ radical is the primary oxidant. The reaction mechanism for the photooxidative degradation of many organic pollutants over titania particles is studied extensively (Mills and Hunte, 1997; Pelizzetti and Minero, 1993) and the following chain reactions is hypothesized (Gaya and Abdullah, 2008).

Photoexcitation: $TiO_2/SC + h\nu \rightarrow e^- + h^+$ (1.6.1)

Oxygen adsorption: $(O_2)_{ads} + e^- \rightarrow O_2^{\bullet -}$ (1.6.2)

Ionization of water: $H_2O \rightarrow OH^- + H^+$ (1.6.3)

Protonation of superoxide: $O_2^{\bullet -} + H^+ \rightarrow HOO^{\bullet}$ (1.6.4)

The hydroperoxyl radical formed in (1.6.4) also has scavenging property as O_2 thus doubly prolonging the lifetime of photo-hole:

$HOO^{\bullet} + e^- \rightarrow HO_2^-$ (1.6.5)

$HOO^- + H^+ \rightarrow H_2O_2$ (1.6.6)

Both the oxidation and reduction take place at the surface of the photoexcited semiconductor photocatalyst and illustrated in Figure 1.6(a).

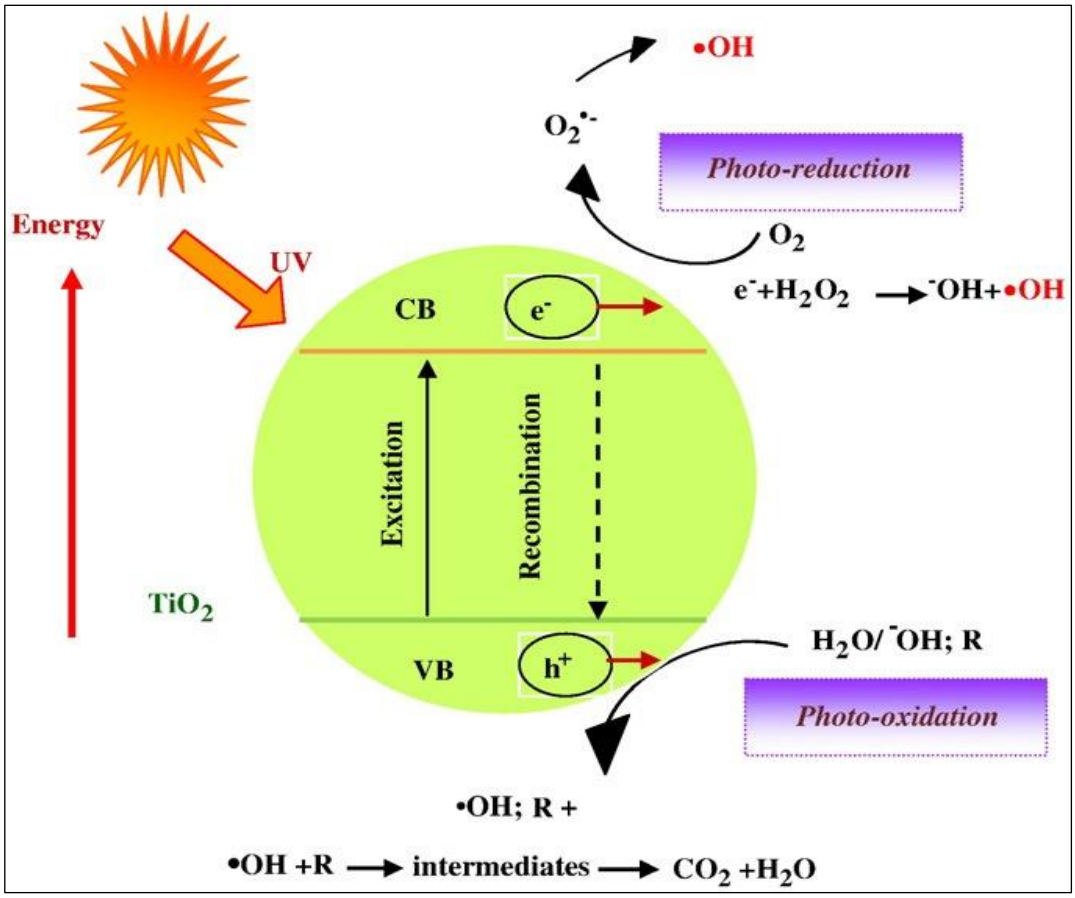

Figure 1.6(a): Schematic diagram illustrating the principle of TiO_2 photocatalysis [Ahmed *et al.*, 2010].

Recombination of electron and hole proceeds unless oxygen is available to scavenge the electrons to generate the superoxide ($O_2^{\bullet -}$). The protonated form, i.e., hydroperoxyl radical ($HO_2^{\bullet}$) and subsequently H_2O_2 is produced. Organic pollutants are attacked by these *in situ* generated radical species. In addition to the radicals, *viz.*, $^{\bullet}OH$, $O_2^{\bullet -}$, the positive holes are also involved in oxidation process (Zang and Farnood, 2005).

The titania-assisted aerobic photocatalytic reaction as opposed to a photosynthetic reaction having ΔG as negative (Carp *et al*., 2004). The corresponding acid HA of the non-metal substituent is formed as one of the byproduct (Gaya and Abdullah, 2008):

$$\text{Organic Contaminants} \xrightarrow[(ii)O_2]{(i)TiO_2} \text{Intermediate(s)} \rightarrow CO_2 + H_2O + HA \qquad (1.6.7)$$
$$(iii)h\nu \geq E_g$$

Several mechanisms are proposed in the photocatalytic degradation of organic compounds over TiO_2 surface. The characteristic time for each elementary reaction is illustrated in Table 1.6 (Gaya and Abdullah, 2008).

Table 1.6: Primary processes and time domains in TiO_2 catalyzed mineralization of organic pollutants [Gaya and Abdullah, 2008].

Primary process	Characteristic time
Charge carrier generation	
$TiO_2 + h\nu \longrightarrow e^- + h^+$	fs (very fast)
Charge carrier trapping	
$h^+ + > Ti^{IV}OH \longrightarrow \{> Ti^{IV}OH^{\bullet +}\}$	10ns (fast)
$e^- + > Ti^{IV}OH \longrightarrow \{> TiOH^{III}\}$	100ps (shallow trap; dynamic equilibrium)
$e^- + > Ti^{IV} \longrightarrow Ti^{III}$	10ns (deep trap)
Charge carrier recombination	
$e^- + \{> Ti^{IV}OH^{\bullet +}\} \longrightarrow > Ti^{IV}OH$	100 ns (Slow)
$h^+ + > Ti^{III}OH^{\bullet +}\} \longrightarrow Ti^{IV}OH$	10 ns (fast)
Interfacial charge transfer	
$\{> Ti^{IV}OH^{\bullet +}\}$ + Organic molecule	100ns (Slow)
$\longrightarrow Ti^{IV}OH$ + Oxidized molecule	ms (Very slow)
$\{> Ti^{III}OH\ \} + O_2 \longrightarrow > Ti^{IV}OH + O_2^{\bullet -}$	

The {>$Ti^{IV}OH^{\bullet +}$} and {>$Ti^{III}OH$} represent the surface-trapped valence band electron and surface-trapped conduction band electrons, respectively. The surface-bound $^{\bullet}OH$ radical represented by {>$Ti^{IV}OH^{\bullet +}$} is chemically equal to the surface-trapped hole allowing the use of the former and latter terms interchangeably (Horvath, 2003). It was reported that a good correlation had occurred between the charge carrier dynamics, their

surface densities and the efficiency of the photocatalytic degradation over TiO_2. A femtosecond spectroscopic analysis is conducted for the TiO_2/SCN^- aqueous system and the results indicated that a dramatic rise in the population of trapped charge carriers is obtained within the first few picoseconds (Colombo and Bowman, 1996). The results also confirmed that for species adsorbed to TiO_2, the hole-transfer reaction is successfully completed within picoseconds. The interfacial photochemical reactions are described as given below (Gaya and Abdullah, 2008):

Photoexcitation: $TiO_2 + h\nu \rightarrow e^-_{CB} + h^+_{VB}$ (1.6.8)

Charge carrier trapping: $e^-_{CB} \rightarrow e^-_{TR}$ (1.6.9)

Charge carrier trapping: $h^+_{VB} \rightarrow h^+_{TR}$ (1.6.10)

Electron-hole recombination: $e^-_{TR} + h^+_{VB}(h^+_{TR}) \rightarrow e^-_{CB} + \text{heat}$ (1.6.11)

Bahnemann et al. (1984) provided a clear evidence of the trapped charge carriers using flash radiolysis. The breaking of bonds in organic molecule takes place due to the interaction of the trapped e^-_{TR} (Ti^{3+}) and h^+_{TR} (presumably $^{\bullet}OH$) pairs onto the TiO_2 particle surface (Anpo *et al*., 1984). Furube et al. (1999) also confirmed the trapped charge carriers occur near the particle surface and do not undergo rapid (~1mps) recombination instantly.

Photocatalytic degradation processes are conducted in presence of water, air, the target contaminant and the photocatalyst. The presence of water is important and crucial in TiO_2 photocatalysis since the 2-propanol photooxidation cannot proceed without water (Domen *et al*., 1982). Figure 1.6(b) displays the steps involved in the photo-induced processes of the photo–mineralization of organic contaminant in presence of TiO_2.

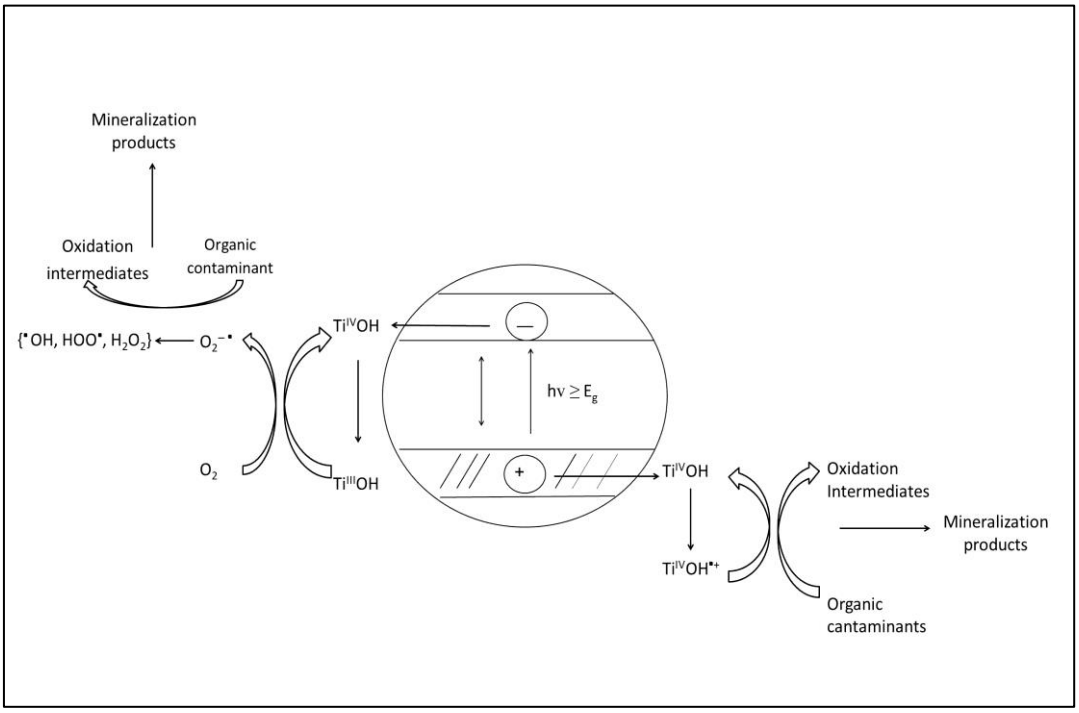

Figure 1.6(b): Conceptual diagram for the primary processes involved in photo-mineralization of organic compounds [Gaya and Abdullah, 2008].

Photo-generated holes are greatly involved in oxidizing the organic molecules directly (Zeltner and Tompkins, 2005) or indirectly through the *in situ* generated $^{\bullet}OH$ (Zhao and Yang, 2003; Fujishima *et al*., 2000):

$$H_2O + h^+ \rightarrow OH^{\bullet} + H^+ \qquad (1.6.12)$$

$$R\text{–}H + OH^{\bullet} \rightarrow R'^{\bullet} + H_2O \qquad (1.6.13)$$

$$R + h^+ \rightarrow R^{+\bullet} \rightarrow \text{Degradation products} \qquad (1.6.14)$$

The kinetics of photocatalytic degradation of organic compounds generally follows the Langmuir-Hinshelwood scheme (Dung *et al*., 2005; Mills and Hunte, 1997).

$$r = -\frac{dC}{dt} = \frac{kKC}{1+KC} \qquad (1.6.15)$$

where *r* represents the initial rate of photo-oxidation, *C* the concentration of the

reactant, *t* the irradiation time, *k* the rate constant of the reaction and *K* is the adsorption coefficient of the reactant. At mM concentrations $C \ll 1$, the equation can be simplified to the apparent rate order equation (Kabra *et al*., 2004; Konstantinou and Albanis, 2004):

$$\frac{\ln C_0}{C} = kKt = K_{app}\, t \qquad (1.6.16)$$

or

$$C_t = C_0\, e^{-K_{app}\, t}$$

where K_{app} is the apparent pseudo-first-order rate constant obtained by the slope of ln C_0/C against time (*t)* and C_0 is the initial concentration of the organic pollutant. Consequently, under the similar condition, the initial degradation rate is given in the following form:

$$r_0 = K_{app}\, C \qquad (1.6.17)$$

A quasi-exhaustive consideration of photo-oxidation studies of organic contaminants evidenced that the pseudo-first-order rate equation above holds true (Valente *et al*., 2006; Chen *et al*., 2007). Further, the Langmuir-Hinshelwood model acts as a basis for the photo–degradation of organic compounds even if it could not directly offer sufficient fitting (Demeestere *et al*., 2004). However, for suspended titania-mediated photocatalytic degradation of organic compounds pseudo-zeroth order is also reported (Dijkstra *et al*., 2001).

The use of titania based photocatalysis suffers from several drawbacks, for example, difficulty of separation from the solution, relatively high electron-hole recombination rate. This, of course, results with lower photocatalytic efficiency. Moreover, the TiO_2 is effective only under UV light ($\lambda < 388$ nm) irradiation because of its large energy band gap (3.2 eV

for anatase), i.e., it obtains only less than 3% of the available solar energy (Chowdhury *et al*., 2015; De Almeida *et al*., 2015). The preparation of porous TiO_2 thin films with high specific surface area is attracting more and more attention in recent past (Cernigoj *et al*., 2006; Bu *et al*., 2006). The photocatalytic activity of TiO_2 is reliant on surface and structural properties of the semiconductor. These factors could impact the adsorption behavior of a pollutant or degradation intermediates and the life time and recombination rate of electron-hole pairs (Furube *et al*., 1999). Because photocatalytic procedures are chemical reactions on the surface, therefore, the increase of surface area could enhance the effectiveness of the process because it involves larger contact surfaces exposed to the pollutants (Yu *et al*., 2000). Particle size is an important parameter in heterogeneous catalysis, because it is directly associated with the efficiency of a catalyst through the definition of its specific surface area (Ahmed *et al*., 2010). The photo-induced phenomenon is affected by quantum size. Anpo et al. (1987) seen blue shift and increase in reaction yield and photocatalytic activity as the diameter of the TiO_2 particles becomes smaller particularly below 100Å. This observation was credited to the suppression of radiation-less transfer and the concurrent enhancement of the activities of the charge carriers. Porous inorganic TiO_2 (anatase) films can be acquired using templating membranes (Schattka *et al*., 2006) or conventional alkoxide sol-gel route with the addition of surfactants (Chen *et al*., 2008). The templates allow to maintain the initial polymer morphology up to final porous structure. Polyethylene glycol is particularly appropriate for obtaining the porous structure of coatings (Bu *et al*., 2004) due to its complete decomposition at relatively low temperature (Kajihara *et al*., 2005). The control of synthesis and deposition processes is crucial for getting homogeneous, ordered and crack-free surface coatings. Crystalline phase, specific surface area, surface OH groups, morphology, band gap, porosity and accumulation of particles are several parameters playing a conclusive role in the photocatalytic effectiveness of titania (Cheng *et*

al., 1995). But, diverse results are obtained in literature. While some authors emphasize the high surface area as determining factor to increase efficiency (Bacsa and Kiwi, 1998) others indicate the influence of crystallinity and particle size (Yin *et al*., 2001).

In order to improve the photocatalytic activity of catalyst, the production of more electrons and holes by overpowering their recombination is perhaps the best possible way to be adopted. Therefore, the recombination rate is significantly decreased by doping the metal ions. Several studies are conducted doping the numerous metals with titania network. This creates an apparent dopant energy levels below to the conduction band energy of titanium dioxide. The dopant metal provides energy band as a trapping electron site and electrons stay for a while prior to further transported to an adsorbed acceptor on the catalyst surface. Therefore, electron and holes are available for further oxidative decomposition reaction (Reda *et al*., 2017). In addition, some of doped metals with titania network leads to the creation of oxygen vacancy in titania lattice or even lattice defect which then provide an impurity energy level below to the conduction band of titanium dioxide. The incorporation of impurity creates strain and unbalanced charge and making oxygen vacancy. This vacancy traps electron and also result in a decrease of electron and hole recombination. In recent past several studies conducted for doping several metals with titania network to improve its photocatalytic activity under UV or visible light irradiation. Transition metals have long been selected as doping elements because of the possible transition of d and f orbital electrons, which allows these elements to be a good electron acceptor and thus obstructs the recombination of photo-induced electron-hole pairs (Bae and Choi, 2003). The most widely studied metals are Ag, Au or Ce doped titania (Stengl *et al*., 2009).

The doping of silver nanoparticles with TiO_2 has shown an enhanced catalytic efficiency of catalyst in the removal of numerous pollutants, since the nanoparticles traps

electrons and restricting the recombination of the electron-hole pairs (Iliev *et al*., 2006). Moreover, the Ag nanoparticles provides the excitation under the visible light irradiation because of the localized surface plasmon resonance (SPR) due to the collective oscillations of the surface electrons (Liu *et al*., 2015). Ag nanoparticles displays greater applicability due to its low cost and high-performance photocatalytic activities (Weerachawanasak *et al*., 2009). It is well known that the free electrons of metals can collectively oscillate when induced by light irradiation. The oscillation frequency of light, electro-magnetic field agrees with that of the free electrons, the SPR effect is generated and light energy is coupled with the metal nanoparticles at the same time (Ohno, 2004). Silver nanoparticles are impregnated with the titania network and employed for the removal of methyl orange. The materials showed remarkably enhanced photocatalytic performance compared to the bare TiO_2 nanoparticles (Aysin *et al*., 2013). The plasmonic photocatalyst Ag/AgCl/TiO_2 was synthesized and showed a high photocatalytic activity in the elimination of methylene orange. The SPR effect of Ag-nanoparticles under visible light irradiation is the possible pathway of degradation (Jing *et al*., 2003). The effect of Ag doping with titanium dioxide using the sol-gel synthesis was conducted by Chao et al. (2003). The Ag doping caused the transformation of anatase to rutile phase of titanium dioxide. The silver deposition has caused to improve the photocatalytic activity of rutile titanium dioxide and detrimental effect is observed for the anatase phase in the oxidation of 2-propanol (Sclafani *et al*., 1998). Similarly, the Ag doped nano-TiO_2 catalyst showed enhanced catalytic performance than the commercial titanium dioxide in the mineralization of organic pollutants (Loganathan *et al*., 2011).

Further, the TiO_2 catalyst as decorated with the noble metals nanoparticles (NPs), *viz*., nanoparticles of Ag or Au helps to achieve several useful results. It serves first to

operate the process in visible light absorption since the noble metal nanoparticles yield with surface plasmon resonance effect under the visible/UV-A light irradiation. The nanoparticles enable to stimulate the localized electric field in the vicinity of TiO_2 that results in facile generation of e^{-}/h^{+} pairs at the surface region of TiO_2 (Ihara *et al*., 1997). Further, the noble metal nanoparticles on TiO_2 also act as co-catalysts which promotes e^{-}/h^{+} separations that favors the surface reactions (e.g., recombination of H atoms to produce H_2 (Seery *et al*., 2007). It is further demonstrated that effective plasmon resonance and the catalytic activity depends largely upon particle size, geometry and the noble metal nanoparticles doped to its sphere (Feldstein *et al*., 1997; El-Sayed, 2001). This doping overcomes the limitations of TiO_2 and enables the use of solar visible light that constitutes *Ca.* 40% in solar radiations. This ultimately reduces the cost of operation and perhaps makes it further viable in the treatment technology. On the other hand, UV-A light active advanced materials were synthesized and employed in the efficient treatment of variety of emerging water pollutants (Park *et al*., 2017; Aazam, 2014). The nanocomposite Fe_2O_3@TiO_2@nanometal (Au, Ag) was synthesized by the sol-gel facile route and an enhanced degradation of pollutant was obtained using the UV-radiations (Kim *et al*., 2016). Tetracycline was treated using the TiO_2/Ge composite material under the UV-A radiations. The results indicated that more than 95% of COD was removed with 240 min of irradiation (Chung *et al*., 2016). Similarly, the carbon quantum dots modified CdSe loaded reduced graphene oxide was utilized in the photocatalytic degradation of tetracycline. The results indicated that the $^{\bullet}OH$, $O_2^{\bullet-}$ and $^1O_2$ radicals were predominantly involved in the degradation mechanism of tetracycline (Huo *et al*., 2017). The Fenton-like catalytic process was conducted using the ferro-ferric oxide nanoparticles coated activated carbon and employed in the efficient degradation of tetracycline from aqueous solutions (Jafari *et al*., 2017).

The doping with rare earth ions also enables the light absorption in the visible range hence, enhances the separation efficiency of photo-induced charge carriers (Qu *et al*., 2011). Several studies indicated that some of the rare earth ions doped titanium dioxide not only suppresses the recombination of photo-induced charge carriers, but also widen the absorption spectrum (Ko *et al*., 2011). Predominantly, cerium ions (Ce^{3+}/Ce^{4+}) are found to be an ideal dopant to modify the crystal structure, electronic structure and optical properties of TiO_2. It makes complexes with various Lewis bases including organic acids, aldehydes, alcohols, and thiols in the interaction of the functional groups with its f-orbital (Ranjit *et al*., 2001). Ce doping with titania network enabled useful properties, *viz*., the redox couple Ce^{3+}/Ce^{4+}, which results from the shift of cerium oxide between CeO_2 and Ce_2O_3 under oxidizing and reducing conditions. Moreover, the variable electronic configurations Ce^{3+} ($4f^15d^0$) and Ce^{4+} ($4f^05d^0$) caused different optical and catalytic properties of materials (Magesh *et al*., 2009). Cerium is one of the four most abundant rare earth metals, it is inexpensive and relatively nontoxic in nature. The Ce-doped TiO_2 is found efficient in the methane steam reforming, CO_2 hydrogenation, mercury oxidation, S-metolachlor degradation, NO_x reduction, CO_2 reduction, NH_3 oxidation, degradation of dye, nitrobenzene degradation, etc., (Makdee *et al*., 2018). Nikl et al. (2015) has combined Ce into $RbGdS_2$ crystal and the samples showed long-term stability with luminescent features. The Ce-doped SnS_2 nanoflakes show higher photocatalytic activity for degradation of organic dye (Kiruthigaa *et al*, 2015). Ce doping enhances the absorption of light compared to the host semiconductor hence, enabled to show enhanced catalytic activity (Zhan *et al*., 2018). It has been indicated that Pt, Cu and Au nanoparticles supported on mixed-metal oxide CeO_x/TiO_2 presented higher activity toward the water-gas shift reaction than in the absence of CeO_x (Fan *et al*., 2015; Loganathan *et al*., 2011).

1.7. SCOPE OF THE PRESENT INVESTIGATION

The emerging water pollutants including the pharmaceuticals, personal care products (PPCPs) or dye compounds is a greater and serious concern since these pollutants are presently entered into the drinking water system and showed serious threat to the humans and aquatic life. Among these emerging water pollutants, the pharmaceuticals including antibiotics (Arikan *et al*., 2009), antipyretic/analgesic drugs (Bunch and Bernot, 2010), environmental estrogen (Bicchi *et al*., 2009), and disinfectants (Cha and Cupples, 2009) are found to be important water contaminants since these are often detected in high concentrations in natural water bodies. The conventional WWTPs are found to be the leading cause for these pharmaceuticals as they accumulate discharges from hospitals, veterinaries, households, industries and pharmacies (Destrieux *et al*., 2017; Lee *et al*., 2017). Because of the differences in the physico-chemical properties of active pharmaceutical ingredients (APIs), the configuration of WWTP facilities and the sewage composition, the effectiveness of treatments can differ significantly requiring a broad range of removal procedures (Kassinos *et al*., 2011a; Luo *et al*., 2014). Numerous studies have confirmed the presence of pharmaceuticals in the influents and effluents of WWTPs (Causanilles *et al*., 2017; Lin *et al*., 2018). Uncontrolled discharge of micropollutants in the aquatic environment poses a global health concern (Rahman *et al*., 2009).

Overall, WWTPs have been mainly intended and modernized for the elimination of easily or moderately biodegradable compounds containing carbon, nitrogen and phosphorus (Nitoi *et al*., 2015), they are not tuned for complete removal of personal care products and pharmaceuticals active substances. Unfortunately, PPCPs elimination by conventional wastewater treatment plants is not achieved effectively (Yang *et al*., 2011). WWTPs cannot entirely eliminate the PPCPs or other organic or synthetic compounds from wastewater, the

removal is affected by treatment technique and operating conditions (Narumiya *et al*., 2013). Therefore, elimination of these pollutants from waste or effluent waters is one of the greatest concerns due to the shortage of clean water sources. In this concern, advanced oxidation processes (AOPs) could constitute a better alternative for PPCPs degradation (Pouran *et al*., 2015). Among AOPs, heterogeneous photocatalysis using UV/TiO_2 process was often used for PPCPs degradation. This is due to the fact that it generates *in situ* the highly reactive oxygen species (ROS), *viz*., hydroxyl radicals and superoxide anion radicals. This enables the mineralization of pollutant species into the end products, *viz.*, CO_2, H_2O and inorganic ions (Rafqah *et al*., 2006; Yu *et al*., 2006; Dalrymple *et al*., 2007).

Therefore, in order to improve the photocatalytic activity of TiO_2 catalysts, a thin film of titania (TiO_2 nanoparticles) immobilized on to a stationary substrate, i.e., on borosilicate glass could be attained via sol-gel dip coating process. These immobilized nano-TiO_2 thin films having the TiO_2 nanoparticles are believed to acquire significantly large specific surface area, which offer good photocatalytic properties in the degradation of several micropollutants from aqueous solutions. The TiO_2 thin films (immobilized nano-TiO_2 thin films as well as the PEG template nano-TiO_2 thin films onto borosilicate glass) as the heterogeneous photocatalysts could increase evidently the degradation of several pollutants. Furthermore, the TiO_2 thin films prepared by template synthetic route using polyethylene glycol (PEG) as filler medium while impregnating with nanoparticles of Ag, Au and Ce could increase evidently the degradation of several pollutants. Thus, the present research work is proposed as an alternative water treatment technology which targets towards the effective and selective oxidation of several organic micropollutants such as triclosan, tetracycline, amoxicillin along with the dye alizarin yellow from aqueous solutions using immobilized nano-TiO_2 thin films as well as the PEG template nano-TiO_2 thin films

(both the nano-TiO_2 thin films are impregnated with Ag, Au and Ce nanoparticles). Additionally, various physico-chemical parametric studies are conducted to enhance the degradation mechanism of these pollutants under the photocatalytic degradation. The reusability of these thin films in the repeated photocatalytic operations for these pollutants is extensively studied for greater implication of proposed technology.

2. METHODOLOGY

2.1 Materials

2.1.1. Chemicals and Apparatus

Preferably the AR/GR grade chemicals were used in the experimentation. Titanium(IV) isopropoxide ($Ti[OCH(CH_3)_2]_4$), poly(ethyleneglycol) ($H(OCH_2CH_2)_nOH$), gold(III) chloride hydrate ($HAuCl_4.xH_2O$), tetracycline hydrochloride ($C_{22}H_{24}N_2O_8.HCl$), alizarin yellow ($C_{13}H_8N_3NaO_5$), triclosan ($C_{12}H_7Cl_3O_2$), amoxicillin ($C_{16}H_{19}N_3O_5S$), sodium borohydride ($NaBH_4$) were obtained from Sigma Aldrich. Co., USA. Acetylacetone ($CH_3COCH_2COCH_3$), ethanol anhydrous (C_2H_5OH), hydrochloric acid (HCl), sodium hydroxide (NaOH), zinc chloride ($ZnCl_2$), cupric sulphate ($CuSO_4.5H_2O$), cadmium nitrate ($Cd(NO_3)_2.4H_2O$), oxalic acid ($C_2H_2O_4.2H_2O$), acetic acid (CH_3COOH), 2-propanol ($CH_3CHOHCH_3$), sodium azide (NaN_3), sodium hydrogen carbonate ($NaHCO_3$), silver nitrate ($AgNO_3$), sodium chloride (NaCl), glycine ($C_2H_5NO_2$) were obtained from Merck India Ltd., India. Moreover, sodium nitrite ($NaNO_2$) and cerium (III) nitrate hexahydrate ($Ce(NO_3)_3.6H_2O$) were obtained from Himedia India Ltd., India. Besides, sodium nitrate ($NaNO_3$), ethylenediaminetetraacetic acid disodium salt were obtained from Loba Chemicals, India. Purified water (18.2 MΩ.cm at 25 ^{0}C) was obtained from Millipore Water Purification system (Model: Elix 3). An electric furnace was used for materials annealing (Nabertherm, Germany; Model No. LT/15/12/P330).

A pH-meter having glass and calomel electrode assembly (*Thermo Scientific, Sn B43460*) was employed for entire pH measurements in aqueous solutions. Before using the pH meter, it was carefully calibrated using the standard buffer solutions.

A lamp, wavelength (λ_{max}) = 360 nm (Model: 9W, PLS9W BLB/2P 1CT, Philips) was procured from Hansung UV Pvt. Co. Ltd., Korea and utilized in the photoreactor.

2.1.2. Reagents

i. Sample Stock solutions: 100.0 mg/L solutions of tetracycline [TC], triclosan [TCS], amoxicillin [AMX] and alizarin yellow [AY] were prepared in aqueous solutions. Solutions were sonicated in sonication bath to increase the solubility of these pollutants.

ii. Standard Buffers (pH 4.00, 7.00 & 12.00) were used for the calibration of pH meter.

iii. HCl and NaOH (0.1 mol/L) solutions were used to adjust the pH of the sample solutions.

2.1.3. Ultra violet-Visible (UV-Vis) Spectroscopy

UV-Vis spectrophotometer was used to measure the absorbance of sample solutions, either at a single wavelength or perform a scan over a range in the spectrum. The UV region ranges from 190 − 400 nm and the visible region from 400 − 800 nm (Kalsi, 2004). This technique can be used both for quantitative and qualitative measurement. The technique is routinely used in analytical chemistry for quantitative determination of different analytes such as transition metal ions, highly conjugated organic compounds, and biological macromolecules (Elsherif *et al*., 2014).

UV-Visible absorption spectrophotometry is the technique based on attenuation of electromagnetic radiation measurement by an absorbing substance (Tissue, 2012). It has a spectral range approximately around 190 – 800 nm, which also differ in terms of energy ranges, and type of excitation from other related regions. This attenuation results from the scattering, absorption, reflection or interferences. Though, accurate measurements of the attenuation can be done recording only the absorbance. Within some limits, the absorbance

is proportional to the concentration of the analyte to determine and to the distance of the light when it passes through the sample during the irradiation. This relationship is called Lambert and Beer's law and it is commonly written as:

$$A = a\ b\ c \qquad \ldots (2.1.3)$$

where A means absorbance, a is the molar extinction coefficient (wavelength-dependent) in L/mol/cm , b is the path length in cm and c is the absorber concentration in mol/L. This linear relationship is influenced by different factors such as the characteristics of the spectrophotometer, photodegradation of the molecules, presence of scattering or absorbing interferences in the sample, fluorescent compounds in the sample, interactions between the analyte and the solvent, and the pH (Passos and Saraiva, 2019).

The absorption of light in the UV-Vis wavelength (between ~ 180 – 800 nm) occurs frequently from many molecules such as a wide number of organic molecules. The main energy changes happen at electronic level but can also happen at vibrational quantum levels (Sommer, 1989). $n \rightarrow \sigma^*$ and $\sigma \rightarrow \sigma^*$ transitions need more energy and are related with absorption in the UV region and $\pi \rightarrow \pi^*$ transition with absorption in the UV-Vis region. The area of the molecule where the electronic transitions happen is called chromophore (Anderson *et al*., 2004). The principle of this technique lies to the fact that molecules containing π-electrons or non-bonding electrons (σ-electrons) can absorb the energy in the form of ultraviolet or visible light to excite these electrons to higher anti-bonding molecular orbitals. The more easily excited the electrons (i.e., lower energy gap between the HOMO and the LUMO) the longer the wavelength of light that absorbs (Kalsi, 1995).

A spectrophotometer is a device which compares the intensity of the transmitted light with that of the incident light. The modern ultra violet-visible spectrometers consist

of light source, monochromator to separate different wavelengths of light, detector, amplifier and the recording devices. The most suitable sources of light is tungsten filament (300-2500 nm). Recently, light emitting diodes (LED) and xenon arc lamps are used for visible wavelengths. Deuterium arc lamp is used for ultraviolet region (190 − 400 nm). Usually a photodiode or a charge-coupled device (CCD) is a detector. Photodiodes with monochromators permit only the light of a single wavelength reaches the detector. Diffraction gratings are used with CCDs, which collects light of different wavelengths on different pixels. In the present investigation, UV-Visible Spectrophotometer (Thermo Fisher Evolution, Model-220, UK) was used to study the degradation kinetics of organic compounds measuring the change in concentration at a fixed wavelength.

2.1.4. Total Organic Carbon Analyser (TOCA)

The TOC Analyzer (*Shimadzu, Japan; Model: TOC-VCPH/CPN*) was fully employed to obtain the total organic carbon content data. The study enables to correlate the apparent mineralization of organic compounds present in water.

Total organic carbon (TOC) is an indirect measure of organic load present in water and measured as carbon content. A typical analysis of TOC measures both the total carbon (TC) present and the inorganic carbon (IC), the latter representing the content of dissolved carbon dioxide and carbonic acid salts. One approach used to measure TOC involves subtracting the measured inorganic carbon from the measured total carbon (TOC=TC–IC), which is the sum of organic carbon and inorganic carbon. The organic carbon is further classified as purgeable organic carbon (POC) and non-purgeable organic carbon (NPOC). NPOC is differentiated into dissolved organic carbon and particulate organic carbon. TOC analysis is performed by acidification of the sample to discharge carbon dioxide and

measuring it as inorganic carbon (IC), then oxidizing and measuring the remaining carbon called non-purgeable organic carbon (NPOC) (Clescerl *et al.*, 1999).

In order to analyse a sample, TOC analysers employ either differential or direct methods of measurements. In the differential method (TC–IC), both total carbon (TC) and total inorganic carbon (IC) is determined by separate measurements and TOC is calculated by subtracting IC from TC. This method is appropriate for samples in which IC is less than or of similar size to TOC. In direct method IC is removed from a sample by purging the acidified sample with a purified gas. TOC is then determined by oxidation. This method is also known as NPOC (non-purgeable organic carbon) due to the fact that POC (purgeable organic carbon) such as benzene, toluene, cyclohexane, and chloroform are partly removed from a sample by gas stripping. The direct method is suitable for surface water, ground water, and drinking water because of (in most cases) less TOC than IC and a negligible amount of POC present in these samples.

TOC measurement involves three stages, *viz*., acidification, oxidation, detection and quantification. Acidification for the removal of the IC and POC gases, oxidation of organic carbon in a sample, detection and quantification of the oxidized carbon (CO_2). All TOC analysers today offered to employ either combustion or low-temperature oxidation techniques. The purpose of the oxidation step is to convert the organics to carbon dioxide which is measured by a detector to provide TOC values. Modern TOC analysers achieve oxidation by low-temperature oxidation, ultraviolet irradiation, thermo-chemical (persulfate) oxidation, UV/persulfate irradiation, high temperature combustion. Out of all components of a TOC analyser, accurate detection and quantification are considered the most vital. Detection techniques include conductivity cells and non-dispersive infrared cells. Conductivity cells rely on aqueous CO_2 to raise acidity levels, causing the conductivity of

the solution to increase. TOC analysers that use a conductometric method is used for the measurement of carbon dioxide in the liquid phase. Non-dispersive infrared (NDIR) cell detection measures carbon dioxide in the gas phase. It is a direct method that specifically measures carbon dioxide by analysing the absorption spectrum in the IR region. Static pressurized concentration (SPC) is a new NDIR technology. In this method, the detector is pressurized. Once the gases contained in the detector reaches equilibrium, carbon dioxide concentration is analysed. A TOC analyser that utilizes this process measures all of the oxidation products contained in the sample in a single reading.

For the present investigation, the TOC analyser (Shimadzu, Japan; Model: TOC-VCPH/CPN) was employed and it is based on catalytic combustion at 680 ^{0}C, i.e., catalytic oxidation/NDIR method, developed by Shimadzu and the model is highly sensitive, capable of measuring parameters such as TC, IC, TOC, NPOC with measuring range and detection limit as TC: 0 to 25000 and IC: 0 to 30000 and 4 µg/L, respectively. TC combustion tube is filled with a platinum catalyst. Since this utilizes the simple principle of oxidation through heating and combustion, pre-treatment and post-treatment using oxidizing agents are not required, which enhances operability. The carbon dioxide generated by oxidation is detected using sensitive Non-dispersive infrared gas analyser (NDIR).

2.2. Methods

2.2.1. Preparation of Silver Nanoparticles

The synthesis of silver nanoparticles was conducted using a known chemical method as described elsewhere (Rashid *et al*., 2013). 0.1 mmol/L silver(I) sulphate and 0.2 mmol/L sodium borohydride solutions were prepared separately. 30 mL of sodium borohydride solution was then taken in a beaker and was kept in an ice bath. Under the stirred conditions the silver sulfate solution was introduced drop wise (about 1 drop per second) to the sodium borohydride solution. Silver(I) was turned to brighter yellow that confirms the reduction of Ag(I) to Ag(0) (equation (2.2.1)) and the formation of Ag(0) nanoparticles. The nanoparticles were stable for several minutes (Tiwari *et al*., 2018).

$$Ag_2SO_4 + 2NaBH_4 \rightarrow 2Ag(0) + H_2 + B_2H_6 + Na_2SO_4 \qquad \ldots(2.2.1)$$

2.2.2. Preparation of Gold Nanoparticles

The synthesis of gold nanoparticles was synthesized by using the known method as demonstrated elsewhere (McFarland *et al*., 2004). 0.1 mmol/L of gold(III) chloride solution was prepared in distilled water. 50 mL of gold(III) solution was taken into a conical flask and it was heated up to its boiling. Then, under the stirred condition 2mL 1% trisodium citrate solution was added quickly to the gold(III) solution. The solution was taken off from the hot plate. The gold(III) rapidly reduces to Au(0) and the color of the solution was quickly changed to deep red. The gold nanoparticles were formed and it was found stable for hours (Lalliansanga *et al*., 2018).

2.2.3. Preparation of Ag^0(NP)/Titania Sol Solutions

The nanostructured TiO_2 was obtained by following a template synthetic method. A polyethylene glycol was introduced to generate the titania network. Titanium isopropoxide (TISP) contained with 2.0 g of poly(ethylene glycol) was dissolved in acetyl-acetone (AcAc). Instantaneously, 10 mL of Ag^0(NP) solution (freshly prepared) was added to this solution. A solution mixture of ethanol (EtOH), acetic acid (AcOH) and distilled water (H_2O) was mixed slowly to the titanium isopropoxide solution. This initiated the hydrolysis and the condensation reaction. The mass ratios of titanium isopropoxide: acetyl acetone: ethanol: acetic acid: water was taken respectively as 2.8 g, 1.3 g, 18.4 g, 0.58 g and 2.25 g. The solution mixture was stirred rapidly for 2 hours followed by sonication for 30 minutes in a sonication bath. A clear sol was obtained which was then aged for *Ca.* 24 hours and employed in the preparation of thin films (Tiwari *et al*., 2018). Similarly, a non–template titania doped *in situ* with the Ag^0(NP) was carried out. This was proceeded with no addition of PEG solid. The two Ag^0(NP) titania sols were named as Ag^0(NP)/TiO_2(A1) and Ag^0(NP)/TiO_2(A2) for the non–template and template titania sols, respectively, (Tiwari *et al*., 2018).

2.2.4. Preparation of Au^0(NP)/Titania Sol Solutions

The polyethylene glycol was used as a template to generate titania network. Titanium(IV) isopropoxide 2.8 g and 1.3 g of acetylacetone were mixed together and 2 g of polyethylene glycol was dissolved in it. At the same time, freshly prepared 10 mL of Au(0) nanoparticle suspension was mixed. Further, a solution mixture of ethanol (18.4 g), acetic acid (0.58 g), and distilled water (2.25 g) was mixed slowly to the titanium isoproxide solution. The solution mixture was stirred vigorously for 2 hours followed by sonication for

30 minutes in a sonication bath. A clear sol Au^0(NP)/TiO_2 was obtained which was aged for *Ca*. 24 hours (Lalliansanga *et al*., 2018). Similarly, a non-template titania doped in situ with the Au^0(NP) was carried out with no addition of PEG solid. Therefore, the two Au^0(NP) titania sols were named as Au^0(NP)/TiO_2(B1) and Au^0(NP)/TiO_2(B2) for the non-template and template titania sols, respectively. These sols were then employed for the fabrication of respective thin films (Lalliansanga *et al*., 2018).

2.2.5. Fabrication of Ag^0/Au^0(NP)/TiO_2 Thin Films

Borosilicate circular glass disks having diameter 2.3 cm and thickness 0.5 mm were carefully cleaned by using 0.1 mol/L HNO_3. The glass disks were washed repeatedly by distilled water and dried in a drying oven (Tiwari *et al*., 2018; Lalliansanga *et al*., 2018). Then the borosilicate glass disks were dipped in vertical position into four different sol solutions Ag^0(NP)/TiO_2(A1), Ag^0(NP)/TiO_2(A2), Au^0(NP)/TiO_2(B1) and Au^0(NP)/TiO_2(B2) separately for 1 hour each. After one hour the glass disks were removed slowly and kept in an open atmosphere for 12 hours. The materials were immobilized on the glass surfaces. The disks were dried carefully at 100 ^{0}C for 1 hour, subsequently it was annealed at 500 ^{0}C for 3 hours in an electric furnace. The coatings were repeated for three times in order to obtain smooth films on the borosilicate glass surfaces. These thin films were then stored in a closed and dry container under dark condition (Tiwari *et al*., 2018; Lalliansanga *et al*., 2018).

2.2.6. Synthesis of Ce-Nanocomposite Materials

The cerium nitrate was reduced with the method described previously (Wan *et al*., 2016). The Cerium (III) nitrate (0.0868 g) 50 mL solution was prepared and taken in a three neck flat bottom flask. The solution mixture was kept under stirring using the magnetic stirrer. Solution was deoxygenated using the continuous flow of N_2. Further, 50 mL of

$NaBH_4$ (0.2 mol/L) solution was slowly added to the cerium nitrate solution under constant stirring. The solution mixture was stirred for 1 hour at room temperature in N_2 atmosphere. On the other hand, the TiO_2 was synthesized by sol-gel synthetic route. The polyethylene glycol was used as templating agent in sol gel process. Titanium(IV) isopropoxide (2.8 g) along with polyethylene glycol (2 g) was introduced and dissolved in acetyl-acetone (1.3 g). 20 mL of reduced cerium solution was immediately introduced. Further, ethanol (18.4 g), acetic acid (0.58 g) and distilled water (2.25 g) was added carefully into the titanium solution which was previously kept under stirring and under N_2 atmosphere. This mixture was stirred continuously for 2 hours at room temperature. Then it was sonicated for 30 minutes. A transparent sol solution of Ce^{3+}/TiO_2(C2) was prepared. The solution was aged *Ca*. 24 hours and then it was utilized for the coatings of glass disks. Similarly, the Ce^{3+}/TiO_2(C1) was prepared without introducing the templating agent polyethylene glycol.

2.2.7. Fabrication of Ce^{3+}/TiO_2 thin films

The borosilicate glass disks (2.3 cm radius and 0.05 cm thickness) were prepared prior to its fabrication as described previously (Tiwari *et al*., 2018). Further, the fabrication process was conducted using the sol solutions Ce^{3+}/TiO_2(C1) and Ce^{3+}/TiO_2(C2) as demonstrated previously (Tiwari *et al*., 2018). The two nanocomposite thin films fabricated were named as Ce^{3+}/TiO_2(C1) and Ce^{3+}/TiO_2(C2). The disks were stored safely in a silica desiccator and utilized as required for the photocatalytic operations.

2.2.8. Preparation of Nanostructured TiO_2 and Nanocomposite Powders

The nanostructured TiO_2 and the nanocomposites powders were acquired using the sol solution mixtures Ag^0(NP)/TiO_2(A1), Ag^0(NP)/TiO_2(A2), Au^0(NP)/TiO_2(B1), Au^0(NP)/TiO_2(B2), Ce^{3+}/TiO_2(C1) and Ce^{3+}/TiO_2(C2). Initially, the sol solutions were dried

at 105 ^{0}C and then annealed at 500 ^{0}C for 4 hours in an electric furnace to obtain the powders of Ag^0(NP)/TiO_2(A1), Ag^0(NP)/TiO_2(A2), Au^0(NP)/TiO_2(B1), Au^0(NP)/TiO_2(B2), Ce^{3+}/TiO_2(C1) and Ce^{3+}/TiO_2(C2). The solid powders were obtained by crushing each solid in a mortar. The powders were kept in the air tight polyethylene bottles for further applications.

2.2.9. Characterization of Thin Films

The XRD pattern of powders *viz*., Ag^0(NP)/TiO_2(A1), Ag^0(NP)/TiO_2(A2), Au^0(NP)/TiO_2(B1), Au^0(NP)/TiO_2(B2), Ce^{3+}/TiO_2(C1) and Ce^{3+}/TiO_2(C2) were characterized by several advanced analytical tools. The X-ray diffraction (XRD) data of thin films were recorded using the X-ray diffraction machine (i.e., PANalytical, Netherland; model X'Pert PRO MPD). It was recorded at the scan rate of 0.033 of 2θ illumination and having the generator settings 30mA, 40kV. The CuKα1 and CuKα2 radiations were employed having wavelengths of 1.5406 and 1.54443 Å.

The BET (Brunauer-Emmett-Teller) specific surface area along with the pore size and pore volumes were obtained using BET surface area analyser (Model ASAP, 2020; Protech Korea) based on the liquid N_2 adsorption and desorption isotherms. The physical conditions in the analysis was maintained as analytical bath temperature: 77.27 K; sample mass: 0.671 g; cold free and warm free spaces 48.83 and 16.50 cm^3, respectively. The BET data was collected using the powder samples Ag^0(NP)/TiO_2(A1), Ag^0(NP)/TiO_2(A2), Au^0(NP)/TiO_2(B1) and Au^0(NP)/TiO_2(B2).

The spectral analysis was conducted with the diffuse reflection spectra (DRS) of solids Ag^0(NP)/TiO_2(A1), Ag^0(NP)/TiO_2(A2), Au^0(NP)/TiO_2(B1) and Au^0(NP)/TiO_2(B2). The UV-VIS NIR spectrophotometer (DS104 Optical Spectrometer, Varian/Model Cary 5G,

USA) was employed to estimate the optical band gap of these solids. The equipment was employed using the diffuse reflectance spectra (DRA) having the absorbance conversion and F(R) conversion. The data was collected within 200 − 1000 nm wavelength at the bandwidth of 1 nm. The UV-Vis-NIR Reflectance spectra of Ce^{3+}/TiO_2(C1) and Ce^{3+}/TiO_2(C2) solids were obtained by using the UV-Vis-NIR Spectrophotometer (Model: Lambda 950 (Perkin Elmer) equipped with 100mm Int. Sphere (Diffuse Reflectance Accessory). Spectrum was recorded in the spectral range of 200 − 2,000 nm at a scan rate of 600nm/min. The measurements were performed at the Korea Basic Science Institute (KBSI), Daegu Center, South Korea.

2.2.10. Morphological Study of Thin Films

The thin films Ag^0(NP)/TiO_2(A1), Ag^0(NP)/TiO_2(A2), Au^0(NP)/TiO_2(B1), Au^0(NP)/TiO_2(B2), Ce^{3+}/TiO_2(C1) and Ce^{3+}/TiO_2(C2) surface morphologies were obtained by taking the SEM (Scanning electron microscope, machine Model FE–SEM SU–70, Hitachi, Japan) images of these thin films. The accelerating voltage, emission current and working distance was measured as 2000V, 9500 nA, and 13100 μm, respectively. The elemental mapping of materials was conducted with the EDX method attached with SEM machine.

Similarly, the solid materials of Ag^0(NP)/TiO_2(A1), Ag^0(NP)/TiO_2(A2), Au^0(NP)/TiO_2(B1), Au^0(NP)/TiO_2(B2), Ce^{3+}/TiO_2(C1) and Ce^{3+}/TiO_2(C2) were subjected for the TEM (Transmission electron microscopic) analysis using the TEM analyzer (Tecnai F20 Transmission Electron Microscope, FEI, USA). Similarly, the elemental mapping was conducted to obtained with the EDX method as attached with TEM machine.

Further, the topographical 3D images of these thin films were obtained by the AFM (Atomic Force Microscope) machine (XE-100 apparatus from Park Systems, Korea) having sharp tips (> 8 nm tip radius; PPP-NCHR type from Nanosensors™). The images were taken over the area of 10×10 μm^2 and the AFM images were recorded under the non-contact mode. The 3D data clearly enabled the pillar height of TiO_2 along with the surface roughness of thin films.

2.2.11. Batch Reactor Studies

2.2.11.1. Photo-catalytic degradation experiment

Stock solutions of each pollutant (100.0 mg/L) were prepared in a purified water. The solutions were sonicated for 10 minutes in a sonication bath which enabled better solubility. Further, the required experimental concentrations of pollutants were obtained by the successive dilution of each stock solution. The pH of pollutant solutions was obtained by the drop wise addition of HCl and NaOH (0.1 mol/L) solutions. The concentration dependence data was collected by varying each micropollutant/dye concentration from 0.5 to 15.0 mg/L, respectively.

In order to conduct the photolytic or photocatalytic operations, a self-assembled photo reactor was used. A black box (dimension 90 x 90 x 90 cm) was made by cardboard and wrapped with black paper. A borosilicate glass beaker (100 mL) was contained with 50.0 mL of pollutant solution and was placed inside the black box. Carefully, the thin film disks of Ag^0(NP)/TiO_2(A1), Ag^0(NP)/TiO_2(A2), Au^0(NP)/TiO_2(B1), Au^0(NP)/TiO_2(B2), Ce^{3+}/TiO_2(C1) and Ce^{3+}/TiO_2(C2) were placed horizontally at the bottom of the reactor vessel. An UV-A lamp (λ_{max}: 360 nm) was mounted *Ca.* 10 cm above to the pollutant solution. The radiations enter the photocatalyst through the pollutant solution that enabled

the photocatalytic oxidation of pollutants. The temperature of reactor was maintained to 25 ± 1^0C using a self-assembled water bath. The sample solution was taken out from the reactor at definite time intervals in order to analyze the pollutant concentrations using a UV-Vis spectrophotometer. A blank experiment was always performed using only UV-A irradiation without the thin film photocatalyst for comparison of photocatalytic degradation of these pollutants. The degradation efficiency of pollutant was obtained using the Equation (2.2.11.1):

$$Removal\ efficiency\ = \frac{C_i - C_f}{C_i} \times 100 \qquad \ldots\ (2.2.11.1)$$

where C_i and C_f are the concentrations of pollutants before and after the photolytic/or photocatalytic treatment.

2.2.11.2. Effect of pH

The pH of the solution is an important factor in the degradation/oxidation of pollutants since it deals with the mechanism involved on the surface of photocatalyst. The catalytic action is significantly influenced with the sorption of pollutants onto catalyst surface and sorption is highly dependent to the pH of the solution. Actually, the catalyst surface charge, the size of the catalyst aggregates in addition to the positions of conductance and valence bands are influenced with solution pH (Chong *et al.,* 2010). Therefore a pH dependence degradation of the pollutants was conducted varying the pH from pH 4.0 to 10.0 with a constant concentration of pollutant (1.0 mg/L). The results acquired were reported as the percent degradation of pollutant as a function of pH of the pollutant solution.

2.2.11.3. Effect of pollutant concentration

Since photocatalytic degradation of organic pollutants is surface phenomenon and organic molecules which adhere effectively to the surface of the photocatalyst are more susceptible to direct oxidation, which indicates initial pollutant concentration is an important factor (Tariq *et al.,* 2007). In general, the percentage degradation of organic pollutants decreased with increase in initial pollutant concentration at a fixed amount of photocatalyst. This is described on the basis that as initial pollutant concentration increases, more organic substances are adsorbed on to the surface of the TiO_2 catalyst, whereas less number of photons able to reach the catalyst surface and therefore less $^{\bullet}OH$ are formed, thus results in less degradation percentage (Wang *et al.,* 2008; Tariq *et al.,* 2007). Therefore, the effect of initial pollutant concentration on the photocatalytic degradation of organic compounds were studied from 0.5 mg/ L to 15.0 mg/L for pollutant at a constant solution pH 6.0. The results were reported as the percent degradation of pollutant as a function of different pollutant concentration after 2 hours irradiation treatment.

2.2.11.4. Degradation kinetics

The degradation kinetics study in wastewater treatment is a useful factor which offers important insights in the degradation pathways and mechanisms involved between the surface reactive species and the adsorbed organic pollutants. Thus, kinetic studies were conducted in order to deduce the efficiency of photocatalyst as well to obtain apparent rate constant values in the degradation of pollutants under the photocatalytic degradation. Further, the kinetics of the degradation was represented using the known pseudo–first order rate equation (eq. 2.2.11.4i):

$$r = -\frac{d[MP]}{dt} = k_{app}\left[k_{photolysis} + k_{photocatalysis}\right][MP] = k_{app}\,[MP] \qquad \ldots(2.2.11.4i)$$

where [MP] represents the concentration of micropollutant/dye and k_{app} is the pseudo-first-order rate constant. Integration of equation (2.2.11.4i) with the extreme conditions, i.e., at t=0 the [MP]=C_0, equation (2.2.11.4i) was reduced to equation (2.2.11.4ii):

$$LN\left(\frac{C_0}{C_t}\right) = k_{app} \cdot t \qquad \ldots(2.2.11.4ii)$$

Straight lines were drawn between the LN (C_o/C_t) against time `t`. The slope of the straight line gives apparent first order rate constant for the degradation of organic compounds.

2.2.11.5. Effect of interfering ions

Wastewater comprises different varieties of dissolved inorganic anions and cations which have either positive or negative effects on the rate of photocatalytic degradation of the parent pollutants (Sun *et al.,* 2006). In order to mimic the natural wastewater matrix, effort was made to measure the applicability of the thin films in the photocatalytic degradation of these pollutants in presence of several interfering ions including sodium chloride, sodium nitrate, cadmium nitrate, copper sulphate, zinc chloride, sodium nitrite, glycine, oxalic acid and EDTA. Taking a ratio between pollutant and interfering ions as 1 : 5. The samples were irradiated for 2 hours at pH 6.0. The percent removal of micropollutant/dye was presented as a function of interfering ions.

2.2.11.6. Mineralization study

The effectiveness of photocatalytic treatment process rely on the degree of mineralization of pollutants which assesses the mineralization of dissolved organic compounds from the reaction media. Therefore, the amount of mineralization followed by

the photocatalytic treatment process was determined by the NPOC (non-purgeable organic carbon) removal. The NPOC values were obtained at varied initial pollutant concentrations (0.5 – 15.0 mg/L) of pollutant at a constant solution pH 6.0 or varying solution pH at a fixed pollutant concentration (1.0 mg/L). The final data obtained was presented as percent NPOC removal as a function of solution pH or pollutant concentration.

2.2.12. Reusability Test of The Thin Films

The reusability of the thin films in photocatalytic processes is an important characteristic since it plays substantially in lowering the operational cost of the process. This shows the utility of heterogeneous thin film catalyst for repeated operations which further enhances the cost of the operation and makes the operation sustainable. Therefore, the reusability tests for the thin films Ag^0(NP)/TiO_2(A2), Au^0(NP)/TiO_2(B2) and Ce^{3+}/TiO_2(C2) were conducted for the micropollutant/dye for six repeated cycles with a fixed initial concentration of pollutant (5.0 mg/L) at pH 6.0 for 2 hours irradiation. After each successive experiment the catalyst thin film was washed with distilled water and dried in an electric oven at 100 ^{0}C for 1 hour. Results were presented as percentage degradation of pollutants as a function of repeated cycle.

3. RESULTS AND DISCUSSIONS

3.1. Characterization of Samples

The materials synthesized *viz.*, Ag^0(NP)/TiO_2(A1), Ag^0(NP)/TiO_2(A2), Au^0(NP)/TiO_2(B1), Au^0(NP)/TiO_2(B2), Ce^{3+}/TiO_2(C1) and Ce^{3+}/TiO_2(C2) were characterized extensively using the advanced analytical methods *viz.*, X-ray diffraction, X-ray photoelectron spectroscopy, BET Surface area diffuse reflectance spectroscopy analyses. Surface imaging was conducted with the SEM, TEM/EDX and AFM analyses.

3.1.1. X-ray Diffraction (XRD) Analysis

The X-ray diffraction data for thin film samples Ag^0(NP)/TiO_2(A1) and Ag^0(NP)/TiO_2(A2) was obtained and graphically shown in Figure 3.1.1(a). The diffraction pattern clearly showed that the thin films were predominantly found to be amorphous in nature. This was possibly due to the fact that these thin films were annealed only at moderate temperature, i.e., 500 ^{0}C. However, characteristic but distorted peak was observed (for both the samples) at the 2θ value of 25.39 which indicated the presence of anatase phase of TiO_2.

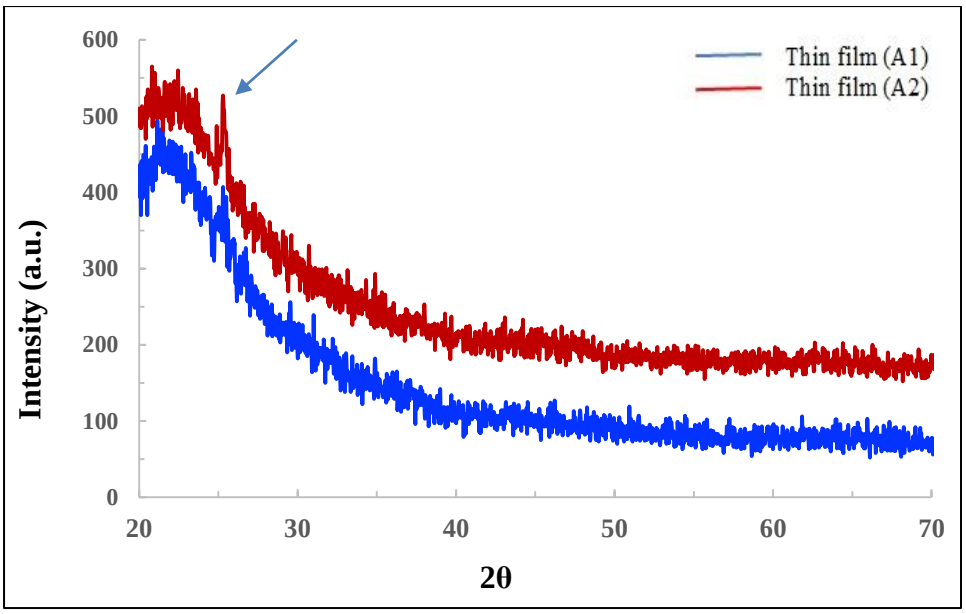

Figure 3.1.1(a): X-ray diffraction pattern of thin film materials A1: Ag^0(NP)/TiO_2(A1) and A2: Ag^0(NP)/TiO_2(A2) [Tiwari *et al*., (2019a)].

The powder of nanocomposite materials *viz*., Ag^0(NP)/TiO_2(A1) and Ag^0(NP)/TiO_2(A2) were then annealed at 800 ^{0}C and XRD data was again obtained. XRD pattern was shown in Figure 3.1.1(b). The TiO_2 annealed at this temperature showed a good crystalline structure. But, it was predominantly converted into the rutile phase. In order to reveal the silver nanoparticles, the low intensity was further resolved for the nanocomposite material Ag^0(NP)/TiO_2(A1). It was interesting to note that (Figure 3.1.1(b) (Inset)) the clear reflections were observed at the 2θ values of 38.27, 44.37, 64.55, which were characteristic diffraction peaks of the silver nanoparticles (Tiwari *et al*., 2019a; Seaton, 1991).

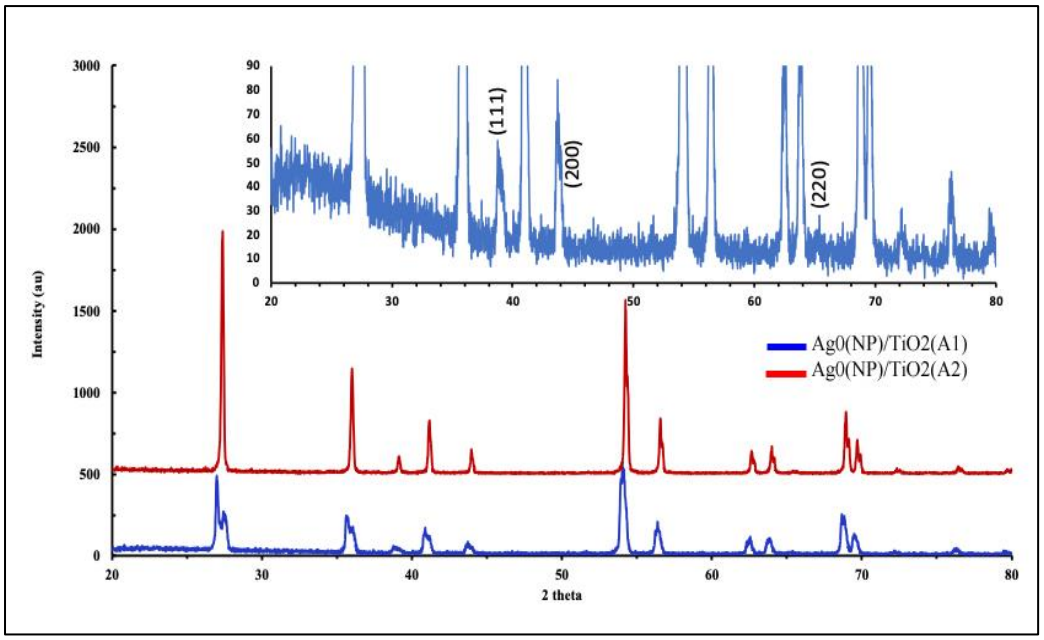

Figure 3.1.1(b): X–ray diffraction pattern of Ag^0(NP)/TiO_2(A1) and Ag^0(NP)/TiO_2(A2) nanocomposite materials annealed at 800 ^{0}C. [Inset: nanocomposite Ag^0(NP)/TiO_2(A1)] [Tiwari *et al*., (2019a)].

Similarly, the X-ray diffraction data for the thin film samples, *viz*., Au^0(NP)/TiO_2(B1) and Au^0(NP)/TiO_2(B2) were obtained and the result was shown in Figure 3.1.1(c). Figure clearly showed that the thin film samples were predominantly amorphous in nature. It was, perhaps, due to the fact that these solids were annealed at moderate temperature, i.e., 500 ^{0}C. However, characteristic but distorted peak was observed (for both the thin film samples) around the 2θ value of 25.5 which indicated that TiO_2 was having the anatase mineral phase. Further, the powder samples were annealed at 800 ^{0}C and the results were shown in Figure 3.1.1(d). The TiO_2 annealed at this temperature possessed a good crystalline structure. However, it was converted in to rutile phase. In order to reveal the gold nanoparticles, the intensity was further resolved using the Au^0(NP)/TiO_2(B1) nanocomposite and it was interesting to note that (Figure 3.1.1(d) (Inset)), a clear reflections were observed

at the 2θ values of 39.27, 44.25, 64.29 which are characteristic diffraction peaks of the gold nanoparticles.

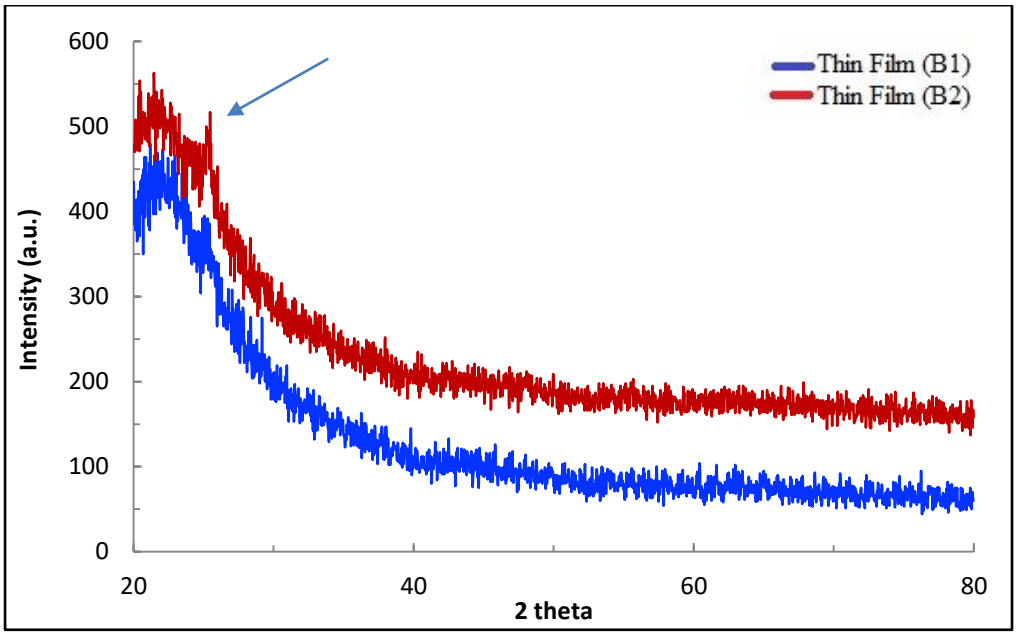

Figure 3.1.1(c): X–ray diffraction spectra of thin film samples B1: Au^0(NP)/TiO_2(B1) and B2: Au^0(NP)/TiO_2(B2) [Tiwari *et al*., (2019b)].

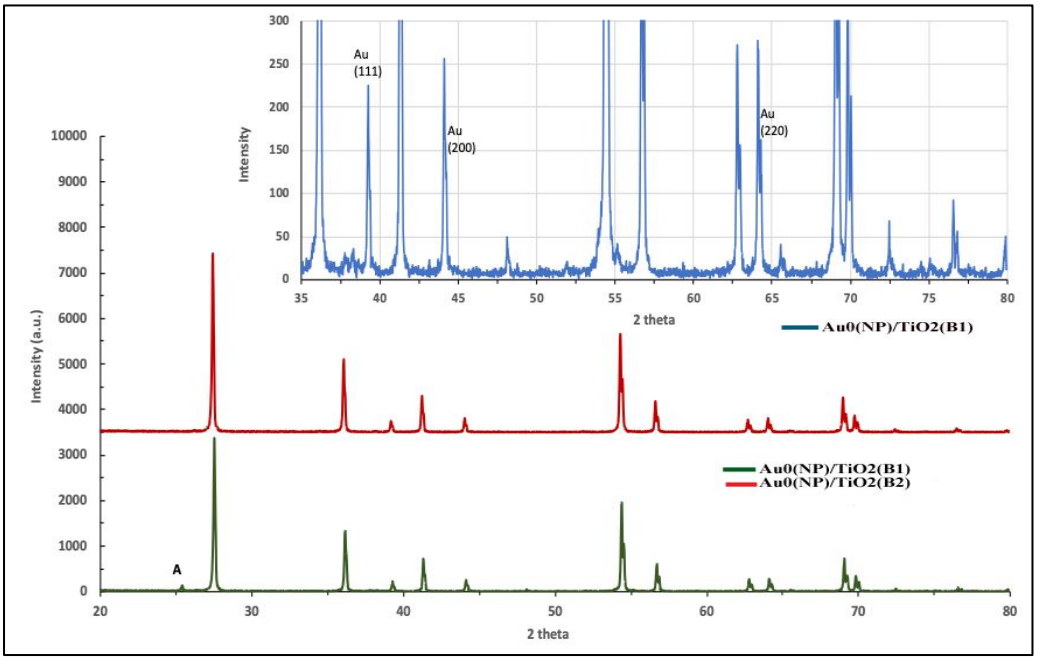

Figure 3.1.1(d): X-ray diffraction pattern of Au^0(NP)/TiO_2(B1) and Au^0(NP)/TiO_2(B2) nanocomposite materials annealed at 800 ^{0}C. [Inset: nanocomposite Au^0(NP)/TiO_2(B1)] [Lalliansanga *et al*., (2019)].

Further, Ce (cerium) photocatalyst thin films *viz*., Ce^{3+}/TiO_2(C1) and Ce^{3+}/TiO_2(C2) were subjected for the X-ray diffraction analysis and the X-ray pattern was displayed in Figure 3.1.1(e). The X-ray pattern indicated that both the samples possessed with fairly good crystalline phase. The X-ray diffraction pattern was further expanded to identify the diffraction peaks and shown the results in Figure 3.1.1(e) (Inset). The diffraction peaks were well matched with the anatase mineral phase of the titanium dioxide (JCPDS No.: 21-1272). Moreover, both the samples Ce^{3+}/TiO_2(C1) and Ce^{3+}/TiO_2(C2) were possessed with similar mineral phase. On the other hand, the Ce particles were not visible with the XRD data, it was perhaps, due to very low loading of cerium with the material.

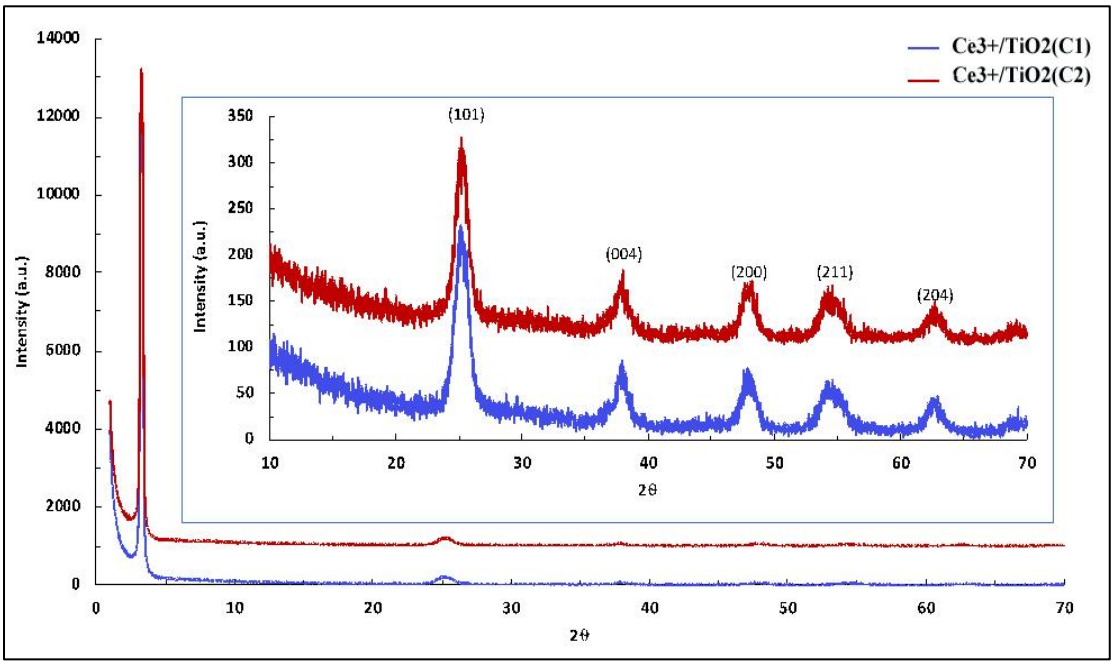

Figure 3.1.1(e): X-ray diffraction pattern of thin film samples Ce^{3+}/TiO_2(C1) and Ce^{3+}/TiO_2(C2).

Since the Ce (Cerium) was not visible with the XRD data therefore, the samples were again analysed with the X-ray photoelectron analysis. The XPS spectra was recorded for the Ce^{3+}/TiO_2(C2) solid and the results were shown in Figure 3.1.1(f)(i). It was evident from the spectrum that the elements Ti (titanium), O (oxygen), and Ce (cerium) were present

in the sample since the corresponding peaks were observed in the spectrum. Further, the Ti, O and Ce spectra were resolved to identify the specific photoelectron peaks with the corresponding energies and represented in Figure 3.1.1(f)(ii), Figure 3.1.1(f)(iii) and Figure 3.1.1(f)(iv), respectively, for the Ti, O and Ce elements. The Ti spectrum showed that 2p peak was splitted into the binding energy levels $2p^{3/2}$ and $2p^{1/2}$ corresponding to the binding energy values 458.18 and 463.98 eV (*cf.* Figure 3.1.1(f)(ii). These XPS peaks corresponded to the Ti^{4+}, i.e., fully oxidized state. It was previously reported that Ti^{4+} $2p^{3/2}$ and $2p^{1/2}$ were occurred respectively at the binding energy values of 458.6 and 464.5 eV (Xiu *et al*., 2018). Slightly lower binding energy values for the 2p values possibly due to the presence of surrounding atoms bonded with the Ti. Similarly, the O1s peak was occurred at the binding energy of 529.68 eV (*cf.* Figure 3.1.1(f)(iii). The single peak of oxygen demonstrated that oxygen was bound with the Ti and forming the Ti–O–Ti linkage (Xiu *et al*., 2018). Previously, it was noted that the O photopeak was observed at the binding energy of 529.8 due to the presence of TiO_2 (Fiorenza *et al*., 2018). The Ce XPS spectra showed the doublet 3d photo-peaks at the binding energies of 887.88 and 881.48 eV for $3d^{5/2}$. Whereas, it was observed at the binding energies of 904.38 and 899.48 eV for the $3d^{3/2}$ states. The presence of Ce^{4+} showed a dominant photo peak at the binding energy 916.5 eV (Eloirdi *et al*., 2018). This indicates that Ce was not present with its +4 oxidation state. Moreover, the Ce^{3+} possessed with the photo peaks around the binding energies of 880.2, 885.0, 899.0, and 904.2 eV (Xiu *et al*., 2018). This showed that the solid was possibly present to its Ce^{3+}. Additionally, the formation of Ce–O–Ce was also not observed since no characteristic photo peak was obtained around 531.4 for O1s (Xiu *et al*., 2018).

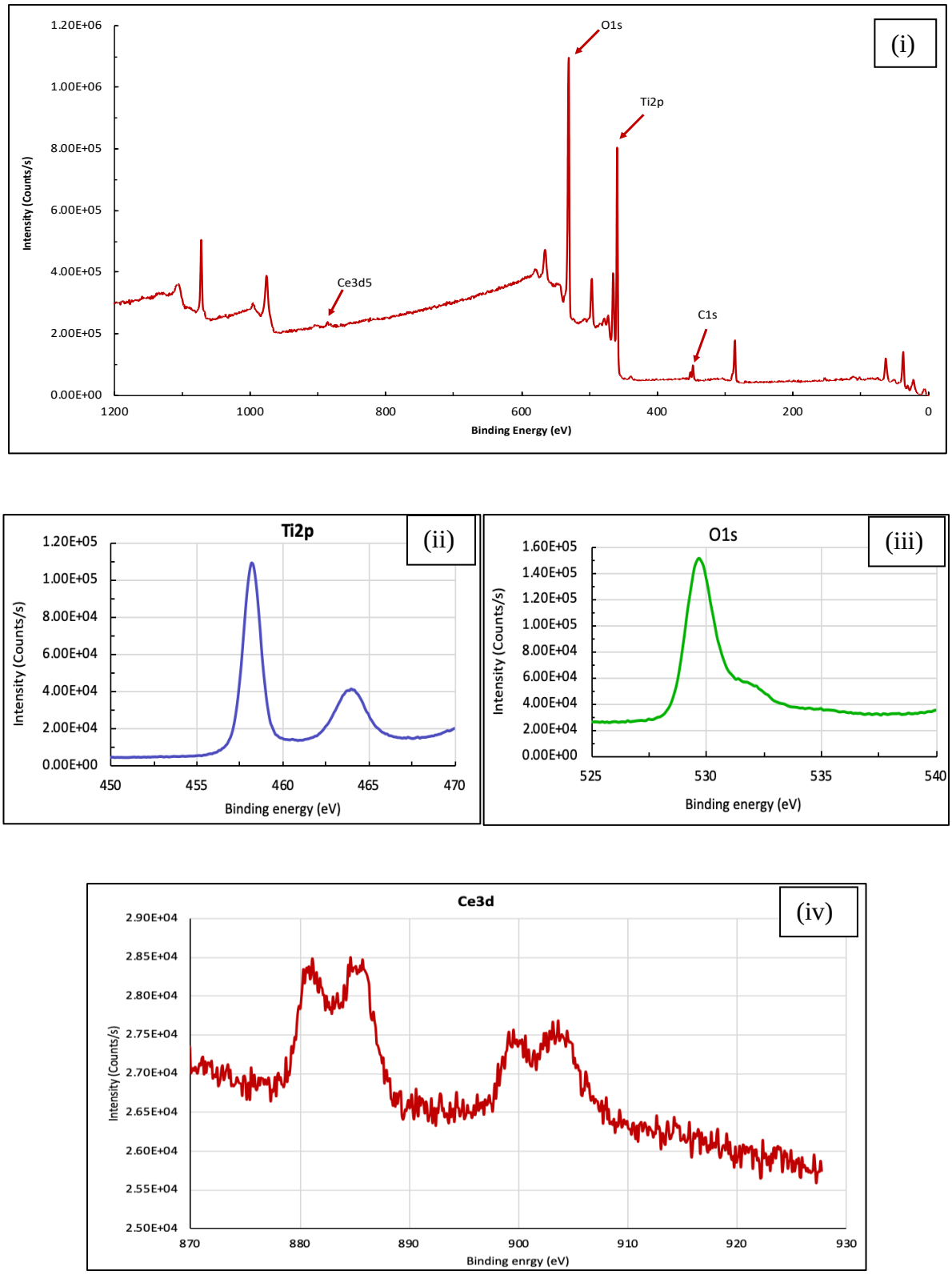

Figure 3.1.1(f): X-ray photoelectron spectra of (i) Ce^{3+}/TiO_2(C2) powder (ii) Ti2p (iii) O1s and (iv) Ce3d.

3.1.2. BET Analysis

The BET analysis of nanocomposite materials *viz.*, Ag^0(NP)/TiO_2(A1) and Ag^0(NP)/TiO_2(A2) were measured by the N_2 adsorption/desorption method and the curves were illustrated in Figure 3.1.2(a) for both the solids. Adsorption/desorption isotherm curves were found to be of H2 type hysteresis loop that confirmed the pores were having narrow mouths with uniform channel-like pore network (Seaton, 1991). Besides, the solid was contained with particles that crossed by cylindrical channels having non-uniform size and shapes (Leofanti *et al*., 1998). The pore size, pore volume and the specific surface area of these two solids were given in Table 3.1.2(a). The Figure clearly revealed that both the samples, i.e., Ag^0(NP)/TiO_2(A1) and Ag^0(NP)/TiO_2(A2) were contained with meso-porosity and the specific surface area of Ag^0(NP)/TiO_2(A2) solid was significantly reduced when it was synthesized with template method. It suggested that using PEG as template material generated a dense network of TiO_2. Besides, pore volume was also decreased for the sample Ag^0(NP)/TiO_2(A2) compared with the non-template synthesized Ag^0(NP)/TiO_2(A1) solid. Interestingly, both the solid samples were possessed with almost identical pore sizes. Other studies showed a type II N_2 adsorption/desorption isotherm was obtained for the magnetic AC (activated carbon)/CeO_2 nanocomposite possessed with micro and meso-pores. Moreover, the specific surface area of the solid was estimated to be 423 m^2 (Tuzen *et al*., 2018). Similarly, the magnetic palygorskite modified with polyamide (MPGP) material was produced and which possessed micro-porosity having surface area of 380 m^2/g (Saleh *et al*., 2018).

Table 3.1.2(a): Pore size, pore volume and BET specific surface area of the $Ag^0(NP)/TiO_2(A1)$ and $Ag^0(NP)/TiO_2(A2)$ solid samples [Tiwari *et al*., 2019a].

Sample	Adsorption Pore Size (nm)	Adsorption Pore Volume (cm^3/g)	BET Specific Surface Area (m^2/g)
$Ag^0(NP)/TiO_2(A1)$	5.613	0.0695	49.55
$Ag^0(NP)/TiO_2(A2)$	5.670	0.0170	12.02

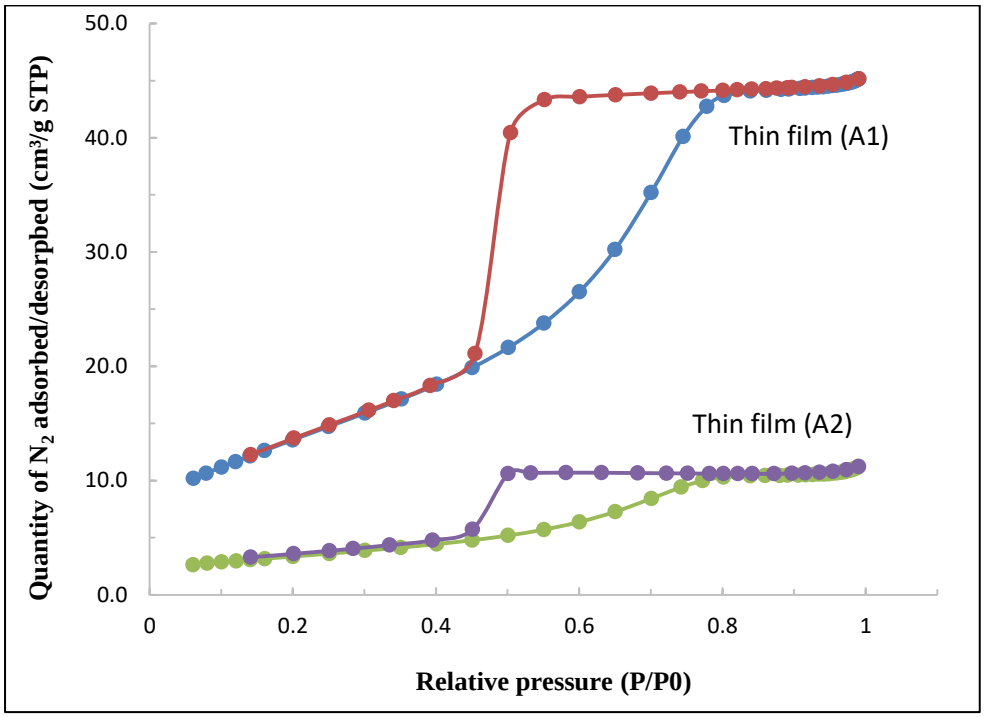

Figure 3.1.2(a): BET adsorption/desorption isotherms for the A1: $Ag^0(NP)/TiO_2(A1)$ and A2: $Ag^0(NP)/TiO_2(A2)$ solid samples [Tiwari *et al*., (2018)].

Similarly, BET analysis of $Au^0(NP)/TiO_2(B1)$ and $Au^0(NP)/TiO_2(B2)$ were conducted by the N_2 adsorption/desorption method and the curves were shown in Figures 3.1.2(b)(i) and 3.1.2(b)(ii). Adsorption/desorption isotherm curves were found to be of H2 type hysteresis loop which disclosed that the uniform-channel like pores were having narrow mouths (Seaton, 1991; Mendioroz *et al*., 1987). Further, the pore size, pore volume

and the specific surface area of these two solids were shown in Table 3.1.2(b). It was clearly revealed that both the samples, i.e., Au^0(NP)/TiO_2(B1) and Au^0(NP)/TiO_2(B2) were possessed with meso-porosity and the specific surface area of the sample Au^0(NP/TiO_2(B2) was significantly decreased while prepared with template synthesis. It was suggested that a dense network of TiO_2 was generated using the template material. Moreover, pore volume was also decreased for the sample Au^0(NP)/TiO_2(B2) comparing to the non-template synthesis of Au^0(NP)/TiO_2(B1) material. Further, it was exciting to note that both the solid samples were possessed with almost identical pore sizes.

Table 3.1.2(b): Pore size, pore volume and BET specific surface area of the Au^0(NP)/TiO_2(B1) and Au^0(NP)/TiO_2(B2) solid samples [Tiwari *et al*., 2019b)].

Samples	**Adsorption Pore Size (nm)**	**Adsorption Pore Volume (cm^3/g)**	**BET Specific Surface Area (m^2/g)**
Au^0(NP)/TiO_2(B1)	5.270	0.0689	41.47
Au^0(NP)/TiO_2(B2)	5.599	0.0344	19.91

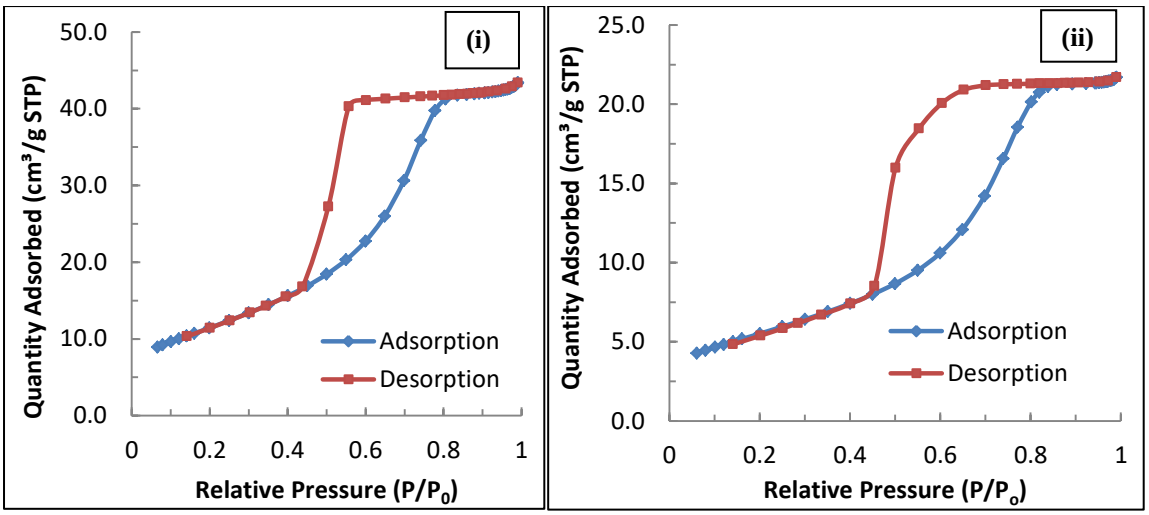

Figure 3.1.2(b): Nitrogen adsorption-desorption isotherms (i) Au^0(NP)/TiO_2(B1) and (ii) Au^0(NP)/TiO_2(B2) solids [Tiwari *et al*., (2019b)].

3.1.3. Diffuse Reflectance Spectroscopic Analysis

The diffuse reflectance spectroscopy analysis was introduced to estimate the band gap of the solids. The Kubelka Munk theory was used and elaborated with the Tauc mathematical equation which was used in the non-linear form of equation (3.1.3):

$$\alpha h\nu = A\left(h\nu - E_g\right)^n \qquad \ldots(3.1.3)$$

The terms 'α' and 'h' represent the absorption coefficient and Planck's constant (J.s), respectively. Similarly, 'A' is the absorption constant, 'ν' is frequency of light, i.e., (C/λ; C: velocity of light) (s^{-1}) and 'E_g' is the band gap energy (eV). The exponent 'n' is dependent to the type of possible electronic transitions having the value 2 for an indirect allowed transition, 3 for indirect forbidden transitions. Similarly, 1/2 for a direct allowed and 3/2 for a direct forbidden transitions (Beshkar *et al*., 2017). The calculations of band gap was obtained using the n=2 for an indirect allowed transition. The curves were drawn between the hν against the $(\alpha h\nu)^2$. The DRS spectra was shown in Figure 3.1.3(a). The Figure clearly revealed that the reflectance break was greatly shifted to the higher wavelength for

Ag^0(NP)/TiO_2(A1) and Ag^0(NP)/TiO_2(A2) solids comparing to bare TiO_2 (with PEG). The reflectance spectra was shown in Figure 3.1.3(a) (Inset). The intermediate band gap energy (E_g) was estimated by extrapolating the flat region of the curve to its zero value. The band gap energies were found to be 3.12, 2.88 and 2.89 eV, respectively, for bare TiO_2, Ag^0(NP)/TiO_2(A1) and Ag^0(NP)/TiO_2(A2) solids. The silver nanoparticles doping greatly decreased the band gap energy of these solids. Similar results were obtained in the copper chromite nanostructured material prepared hydrothermally and shown the E_g value 3.38 eV (Zinatloo–Ajabsir *et al*., 2018). On the other hand the nanostructured $Nd_2Sn_2O_7$ was obtained using the pomegranate juice at low temperature. The solid showed the band gap of 2.8 eV and was efficiently employed as visible light driven photocatalyst (Moyo *et al*., (2015).

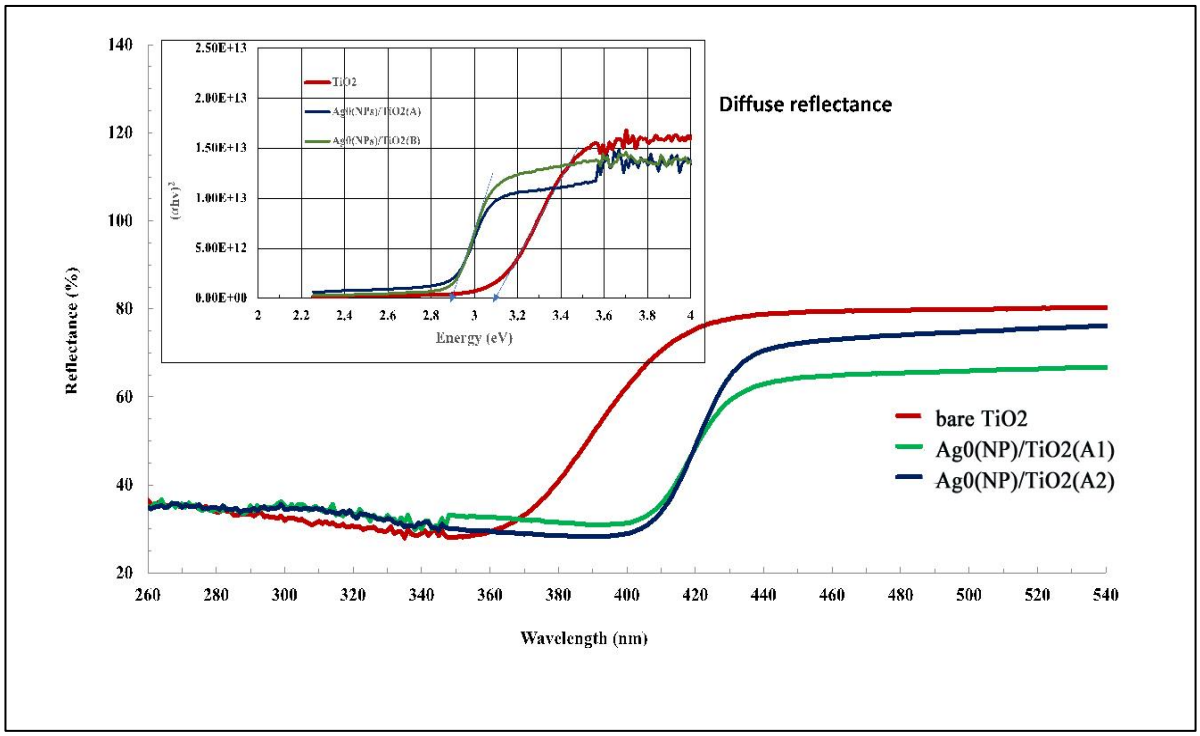

Figure 3.1.3(a): Diffuse reflectance spectra of bare TiO_2, Ag^0(NP)/TiO_2(A1) and Ag^0(NP)/TiO_2(A2) solids. [Inset: The intermediate E_g determination of bare TiO_2, Ag^0(NP)/TiO_2(A1) and Ag^0(NP)/TiO_2(A2) solids] [Tiwari *et al*., (2019a)].

Further, the DRS spectra for the samples bare TiO_2 (with PEG), Au^0(NP)/TiO_2(B1) and Au^0(NP)/TiO_2(B2) was shown in Figure 3.1.3(b). It was evident from the Figure that the reflectance break was greatly shifted to the higher wavelength for Au^0(NP)/TiO_2(B1) or Au^0(NP)/TiO_2(B2) solids compared to the bare TiO_2. Further, the intermediate band gap energy (E_g) was estimated by extrapolating the flat region of the curve to its zero value (Figure 3.1.3(b) (Inset)). The band gap energies were found to be 3.12, 2.86 and 2.87 eV, respectively, for the bare TiO_2, Au^0(NP)/TiO_2(B1) and Au^0(NP)/TiO_2(B2) solids. Hence, the gold nanoparticles doping greatly decreased the band gap energy of these solids.

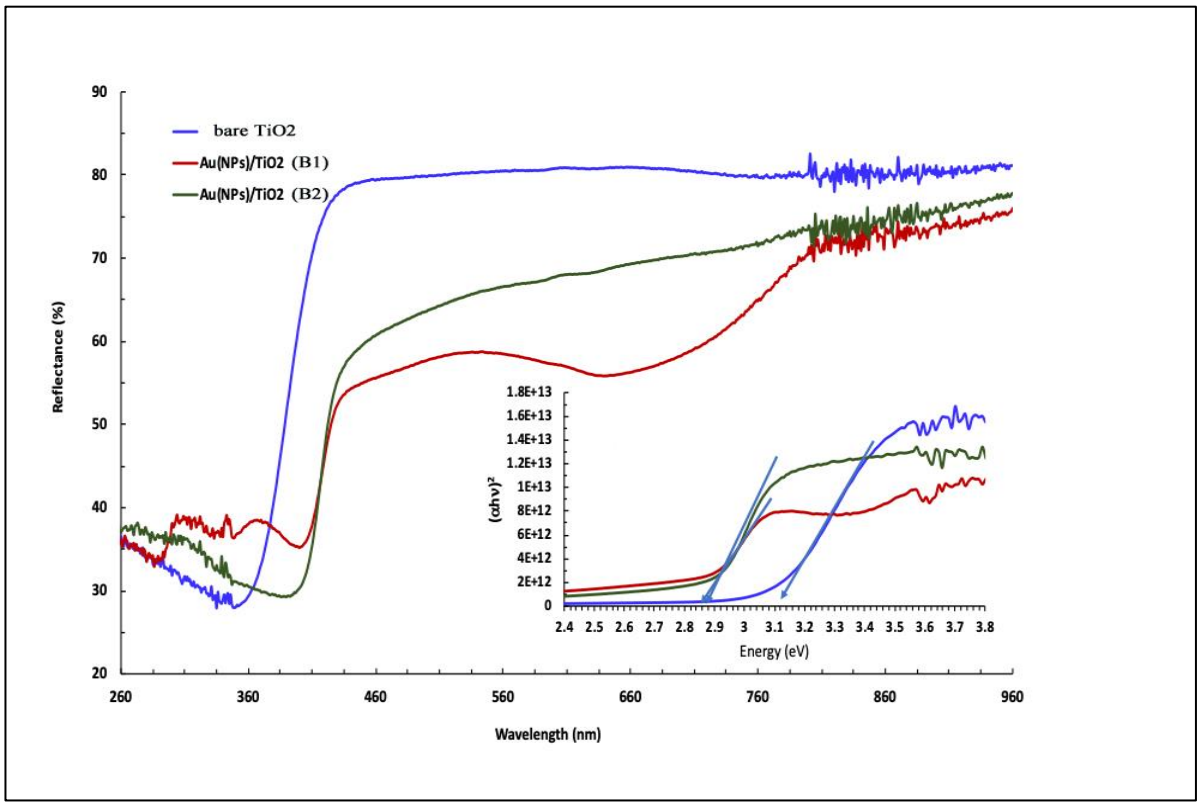

Figure 3.1.3(b): Diffuse reflectance spectra of bare TiO_2, Au^0(NP)/TiO_2(B1) and Au^0(NP)/TiO_2(B2) solids. [Inset: The intermediate E_g determination of TiO_2, Au^0(NP)/TiO_2(B1) and Au^0(NP)/TiO_2(B2) solids] [Lalliansanga *et al.*, (2019)].

3.1.4. SEM Analysis

The SEM images of the two nanocomposite materials *viz*., Ag^0(NP)/TiO_2(A1) and Ag^0(NP)/TiO_2(A2) were shown in Figures 3.1.4(i)(a) and 3.1.4(i)(b). The Figures revealed that TiO_2 particles were orderly distributed over the borosilicate surfaces. As a result, an uniform film consisting of Ag^0(NP)/TiO_2(A1) or Ag^0(NP)/TiO_2(A2) was formed. It was noted that Ag^0(NP)/TiO_2(A1) film was relatively smooth and no remarkable cracks were observed on the surface. Likewise, thin film Ag^0(NP)/TiO_2(A2) showed small sized particles of titanium dioxide distributed unifirmly onto the substrate surface. The heterogeneous structure of thin films hardly showed cracks onto the surface. The distribution reflections due to the silver nanoparticles were apparently observed by SEM images.

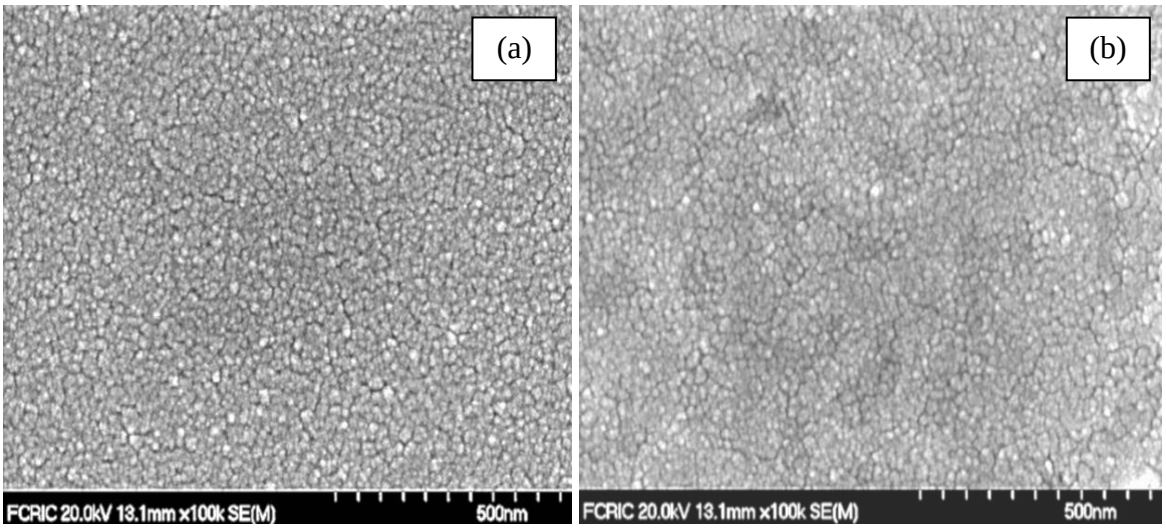

Figure 3.1.4(i): Scanning electron microscopic images of (a) Ag^0(NP)/TiO_2(A1) and (b) Ag^0(NP)/TiO_2(A2) thin films [Tiwari *et al*., (2019a)].

The SEM images of the two nanocomposites *viz.*, Au^0(NP)/TiO_2(B1) and Ag^0(NP)/TiO_2(B2) were shown in Figures 3.1.4(ii)(a) and 3.1.4(ii)(b). The TiO_2 was found to be slightly aggregated and gold was uniformly dispersed within the TiO_2 surface (Tahir *et*

al., 2016). On the other hand the carbon nanotube/silica or activated carbon/silica heterogeneous nanocomposites were obtained by facile method. Further, the SEM images of these solids showed the nanoparticles of silica were evenly distributed within the composite material (Saleh, 2015).

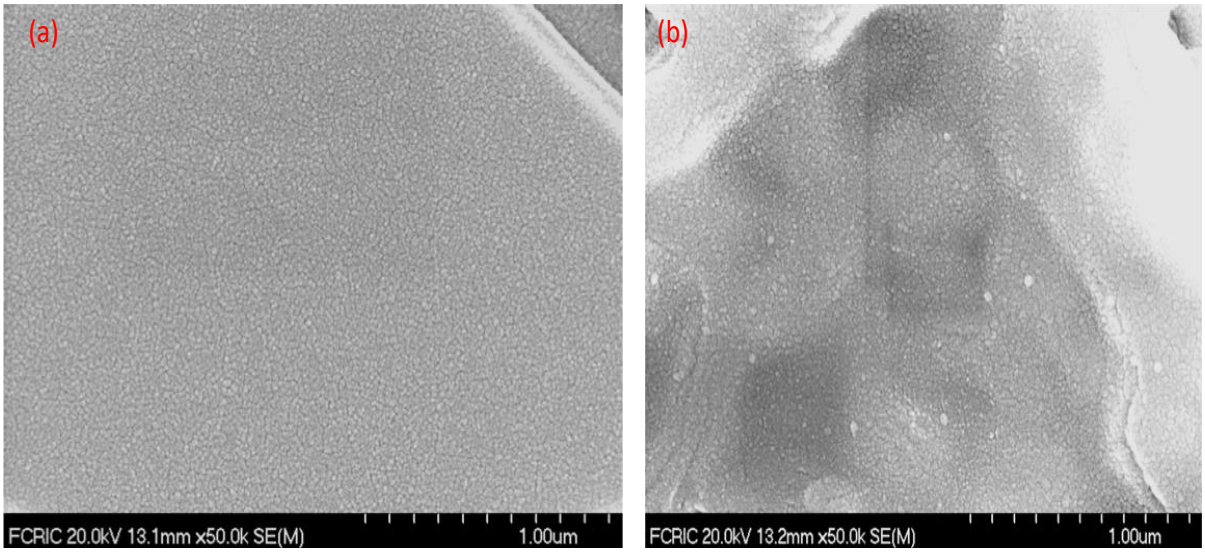

Figure 3.1.4(ii): Scanning electron microscopic images of (a) Au^0(NP)/TiO_2(B1) and Au^0(NP)/TiO_2(B2) thin films [Lalliansanga *et al*., (2019)].

Further, the field emission scanning electron microscopic (FE-SEM) images were obtained for the nanocomposite material thin films *viz*., Ce^{3+}/TiO_2(C1) and Ce^{3+}/TiO_2(C2) and shown in Figures 3.1.4(iii)(a) and 3.1.4(iii)(b). The Figure clearly indicated that the surface of the borosilicate glass disk was fully covered with titanium dioxide. A small sized particles of titanium dioxide was formed on the surface. Further, the sample Ce^{3+}/TiO_2(C1) thin film showed that the titanium dioxide particles were clustered or amalgamated at places whereas the templated synthesized titanium dioxide Ce^{3+}/TiO_2(C2) possessed more evenly distributed titanium dioxide particles on the surface. The cracks were observed on both the thin films. However, cracks were more pronounced on the surface of Ce^{3+}/TiO_2(C1) thin

film. It was interesting to observe that both the thin films were possessed with mesoporosity on its surface. But, it was hard to identify the cerium nanoparticles on the surface of these thin films. It was perhaps due to the low loading of the cerium compared to the bulk titanium dioxide. It was reported previously that the Ti^{3+}–TiO_2/Ce^{3+}–CeO_2 material possessed with thin nanosheet-like structure. Further, because of the monodisperse/ ultraminiature CeO_2 nanoparticles with ultra-thin TiO_2 nanosheets, the CeO_2 nanoparticles were not visible by the SEM images (Xiu *et al*., 2018).

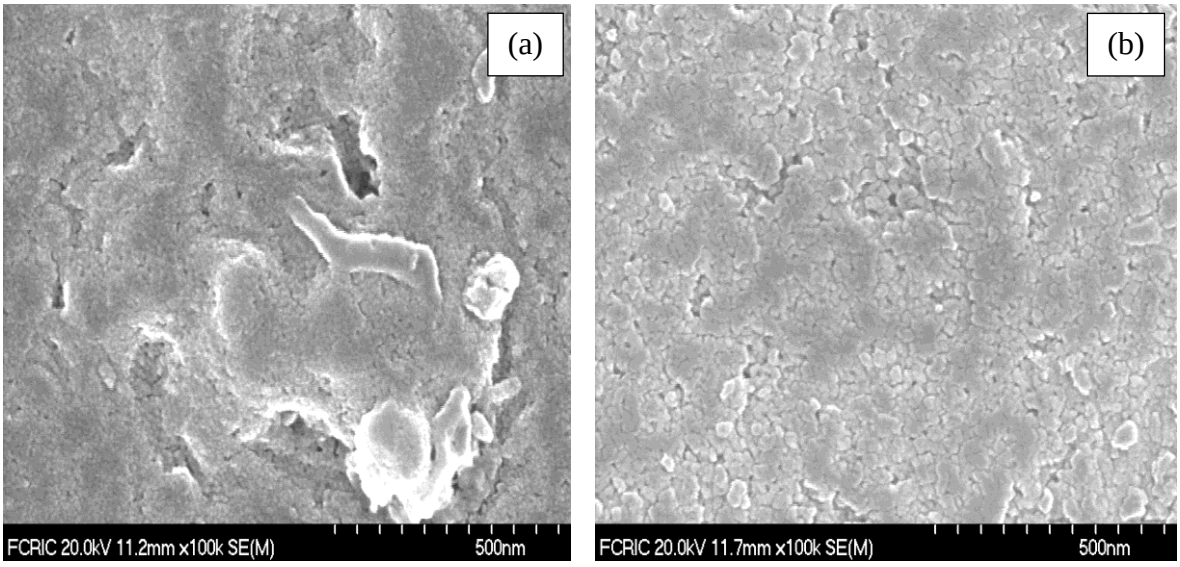

Figure 3.1.4(iii): FE-SEM images of (a) Ce^{3+}/TiO_2(C1) and (b) Ce^{3+}/TiO_2(C2) thin film materials.

3.1.5. Transmission Electron Microscopic (TEM) Analysis

TEM images of the two nanocomposite materials *viz*., Ag^0(NP)/TiO_2(A1) and Ag^0(NP)/TiO_2(A2) were shown in Figures 3.1.5(i)(a) and 3.1.5(i)(b). TEM images showed that Ag–nanoparticles were evenly distributed within the TiO_2 structure. The particle sizes were ranged from 10 – 15 nm in both the samples, i.e., Ag^0(NP)/TiO_2(A1) and Ag^0(NP)/TiO_2(A2) solids. It was remarkable to note that particles of TiO_2 in sample

Ag^0(NP)/TiO_2(A2) was aggregated at places and forming relatively bigger size particles. Besides, the Ag-nanoparticles were spread within the titania network. It was further observed that the Ag-nanoparticles were found relatively at an increased content with the template synthesized solid Ag^0(NP)/TiO_2(A2) than the Ag^0(NP)/TiO_2(A1) solid. The interplanar distance of the Ag-nanoparticles were estimated to be 0.20 and 0.17 nm for the Ag^0(NP)/TiO_2(A1) and Ag^0(NP)/TiO_2(A2) solids, respectively, [Tiwari *et al*., (2018)].

TEM/EDX mapping for the elements of Ti (Titanium), O (Oxygen) and Ag (Silver) in the nanocomposite materials for the Ag^0(NP)/TiO_2(A1) and Ag^0(NP)/TiO_2(A2) were shown in Figures 3.1.5(ii)(a) and 3.1.5(ii)(b). The O atoms were intimately attached with Ti atoms. This confirmed the presence of TiO_2. Besides, both the samples showed the presence of Ag-nanoparticles that were orderly and distinctly dispersed within the titania framework. Further, elemental mapping revealed that the *in situ* impregnation of Ag(NPs) enabled an uniform distribution of nanoparticles within titanium dioxide network and it also proved that the Ag(NPs) were restricted to form bigger aggregates of silver.

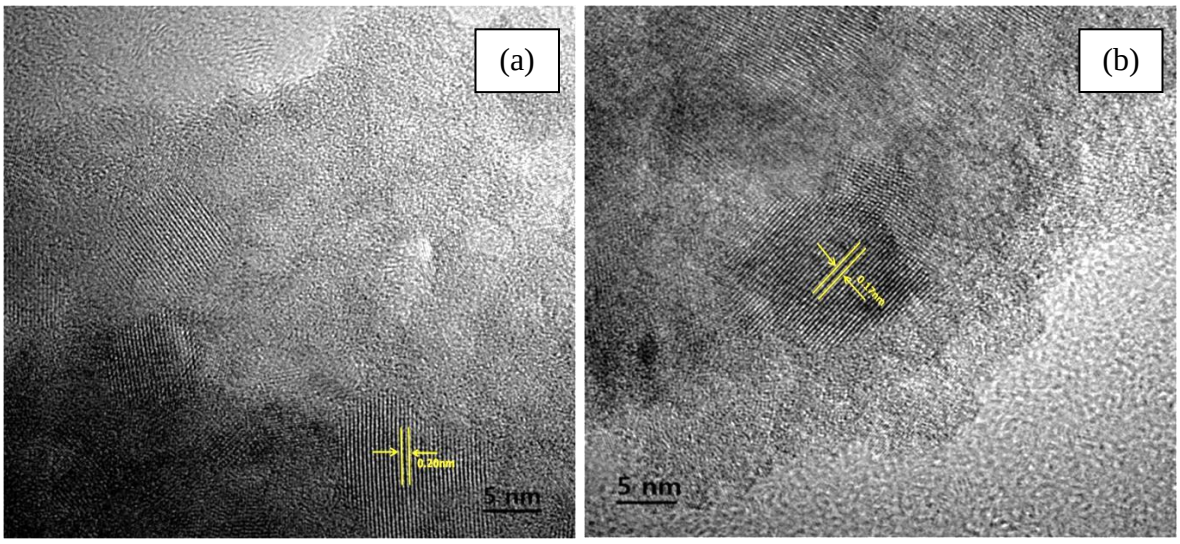

Figure 3.1.5(i): Transmission electron microscopic images of (a) Ag^0(NP)/TiO_2(A1) and (b) Ag^0(NP)/TiO_2(A2) thin films [Tiwari *et al*., (2018)].

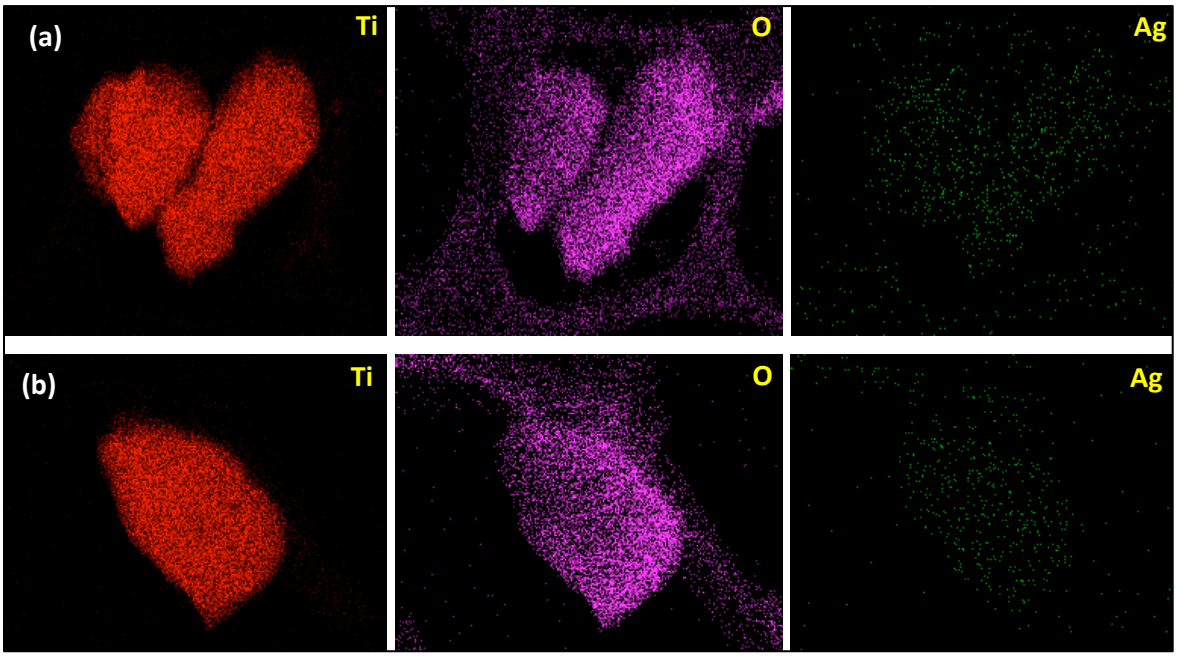

Figure 3.1.5(ii): TEM/EDX mapping of nanocomposite materials (a) Ag^0(NP)/TiO_2(A1) and (b) Ag^0(NP)/TiO_2(A2) [Tiwari et al., (2019a)].

On the other hand, the TEM images of the two nanocomposite materials *viz*., Au^0(NP)/TiO_2(B1) and Au^0(NP)/TiO_2(B2) were shown in Figures 3.1.5(iii)(a) and 3.1.5(iii)(b). The Figure showed that Au-nanoparticles were rather uniformly distributed within titanium dioxide network and particles were ranged within 5 ~ 10 nm. Fairly a good heterogeneous and disordered structure was obtained. Further, the profile analysis of these solids indicated that the average interplanar distance of the Au-nanoparticles were found to be 0.14 nm and 0.20 nm for the solids Au^0(NP)/TiO_2(B1) and Au^0(NP)/TiO_2(B2), respectively, [Lalliansanga *et al*., (2019)].

Further, the TEM/EDX elemental mapping was conducted for the nanocomposite materials Au^0(NP)/TiO_2(B1) and Au^0(NP)/TiO_2(B2) and results were shown in Figures 3.1.5(iv)(a) and 3.1.5(iv)(b). The EDX mapping was recorded for the elements Ti (Titanium), O (Oxygen) and Au (Gold). The Figure clearly indicated that the oxygen was

intimately bound with Ti that confirmed the presence of TiO_2 and forming a chemical bond between the titanium and oxygen (Ti–O). Besides, the Figure clearly revealed that the Au-nanoparticles were very evenly and distinctly distributed within the titanium dioxide network. The Au-nanoparticles were not aggregated on the surface of titanium dioxide. Therefore, the *in situ* impregnation of Au-nanoparticles enabled to distribute evenly within the titanium dioxide network. Similar EDX results were reported for the composite material TiO_2–Pt/Graphene oxide solid that confirms the presence of Ti, O, Pt elements and uniform distribution of Pt nanoparticles over the graphene sheets. The results further inferred that the intimate contact within these components provided an enhanced photocatalytic activity of catalyst by the efficient carrier mobility (Rosu *et al*., 2017).

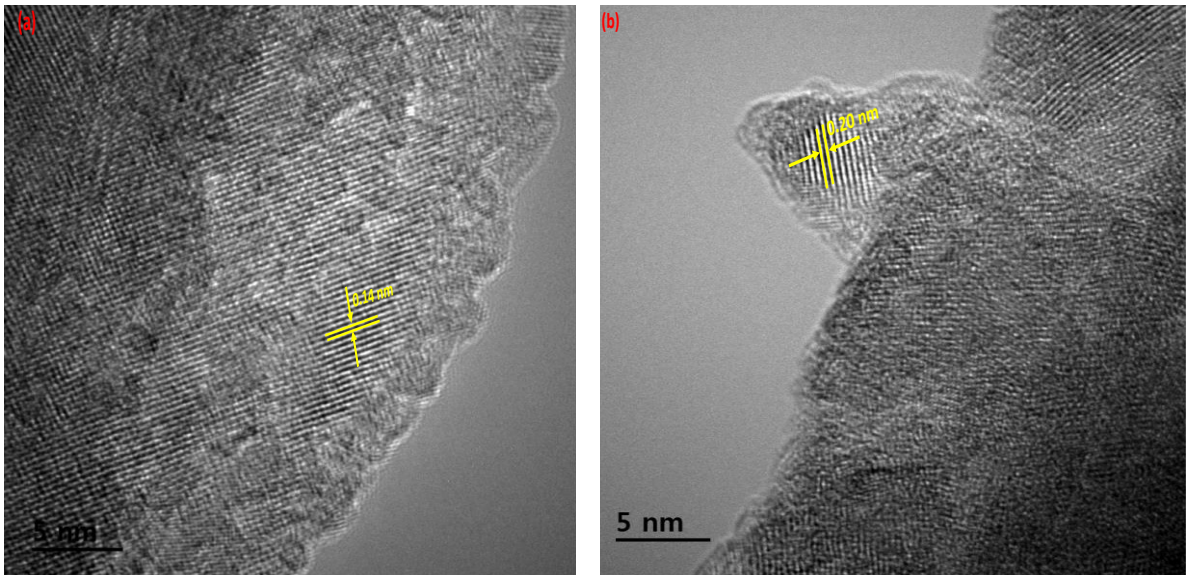

Figure 3.1.5(iii): Transmission electron microscopic images of (a) Au^0(NP)/TiO_2(B1) and (b) Au^0(NP)/TiO_2(B2) nanocomposite materials [Lalliansanga *et al*., (2019)].

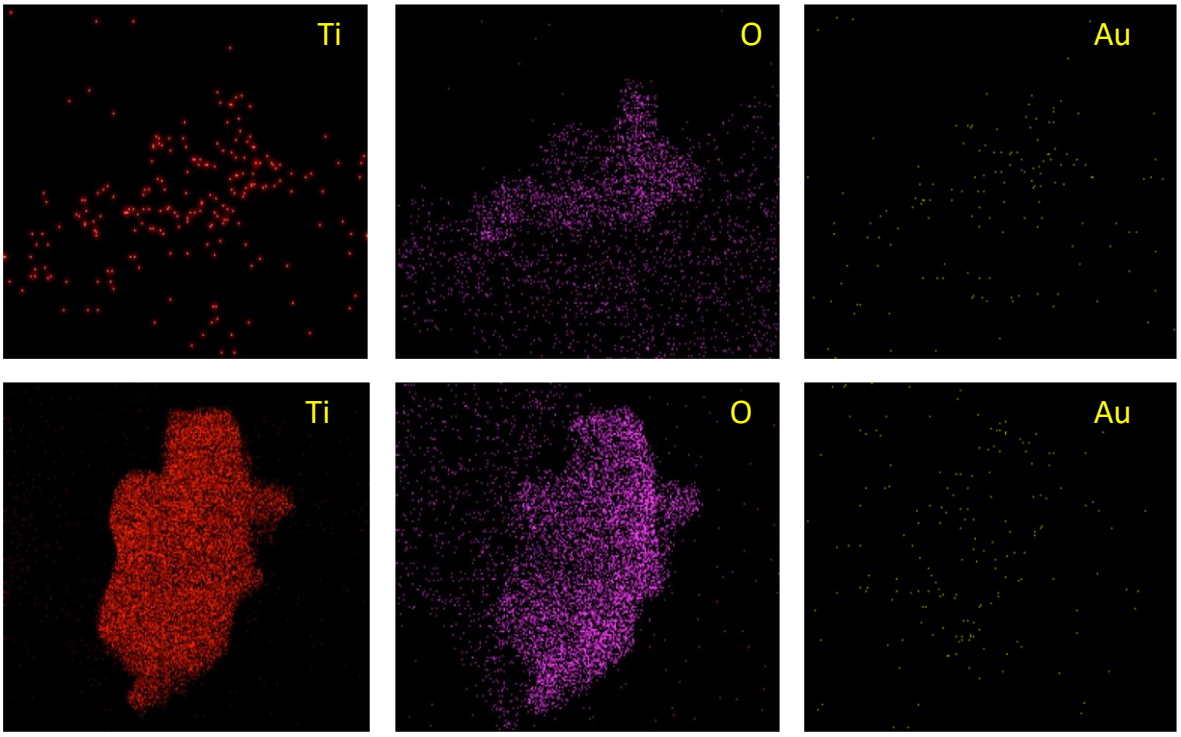

Figure 3.1.5(iv): TEM/EDX mapping of nanocomposite materials (a) Au^0(NP)/TiO_2(B1) and (b) Au^0(NP)/TiO_2(B2) [Lalliansanga *et al*., (2018)].

Further, the TEM images were also obtained for the nanocomposite materials *viz.*, Ce^{3+}/TiO_2(C1) and Ce^{3+}/TiO_2(C2) which were represented in Figures 3.1.5(v)(a) and 3.1.5(v)(b). It was clear from the TEM images that small sized titanium dioxide particles were forming a uniform network. The size of the particles were *Ca.* 12 – 15 nm in both the samples. The titanium dioxide was extensively contained with small sized cerium ions. The Ce particles were very evenly distributed within the titania network. Further, the interplanar distance of Ce particles were estimated in the two samples *viz.*, Ce^{3+}/TiO_2(C1) and Ce^{3+}/TiO_2(C2) and results were shown in Figures 3.1.5(v)(c) and 3.1.5(v)(d), respectively. The interplanar distance of the Ce particles were found to be 0.29 and 0.33 nm for the Ce^{3+}/TiO_2(C1) and Ce^{3+}/TiO_2(C2) solids, respectively. It was reported previously that the CeO_2 nanocube possessed the lattice spacing of 0.27 nm which corresponds to the (200) crystallographic planes of cubic fluorite CeO_2 (Chen *et al*., 2017). Similarly, the interplanar

distance of 0.31 nm and 0.27 nm corresponds to the (111) and (200) crystal planes of CeO_2, respectively, as studied for cerium-based TiO_2 (Wang *et al*., 2017).

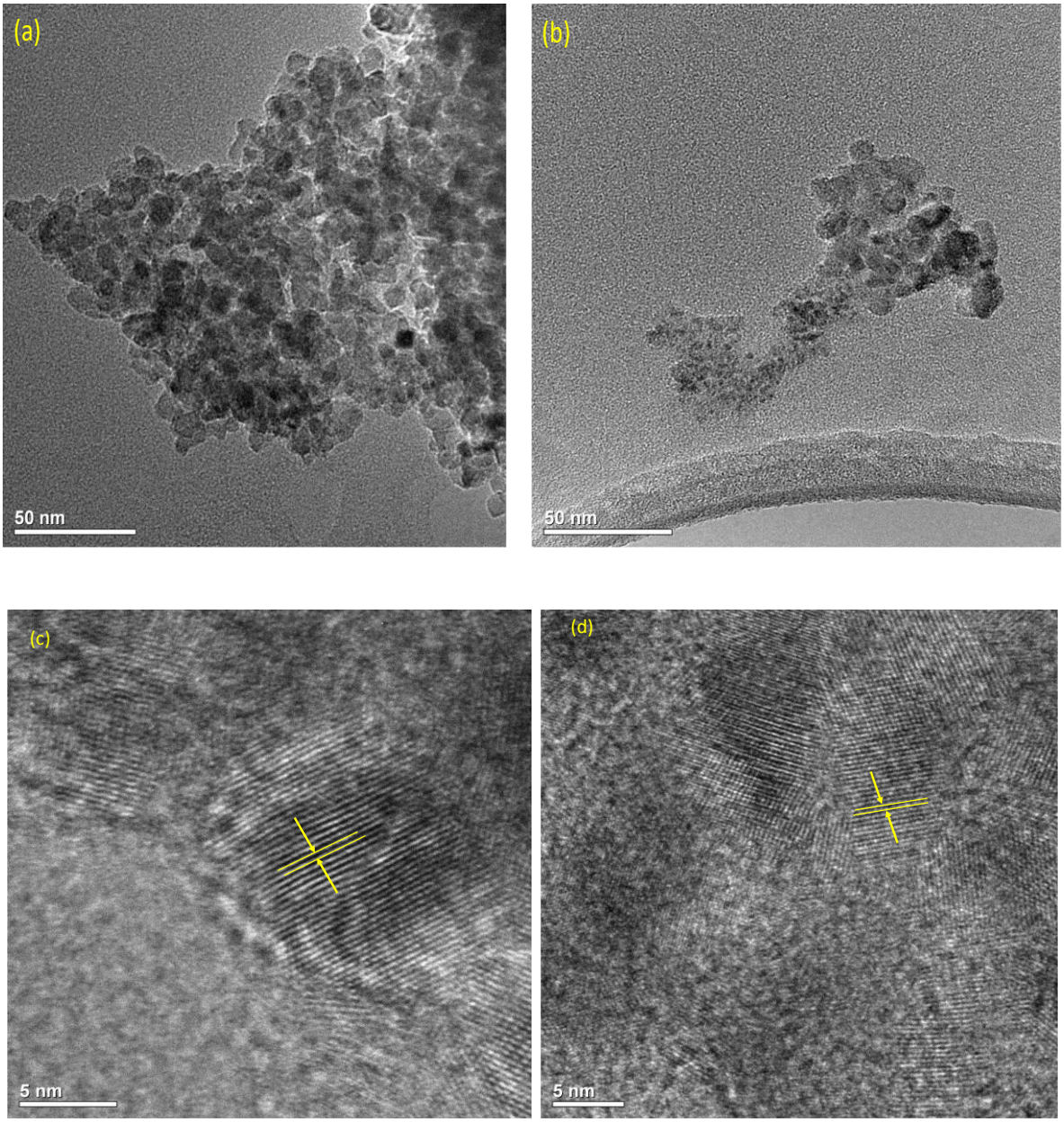

Figure 3.1.5(v): TEM images of the (a) Ce^{3+}/TiO_2(C1), (b) Ce^{3+}/TiO_2(C2) and interplanar distance of Ce in (c) Ce^{3+}/TiO_2(C1) and (d) Ce^{3+}/TiO_2(C2) powders.

Further, the elemental mapping of the Ti, O and Ce elements was conducted for the samples Ce^{3+}/TiO_2(C1) and Ce^{3+}/TiO_2(C2) and results were shown in Figures 3.1.5(vi)(a)

and 3.1.5(vi)(b), respectively. It was evident from the Figure that the titanium was intimately contained with the oxygen atoms. This confirmed the presence of TiO_2 since Ti was chemically bonded with the O and forming Ti–O bond. Further, it was interesting to note that within the titania network small sized Ce was uniformly distributed. Moreover, the Ce particles were not aggregated within the TiO_2 surface. Therefore, the *in situ* doping of Ce enabled to disperse evenly the Ce particles within the titanium dioxide. A similar TEM elemental mapping was obtained for the distribution of Au nanoparticles within the titania network (Lalliansanga *et al*., 2018).

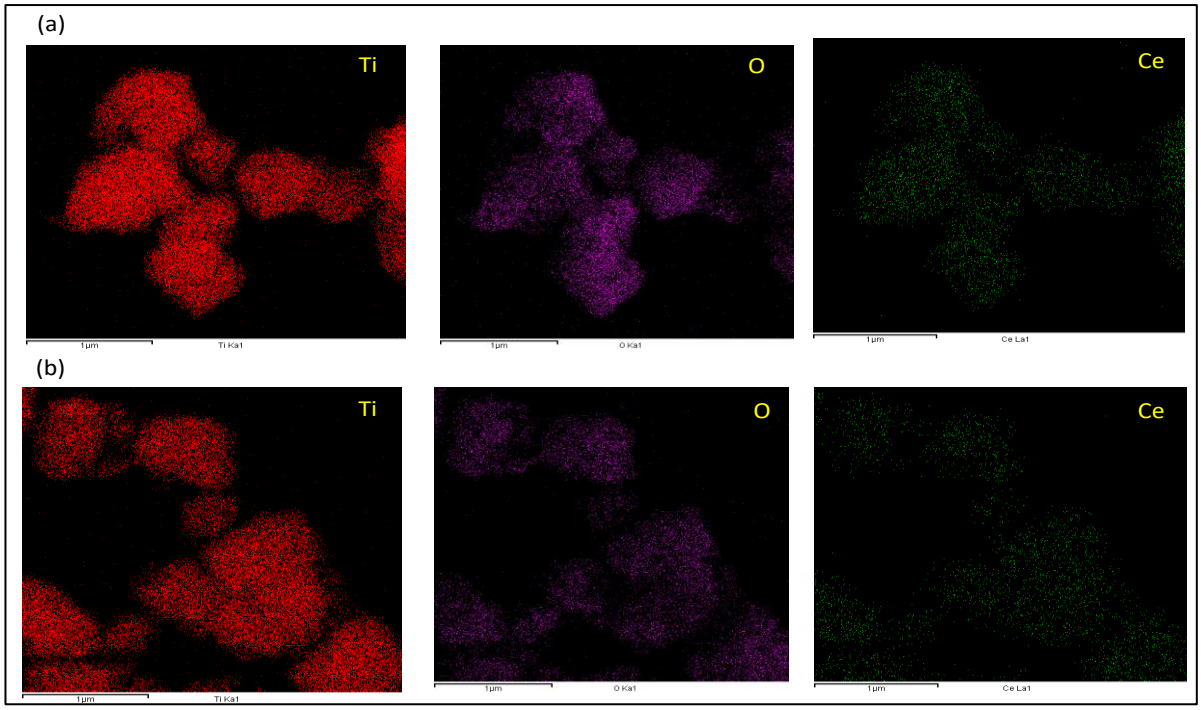

Figure 3.1.5(vi): Elemental mapping of the (a) Ce^{3+}/TiO_2(C1), and (b) Ce^{3+}/TiO_2(C2) powders in TEM/EDX analysis.

3.1.6. Atomic Force Microscopic (AFM) Analysis

The three dimensional AFM images of Ag^0(NP)/TiO_2(A1) and Ag^0(NP)/TiO_2(A2) thin films were shown in Figure 3.1.6(i)(a) and 3.1.6(i)(b). It was observed that the TiO_2 particles forming pillars onto the surface of borosilicate glass. The thin film Ag^0(NP)/TiO_2(A1) showed distinct and spatially distributed pillars on the surface and the pillar height was estimated to be *Ca.* 35 nm. On the other hand a uniform and more regular pillars of TiO_2 were obtained with the Ag^0(NP)/TiO_2(A2) thin film sample. It possessed even more heterogeneous surface structure. The pillar height was found to be *Ca.* 250 nm. This indicated that the template synthesis enabled to produce relatively increased height of pillars on the solid surface. Similarly, the root mean square roughness (Rq) and mean roughness (Ra) were found to be 0.759 nm and 0.406 nm (for Ag^0(NP)/TiO_2(A1)) and 14.095 nm and 10.640 nm (for Ag^0(NP)/TiO_2(A2)) thin films, respectively. These results were further revealed that the template synthesis enabled to obtain enhanced heterogeneity contained with long length pillars of titanium oxide on the surface of solid.

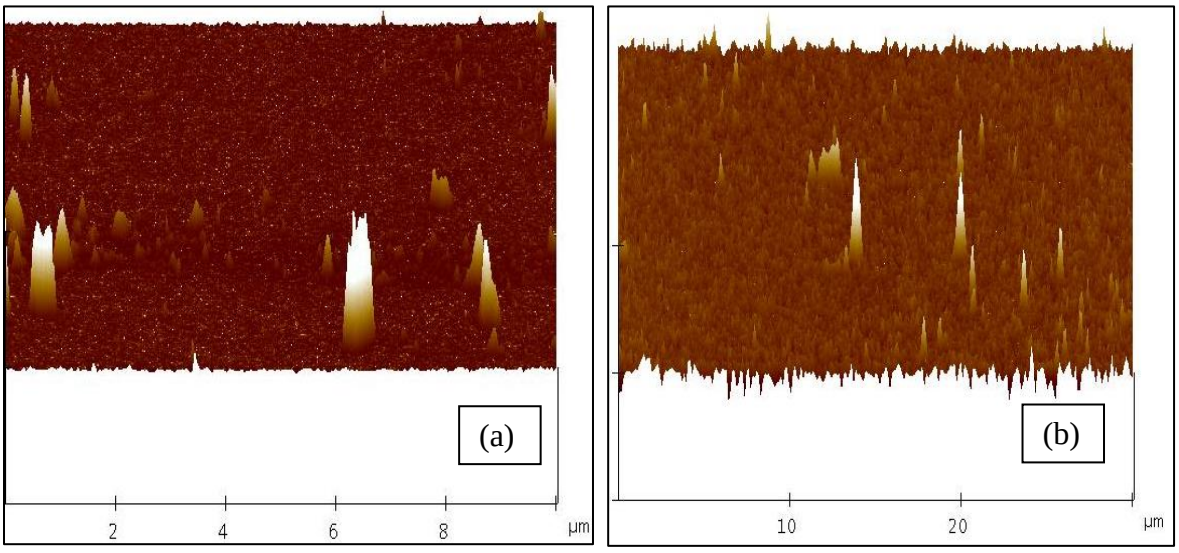

Figure 3.1.6(i): Atomic force microscopic images of (a) Ag^0(NP)/TiO_2(A1) (Scale 35 nm) and (b) Ag^0(NP)/TiO_2(A2) (Scale 250 nm) [Tiwari *et al*., (2018)].

Further, the AFM images of Au^0(NP)/TiO_2(B1) and Au^0(NP)/TiO_2(B2) thin films were shown in Figures 3.1.6(ii)(a) and 3.1.6(ii)(b). It was observed that nanopillars of TiO_2 was generated onto the surface of borosilicate glass. The thin film Au^0(NP)/TiO2(B1) showed scattered pillars on the surface having the pillar height of *Ca.* 50 nm. On the other hand a uniform pillars were formed with the sample Au^0(NP)/TiO_2(B2) and very heterogeneous surface structure was generated. The pillar height was found to be *Ca.* 300 nm. This specified that template synthesis of Au/TiO_2 caused to increase the length of the pillars of TiO_2 onto the borosilicate surface. Further, the root mean square roughness (Rq) and mean roughness (Ra) was found to be 7.314 nm and 1.333 nm (for Au^0(NP)/TiO_2(B1)) and 124.330 nm and 94.659 nm (for Au^0(NP)/TiO_2(B2)) thin films, respectively. It was evident again that the template synthesis enabled to obtain the heterogeneous surface structure with enhanced pillars on the surface.

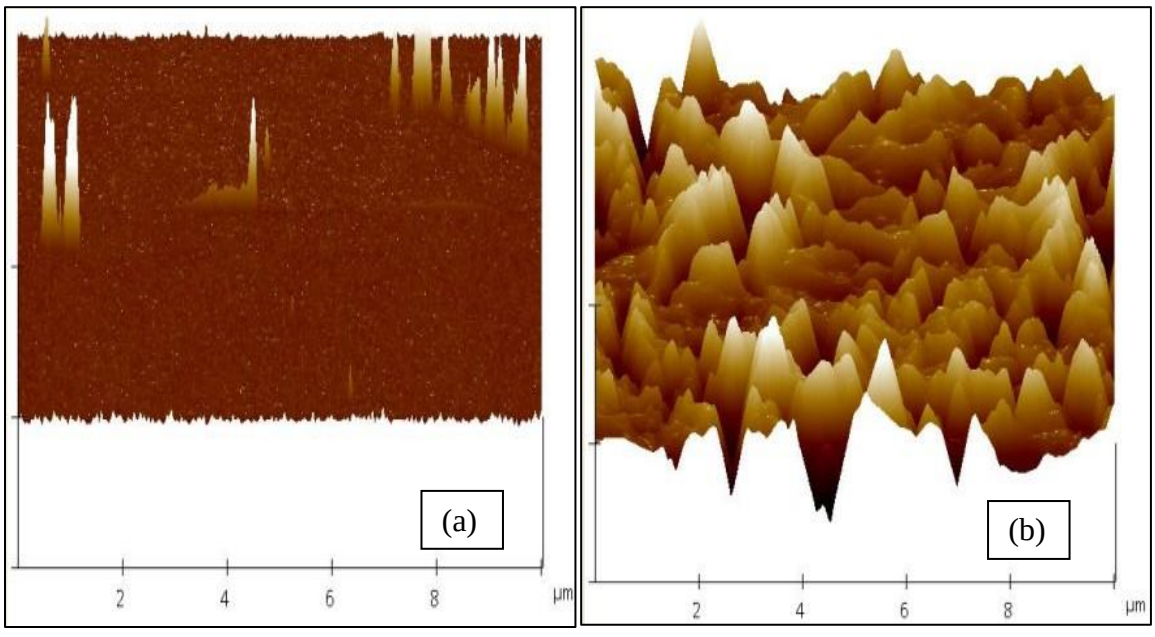

Figure 3.1.6(ii): Atomic force microscopic images of (a) Au^0(NP)/TiO_2(B1) (Scale 50 nm) and (b) Au^0(NP)/TiO_2(B2) (Scale 600 nm) [Tiwari et al., (2019b)].

Similarly, the 3D atomic force image profiling was conducted for the nanocomposite Ce^{3+}/TiO_2(C1) and Ce^{3+}/TiO_2(C2) thin films and the results were illustrated in Figures 3.1.6(iii)(a) and 3.1.6(iii)(b), respectively. It is evident from the Figures that both the thin film samples possessed with heterogeneous structures and the titanium dioxide forming some pillars on the surface. The image root mean square roughness (Rq) and mean roughness (Ra) was found to be 2.78 nm and 2.14 nm (for Ce^{3+}/TiO_2(C1)) and 1.83 nm and 1.46 nm (for Ce^{3+}/TiO_2(C2)) thin films, respectively. Similarly, the maximum surface roughness (R_{max}) values were found to be 30.1 nm and 18.2 nm for the Ce^{3+}/TiO_2(C1) and Ce^{3+}/TiO_2(C2) thin films, respectively. These results clearly indicated that the thin film Ce^{3+}/TiO_2(C1) possessed more heterogeneous surface structure compared to the templated Ce^{3+}/TiO_2(C2) thin film. Further, these results were in a line to the FE–SEM images of obtained previously for these thin films.

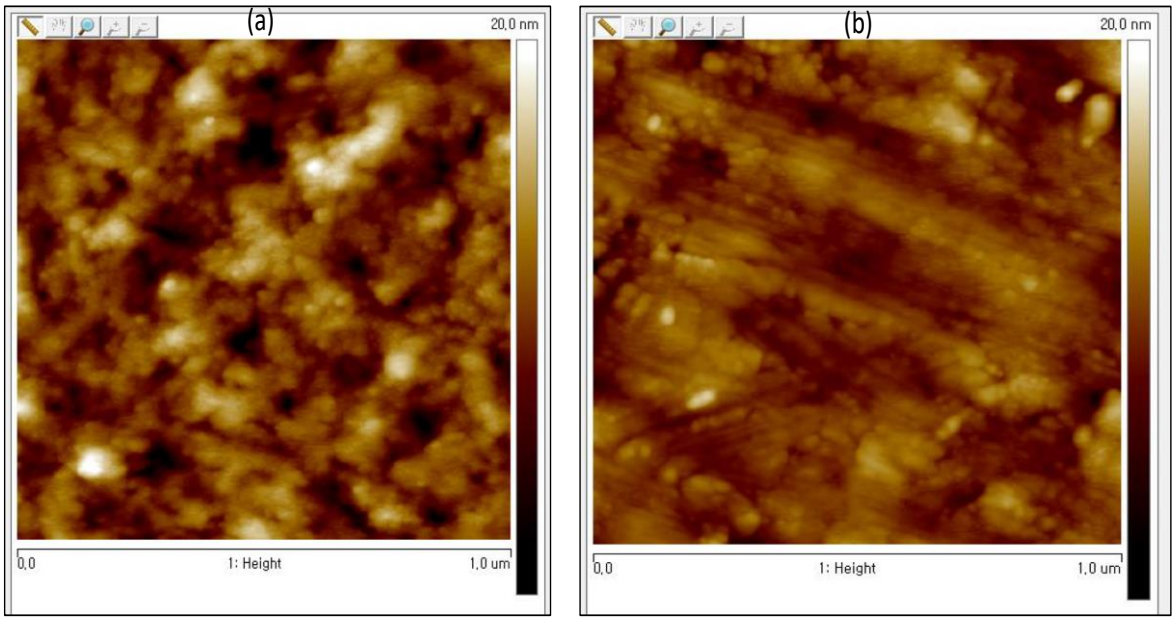

Figure 3.1.6(iii): 3D atomic force microscopic images of (a) Ce^{3+}/TiO_2(C1) and (b) Ce^{3+}/TiO_2(C2) thin films.

3.2. Heterogeneous Photocatalytic Degradation of Triclosan and Alizarin Yellow using Meso-porous Thin Films (Triclosan by Ag^0(NP)/TiO_2 and Alizarin Yellow by Ag^0(NP)/TiO_2, Au^0(NP)/TiO_2 thin films).

3.2.1. Batch Reactor Studies

3.2.1.1. Effect of pH in the degradation of Triclosan (TCS)

The removal of triclosan as a function of pH enabled in elucidating the mechanism involved in degradation. The catalyst surface charge, the size of the catalyst aggregates as well as the positions of conductance and valence bands were influenced with change in pH (Chong *et al.,* 2010). Therefore, photolytic and photocatalytic elimination of triclosan was conducted at varied pH (pH 4.0 – 10.0) values. The efficiency of triclosan degradation as a function of pH was illustrated in Figure 3.2.1.1 and Table 3.2.1.1. The samples were irradiated for 2 hours. Figure 3.2.1.1 showed that increasing the pH from pH 4.0 to 10.0 had caused a gradual decrease in oxidation of triclosan. Quantitatively, increasing the solution pH from 4.0 to 10.0 caused to suppress the removal efficiency from 63.65 to 43.11%, respectively, for the Ag^0(NP)/TiO_2(A2) catalyst. This decrease in efficiency of elimination with the increase in pH could be explained by surface behaviour of nanocomposites along with the species distribution of triclosan in aqueous medium at varied pH values. Triclosan behaves like a weak monoprotic acid having the dissociation constant value pK_a^1 7.9 (Muzvidziwa *et al*., 2017). Therefore, the species distribution of triclosan was conducted and results were illustrated in Figure 3.2.1.1, simultaneously. This clearly showed that at pH > 7.9, the triclosan molecule possessed dominantly the negative charged species TCS^-. However, at pH < 7.9 the neutral species of triclosan, i.e., TCS^0 was prevalent. On the other hand, the pH_{PZC} of these solids were found to be 6.6 and 6.8, respectively, for the solids titanium oxide, Ag^0(NP)/TiO_2(A1) and Ag^0(NP)/TiO_2(A2). This conferred that titanium

dioxide surface showed net positive charge at pH < 6.6 ~ 6.8 that turned to negatively charged at pH > 6.6 ~ 6.8 as depicted in equation (3.2.1.1):

$$\equiv S - OH_2^+ \leftrightarrow \quad \equiv S - OH^0 \leftrightarrow \quad \equiv S - O^- \qquad \ldots(3.2.1.1)$$

pH_{PZC}

This showed that at higher pH values both catalyst surface and the triclosan species (TCS^-) were possessed with net negative charge and hence, caused to repel each other. This hindered the electrostatic attraction of triclosan species onto the catalyst surface and therefore, resulted in less sorption of triclosan on the catalyst surface. Hence, the dissociated species of triclosan (TCS^-) was invariably less degraded at higher pH values. However, at lower pH conditions the un-dissociated species of triclosan (TCS^0) were readily oxidized. The results therefore, showed that the dissociated phenolate species of triclosan were relatively stable in photocatalytic degradation compared to the un-dissociated species. The results were contrary to the previous observations mentioned that the phenolic form of triclosan was more stable than the phenolate form of triclosan (Aranami and Readman, 2007). However, a similar decrease in pseudo-second order rate constant (k_{app}) was obtained with an increase in pH from 7.0 to 10.0 while triclosan was degraded by ferrate(VI) (Yang *et al*., 2011).

Further, the oxidation of triclosan was significantly favored by nanocomposite photocatalysts compared to photolysis. This demonstrated, the thin film of nanocomposites *viz*., Ag^0(NP)/TiO_2(A1) or Ag^0(NP)/TiO_2(A2) had shown an enhanced catalytic activity that caused to promote the removal efficiency of triclosan. Additionally, the photocatalyst Ag^0(NP)/TiO_2(A2) possessed relatively higher catalytic activity than the Ag^0(NP)/TiO_2(A1) catalyst. This was possibly due to the enhanced surface heterogeneity of thin film Ag^0(NP)/TiO_2(A2) compared to Ag^0(NP)/TiO_2(A1) as observed with AFM analysis. On the

other hand, the photocatalytic removal of triclosan using the unmodified TiO_2 thin film was obtained for simple comparison with the Ag^0(NP) doped TiO_2 and the results were included in the Figure 3.2.1.1. It was shown from the Figure that photocatalytic removal of triclosan was significantly increased with the Ag^0 doped TiO_2 compared to the bare TiO_2 using the UV-A radiations.

Table 3.2.1.1: Effect of pH in the photocatalytic degradation of triclosan by using UV-A only, Ag^0(NP)/TiO_2(A1) and Ag^0(NP)/TiO_2(A2) thin films.

	% Removal			
	(pH)			
	4	**6**	**8**	**10**
UV-A	23.4	20.3	15.9	14.3
Ag^0(NP)/TiO_2(A1)	51.6	48.4	39.7	34.9
Ag^0(NP)/TiO_2(A2)	63.65	59.3	47.85	43.11

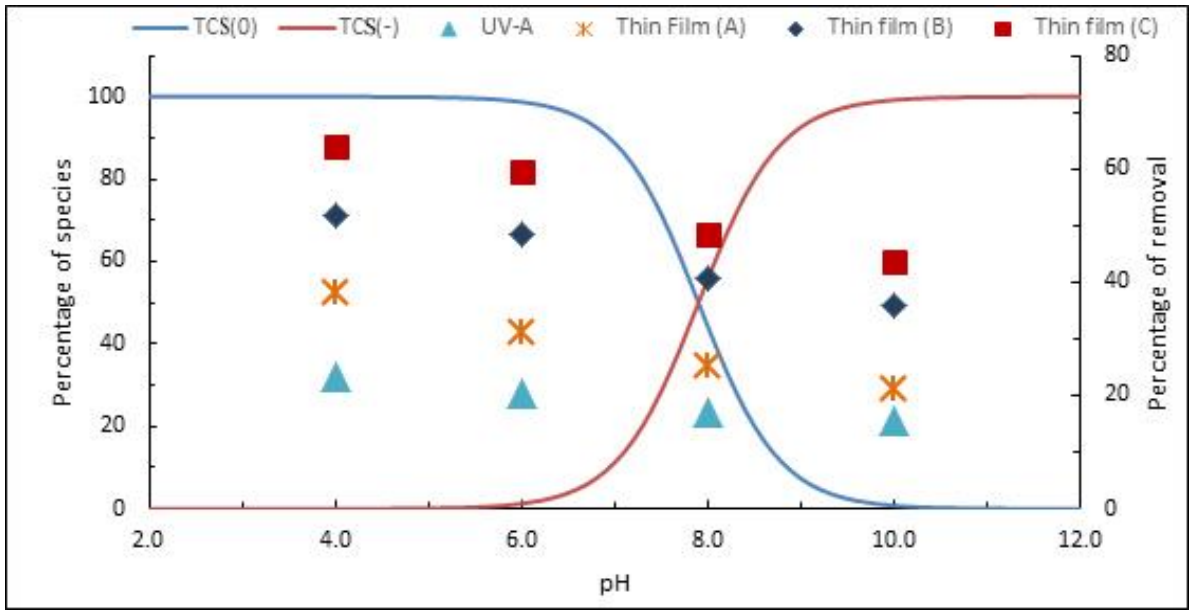

Figure 3.2.1.1. Percentage distribution of species of triclosan as a function of pH (Smooth line) and percentage removal of triclosan as a function of pH (scattered points) under the photolytic and photocatalytic operations [Initial concentration of triclosan: 1.0 mg/L; Thin Film(A): bare TiO_2 thin film; Thin Film (B): Ag^0(NP)/TiO_2(A1) and Thin Film (C): Ag^0(NP)/ TiO_2(A2); Temperature: 25±1 ^{0}C].

3.2.1.2. Effect of pH in the degradation of Alizarin Yellow (AY)

Variations of pH effected the electron charge on the surface of the catalyst (Modirshahla *et al.*, 2011) and the dye degradation process under UV light irradiation (Gözmen *et al*, 2009). The pH influenced not only the surface properties of the photocatalyst but also dye dissociation and hydroxyl radical formation (Liu *et al.*, 2015i). The effect of the solution pH on the adsorption could be explained generally by the modification of the electrical double layer of the solid-electrolyte interface, which consequently affected the electrostatic interactions (Liu *et al.*, 2015i). Therefore, the pH dependence study was conducted varying the solution pH from 4.0 to 10.0 at a constant alizarin yellow concentration (1.0 mg/L). The results of photocatalytic removal of alizarin yellow by Ag^0(NP)/TiO_2(A1) and Ag^0(NP)/TiO_2(A2) thin films were presented in Table 3.2.1.2(a) and

Figure 3.2.1.2(a). Percent degradation was increased by increasing the solution pH from 4.0 – 6.0. Though, further increase in pH, i.e., pH from 6.0 to 10.0 caused a significant decrease in percentage removal of alizarin yellow. Quantitatively, increasing the pH from 4.0 to 6.0 caused to increase the efficiency of alizarin yellow removal from 43.78 to 52.3% using the Ag^0(NP)/TiO_2(A2) thin film. However, increasing further the pH from 6.0 to 10.0 caused to decrease the efficiency of percentage removal of alizarin yellow from 52.3 to 35.79% respectively. A similar trend of degradation of alizarin yellow was observed for the Ag^0(NP)/TiO_2(A1) thin film. This pH dependence degradation of alizarin yellow using the nanocomposite photocatalysts could be explained based on the speciation studies of alizarin yellow and the surface properties of nanocomposite in aqueous solutions as a function of pH. Therefore, a systematic speciation studies of alizarin yellow was conducted separately at varied pH conditions. It was reported that the alizarin yellow molecule had two dissociable hydrogens (the phenolic and carboxylic) and were having the pK_{a1} and pK_{a2} values of 5.0 and 11.0 (Nazar *et al*., 2010). The Mono-anionic form of alizarin yellow that chiefly existed within the pH region 6.0 ~ 10.0. However, it was reported that mono-ionic species existed in an equilibrium state between the anionic and non-ionic state forming the hydrogen bonds with the two phenolic and carboxylic oxygen atoms (Nazar *et al*., 2010). However, further increase in pH > 10.0, the second hydrogen was dissociated and the alizarin yellow becomes the di–anionic species and carrying the net negative charges. It was known that anatase titanium dioxide possessed the point of zero charge values in the pH range 4.8 ~ 6.5 and accepted average value was 5.9 (Kosmulski, 2009). Hence, it was concluded that thin films carried positive charge at pH < 5.9 whereas carried negative charge at pH > 5.9 as shown in equation (3.2.1.2(a)):

$$\equiv Ti - OH_2^+ \leftrightarrow \quad \underset{pH_{PZC}}{\equiv Ti - OH^0} \quad \leftrightarrow \quad \equiv Ti - O^- \qquad \ldots(3.2.1.2(a))$$

Therefore, it was evident that at high pH values (pH 6 ~ 10) both the nanocomposite and alizarin yellow were possessed with net negative charges that eventually caused to repel the alizarin yellow by the solid surface that hindered the electrostatic attraction of alizarin yellow by the nanocomposite. This led to restrict the sorption of the alizarin yellow onto the solid surface to enable it for a chemisorption at the nanocomposite surface. This caused a marked decrease in percentage of alizarin yellow removal at high pH values. Furthermore, relatively a high percentage removal of alizarin yellow at pH 6.0 was explained with the fact that at this pH the anionic species of alizarin yellow were seemingly attracted by the positively charged surface of nanocomposite solid that caused an enhanced sorption of alizarin yellow species and hence, underwent with an enhanced catalytic degradation of alizarin yellow. A similar very high sorptive removal of several anionic dyes was recorded at pH *Ca.* 5 which was significantly decreased at pH 10.0 using the isoreticular nano-porous Zn(II) -MOFs (metal oxide framework) known as TMU-16 and TMU-16-NH_2 (Roushani *et al*., 2016). The enhanced removal of alizarin yellow at pH 6.0 was also supported with the fact that the hydroxyl ions were readily oxidized to the hydroxyl radicals at surface of catalyst and were found to be predominant and stable at the neutral pH conditions (Buxton *et al*., 1988) which further synergised the degradation of alizarin yellow in aqueous solutions. However, at lower pH conditions the low percentage removal of alizarin yellow was explained due to the reason that the alizarin yellow species were predominantly present to its un-dissociated species and the surface of thin film also contained with high positive charge density. Therefore, relatively less sorption of alizarin yellow resulted a slight decrease in percentage degradation of alizarin yellow. Moreover, at low pH conditions the hydroxyl species were also readily reduced as combined with the H^+ ions that hindered the $^{\bullet}OH$ induced degradation of alizarin yellow (equation 3.2.1.2(b)) (Tang and Huang, 1996; Benitez *et al*., 2007: Feizpoor *et al*., 2018; Salavati-Niasari *et al*., 2016). Similarly, the

photocatalytic degradation of Congo red was decreased by increasing the pH from 3.0 to 10.0 whereas the dye Bismarck brown removal was increased by increasing the similar pH, i.e., 3.0 to 10.0 using the Ag/reduced graphene oxide nanocomposite (Borthakur *et al*., 2017).

$$^{\bullet}OH + H^{+} + e^{-} \rightarrow H_2O \qquad \ldots (3.2.1.2(b))$$

Similar degradation trend was reported previously for the photocatalytic degradation of alizarin yellow by the nanopillar TiO_2 using the UV irradiation (Tiwari *et al*., 2015). Similarly, relatively high percentage oxidative removal of alizarin red S was obtained at pH 7.0 using the biomimetic peroxidase-like catalyst 5,10,15,20-tetrakis(4-sulfonatophenyl)porphine-Mn(III) (Zucca *et al*., 2008).

Table 3.2.1.2(a): Effect of pH in the photocatalytic degradation of alizarin yellow by using UV-A only, Ag^0(NP)/TiO_2(A1) and Ag^0(NP)/TiO_2(A2) thin films.

	% Removal			
	(pH)			
	4	**6**	**8**	**10**
UV-A	3.4	11.1	8	4.8
Ag^0(NP)/TiO_2(A1)	37.3	44.5	38.1	32.3
Ag^0(NP)/TiO_2(A2)	43.78	52.3	39.58	35.79

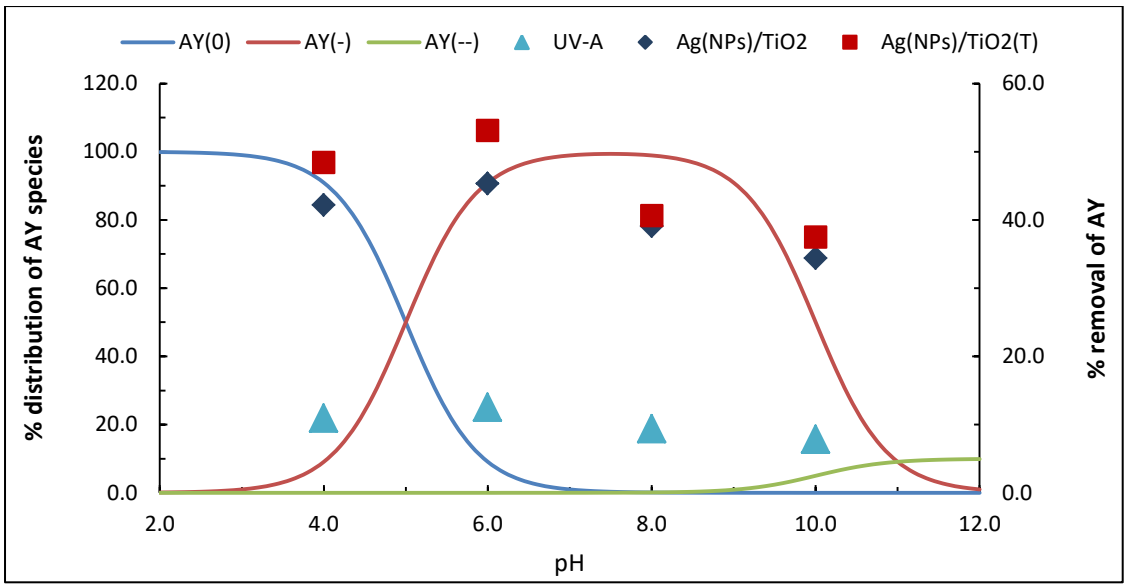

Figure 3.2.1.2(a): Percentage distribution of alizarin yellow species at different pH values (Smooth Line) and percentage oxidative removal of alizarin yellow at different pH values (Scattered Points) for photolytic and photocatalytic operations using the Ag(NPs)TiO_2: Ag^0(NP)TiO_2(A1) and Ag(NPs)TiO_2(T): Ag^0(NP)TiO_2(A2) thin films [Initial concentration of alizarin yellow: 1.0 mg/L; Temperature 25±1 ^{0}C].

Similarly, the percentage removal of alizarin yellow as a function of solution pH was obtained and illustrated in Figure 3.2.1.2(b) (Secondary axis) using the Au^0(NP)/TiO_2(B1) and Au^0(NP)/TiO_2(B2) thin film catalysts. The concentration of alizarin yellow (1.0 mg/L) was taken and the UV-A illumination was given for 2 hours. Figure 3.2.1.2(b) and Table 3.2.1.2(b) showed that photocatalytic removal of alizarin yellow was increased by increase in pH from 4.0 to 6.0. However, further increase in pH, i.e., pH 6.0 to 10.0 had caused to decrease the percentage degradation of alizarin yellow. Moreover, the percentage of alizarin yellow removal was increased from 48.89 to 58.66% with an increase in pH from 4.0 to 6.0 employing the nanocomposite Au^0(NP)/TiO_2(B2) thin film. However, further increase in pH 6.0 to 10.0 had suppressed the removal efficiency of alizarin yellow from 58.66 to 39%,

respectively. Similarly, the degradation trend of alizarin yellow by Au^0(NP)TiO_2(B1) and Au^0(NP)TiO_2(B2) photocatalysts was same as that of alizarin yellow by Ag^0(NP)TiO_2(A1) and Ag^0(NP)TiO_2(A2) photocatalysts.

Alizarin Yellow molecule contain invariably two dissociable hydrogens (i.e., attached with the phenolic and carboxylic groups (*cf.* Figure 3.2.1.2(i)). The speciation studies indicated that the mono-anionic species of alizarin yellow was dominantly present within the pH region 6.0 ~ 10.0 (*cf.* Figure 3.2.1.2(b) (Primary axis)). However, the mono-ionic species exist in equilibrium with the non-ionic species as resulted with the hydrogen bonding between the two phenolic and carboxylic oxygen atoms (*cf.* Figure 3.2.1.2(i)) (Nazar *et al*., 2010). At higher pH conditions (pH 6 ~ 10) both the nanocomposite and alizarin yellow were carrying the net negative charges which greatly hindered the electrostatic attraction of alizarin yellow by the nanocomposite materials. Therefore, this restricted the sorption of alizarin yellow by the surface active sites of nanocomposites or even it restricted the sorbing species to enter within the Stern plane to enable it for a chemisorption of alizarin yellow at the solid surface. This led to a mark decrease in removal of alizarin yellow at high pH values. Moreover, relatively high percentage removal of alizarin yellow at pH 6.0 were explicable by the fact that at this pH the anionic species of alizarin yellow was seemingly attracted by the positively charged surface of nanocomposite which enabled an enhanced sorption of alizarin yellow species onto the surface of catalyst and hence; underwent with an enhanced catalytic degradation of alizarin yellow.

Figure 3.2.1.2(b) further indicated that the percentage efficiency of alizarin yellow removal was markedly higher using the nanocomposite Au^0(NP)/TiO_2(B1) or Au^0(NP)/TiO_2(B2) photocatalysts than the corresponding blank process using UV-A illumination. Therefore, this again demonstrated that nanocomposite thin films possessed an

enhanced catalytic activity, at least, in the degradation of alizarin yellow in aqueous media. Moreover, the template synthesized photocatalyst Au^0(NP)/TiO_2(B2) showed relatively higher removal efficiency of alizarin yellow than the non-template nanocomposite Au^0(NP)/TiO_2(B1). This indicated that templated synthesized TiO_2 with *in situ* impregnation of Au-nanoparticles resulted a dense titania network which showed an enhanced photocatalytic efficiency.

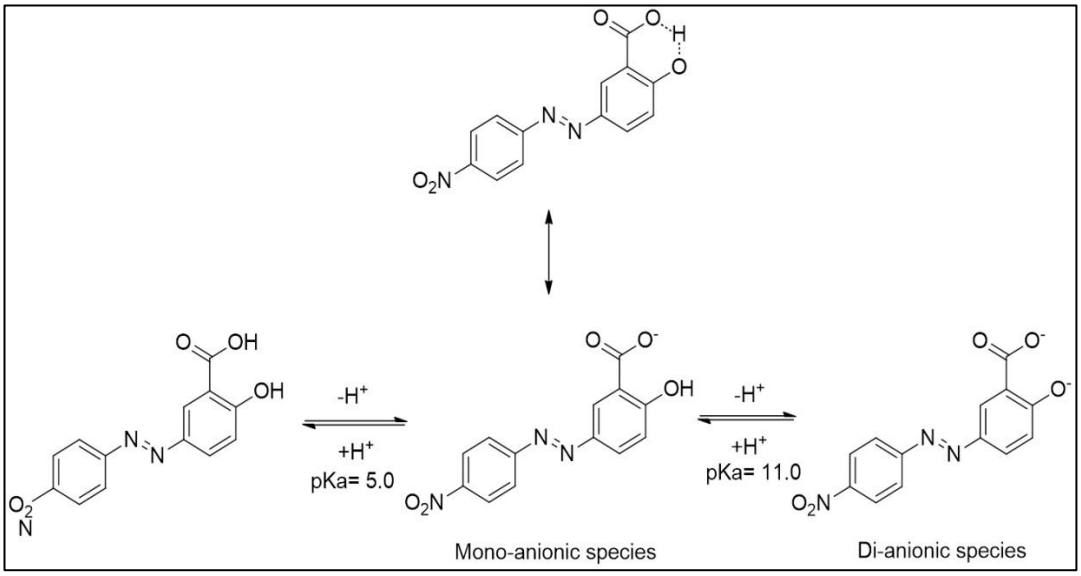

Figure 3.2.1.2(i). pH dependence dissociation of alizarin yellow in aqueous solution.

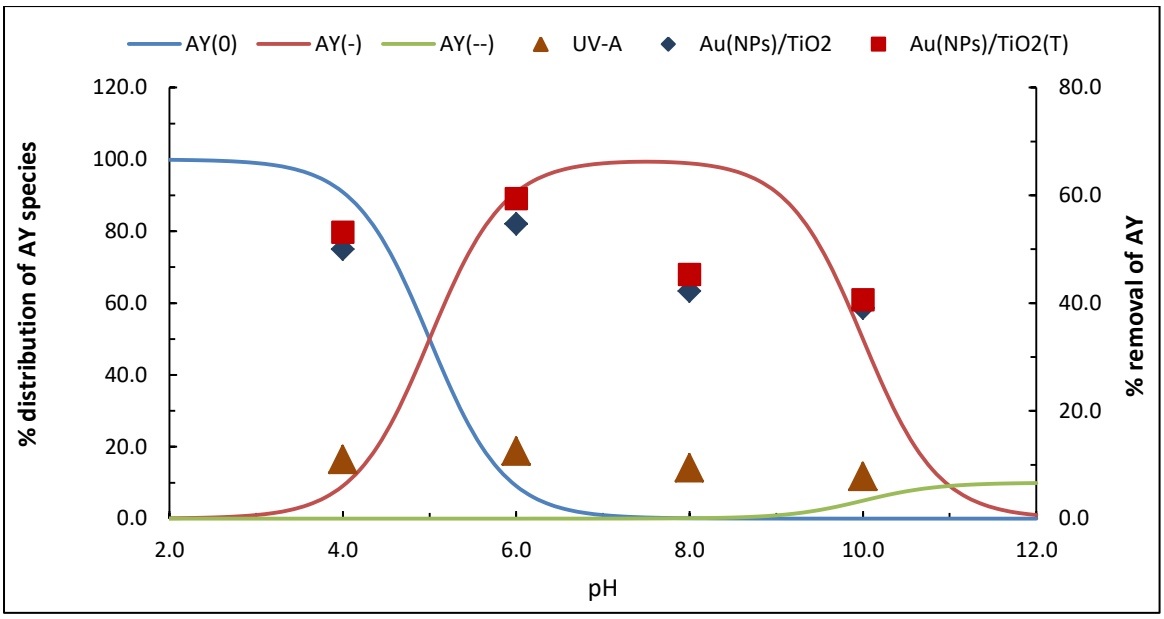

Figure 3.2.1.2(b). Percentage distribution of alizarin yellow species as a function of pH (Smooth Line) and percentage removal of alizarin yellow at various pH values (Scattered Points) for catalytic and photolytic treatments. Au^0(NPs)/TiO_2: Au^0(NP)/TiO_2(B1) and Au^0(NPs)/TiO_2(T): Au^0(NP)/TiO_2(B2) thin films [Initial concentration of alizarin yellow: 1.0 mg/L; Temperature 25±1 ^{0}C].

Table 3.2.1.2(b): Effect of pH in the photocatalytic degradation of alizarin yellow by using UV-A only, Au^0(NP)/TiO_2(B1) and Au^0(NP)/TiO_2(B2) thin films.

	% Removal			
	(pH)			
	4	**6**	**8**	**10**
UV-A	3.4	11.1	8	4.8
Au^0(NP)/TiO_2(B1)	45.8	54	41.3	37.1
Au^0(NP)/TiO_2(B2)	48.89	58.66	44.35	39

3.2.1.3. Effect of concentration in the degradation of Triclosan (TCS)

Triclosan concentration varied from 0.5 to 15.0 mg/L at pH 6.0 was taken for the photocatalytic oxidation. The removal efficiency of triclosan was presented as a function of triclosan concentration and it was depicted in Figure 3.2.1.3 and Table 3.2.1.3. Figure 3.2.1.3 showed that increasing the concentration of triclosan had greatly suppressed the percentage degradation of triclosan. The percentage efficiency of triclosan removal was decreased from 72.65 to 18.88% while increasing the triclosan concentration from 0.5 mg/L to 15.0 mg/L using the Ag^0(NP)/TiO_2(A2) nanocomposite. The decrease in removal efficiency at increased pollutant concentration was due to the fact that the catalyst surface possessed relatively large number of available active sites for lesser extent of pollutant species at lower concentrations (Nasseri *et al*., 2017). Earlier it was mentioned that at an increased pollutant concentration, the scavenging effect caused for decrease in removal efficiency (Chen *et al*., 2011a). Similarly the C/C_0 (where C is the concentration of triclosan (mg/L) after treatment (max. 2 hours) and C_0 is the initial triclosan concentration (mg/L)) was drawn against the initial concentration of triclosan for photolytic and photocatalytic treatment. The results were shown in Figure 3.2.1.3 (secondary axis; dotted lines). It was evident to note that C/C_0 values were increased with the increase in triclosan concentration. Further, the C/C_0 values were found lowest for nanocomposite Ag^0(NP)/TiO_2(A2) compared to Ag^0(NP)/TiO_2(A1) photocatalytic or simple UV-A photolysis processes.

It was again restated that the thin films Ag^0(NP)/TiO_2(A1) and Ag^0(NP)/TiO_2(A2) showed significantly higher photocatalytic efficiency in the degradation of triclosan from aqueous solutions compared to the UV-A only irradiated sample. Further, the PEG template thin film Ag^0(NP)/TiO_2(A2) possessed an enhanced photocatalytic activity than the Ag^0(NP)/TiO_2(A1) thin film in the degradation of the triclosan from aqueous solution since

more triclosan molecules were effectively trapped inside the small meso pores provided by the Ag^0(NP)/TiO_2(A2) catalyst surface. Hence, triclosan was effectively oxidised by the reactive species.

Table 3.2.1.3: Effect of concentration in the photocatalytic degradation of triclosan (TCS) using UV-A, Ag^0(NP)/TiO_2(A1) and Ag^0(NP)/TiO_2(A2).

	% Removal				
	[Initial concentration of TCS (mg/L)]				
	0.5	**1.0**	**5.0**	**10.0**	**15.0**
UV-A	17.3	20.3	10.2	2.7	1.9
Ag^0(NP)/TiO_2(A1)	55.2	48.4	32.6	14.4	11.1
Ag^0(NP)/TiO_2(A2)	72.65	59.3	38.94	25.05	18.88

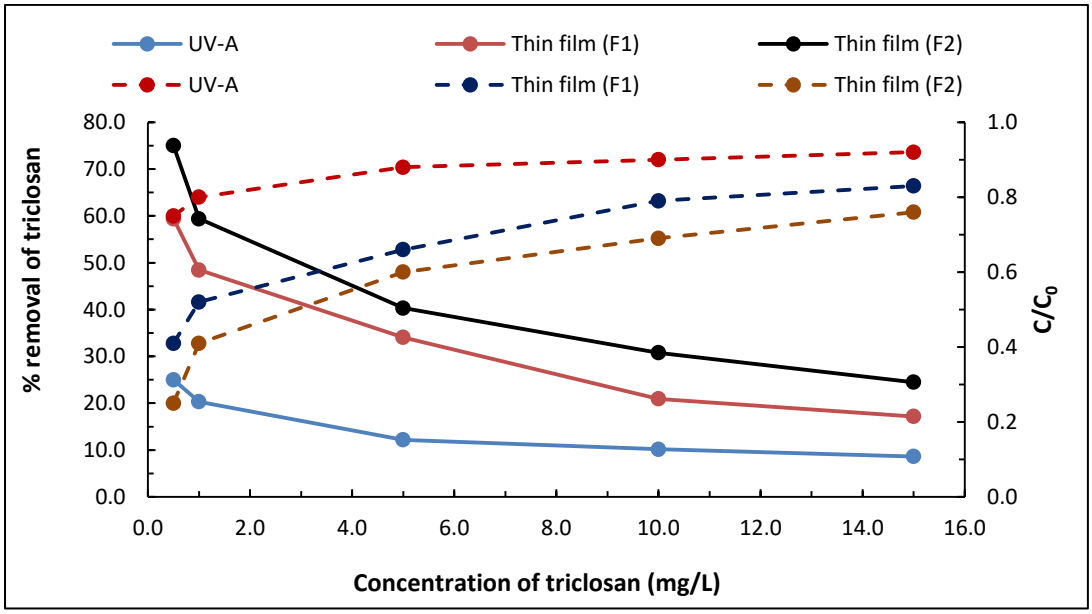

Figure 3.2.1.3: Percentage removal of triclosan (dotted lines) as a function of triclosan initial concentrations and the C/C_0 values (smooth line) against the triclosan concentration under the photolytic and photocatalytic processes [pH: 6.0; F1: Ag^0(NP)/TiO_2(A1) thin film; F2: Ag^0(NP)/TiO_2(A2) thin film; Temperature 25±1 ^{0}C].

3.2.1.4. Effect of concentration in the degradation of Alizarin Yellow (AY)

Initial concentration of alizarin yellow was increased from 0.5 mg/L to 15.0 mg/L at pH 6.0. The dye solution was irradiated for a total length of time 2 hours. Further the degradation efficiency of alizarin yellow was obtained and presented as a function of alizarin yellow concentration and shown in Figure 3.2.1.4(a). Figure 3.2.1.4(a) revealed that increasing the initial concentration of alizarin yellow had caused significantly the percentage degradation of alizarin yellow for both photolytic and photocatalytic processes. Quantitatively, the removal efficiency of alizarin yellow was decreased from 64.68 to 15.52% with a corresponding increase in alizarin yellow concentration from 0.5 mg/L to 15.0 mg/L employing the nanocomposite Ag^0(NP)/TiO_2(A2) film.

The decrease in degradation efficiency at increased dye concentration was due to the revealing fact that the dye species have relatively lower possibility of contact at higher dye concentrations. Moreover, catalyst surface possessed relatively large number of available active sites at surface for lesser number of pollutant species at lower concentrations. Similar results were obtained elsewhere where increased in pollutant concentration was greatly hampered the removal efficiency and this was due to the scavenging effect (Lalhriatpuia *et al*., 2016; Nasseri *et al*., 2017). A similar decrease in the degradation of alizarin red S by the ZnS and cadmium doped ZnS nanoparticles were obtained and mentioned that at an increased concentration of alizarin red S enabled to aggregate dye molecules at the surface which screened the catalyst surface to interact with other dye molecules either with the holes or hydroxyl radicals. Therefore, reduces the percentage degradation of dye at an enhanced pollutant concentration (Jabeen *et al*., 2017).

Table 3.2.1.4(a): Effect of concentration in the photocatalytic degradation of alizarin yellow.

	% Removal				
	[Initial concentration of AY (mg/L)]				
	0.5	**1.0**	**5.0**	**10.0**	**15.0**
UV-A	13	11.1	4.5	0.2	0.1
Ag^0(NP)/TiO_2(A1)	54.9	44.5	29.6	14.7	11
Ag^0(NP)/TiO_2(A2)	64.68	52.3	35.35	20.1	15.52

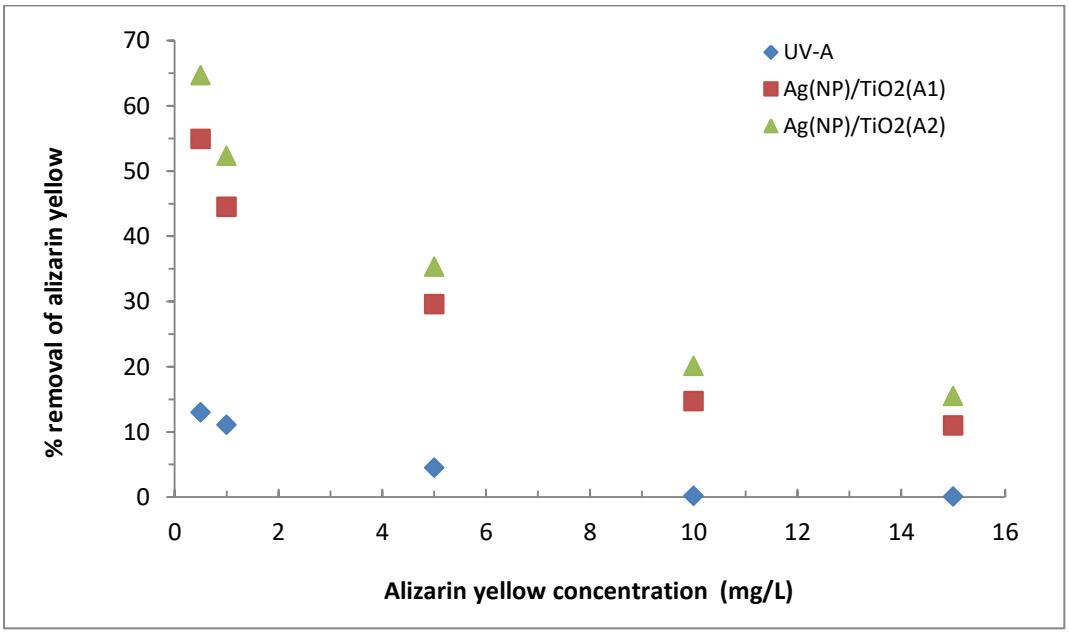

Figure 3.2.1.4(a): Effect of concentration in the photocatalytic degradation of alizarin yellow (AY) by using UV-A only, Ag^0(NP)/TiO_2(A1) and Ag^0(NP)/TiO_2(A2) thin films [pH: 6.0; Irradiation time: 2 hours; Temperature 25±1 ^{0}C].

Further, the concentration dependence degradation of alizarin yellow was also conducted using Au^0(NP)TiO_2(B1) and Au^0(NP)TiO_2(B2) thin films. The degradation process was studied by varying the alizarin yellow concentration from 0.5 to 15.0 (mg/L) at

a constant solution pH 6.0. The results of photocatalytic removal of alizarin yellow were presented in Table 3.2.1.4(b) and Figure 3.2.1.4(b). Similarly, the degradation trend of alizarin yellow by $Au^0(NP)TiO_2(B1)$ and $Au^0(NP)TiO_2(B2)$ photocatalysts was same as that of alizarin yellow by $Ag^0(NP)TiO_2(A1)$ and $Ag^0(NP)TiO_2(A2)$ photocatalysts. The increase in concentration of alizarin yellow inhibited the percentage removal substantially. It was further demonstrated that the pollutant molecules were increased significantly at higher initial concentration, though the content of free radicals that take part in decomposing the organic molecules were constant. This eventually reduced the percent degradation of dye at higher initial concentration (Caliskan *et al*., 2017). The photocatalyst $Au^0(NP)TiO_2(B2)$ showed higher degradation efficiency than the corresponding non-template thin film $Au^0(NP)TiO_2(B1)$, which in turn showed much higher degradation efficiency than the corresponding blank process using UV–A illumination only. Therefore, it was again confirmed that nanocomposite thin film had an enhanced catalytic activity at least in the degradation of alizarin yellow in aqueous media.

Table 3.2.1.4(b): Effect of pH in the photocatalytic degradation of alizarin yellow by using UV-A only, $Au^0(NP)TiO_2(B1)$ and $Au^0(NP)TiO_2(B2)$ thin films.

	% Removal				
	[Initial concentration of AY (mg/L)]				
	0.5	**1.0**	**5.0**	**10.0**	**15.0**
UV-A	13	11.1	4.5	0.2	0.1
$Au^0(NP)TiO_2(B1)$	64.5	54	36.7	23.8	16.9
$Au^0(NP)TiO_2(B2)$	71.11	58.66	38.56	25.13	18.87

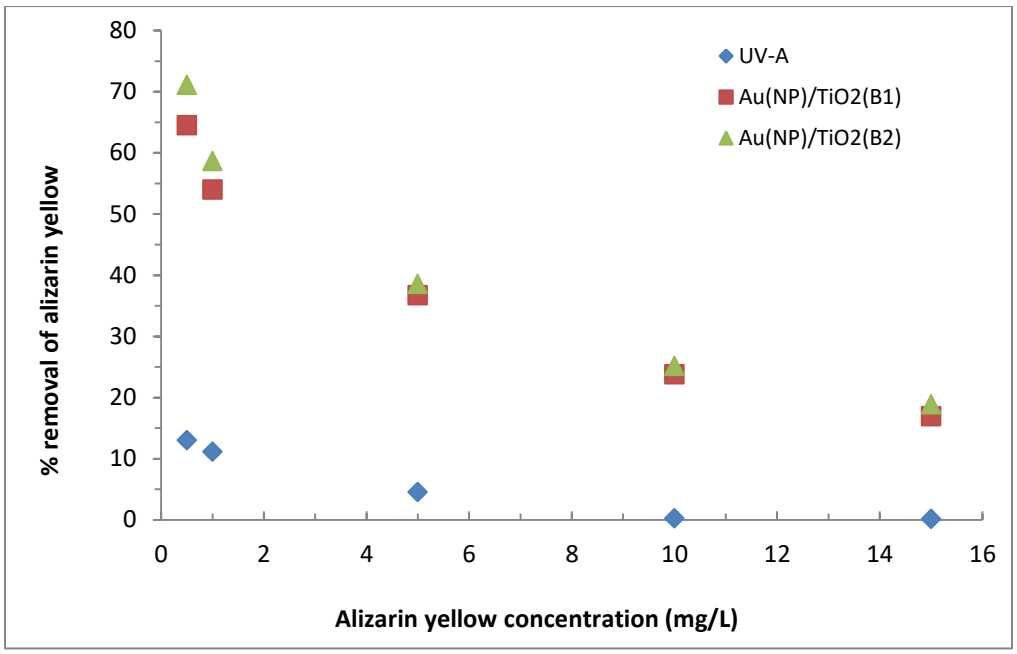

Figure 3.2.1.4(b): Effect of concentration in the photocatalytic degradation of alizarin yellow by using UV-A only, $Au^0(NP)/TiO_2(B1)$ and $Au^0(NP)/TiO_2(B2)$ thin films [pH: 6.0; Irradiation time: 2 hours; Temperature 25±1 ^{0}C].

3.2.1.5. Degradation Kinetics of Triclosan (TCS)

The time dependent degradation of triclosan under photolysis and photocatalytic studies were conducted in order to deduce the reaction kinetics involved and to obtain apparent rate constant values. The value of C_t/C_0 was presented graphically and returned in Figure 3.2.1.5(a) (inset) (where C_0 was the initial concentration of triclosan and C_t was the concentration of triclosan at time `t`). The Figure clearly demonstrated that a sharp decrease in degradation was observed in presence of thin films $Ag^0(NP)/TiO_2(A1)$ and $Ag^0(NP)/TiO_2(A2)$ after 2 hours irradiation (initial concentration of triclosan: 1.0 mg/L at pH: 6.0). The calculated C_t/C_0 values were 0.41, 0.52 and 0.80 for the $Ag^0(NP)/TiO_2(A2)$, $Ag^0(NP)/TiO_2(A1)$ and UV-A (blank) treatment, respectively. Further, significantly lower values of C_t/C_0 were obtained using the $Ag^0(NP)/TiO_2(A2)$ thin film comparing to the

Ag^0(NP)/TiO_2(A1) thin film. This indicated the affinity of the triclosan towards the thin film surface and enhanced photocatalytic degradation of triclosan at the surface.

Further, the kinetics of the triclosan degradation was represented using the known pseudo-first-order rate equation (Eq. 3.2.1.5(i)):

$$r = -\frac{d[TCS]}{dt} = k_{app}\left[k_{photolysis} + k_{photocatalysis}\right][TCS] = k_{app}\,[TCS] \quad \ldots (3.2.1.5(i))$$

where [TCS] represents to the concentration of triclosan and k_{app} is the pseudo-first-order rate constant. It was obvious that the k_{app} depended on the concentration of triclosan. Integration of equation 3.2.1.5(i) with the extreme conditions, i.e., at t = 0 the [TCS] = C_0. The equation 3.2.1.5(i) became:

$$LN\left(\frac{C_0}{C_t}\right) = k_{app} \cdot t \quad \ldots (3.2.1.5(ii))$$

The result obtained from a plot of the LN(C_0/C_t) against time `t` was presented graphically in Figure 3.2.1.5(a) (inset) with initial concentration of triclosan (1.0 mg/L) at pH 6.0. Besides, the pseudo-first-order rate constants (k_{app}) and R^2 values obtained for Ag^0(NP)/TiO_2(A2), Ag^0(NP)/TiO_2(A1) and UV-A only treatment were evaluated and results were presented in graphically in Figure 3.2.1.5(a) and Table 3.2.1.5. It was observed that the photodegradation of triclosan had reasonably fitted well to the pseudo-first-order kinetics using the Ag^0(NP)/TiO_2(A1) and Ag^0(NP)/TiO_2(A2) thin films (*cf.* Figure 3.2.1.5(a) and 3.2.1.5(a) (Insets; Linear and Non-linear fitting)). Further, the rate constant was increased with the decrease in triclosan concentration. Moreover, significantly low value of rate constant was recorded for the photolytic oxidation of triclosan than the photocatalytic oxidation. This reaffirmed the potential use of immobilized nanocomposites in the degradation of triclosan. The Ag^0(NP)/TiO_2(A2) thin film was found to be more efficient comparing to the Ag^0(NP)TiO_2(A1) thin film. This again confirmed the potential use of

template synthesis of thin film using the PEG as modifier. Similarly, the triclosan degradation by the electro-Fenton process showed to be the pseudo-first-order rate kinetics (Sires *et al*., 2007). Moreover, the pseudo-first order rate kinetics was demonstrated for the biological degradation triclosan in an activated sludge under the aerobic conditions (Mohamed and Mkhalid, 2015).

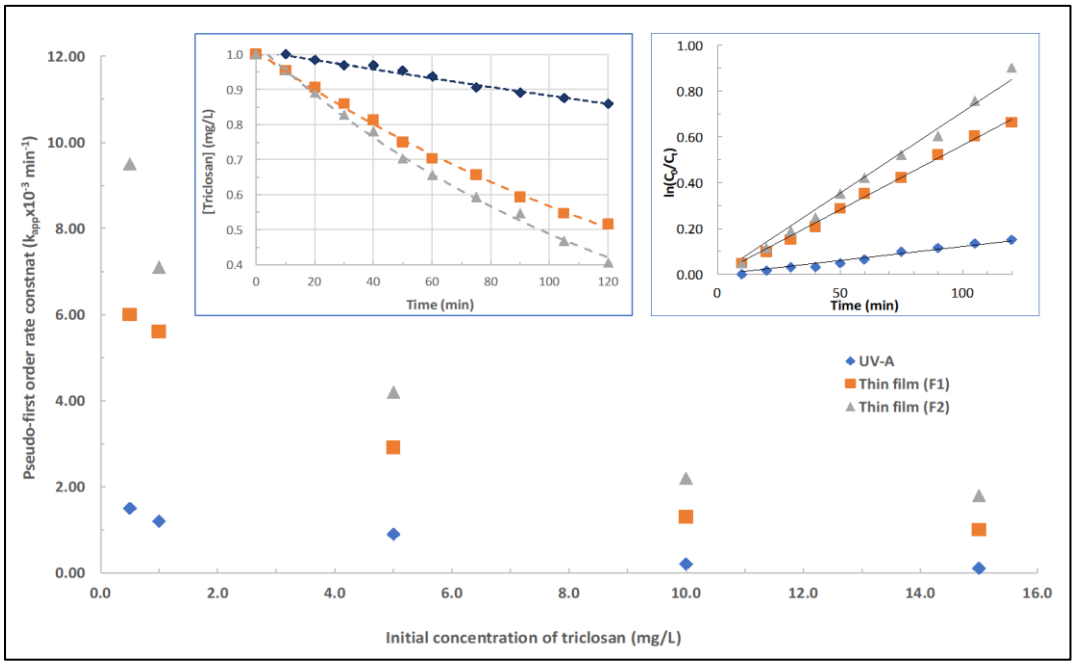

Figure 3.2.1.5(a): The pseudo-first-order rate constant as a function of initial concentration of triclosan under the photolytic and photocatalytic processes [Insets Linear and Non-linear fitting of data for the pseudo-first-order rate kinetics; Initial concentration of triclosan: 1.0 mg/L at pH: 6.0; Temperature: 25±1 ^{0}C; F1: Ag^0(NP)/TiO_2(A1); and F2: Ag^0(NP)/TiO_2(A2)].

Table 3.2.1.5: Kinetic data obtained for the degradation of triclosan using Ag^0(NP)/TiO_2(A1) and Ag^0(NP)/TiO_2(A2) thin film photocatalysts along with UV-A only photolysis at different initial triclosan concentrations.

	Pseudo-first order rate constant (k_{app}x10^{-3})/min				
	[Initial concentration of TCS (mg/L)]				
	0.5	**1.0**	**5.0**	**10.0**	**15.0**
UV-A only	1.6 (0.972)	1.7 (0.986)	0.9 (0.993)	0.2 (0.959)	0.1 (0.942)
Ag^0(NP)/TiO_2 (A1)	6 (0.973)	5.6 (0.997)	2.9 (0.934)	1.3 (0.986)	1 (0.996)
Ag^0(NP)/TiO_2 (A2)	9.7 (0.977)	7.1 (0.991)	4.1 (0.993)	2.2 (0.989)	1.8 (0.988)

R^2 values are given in parenthesis.

Further, the L-H (Langmuir-Hinshelwood) model was used to describe the dependence of the observed reaction rate on the initial solute concentrations (Turchi and Ollis, 1990). The derived equation (3.2.1.5(i)) was used to its linear form:

$$r_0 = \frac{k_r \cdot K \cdot C_0}{1 + K \cdot C_0} \quad \ldots(3.2.1.5(iii))$$

or

$$\frac{1}{r_0} = \frac{1}{K \cdot k_r} \cdot \frac{1}{C_0} + \frac{1}{k_r} \quad \ldots(3.2.1.5(iv))$$

where 'C_0' is the concentration of the triclosan at time 't', K is the constant related to adsorption and k_r is to the reaction properties of the substrate (triclosan), '$1/r_0$' is the dependent variable, '$1/C_0$' the independent variable, $1/k_r$ is the linear coefficient and ($1/(k_r . K)$) the slope of the straight line. Using the L-H equation, the adsorption constant and the rate constant were evaluated while plotting $1/r_0$ against $1/C_0$. A plot of $1/r_0$ against $1/C_0$ (Figure 3.2.1.5(b)) gave the L-H adsorption constant 'K' (L/mg) and the rate constant 'k_r'

(mg/L/min) for the degradation of triclosan by the two thin films Ag^0(NP)/TiO_2(A1) and Ag^0(NP)/TiO_2(A2). The results obtained for the k_r and K were found to be 0.0196 and 0.368 (R^2: 0.989; for Ag^0(NP)/TiO_2(A1) sample) and 0.028 and 0.398 (R^2: 0.988; for Ag^0(NP)/TiO_2(A2) sample), respectively, in the oxidation of triclosan. The values of R^2 obtained for Ag^0(NP)/TiO_2(A1) and Ag^0(NP)/TiO_2(A2) thin films showed that the L-H kinetics was fitted reasonably well to the photocatalytic degradation of triclosan.

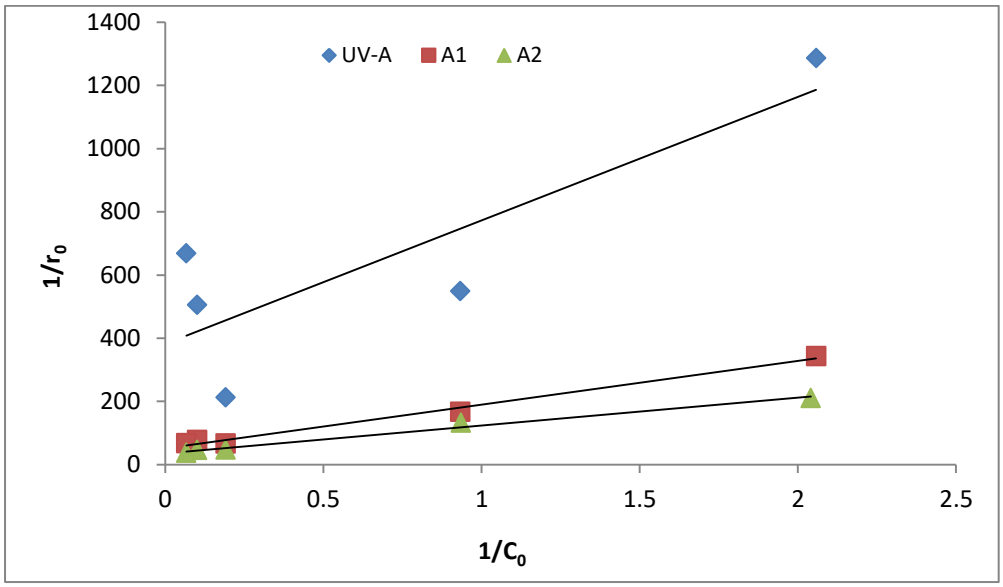

Figure 3.2.1.5(b): Langmuir-Hinshelwood plot for the photocatalytic degradation of triclosan using A1: Ag^0(NP)/TiO_2(A1) and A2: Ag^0(NP)/TiO_2(A2) photocatalytic thin films and UV-A only photolysis [TCS concentration: 0.5 – 15.0 mg/L; pH: 6.0; Temperature: 25±1 ^{0}C].

3.2.1.6. Degradation Kinetics of Alizarin Yellow (AY)

The time dependent degradation of alizarin yellow under photolysis and photocatalytic studies were conducted in order to deduce the reaction kinetics involved and to obtain apparent rate constant values. The value of C_t/C_0 was presented graphically in Figure 3.2.1.6(a) (Inset) for the degradation of alizarin yellow (initial concentration of AY: 1.0 mg/L at pH~6.0) as a function of time (where C_0 was initial concentration of AY and C_t

was the concentration of AY at time `t`). The Figure clearly indicated a sharp decrease of alizarin yellow degradation was occurred with respect to time in presence of thin films Ag^0(NP)/TiO_2(A1) and Ag^0(NP)/TiO_2(A2) whereas the UV-A only irradiation showed almost no degradation of alizarin yellow within 2 hours of irradiation. The computed C_t/C_0 values at the end of 2 hours of irradiations were 0.89, 0.56 and 0.48 for the UV-A only, Ag^0(NP)/TiO_2(A1) and Ag^0(NP)/TiO_2(A2) thin films, respectively. Relatively, a lower value of C_t/C_0 was obtained using the Ag^0(NP)/TiO_2(A2) thin film than the Ag^0(NP)/TiO_2(A1) thin film, this again indicated the higher efficiency of the PEG template thin films for the degradation of alizarin yellow from aqueous solution.

The pseudo-first-order rate equation for the degradation of alizarin yellow could be represented as:

$$r = -\frac{d[AY]}{dt} = k_{app}\left[k_{photolysis} + k_{photocatalysis}\right][AY] = k_{app}\,[AY] \quad \ldots \quad (3.2.1.6(i))$$

where [AY] represents the concentration of alizarin yellow and k_{app} is the pseudo-first-order rate constant. It was obvious that the k_{app} depended on the concentration of alizarin yellow. Integration of equation 3.2.1.6(i) with the extreme conditions, i.e., at t = 0 the [AY] = C_0. The equation (3.2.1.6(i)) could be written as:

$$LN\left(\frac{C_0}{C_t}\right) = k_{app} \cdot t \qquad \ldots(3.2.1.6(ii))$$

A linear relationship between alizarin yellow concentration and irradiation time were obtained plotting LN(C_0/C_t) against time `t` and the results obtained were presented in Figure 3.2.1.6(a) (inset) also non-linear fitting was conducted and returned in Figure 3.2.1.6(a) (inset) having the initial concentration of 1.0 mg/L at pH 6.0. Besides, the pseudo-first-order rate constants (k_{app}) and R^2 values obtained for Ag^0(NP)/TiO_2(A2), Ag^0(NP)/TiO_2(A1) and UV-A only treatment were evaluated and results were presented in

Table 3.2.1.6(a) and Figure 3.2.1.6(a). It was clear from the Table that the photodegradation of alizarin yellow was reasonably fitted well to the pseudo-first-order kinetics using the Ag^0(NP)/TiO_2(A1) and Ag^0(NP)/TiO_2(A2) thin films. Besides, the Ag^0(NP)/TiO_2(A2) thin film was found to be more efficient comparing to the Ag^0(NP)/TiO_2(A1) thin film which again indicated the potential use of template synthesis of thin films using the PEG as filler media. Similarly, the Nano-TiO_2 supported on latex paint film showed the pseudo-first-order kinetics in the photocatalytic removal of ammonia (Geng *et al.*, 2008). The oxidative removal of methylene blue using the P25 titanium dioxide showed pseudo-first-order kinetics and the experimental data was fitted well to the model at sufficient accuracy (Xu *et al.*, 2014).

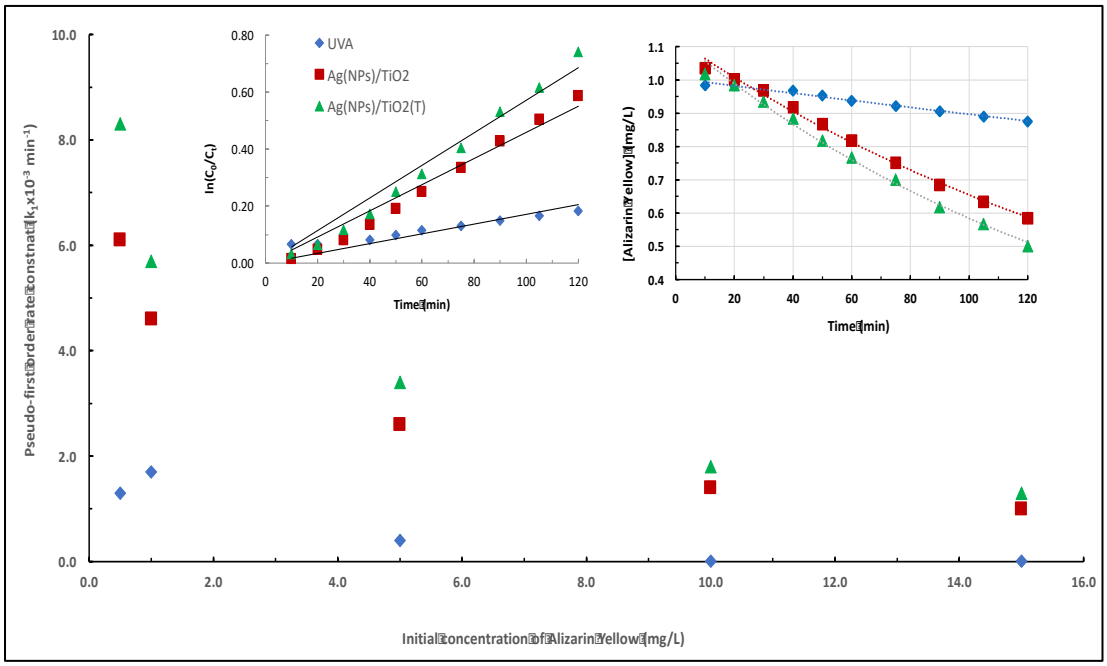

Figure 3.2.1.6(a): Kinetics of photocatalytic degradation of alizarin yellow as a function of time using Ag^0(NPs)/TiO_2: Ag^0(NP)/TiO_2(A1); and Ag^0(NPs)/TiO_2(T): Ag^0(NP)/TiO_2(A2) thin film photocatalysts along with simple photolysis [AY concentration: 1.0 mg/L; pH: 6.0; Temperature: 25±1 ^{0}C].

Table 3.2.1.6(a): Kinetic data obtained for the degradation of alizarin yellow using Ag^0(NP)/TiO_2(A1) and Ag^0(NP)/TiO_2(A2) thin film photocatalysts along with UV-A only photolysis at different initial AY concentrations.

	Pseudo-first order rate constant (k_{app}x10^{-3})/min				
	[Initial concentration of AY (mg/L)]				
	0.5	**1.0**	**5.0**	**10.0**	**15.0**
UV-A only	1.3 (0.937)	0.9 (0.933)	0.4 (0.966)	0 (0.441)	0 (0.403)
Ag^0(NP)/TiO_2 (A1)	6.1 (0.969)	4.6 (0.971)	2.6 (0.921)	1.4 (0.984)	1 (0.995)
Ag^0(NP)/TiO_2 (A2)	8.3 (0.991)	5.7 (0.975)	3.4 (0.992)	1.8 (0.991)	1.3 (0.982)

R^2 values are given in parenthesis.

The photocatalytic degradation of alizarin yellow was modelled with the Langmuir-Hinshelwood (L-H) model to its linear form equation, equation 3.2.1.6(i) could be written as:

$$r_0 = \frac{k_r \cdot K \cdot C_0}{1 + K \cdot C_0} \quad \ldots(3.2.1.6(iii))$$

or

$$\frac{1}{r_0} = \frac{1}{K \cdot k_r} \cdot \frac{1}{C_0} + \frac{1}{k_r} \quad \ldots(3.2.1.6(iv))$$

where 'C_0' is the concentration of alizarin yellow at time '*t*', *K* is the constant related to adsorption and k_r is to the reaction properties of the substrate (alizarin yellow), '$1/r_0$' is the dependent variable, '$1/C_0$' the independent variable, $1/k_r$ is the linear coefficient and ($1/(k_r . K)$) the slope of the straight line. Using the L-H equation, the adsorption constant and the rate constant were evaluated while plotting $1/r_0$ against $1/C_0$. The values of *K* and k_r were determined from the slope and intercept of these plots presented graphically in Figure

3.2.1.6(b). The results obtained for the k_r (mg/L/min) and K (L/mg) were found to be 0.017 and 0.417 (R^2: 0.990; for Ag^0(NP)/TiO_2(A1) sample) and 0.021 and 0.460 (R^2: 0.972; for Ag^0(NP)/TiO_2(A2) sample), respectively, in the oxidation of alizarin yellow. Thus, the L-H kinetic was reasonably fitted well to the photocatalytic degradation of alizarin yellow using the thin film photocatalysts.

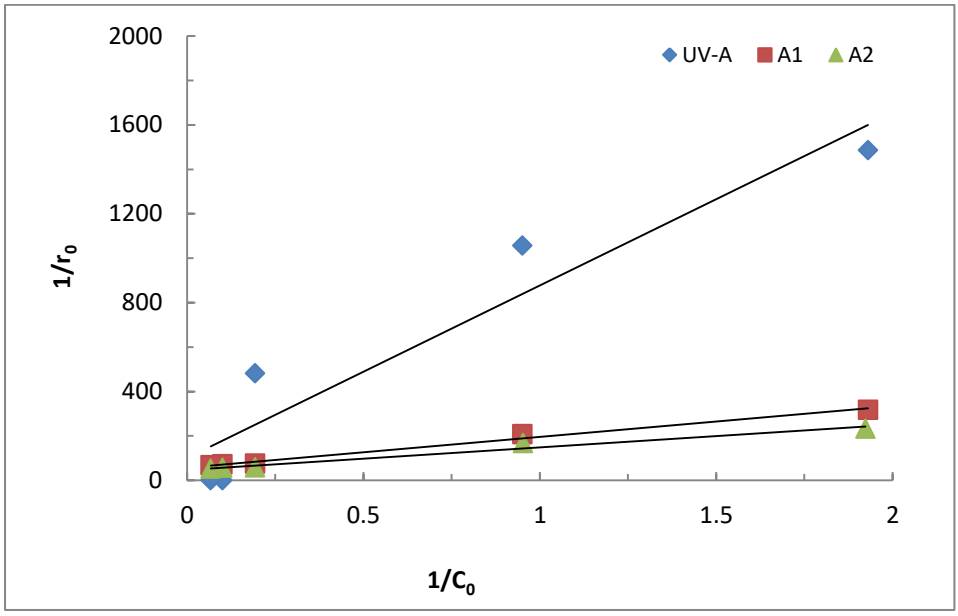

Figure 3.2.1.6(b): Langmuir-Hinshelwood plot for the photocatalytic degradation of alizarin yellow using A1: Ag^0(NP)/TiO_2(A1) and A2: Ag^0(NP)/TiO_2(A2) photocatalytic thin films and UV-A only photolysis [AY concentration: 0.5 – 15.0 mg/L; pH: 6.0; Temperature: 25±1 ^{0}C].

On the other hand, the degradation kinetics of alizarin yellow using Au^0(NP)/TiO_2(B1) and Au^0(NP)/TiO_2(B2) photocatalysts were also established. The value of C_t/C_0 was presented graphically in Figure 3.2.1.6(c) (Inset) (initial concentration of AY: 1.0 mg/L at pH~6.0) as a function of time (where C_0 is initial concentration of AY and C_t is the concentration of AY at time `t`). The k_{app} (pseudo-first-order rate constant) values were calculated for all studied concentrations and presented in Figure 3.2.1.6(c) and Table

3.2.1.6(b). A decrease in alizarin yellow concentration greatly enhanced the k_{app} values. Further, it was interesting to observe that the k_{app} value for the catalytic (i.e., Au^0(NP)/TiO_2(B1) and Au^0(NP)/TiO_2(B2) photocatalysts) removal of alizarin yellow was found relatively higher than photolytic process carried by the UV-A light. This further confirmed the greater applicability of catalyst in the oxidative removal of alizarin yellow. Similarly, the Au^0(NP)/TiO_2(B2) thin film was found to be more efficient comparing to the Au^0(NP)/TiO_2(B1) thin film.

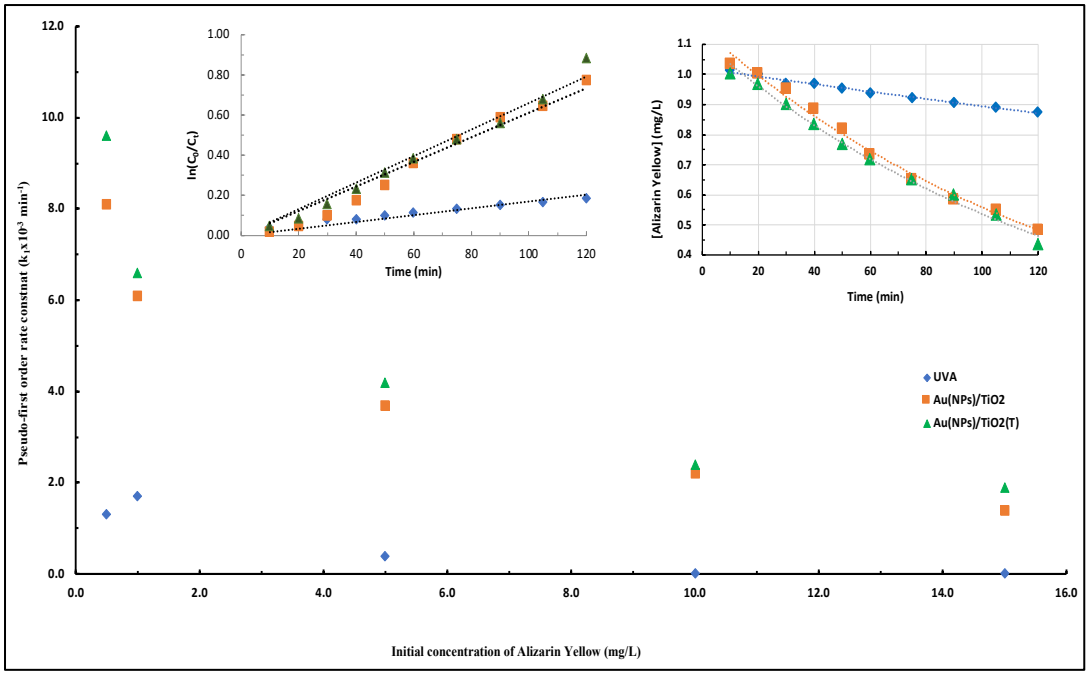

Figure 3.2.1.6(c): The pseudo-first order rate constant values for various concentrations of alizarin yellow for photolytic and photocatalytic operations [Insets Linear and Non-linear fitting of time dependence results for the pseudo-first order rate kinetics [Initial concentration of alizarin yellow: 1.0 mg/L at pH: 6.0; Temperature: 25±1 ^{0}C]. Au^0(NPs)/TiO_2: Au^0(NP)/TiO_2(B1); and Au^0(NPs)/TiO_2(T): Au^0(NP)TiO_2(B2) photocatalytic thin films.

Table 3.2.1.6(b): Kinetic data obtained for the degradation of alizarin yellow using Au^0(NP)/TiO_2(B1) and Au^0(NP)/TiO_2(B2) thin film photocatalysts along with UV-A only photolysis at different initial AY concentrations.

	Pseudo-first order rate constant ($k_{app}x10^3$)/min				
	[Initial concentration of AY (mg/L)]				
	0.5	**1.0**	**5.0**	**10.0**	**15.0**
UV-A only	1.3 (0.937)	0.9 (0.933)	0.4 (0.966)	0 (0.441)	0 (0.403)
Au^0(NP)/TiO_2 (B1)	8.1 (0.983)	6.1 (0.966)	3.7 (0.989)	2.2 (0.994)	1.4 (0.991)
Au^0(NP)/TiO_2 (B2)	9.6 (0.987)	6.6 (0.979)	4.2 (0.989)	2.4 (0.997)	1.9 (0.984)

R^2 values are given in parenthesis.

The photocatalytic degradations of alizarin yellow by using Au^0(NP)/TiO_2(B1) and Au^0(NP)/TiO_2(B2) thin films was again modelled with the Langmuir-Hinshelwood (L-H) model to its linear form equation. Using the L-H equation, the adsorption constant and the rate constant were also evaluated. The values of K and k_r were determined from the slope and intercept of these plots presented graphically in Figure 3.2.1.6(d). The results obtained for the k_r (mg/L/min) and K (L/mg) were found to be 0.026 and 0.279 (R^2: 0.988; for Au^0(NP)/TiO_2(B1) sample) and 0.029 and 0.335 (R^2: 0.969; for Au^0(NP)/TiO_2(B2) sample), respectively, in the oxidation of alizarin yellow. Thus, the L-H kinetic was reasonably fitted well to the photocatalytic degradation of alizarin yellow using the thin film photocatalysts.

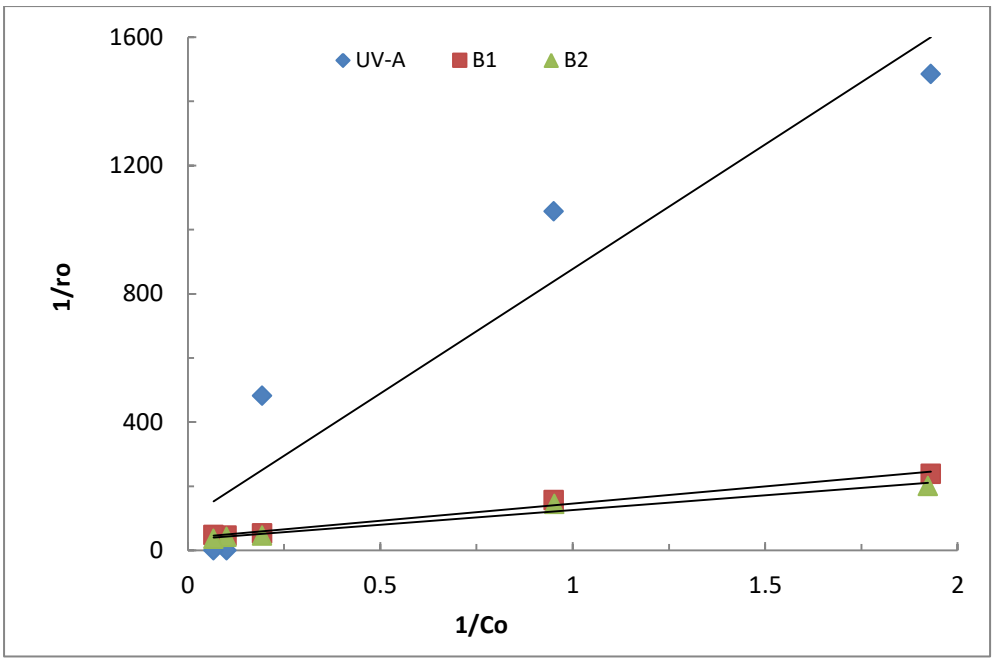

Figure 3.2.1.6(d): Langmuir-Hinshelwood plot for the photocatalytic degradation of alizarin yellow using B1: Au^0(NP)/TiO_2(B1) and B2: Au^0(NP)/TiO_2(B2) photocatalytic thin films and UV-A only photolysis [AY concentration: 0.5 – 15.0 mg/L; pH: 6.0; Temperature: 25±1 ^{0}C].

3.2.1.7. Effect of Interfering Ions on Triclosan Removal

Considerable amount of inorganic anions such as chloride, nitrate, sulphate, carbonate, etc., were present in wastewater. These ions changed the ionic strength of the medium and hence affected the catalytic activity of the photocatalyst. Consequently, the effect of several interfering ions (50.0 mg/L), *viz*., cadmium nitrate, copper sulphate, zinc chloride, sodium chloride, sodium nitrate, sodium nitrite, glycine, oxalic acid and EDTA in the photocatalytic degradation of triclosan from aqueous solution were evaluated using the Ag^0(NP)/TiO_2(A2) photocatalyst. The samples were irradiated for 2 hours and the initial concentration of triclosan was kept constant to 5.0 mg/L at pH 6. The triclosan concentration was obtained with the UV-Vis spectrophotometer. The percent removal of triclosan was presented as a function of interfering ions and returned in Figure 3.2.1.7(a). The Figure

clearly showed that the degradation of triclosan was inhibited at different extent in presence of different interfering ions. However, it was interesting to note that the presence of EDTA, $NaNO_2$, $ZnCl_2$ and Oxalic acid had caused to suppress significantly the degradation of triclosan. The presence of other ions affected to a lesser extent in the photocatalytic degradation of triclosan. The order of inhibition caused by these interfering ions were found to be $NaNO_2$ > Oxalic acid > $ZnCl_2$ > EDTA > Glycine > NaCl > $Cd(NO_3)_2$ > $CuSO_4$ > $NaNO_3$. Photocatalytic degradation were predominantly driven by the highly oxidizing species, *viz.*, photogenerated valence band holes (h^+) or hydroxyl radicals ($^{\bullet}OH$). EDTA was known to eliminate the h^+ significantly in TiO_2 photocatalyst (Jia *et al*., 2017). Oxalate ion ($C_2O_4^{2-}$) was reported as a widely recognized h^+ eradicator and it was used as a probe species to determine the occurrence of direct h^+ oxidation in the photocatalytic system (Yap and Lim, 2011). Therefore, these results clearly indicated that hole (h^+) radical either free or surface trapped acted as one of the oxidising species for the degradation of triclosan from aqueous solution.

It is important to analyse the radical induced photocatalytic degradation of triclosan since they altered the kinetic profile of the reaction, providing information about the participation of different reactive oxidising species. Therefore, the effect of scavengers in the degradation of triclosan was studied using the variety of scavengers used to scavenge the reactive oxidising species, *viz*., h^+, $^{\bullet}OH$ or $O_2^{\bullet-}$. The 2-propanol and HCO_3^- were reported to be the good scavengers of the $^{\bullet}OH$ radical (Xu *et al*., 2015). Sodium azide (NaN_3) was known to scavenge the singlet oxygen ($^1O_2$) produced readily by the interaction of superoxide radical and photogenerated holes. The singlet oxygen was highly reactive species that degraded pollutants readily (Li *et al*., 2011). Hence, the degradation of triclosan (5.0 mg/L at pH 6) in presence of scavengers, *viz*., 2-propanol, sodium azide and sodium bicarbonate (1000.0 mg/L) was studied and results were shown in Figure 3.2.1.7(b). It was

evident from the Figure that in presence of 2-propanol and sodium bicarbonate the percentage removal of triclosan was significantly inhibited that clearly pointed that the $^{\bullet}OH$ radical was greatly involved in the degradation process. On the other hand, the scavenger, 2-propanol significantly suppressed the catalytic activity of the thin film $Ag^0(NP)/TiO_2(A2)$ since a marked decrease in percent removal of triclosan was observed. The presence of sodium azide caused to suppress the degradation of triclosan which indicated that singlet oxygen was also greatly involved in the degradation process. The results clearly indicated that these radicals were scavenging greatly the involved radical species and the removal of triclosan was greatly inhibited.

3.2.1.7.1. Mechanism of Degradation

Overall, the study therefore explained that the absorption of UV-A radiations by the $Ag^0(NP)/TiO_2(A2)$ photocatalyst caused to excite the electrons from the valence band to conduction band in the photocatalyst $Ag^0(NP)/TiO_2(A2)$ where the silver nanoparticles trapped efficiently the excited electrons at the conduction band. This eventually restricted the recombination of electron/hole pairs in the photocatalyst $Ag^0(NP)TiO_2(A2)$. The trapped electrons were able to generate the superoxide radical followed by the formation of $^{\bullet}OH$ radicals. On the other hand, the hole was created in the valence band that interacted with the O_2 molecule and produced the $O_2^{\bullet}$ radical species. This resulted the formation of $^{\bullet}OH$ radicals. Therefore, the reactive radical species were predominantly involved in the degradation of triclosan.

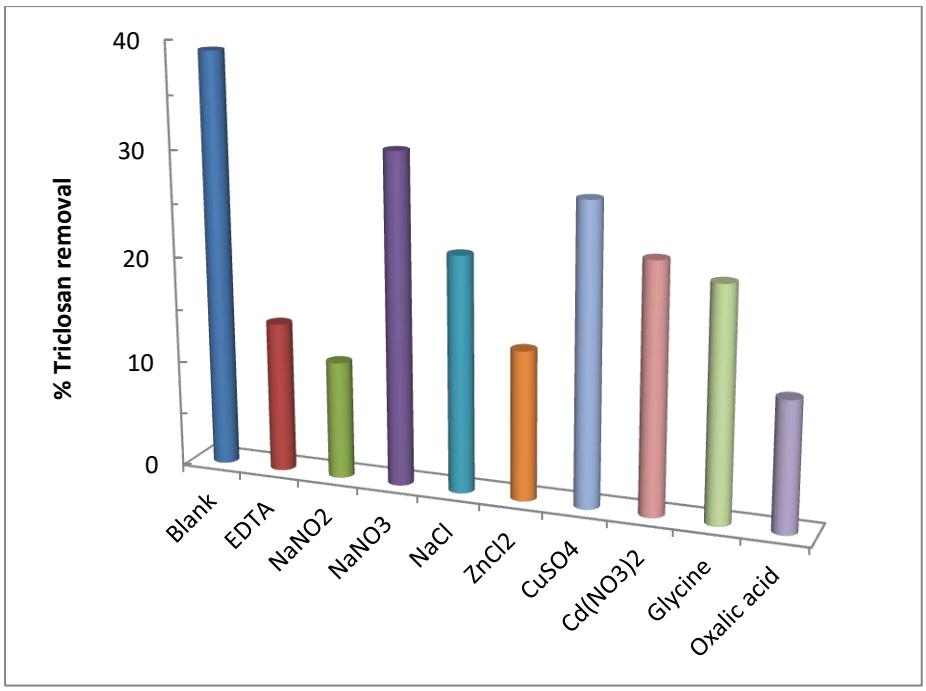

Figure 3.2.1.7(a): Photocatalytic degradation of triclosan in presence of interfering ions using Ag^0(NP)/TiO_2(A2) thin film [TCS concentration 5.0 mg/L; Ion concentration: 50.0 mg/L; pH: 6.0; Temperature: 25±1 ^{0}C].

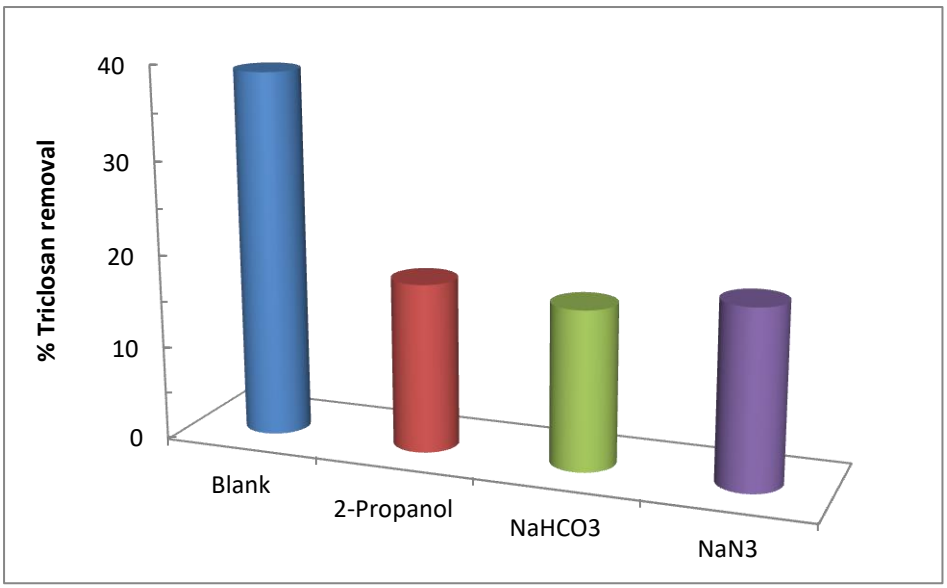

Figure 3.2.1.7(b): Effect of scavengers in the photocatalytic degradation of triclosan using the Ag^0(NP)/TiO_2(A2) thin film [TCS concentration: 5.0 mg/L; Scavenger concentration: 1000.0 mg/L; pH: 6.0; Temperature: 25±1 ^{0}C].

3.2.1.8. Effect of Interfering Ions on Alizarin Yellow (AY) Removal

The presence of co-existing ions enabled to simulate, partially, the treatment to the real matrix samples. Therefore, the experiments were conducted to obtain the photocatalytic removal of alizarin yellow in presence of several co-existing ions, *viz*., sodium chloride, sodium nitrite, sodium nitrate, copper sulphate, cadmium nitrate, zinc chloride, glycine, oxalic acid and EDTA. The $Ag^0(NP)TiO_2$(A2) thin film photocatalyst was used in the degradation process. The concentration of alizarin yellow was kept constant to 5.0 mg/L at pH 6.0 and the interfering ions concentration was kept constant to 50.0 mg/L. Further, the removal of alizarin yellow in presence of these co-existing ions was shown in Figure 3.2.1.8(a). The Figure showed that the presence of these ions affected the removal of alizarin yellow to a varied extent. However, a marked decrease in removal efficiency was observed in presence of $CuSO_4$, glycine and EDTA. However, the presence of other ions affected the removal of alizarin yellow to the lesser extent. The order of inhibition caused by the presence of these co-existing ions are: $CuSO_4$ > glycine > EDTA > NaCl > $NaNO_3$ > $ZnCl_2$ > $NaNO_2$ > oxalic acid > $Cd(NO_3)_2$, respectively.

3.2.1.8.1. Degradation Mechanism

Anatase TiO_2 possessed band gap of 3.2 eV and that requires photon of substantial energy, i.e., UV light to excite electrons from valence band (VB) to conduction band (CB) enabling to produce the electron/hole (e^-/h^+) pairs. These pairs initiate virtually the oxidation or reduction processes onto the surface of photocatalyst via the formation of radical species, *viz*., $^{\bullet}OH$, H_2O_2 or $O_2^{\bullet-}$ in presence of water and oxygen (Mohamed and Mkhalid, 2015). However, the radical formation is restricted to a greater extent with the fast recombination of pairs. On the other hand, the presence of Ag-nanoparticles induced useful catalytic properties. It was reported that by the absorption of photons, the nanoparticles

produces a localized surface plasmon resonance (LSPR) (de Souza and Corio, 2013; Nogawa *et al*., 2012). The LSPR characterized the absorption of light in the visible region. Hence, the Ag-nanoparticles enhanced the local field energy with the absorption of visible radiations and lifted electron from the VB to CB. This eventually enabled to enhance the photocatalytic or energy conversion processes (Lu *et al*., 2012; Linic *et al*., 2011).

Further, the radical scavengers, *viz.*, 2-propanol or HCO_3^- are known to scavenge the $^{\bullet}OH$ radicals (Lalhriatpuia *et al*., 2015; Xu *et al*., 2015). The EDTA molecule causes to inhibit significantly the formation of h^+ in TiO_2 photocatalyst (Jia *et al*., 2017). Similarly the sodium azide (NaN_3) scavenges singlet oxygen which is generated due to interaction of superoxide radical and photo generated holes. The singlet oxygen is known to be highly reactive species that readily decomposes the organics in water media (Barka *et al*., 2010). Hence, the photocatalytic degradation of alizarin yellow (5.0 mg/L at pH 6.0) in presence of 2-propanol, HCO_3^- and sodium azide (1000.0 mg/L) was conducted. The nanocomposite Ag^0(NP)/TiO_2(A2) disk was used as catalyst. The removal efficiency of alizarin yellow was shown in Figure 3.2.1.8(b). The Figure indicated that the presence of these scavengers, *viz.*, 2-propanol, sodium azide and sodium bicarbonate along with the EDTA (studied before) showed a marked decrease in the percentage degradation of alizarin yellow from aqueous solutions. Among these scavengers, the sodium bicarbonate and EDTA caused significantly to suppress the degradation of alizarin yellow. These results, therefore, showed that the degradation process take place predominantly by the $^{\bullet}OH$ radicals. Moreover, the holes were involved in generating the $^{\bullet}OH$ radicals that synergised the oxidation of alizarin yellow. The singlet oxygen was partly taking part in the degradation mechanism since the removal of alizarin yellow was decreased to some extent in presence of sodium azide.

Therefore, based on these studies, the photocatalytic degradation of alizarin yellow followed two different ways. UV-A (λ=360 nm) photons excited e^- from valence band to conduction band in the titanium dioxide solid and the Ag(NPs) trapped excited electrons at conduction band. Therefore, this inhibited the e^-/h^+ pairs recombination. Further, e^- trapped around conduction band caused to produce the superoxide radical and hence the generation of hydroxyl radicals. On the hand, hole created at VB, interacted with the available O_2 and resulted the generation of $O_2^{\bullet}$. This eventually again produced the $^{\bullet}OH$. These hydroxyl radical species were taking part in the oxidative process. Additionally, Ag(NPs) that absorbed the UV-A radiations and generated local electromagnetic field. This LSPR resulted the excitation of electron in semiconductor titanium dioxide and hence, the formation of e^-/h^+. This further generated the $^{\bullet}OH$ that simultaneously involved in oxidative removal of alizarin yellow.

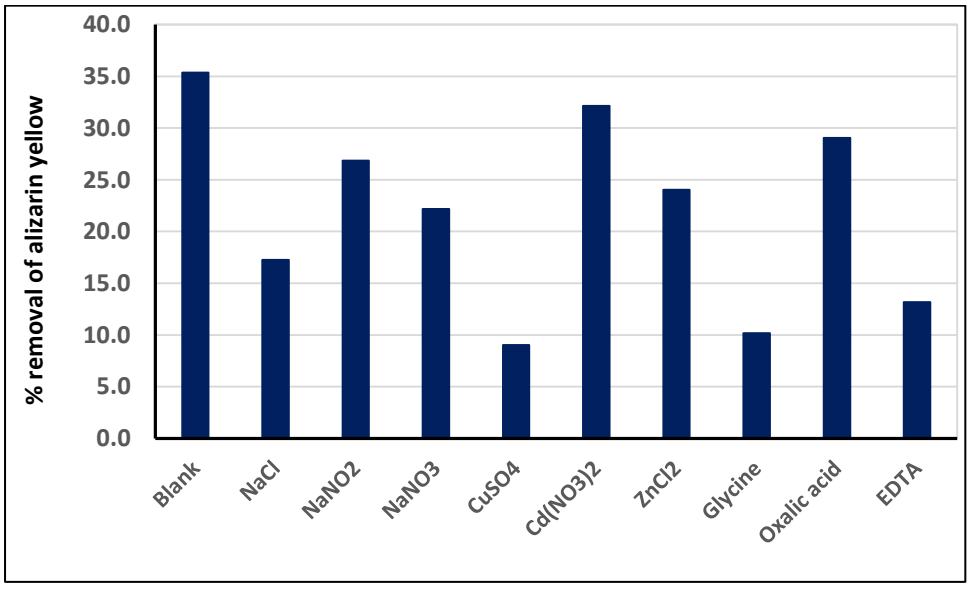

Figure 3.2.1.8(a): Photocatalytic degradation of AY in presence of interfering ions using Ag^0(NP)/TiO_2(A2) thin film catalyst [AY concentration: 5.0 mg/L; Co-existing ion concentration: 50.0 mg/L; pH: 6.0; Temperature: 25±1 ^{0}C].

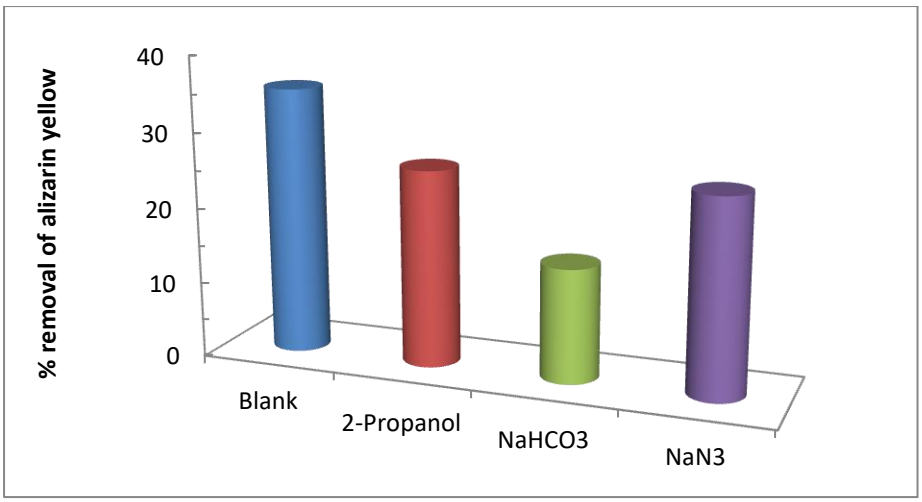

Figure 3.2.1.8(b): Effect of scavengers in the photocatalytic degradation of AY using the Ag^0(NP)/TiO_2(A2) thin film catalyst [AY concentration: 5.0mg/L; Scavenger concentration: 1000.0 mg/L; pH: 6.0; Temperature: 25±1 ^{0}C].

Further, the effect of co-existing ions on alizarin yellow degradation was studied using photocatalyst Au^0(NP)/TiO_2(B2). The concentration of alizarin yellow was kept constant to 5.0 mg/L at pH 6.0 and the co-existing ions concentration was kept constant to 50.0 mg/L. The removal of alizarin yellow in presence of these co-ions was shown in Figure 3.2.1.8(c). The order of inhibition in presence of these co-existing ions was: $ZnCl_2$ < $NaNO_2$ < $Cd(NO_3)_2$ < NaCl < oxalic acid < $NaNO_3$ < Glycine < $CuSO_4$ < EDTA, respectively. Results indicated that a marked decrease in the removal efficiency of alizarin yellow was occurred in presence of EDTA. This suggested that the hole (h^+) has acted as one of the oxidising species in the degradation of alizarin yellow from aqueous solution.

The degradation of alizarin yellow (5.0 mg/L at pH: 6.0) was also studied in presence of scavenger species, *viz*., 2-propanol, $NaHCO_3$ and sodium azide (1000.0 mg/L) employing Au^0(NP)TiO_2(B2) photocatalyst. The degradation of alizarin yellow in presence of these scavengers was shown in Figure 3.2.1.8(d). The Figure indicated that the presence of these scavengers affected significantly the percentage removal of alizarin yellow. Among these scavengers, EDTA and NaN_3 suppressed significantly the degradation of alizarin

yellow. These results, therefore, inferred that the holes were involved in generating the $^{\bullet}OH$ radicals that caused to oxidize the alizarin yellow. Similarly, the singlet oxygen was partly taking part in the degradation pathway. Additionally, the decrease in percentage removal of alizarin yellow in presence of 2-propanol or HCO_3^- indicated the direct involvement of $^{\bullet}OH$ radical in the degradation of alizarin yellow.

Therefore, the photocatalytic removal of alizarin yellow by nanocomposite Au^0(NP)/TiO_2(B2) thin film was proposed in two different mechanistic pathways. The UV-A (λ=360 nm) photons excited the electrons from valence band to conduction band in titanium dioxide. The Au(NPs) trapped the excited electron around conduction band. Hence, this restricted the possibility of recombination of e^-/h^+ in TiO_2. The trapped electron underwent to form superoxide radical and hence the generation of $^{\bullet}OH$. On the other hand, h^+ which was formed in the valence band, combined with the O_2 and generates the $O_2^{\bullet}$. This again produced the $^{\bullet}OH$. Therefore, the reactive $^{\bullet}OH$ radicals were, perhaps, involved in the degradation of alizarin yellow. Moreover, the Au(NPs) absorbs photons energy in the UV-A region that generated local electromagnetic field. This caused local excitation of electrons in semiconductor titanium dioxide and hence, the formation of e^-/h^+ pairs. This further generated hydroxyl radicals and simultaneously involved in the oxidative degradation of alizarin yellow.

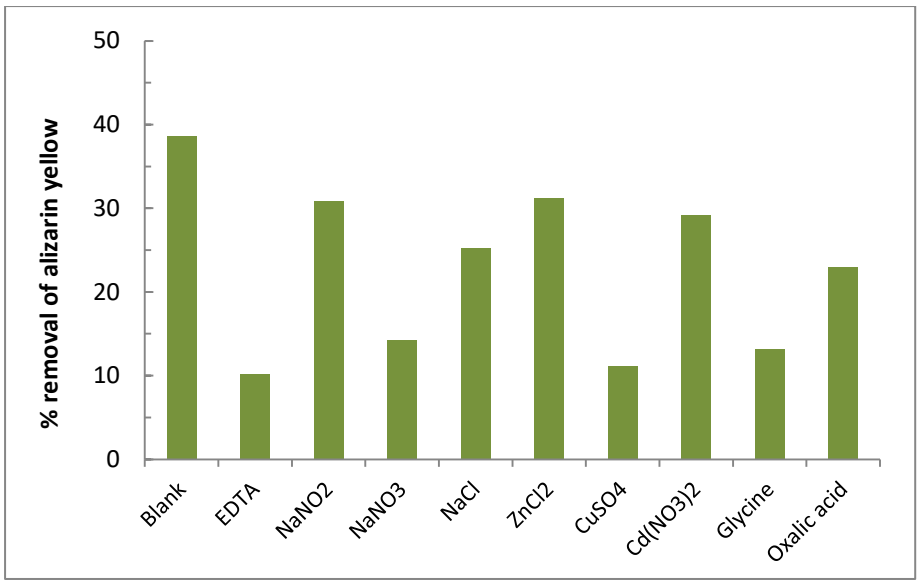

Figure 3.2.1.8(c): Photocatalytic degradation of alizarin yellow in presence of interfering ions using Au^0(NP)/TiO_2(B2) thin film catalyst [AY concentration: 5.0 mg/L; Co-existing ion concentration: 50.0 mg/L; pH: 6.0; Temperature: 25±1 ^{0}C].

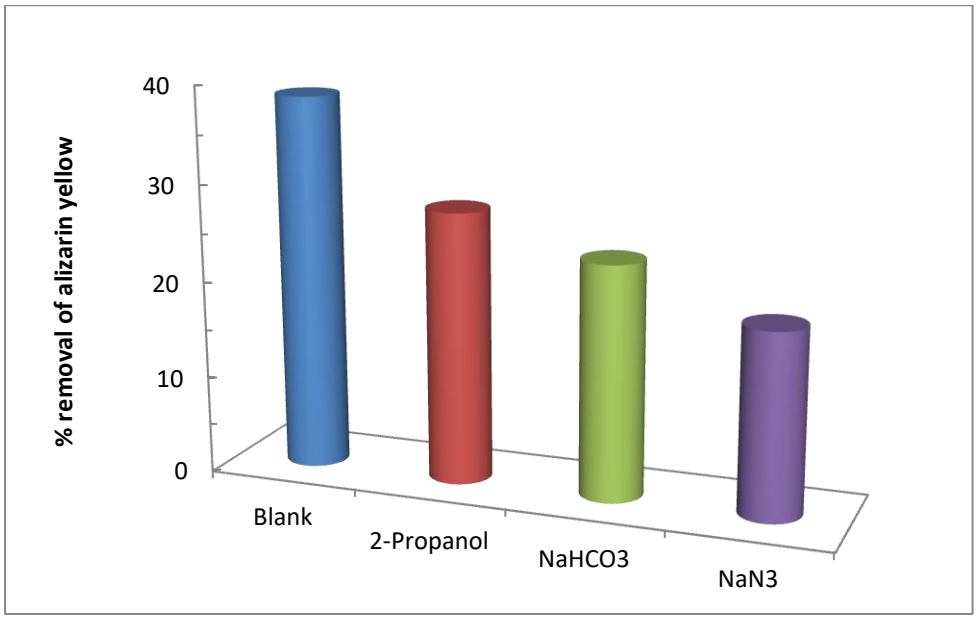

Figure 3.2.1.8(d): Effect of scavengers in the photocatalytic degradation of alizarin yellow using the Au^0(NP)/TiO_2(B2) thin film catalyst [AY concentration: 5.0 mg/L; Scavenger concentration: 1000.0 mg/L; pH: 6.0; Temperature: 25±1 ^{0}C].

3.2.1.9. Mineralization of Triclosan

The essential feature of photocatalytic degradation of pollutant is the actual mineralization of pollutant species from aqueous solutions. Therefore, the NPOC (Non-Purgeable Organic Carbon) data was collected for the treated triclosan samples. The mineralization of triclosan was studied varying the triclosan concentration from 0.5 to 15.0 mg/L at constant pH 6.0 employing the UV-A only, Ag^0(NP)/TiO_2(A1) and Ag^0(NP)/TiO_2(A2) thin film catalyst. The results were collected after the 2 hours of photo-irradiation. The percent of NPOC removal as a function of triclosan concentration was computed and presented in Figure 3.2.1.9(a) and also shown in Table 3.2.1.9(a). The results clearly showed that increasing the concentration of triclosan a sharp decrease in NPOC was observed. Quantitatively, increasing the concentration of triclosan from 0.5 to 15.0 mg/L the percent of NPOC was decreased from 68.74 to 20.12% (using Ag^0(NP)/TiO_2(A2) thin films); 53.30 to 12.04% (using Ag^0(NP)/TiO_2(A1) thin films) and 21.66 to 5.74% (using UV-A only). The increase in concentration greatly suppressed the percentage mineralization of triclosan. It was again observed that similar to the concentration dependence study, the Ag^0(NP)/TiO_2(A1) and Ag^0(NP)/TiO_2(A2) thin films showed relatively higher efficiency in the mineralization of triclosan compared to the UV-A photolysis.

On the other hand, the percent NPOC removal as a function of pH was studied in order to optimise the best possible pH of treatment to achieve maximum mineralization of the triclosan in the photocatalytic treatment. The triclosan solution ([TCS]: 1.0 mg/L) was treated at different pH values (pH 4.0 to 10.00) for 2 hours using the UV-A only, Ag^0(NP)/TiO_2(A1) and Ag^0(NP)/TiO_2(A2) thin film catalysts. The percent NPOC removal was presented as a function of pH in Figure 3.2.1.9(b) and Table 3.2.1.9(b). It was cleared from the Figure that the maximum NPOC removal was achieved at pH 4.0 using the UV-A

only, Ag^0(NP)/TiO_2(A1) and Ag^0(NP)/TiO_2(A2) thin films. Quantitatively, at pH 4.0, 57%, 46% and 19.50% NPOC removal was achieved with Ag^0(NP)/TiO_2(A2), Ag^0(NP)/TiO_2(A1) and UV-A only treatment, respectively. These results were again in conformity with the pH dependence removal of triclosan in the photocatalytic degradation. This clearly revealed that the thin films greatly favoured an enhanced NPOC removal, i.e., greater mineralization of triclosan was attained using the photocatalyst thin films compared to the photolysis using UV-A illumination only. Despite the partial mineralization of triclosan as achieved by the photocatalytic treatment, however, a complete mineralization could be achieved with repeated treatment or even prolonged treatment of the samples.

Table 3.2.1.9: Percentage removal of NPOC for triclosan as a function of **(a)** concentration and **(b)** pH [A1: Ag^0(NP)/TiO_2(A1) and A2: Ag^0(NP)/TiO_2(A2)].

(a)	**% NPOC Removal**				
	TCS concentration (mg/L)				
	0.5	**1.0**	**5.0**	**10.0**	**15.0**
UV-A	21.66	18.43	10.23	7.78	5.74
A1	53.3	42.5	28.83	17.53	12.04
A2	68.74	53.78	36.05	25.54	20.12

(b)	**% NPOC Removal**			
	pH			
	4.0	**6.0**	**8.0**	**10.0**
UV-A	19.50	18.43	16.43	14.65
A1	46	42	39	33
A2	57	54	48	41

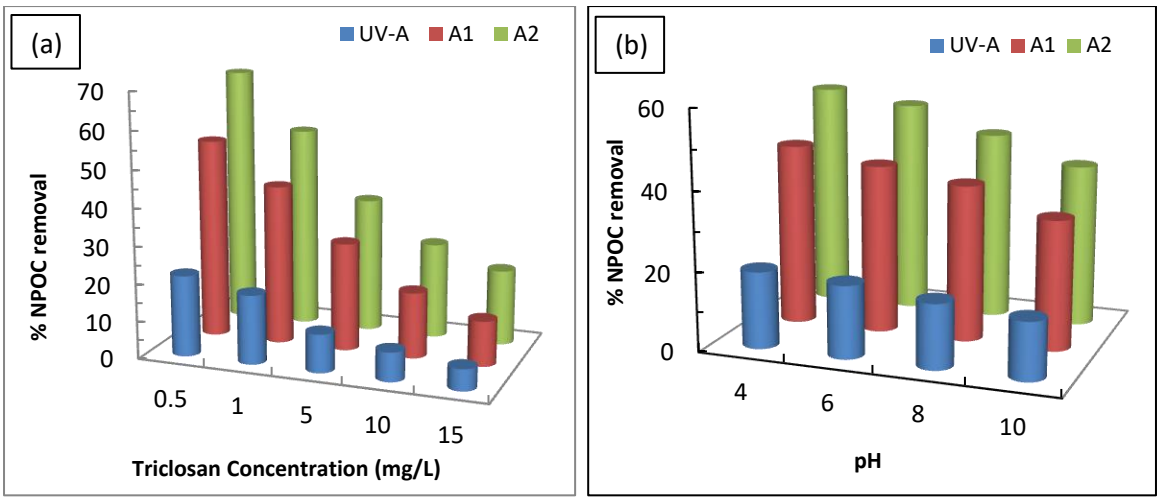

Figure 3.2.1.9: Percent mineralization of triclosan **(a)** as a function of initial triclosan concentration and **(b)** as a function of pH in the photolytic and photocatalytic degradations of triclosan [A1: $Ag^0(NP)TiO_2(A1)$ and A2: $Ag^0(NP)TiO_2(A2)$].

3.2.1.10. Mineralization of Alizarin Yellow (AY)

The mineralization of alizarin yellow was obtained in the photolytic and photocatalytic treatment processes. The NPOC values were obtained at varied initial concentrations of alizarin yellow as well as a function of pH. The percent of NPOC removal as a function of alizarin yellow concentration was presented graphically in Figure 3.2.1.10(a) and in Table 3.2.1.10(a). The concentration of alizarin yellow was increased from 0.5 to 15.0 mg/L at a constant solution pH 6.0 and employing the UV-A only, $Ag^0(NP)/TiO_2(A1)$ and $Ag^0(NP)/TiO_2(A2)$ photocatalysts. The results were obtained at the end of 2 hours of photo-irradiation. It was apparent from the Figure that a sharp decrease in NPOC was observed with increasing the initial concentration of alizarin yellow. Quantitatively, increasing the concentration of alizarin yellow from 0.5 to 15.0 mg/L the percent of NPOC was decreased from 61.33 to 17.09% (using the $Ag^0(NP)/TiO_2(A2)$ thin film); from 51.63 to 13.62% (using $Ag^0(NP)/TiO_2(A1)$ thin film); 10.69 to 3.75% (using UV-A only), respectively. It was again observed that similar to the concentration

dependence study, the Ag^0(NP)/TiO_2(A2) thin film showed relatively higher efficiency in the removal of alizarin yellow compared to the Ag^0(NP)/TiO_2(A1) thin film catalyst.

The effect of solution pH in the mineralization of alizarin yellow was also obtained taking constant alizarin yellow concentration 1.0 mg/L. The solution pH was varied from pH 4.0 to 10.0) and photo illumination was allowed for 2 hours. The percent of NPOC removal was presented as a function of pH and presented in Figure 3.2.1.10(b) as well as in Table 3.2.1.10(b). The results indicated that the maximum NPOC was removed at pH 6.0. Quantitatively, at pH 6.0, 48%, 41% and 10.21% NPOC removal was achieved using the Ag^0(NP)/TiO_2(A2), Ag^0(NP)/TiO_2(A1) and UV-A only treatment, respectively. It was evident from the results that high pH values greatly hindered the percent removal of NPOC. These results were in consistent with the pH dependence removal of alizarin yellow using the Ag or Au-nanoparticles/TiO_2 photocatalysts.

Table 3.2.1.10: Percentage removal of NPOC for alizarin yellow as a function of **(a)** concentration **(b)** pH [A1: Ag^0(NP)/TiO_2(A1) and A2: Ag^0(NP)/TiO_2(A2)].

(a)	**% Removal of NPOC**				
	AY concentration (mg/L)				
	0.5	**1.0**	**5.0**	**10.0**	**15.0**
UV-A	10.69	10.21	5.45	4.81	3.75
A1	51.63	41.18	28.26	16.12	13.62
A2	61.33	48.36	31.85	21.89	17.09

(b)	**% Removal of NPOC**			
	pH			
	4.0	**6.0**	**8.0**	**10.0**
UV-A	8.07	10.21	7.20	6.83
A1	38	41	36	33
A2	44	48	38	36

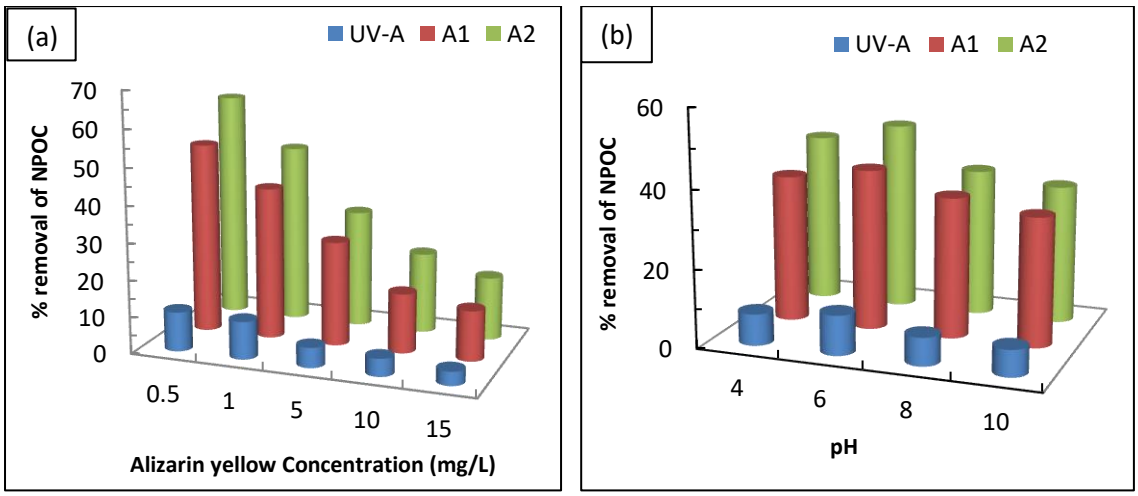

Figure 3.2.1.10: Percentage mineralization of alizarin yellow **(a)** as a function of initial AY concentration and **(b)** as a function of pH in the photolytic and photocatalytic degradations of AY [A1: Ag^0(NP)/TiO_2(A1) and A2: Ag^0(NP)/TiO_2(A2)].

Similarly, the percentage removal of NPOC for alizarin yellow removal was obtained using Au^0(NP)/TiO_2(B1) and Au^0(NP)/TiO_2(B2) thin films. The percent of NPOC removal as a function of alizarin yellow concentration was presented graphically in Figure 3.2.1.10(c) and in Table 3.2.1.10(c). The concentration of alizarin yellow was increased from 0.5 to 15.0 mg/L at a constant solution pH 6.0 and employing the UV-A only, Au^0(NP)/TiO_2(B1) and Au^0(NP)/TiO_2(B2) photocatalysts. The results were obtained at the end of 2 hours of photo-irradiation. Increasing the concentration of alizarin yellow from 0.5 to 15.0 mg/L the percentage of NPOC was decreased from 63.64 to 22.65% (using the Au^0(NP)/TiO_2(B2) thin film); from 62.56 to 20.2% (using Au^0(NP)/TiO_2(B1) thin film); 10.69 to 3.75% (using UV-A only), respectively.

Further, the percentage removal of NPOC for alizarin yellow as a function of solution pH (pH 4.0 to 10.0) was shown in Figure 3.2.1.10(d) and Table 3.2.1.10(d). The Figure clearly indicated that initially the percentage of NPOC removal was increased with

an increase in pH, i.e., pH 4.0 to 6.0. However, further increase in pH from 6.0 to 10.0, the removal efficiency of NPOC was suppressed to a greater extent. Moreover, NPOC removal was increased from 50 to 55% with the increase in pH from 4.0 to 6.0 using nanocomposite Au^0(NP)/TiO_2(B2) photocatalyst. However, increasing the pH from 6.0 to 10.0 had caused to decrease the mineralization of alizarin yellow from 55% to 39%, respectively, using the Au^0(NP)/TiO_2(B2) photocatalyst. Similar trend was observed for the photocatalyst Au^0(NP)/TiO_2(B1). The percent mineralization of alizarin yellow was found relatively high using the template synthesized nanocomposite Au^0(NP)/TiO_2(B2) compared to the non-template synthesized material Au^0(NP)/TiO_2(B1). This again showed the greater utility of template synthesized material. On the other hand, the photolysis process showed insignificant percentage removal of NPOC of alizarin yellow. Overall, it was noted that a single photocatalytic operation could enable to mineralize a significant percentage of alizarin yellow in aqueous solutions.

Table 3.2.1.10: Percentage removal of NPOC for alizarin yellow as a function of **(c)** concentration and **(d)** pH [B1: Au^0(NP)/TiO_2(B1) and B2: Au^0(NP)/TiO_2(B2)].

(c)	**% NPOC Removal**				
	AY concentration (mg/L)				
	0.5	**1.0**	**5.0**	**10.0**	**15.0**
UV-A	10.69	10.21	5.45	4.81	3.75
B1	62.56	50.11	33.89	25.34	20.2
B2	63.64	54.73	37.70	28.26	22.65

(d)	**% NPOC Removal**			
	pH			
	4.0	**6.0**	**8.0**	**10.0**
UV-A	8.07	10.21	7.20	6.83
B1	48	50	39	37
B2	50	55	43	39

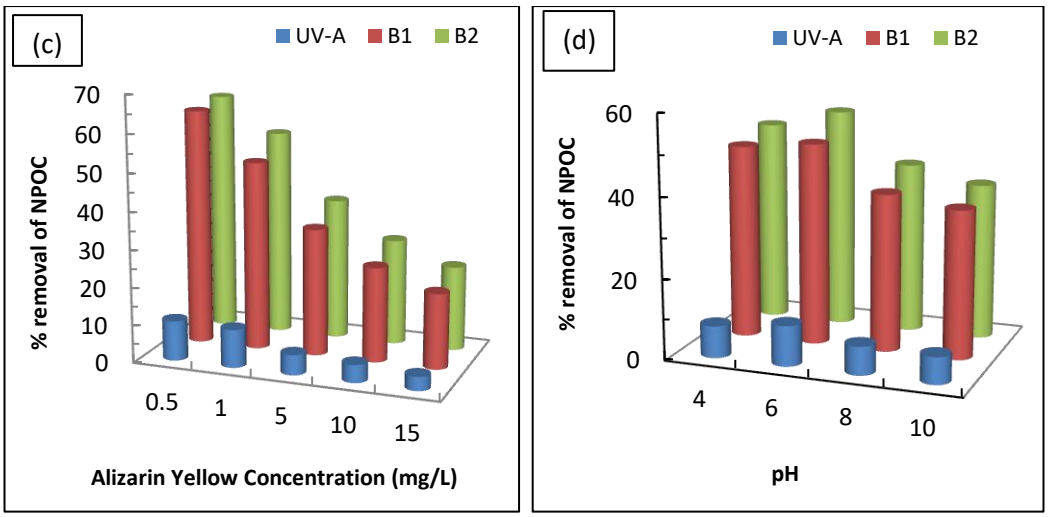

Figure 3.2.1.10: Percent mineralization of alizarin yellow **(c)** as a function of initial alizarin yellow concentration and **(d)** as a function of pH in the photolytic and photocatalytic degradations of alizarin yellow [B1: Au^0(NP)/TiO_2(B1) and B2: Au^0(NP)/TiO_2(B2)].

3.2.2. Stability of thin film photocatalyst

Stability of nanocomposite thin film Ag^0(NP)/TiO_2(A2) is important for prolonged and continuous use of catalyst in wastewater treatment plants. Nevertheless, it demonstrates the long term use of catalyst. Therefore, the nanocomposite Ag^0(NP)/TiO_2(A2) thin film was intended to employ for the six cycle of repeated operations. The results were presented in Figure 3.2.2(a). At the completion of each photocatalytic operation, the thin film was washed with distilled water and dried in a drying oven at 105 ^{0}C for 3 hours and it was again used for the next cycle of operations. The initial concentration of micropollutant (triclosan or alizarin yellow) was 5.0 mg/L at a constant pH 6.0. The results clearly showed that even at the end of six cycle of operations, the percentage efficiency of Ag^0(NP)/TiO_2(A2) photocatalyst was not hampered and almost an identical removal was obtained for triclosan or alizarin yellow. More quantitatively, at the completion of six cycle of operations the percentage removal of triclosan was decreased only from 38.98% to 38.33% (i.e., a decrease

of 0.65%) and alizarin yellow was decreased only from 35.37% to 34.40% (i.e., a decrease of 0.97%). These results showed that the nanocomposite Ag^0(NP)/TiO_2(A2) thin film possessed fairly a good stability at least in successive photocatalytic operations. Hence, this eventually enhanced the applicability of the nanocomposite thin film in the wastewater treatment. It was reported previously that methyl orange removal using the TiO_2 supported on spherical activated carbon (TiO_2/SAC) was significantly decreased even at the completion of 5 cycles of operations (Yoon *et al*., 2012).

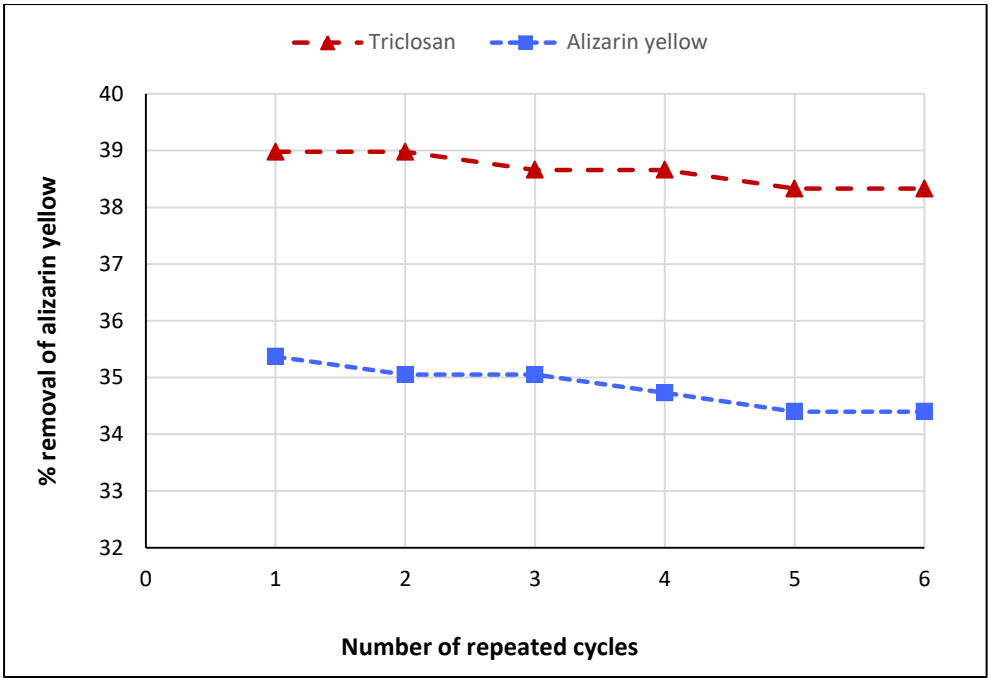

Figure 3.2.2(a). Repeated use of nanocomposite Ag^0(NP)/TiO_2(A2) photocatalyst in the photocatalytic elimination of triclosan and alizarin yellow using the UV-A illumination [Initial concentration of TCS or AY: 5.0 mg/L; pH: 6.0].

Further, the stability test of the thin film Au^0(NP)/TiO_2(B2) was also obtained in the photocatalytic removal of alizarin yellow. The nanocomposite Au^0(NP)/TiO_2(B2) thin film was intended to employ in the six cycle of operations using the same disk. The results of six operations were shown in Figure 3.2.2(b). The initial concentration of alizarin yellow was

5.0 mg/L at pH 6.0. The disk was cleaned at the end of each reactor operation; it was cleaned with purified water followed by drying at 105 ^{0}C. The dried disk was then again employed for the next cycle of treatment. Figure 3.2.2(b) clearly showed that even for six cycles of treatment the nanocomposite Ag^0(NP)/TiO_2(B2) thin film possessed fairly high stability since the degradation efficiency of alizarin yellow was not affected significantly. Quantitatively, at the end of sixth repeated operation, the percentage degradation of alizarin yellow was decreased from 38.58% to 37.30% only (i.e., a decrease of 1.28%). This indicated that the nanocomposite thin film was fairly stable at least for the long term implication of thin film. These studies further demonstrated the applicability of nanocomposite coated disk for efficient and prolonged treatment of wastewater. However, the use of TiO_2 catalyst powder for repeated operations showed marked decrease in catalytic efficiency. This was due to the aggregation of dye particles around the TiO_2 particles which substantially decreased the efficincy of catalyst (Saggioro *et al*., 2011). Similarly, the use of Ag/rGO nanocomposite photocatalyst showed *Ca.* 10% decrease in the removal efficiency of azo dyes, *viz.*, congo red and bismarck brown for repeated uses (Borthakur *et al*., 2017). However, use of nanocomposite thin film could enable to provide a prolonged catalytic operations. Similar stabilty was reported previously using the 6 wt% MWCNT/Au-TiO_2 catalyst in oxidative removal of cyanide for 5 repeated operations (Mohamed and Mkhalid, 2015).

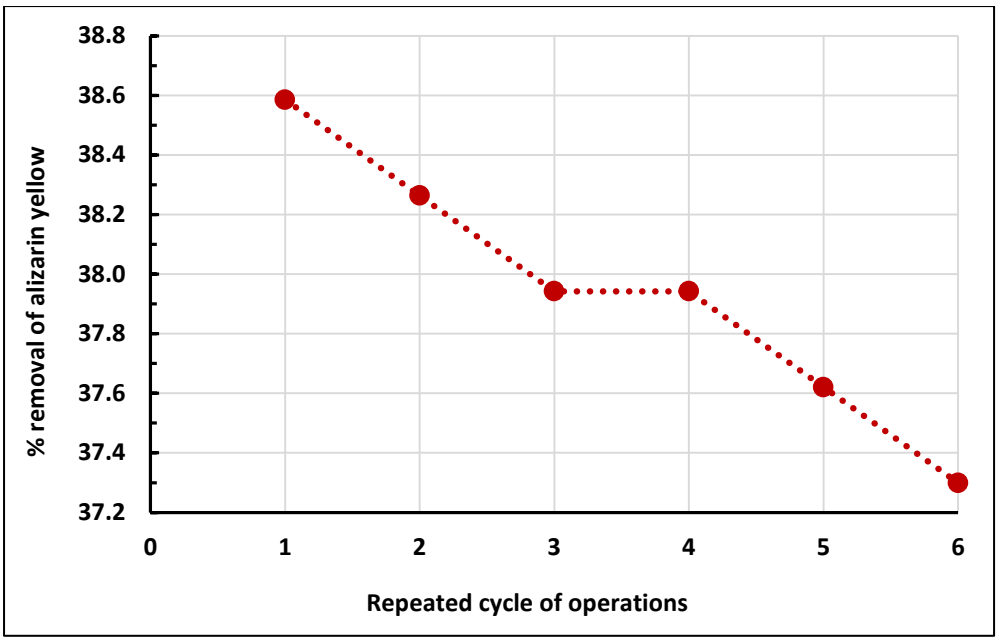

Figure 3.2.2(b). Repeated use of nanocomposite Au^0(NP)/TiO_2(B2) photocatalyst in the photocatalytic removal of alizarin yellow using the UV-A illumination [Initial concentration of AY: 5.0 mg/L; pH: 6.0].

3.3. Photocatalytic Degradation using Ce^{3+}/TiO_2 Thin Films (Removal of Amoxicillin, Tetracycline and Alizarin Yellow)

3.3.1. Batch Reactor Studies

3.3.1.1. Effect of pH

The elimination mechanism was deduced with the help of pH dependence degradation of amoxicillin and tetracycline in photocatalytic reactor operations. The degradation of these antibiotics (amoxicillin and tetracycline) was conducted in a wide range of pH (pH 4.0 – 10.0) keeping the initial antibiotic concentration 1.0 mg/L with a total illumination of 2 hours. The blank degradation was also conducted using the UV-A illumination only in order to compare the photocatalytic degradation of these antibiotics at the studied pH. The percentage elimination of amoxicillin and tetracycline at varied pH values was shown in Figures 3.3.1.1(a) and 3.3.1.1(b) (Secondary axis), and Tables 3.3.1.1(a) and 3.3.1.1(b)**,** respectively. It was evident from the Figure (Figure 3.3.1.1(a)) that the amoxicillin elimination was increased with the increase in pH from pH 4.0 to 6.0, however, further increase in pH caused for decrease in percentage removal of amoxicillin. Quantitatively, increasing the pH from 4.0 to 6.0 the amoxicillin percentage removal was increased from 55.39 to 60.97%. However, further increase in pH from 6.0 to 10.0 the percentage of amoxicillin elimination was decreased from 60.97% to 49.82% using the Ce^{3+}/TiO_2(C2) photocatalyst. The removal behaviour of amoxicillin with varied pH values could be understood with the surface properties of photocatalysts as well as the speciation of amoxicillin in aqueous solutions. Therefore, the two photocatalysts Ce^{3+}/TiO_2(C1) and Ce^{3+}/TiO_2(C2) powders were subjected for the determination of pH_{PZC} (point of zero charge) using the known acid base titration method (Lalhmunsiama *et al*., 2016). The pH_{PZC} of Ce^{3+}/TiO_2(C1) and Ce^{3+}/TiO_2(C2) was found to be 7.1 and 7.5, respectively. Therefore, the surface of the catalyst was negatively charged above to this pH and positively charged

below to this pH. On the other hand the amoxicillin molecule showed acidic dissociation with the change in pH values. The amoxicillin possessed with three dissociable hydrogens dissociated depending on the pK_a values 2.4, 7.4 and 9.6, respectively, representing the pK_a^1, pK_a^2 and pK_a^3 (Elmolla and Chaudhuri, 2010; Chemie, 2005). Therefore, using the pK_a values the speciation studies were conducted and results were shown in Figure 3.3.1.1(a) (Primary Axis). It was evident from the Figure 3.3.1.1(a) that the amoxicillin molecule dominantly present in either neutral or positively charged species up to the pH 7.0. However, at pH > 7.0, the negatively charged species, *viz*., AMX^- or AMX^{2-} dominated. Therefore, the surface of photocatalyst and species of amoxicillin both possessed with negative charged which hindered the electrostatic attraction of amoxicillin species on the catalyst surface hence, caused for decrease in degradation at pH above 6.0. Similarly, at lower pH value, i.e., pH 4.0, relatively less removal of amoxicillin was observed. Again based on the surface properties, the surface of the catalyst possessed net positive charge density and the positively charged species of amoxicillin dominated. This hindered the surface adsorption of amoxicillin onto the catalyst surface. Therefore, the elimination of amoxicillin was suppressed at pH below and above to 6.0. In addition to the surface charge and speciation studies of amoxicillin, it was reported previously that amoxicillin was fairly stable toward hydrolysis at pH 5.0 (Zia *et al*., 1977). However, strong acidic and alkaline conditions, i.e., pH 2.0 and 10.0 favoured greatly the hydrolysis of amoxicillin which suppressed the removal of amoxicillin from aqueous solutions (Yang *et al*., 2017). Therefore, an appropriate pH 5.0 was suggested for the removal of amoxicillin using In-based MOF/graphene oxide composite (Yang *et al*., 2017). However, the other studies stated that pH 11.0 greatly favoured the removal of amoxicillin using the UV/ZnO photocatalytic process (Elmolla and Chaudhuri, 2010). The results were supported with the fact that higher pH values caused excess of OH^- ions on the ZnO surface which enabled the formation of

$^{\bullet}$OH radicals (Kansal *et al*., 2007) and the hydrolysis of amoxicillin caused instability of β-lactam ring at very high pH 11.0 (Hou and Poole, 1971).

On the other hand, as shown in Figure 3.3.1.1(b) that the removal of tetracycline was increased with the increase in solution pH. Quantitatively, increasing the pH from 4.0 to 10.0 the corresponding increase in tetracycline percentage elimination was increased from 52.69 to 76.35% using the Ce^{3+}/TiO_2(C2) photocatalyst. The speciation of tetracycline which was conducted previously using the acid dissociation constants values of 3.3, 7.7 and 9.7 corresponded to the pK_a^1, pK_a^2 and pK_a^3 values, respectively, again shown in Figure 3.3.1.1(b) (Tiwari *et al*., 2018; Feldstein *et al*., 1997) The tetracycline molecule stabilized to its zwitterion (TCH_2^0 or $TCH_2^{0\,+\,-}$) structures within the pH region 3.3 – 7.7. This was because of the loss of a proton from phenolic diketone moiety. Further, the molecule turns to its anionic species (TCH^- or $TCH^{+\,-\,-}$) at pH > 7.7 by acidic dissociation of proton. Hence, the tetracycline possessed net negative charge density at pH > 7.7. Moreover, as shown in Figure 3.3.1.1(b), the tetracycline molecule dissociated the third proton from the tricarbonyl and phenolic diketone moiety at pH ≥ 9.7, which gave the di-anionic species of tetracycline (Feldstein *et al*., 1997). Therefore, these results showed that at high pH conditions both catalyst surface and the tetracycline species were possessed with net negative charge density. This, perhaps, hindered the sorption of tetracycline onto the catalyst surface and less removal was expected. However, the pH studies showed that increase in pH greatly favoured the elimination of tetracycline. Similarly, the adsorption studies conducted separately using the hybrid clay materials showed very high uptake of tetracycline was obtained and indeed it was almost unaffected within the pH region 2.0 to 10.0 (Thanhmingliana *et al*., 2015). This implied that tetracycline showed greater affinity towards the catalyst surface. Moreover, enhanced amount of hydroxide anions were present at high

pH values which resulted the formation of more hydroxyl radicals by oxidation of holes at the catalyst surface (Kansal *et al*., 2007). This, therefore, favoured the enhanced degradation of tetracycline at high pH conditions. Similar, results were reported previously for the photocatalytic degradation of tetracycline using the Ag^0(NP)/TiO_2 nanocomposite (Tiwari *et al*., 2018).

The photolytic elimination (i.e., blank) of amoxicillin and tetracycline was shown in Figure 3.3.1.1(a) and 3.3.1.1(b), respectively. It was clearly observed that the percentage elimination of these two antibiotics was significantly increased in presence of photocatalysts (i.e., Ce^{3+}/TiO_2(C1) and Ce^{3+}/TiO_2(C2)) thin films compared to the blank test. This further implied that the thin films employed showed fairly good photocatalytic activity towards the degradation of amoxicillin and tetracycline in aqueous solutions. Moreover, comparing the two thin film photocatalysts, *viz.*, Ce^{3+}/TiO_2(C1) and Ce^{3+}/TiO_2(C2), the templated synthesized catalyst Ce^{3+}/TiO_2(C2) possessed enhanced catalytic action in the degradation of amoxicillin and tetracycline.

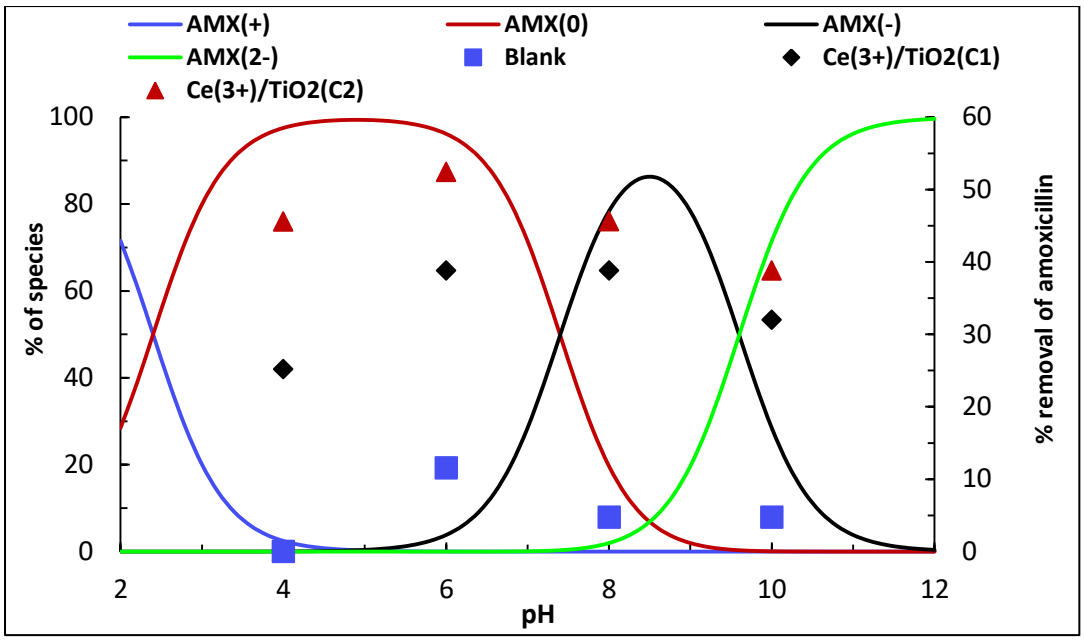

Figure 3.3.1.1(a): Effect of pH in the photocatalytic degradation of amoxicillin (AMX) using Ce^{3+}/TiO_2(C1) and Ce^{3+}/TiO_2(C2) thin films. AMX (1.0 mg/L); Irradiation time: 2 hours; Temperature 25±1 ^{0}C.

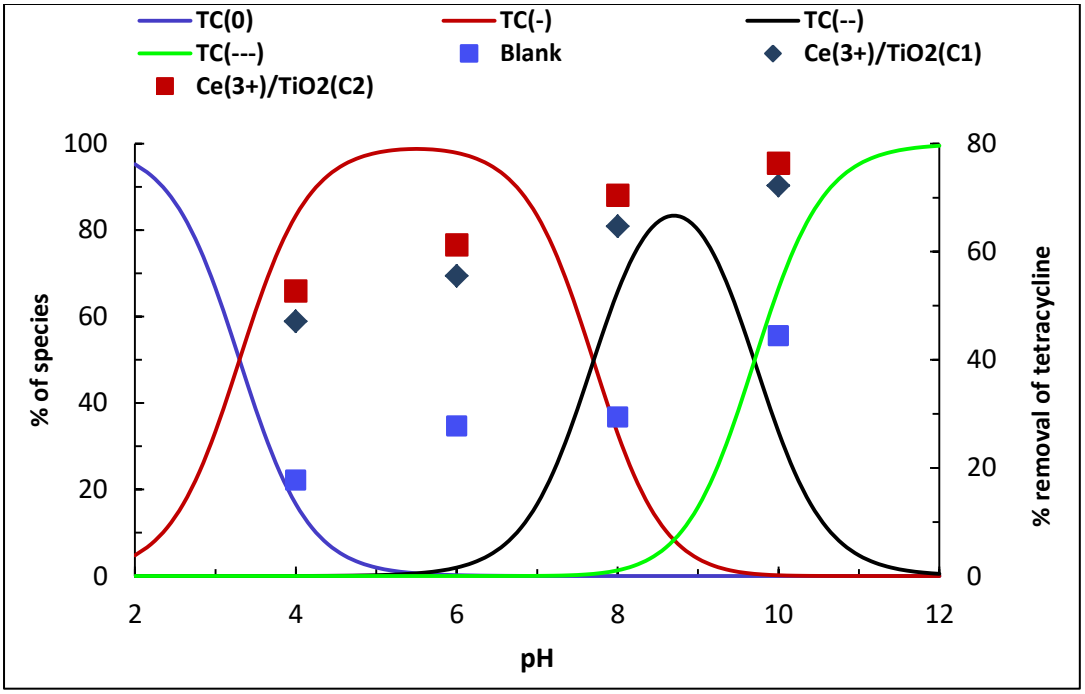

Figure 3.3.1.1(b): Effect of pH in the photocatalytic degradation of tetracycline (TC) using Ce^{3+}/TiO_2(C1) and Ce^{3+}/TiO_2(C2) thin films: TC (1.0 mg/L); Irradiation time: 2 hours; Temperature 25±1 ^{0}C.

Table 3.3.1.1(a): Effect of pH in the photocatalytic degradation of amoxicillin (AMX). ([AMX]:1.0 mg/L; Irradiation time: 2 hours; Temperature 25±1 ^{0}C).

	% Removal (pH)			
	4	**6**	**8**	**10**
UV-A	16.6	27.7	22.2	22.2
Ce^{3+}/TiO_2(C1)	38.9	50	50	44.4
Ce^{3+}/TiO_2(C2)	55.39	60.97	55.39	49.82

Table 3.3.1.1(b): Effect of pH in the photocatalytic degradation of tetracycline (TC). ([TC]:1.0 mg/L; Irradiation time: 2 hours; Temperature 25±1 ^{0}C).

	% Removal (pH)			
	4	**6**	**8**	**10**
UV-A	17.7	27.7	29.4	44.4
Ce^{3+}/TiO_2(C1)	47.1	55.5	64.7	72.2
Ce^{3+}/TiO_2(C2)	52.69	61.22	70.43	76.35

Further, the pH dependence degradation of alizarin yellow was also studied at varied pH (pH 4.0 – 10.0) at a constant alizarin yellow concentration (1.0 mg/L) under the photolysis and photocatalytic processes using UV-A light. The percentage removal of alizarin yellow was illustrated as a function of solution pH in Figure 3.3.1.1(c) and Table 3.3.1.1(c). The photocatalytic removal of alizarin yellow using the photocatalysts Ce^{3+}/TiO_2(C1) or Ce^{3+}/TiO_2(C2) was increased by increasing the solution pH from 4.0 − 6.0. But further increase in pH, i.e., pH from 6.0 to 10.0 caused a significant decrease in

percentage removal of alizarin yellow. Quantitatively, increasing the pH from 4.0 to 6.0 caused to increase the efficiency of alizarin yellow removal from 48.89 to 57.07% using the nanocomposite thin film Ce^{3+}/TiO_2(C2). However, further increase in pH from 6.0 to 10.0 resulted a decrease in percentage removal of alizarin yellow from 57.07 to 47.03% using nanocomposite thin film Ce^{3+}/TiO_2(C2). A similar trend of degradation of alizarin yellow was observed for the photocatalyst Ce^{3+}/TiO_2(C1) thin film.

The pH dependence degradation of alizarin yellow using the nanocomposite photocatalysts could be described based on the speciation studies of alizarin yellow and the surface properties of nanocomposite in aqueous solutions as a function of pH. It was evident that at high pH values (pH 6 ~ 10) both the nanocomposite and alizarin yellow possessed net negative charges that eventually caused to repel the alizarin yellow by the solid surface that obstructed the electrostatic attraction of alizarin yellow by the nanocomposite. This led to limit the sorption of the alizarin yellow onto the solid surface or even it hampered the sorbing species to enter within the Stern plane to enable it for a chemisorption of alizarin yellow at the nanocomposite surface. This caused a marked decrease in percentage of alizarin yellow removal at high pH values. Similarly, the electro-Fenton degradation of acid red 18 dye showed that increasing the pH from 2 – 3 caused to a minimal increase in degradation efficiency of dye. However, increasing further the pH from 3 – 9, the degradation of dye was decreased significantly from 99.2 to 78.8% (Malakootian and Moridi, 2017).

Table 3.3.1.1(c): Effect of pH in the photocatalytic degradation of alizarin yellow (AY). ([AY]: 1.0 mg/L; Irradiation time: 2 hours; Temperature 25±1 ^{0}C).

	% Removal (pH)			
	4	**6**	**8**	**10**
UV-A	3.4	11.1	8	4.8
Ce^{3+}/TiO_2(C1)	45.8	54	41.3	37.1
Ce^{3+}/TiO_2(C2)	48.89	57.07	49.12	47.03

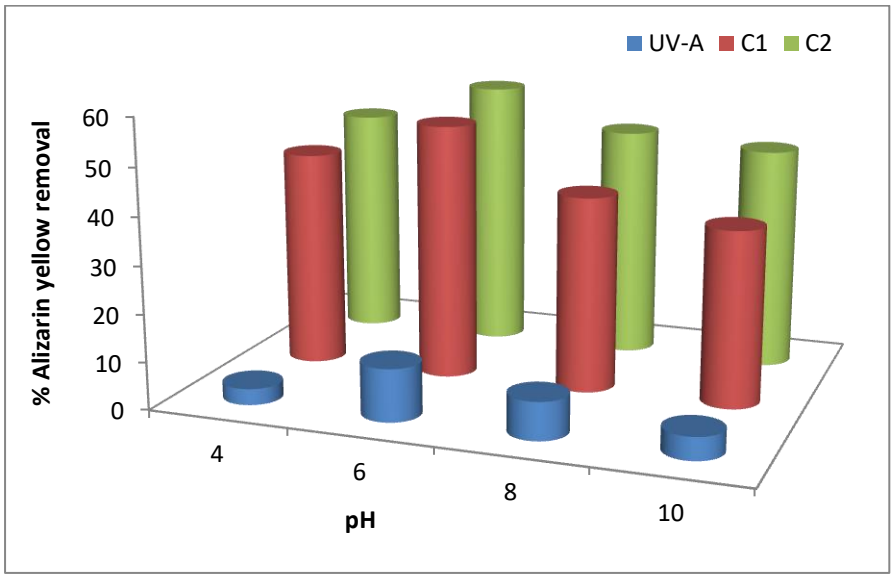

Figure 3.3.1.1(c): Effect of pH in the photocatalytic degradation of alizarin yellow (AY): (C1: Ce^{3+}/TiO_2(C1); C2: Ce^{3+}/TiO_2(C2)); [AY]: 1.0 mg/L; Irradiation time: 2 hours; Temperature 25±1 ^{0}C).

3.3.1.2. Effect of Pollutant Concentration

The pollutant concentration was increased to study the photocatalytic degradation of amoxicillin and tetracycline. Therefore, the amoxicillin and tetracycline concentration were increased from 0.5 to 15.0 mg/L and from 1.0 to 20 mg/L, respectively. The solution pH

taken was 6.0 and total irradiation time was 2 hours. The results were presented in Figure 3.3.1.2(a) and also given in Table 3.3.1.2(a) & 3.3.1.2(b). The increase in dilution of antibiotics greatly favored the percentage removal of these two antibiotics. Quantitatively, decreasing the concentration of amoxicillin from 15.0 mg/L to 0.5 mg/L had caused to increase the percentage elimination of tetracycline from 28.44% to 66.54% employing the Ce^{3+}/TiO_2(C2) photocatalyst. On the other hand, the percentage removal of tetracycline was increased from 25.53% to 61.22% by increasing the dilution from 20.0 mg/L to 1.0 mg/L using the photocatalyst Ce^{3+}/TiO_2(C2). The increase in degradation efficiency of these two antibiotics with the increase in dilution was primarily due to the reason that the contact possibilities of antibiotic towards the solid surface was relatively high at lower pollutant concentrations (Lalliansanga *et al*., 2018; Tiwari *et al*., 2019a) . It was reported previously that the content of free radicals which were responsible for the oxidation of pollutants was constant, however, the number of pollutant molecules were increased at higher initial concentration. Hence, this caused for less percentage removal of pollutant at increased pollutant concentration (Caliskan *et al*., 2017).

Table 3.3.1.2(a): Effect of concentration in the photocatalytic degradation of amoxicillin (AMX). [pH: 6.0; Temperature 25±1 ^{0}C].

	% Removal				
	Initial concentration of AMX (mg/L)				
	0.5	**1.0**	**5.0**	**10.0**	**15.0**
UV-A	33.3	27.7	16.9	2.1	0.5
Ce^{3+}/TiO_2(C1)	55.5	50	38.6	23.4	21.6
Ce^{3+}/TiO_2(C2)	66.54	60.97	45.82	32.39	28.44

Table 3.3.1.2(b): Effect of concentration in the photocatalytic degradation of tetracycline (TC). [pH: 6.0; Temperature 25±1 ^{0}C].

	% Removal				
	Initial concentration of TC (mg/L)				
	1.0	**5.0**	**10.0**	**15.0**	**20.0**
UV-A	27.7	25.5	17.5	14.8	10.8
Ce^{3+}/TiO_2(C1)	55.5	41.5	28.6	22.9	17.6
Ce^{3+}/TiO_2(C2)	61.22	52.15	35.47	32.76	25.53

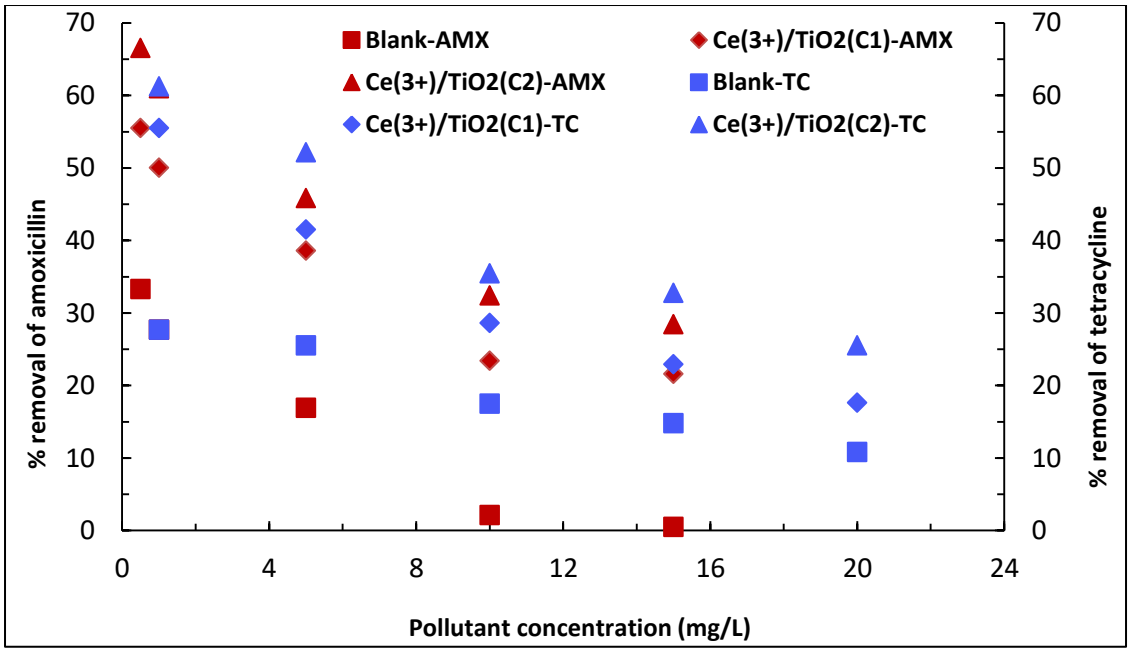

Figure 3.3.1.2(a): Removal efficiency of amoxicillin (Primary axis) and tetracycline (Secondary axis) at different concentration of antibiotics for blank and photocatalytic operations using the Ce^{3+}/TiO_2(C1) and Ce^{3+}/TiO_2(C2) photocatalysts [pH: 6.0; Temperature 25±1 ^{0}C].

It was again observed that the thin film catalysts Ce^{3+}/TiO_2(C1) and Ce^{3+}/TiO_2(C2) showed significantly higher photocatalytic efficiency in the degradation of amoxicillin and

tetracycline from aqueous solutions compared to the UV-A only irradiated sample. Further, the PEG template thin film Ce^{3+}/TiO_2(C2) catalyst possessed an enhanced photocatalytic activity than the Ce^{3+}/TiO_2(C1) catalyst in the degradation of the amoxicillin or tetracycline from aqueous solution which enhanced the applicability of template synthesized catalyst at least in the degradation of these two antibiotics from aqueous solutions.

Further, alizarin yellow concentration dependence study was carried out at varied concentrations, i.e., 0.5 to 15.0 mg/L at pH 6.0. The final concentration after 2 hours irradiation was obtained and the results were presented as percent removal of alizarin yellow as a function of initial concentration and illustrated graphically in Figure 3.3.1.2(b) as well as in Table 3.3.1.2(c). It was obvious that the percentage degradation was increased with decreasing the alizarin yellow concentration. Quantitatively, decreasing the alizarin yellow concentration from 15.0 to 0.5 mg/L increased percentage removal from 18.98 to 67.9% (by Ce^{3+}/TiO_2(C2) thin film); from 17 to 64.5% (by Ce^{3+}/TiO_2(C1) thin film) and from 0.1 to 13% (by UV-A only), respectively. It was evident that the increase in alizarin yellow concentration significantly hindered the removal efficiency of alizarin yellow for all these photolysis or photocatalytic processes. This was attributed due to the fact that the contact possibilities of alizarin yellow were relatively high at lower concentration. However, relative availability of active surface sites was decreased with increasing the alizarin yellow concentrations. Similar results were reported for the degradation of dye in the photocatalytic degradation and pointed that the surface of catalysts saturates at the higher concentration of pollutants (Chen and Huang, 2011; Saquib and Muneer, 2003).

Table 3.3.1.2(c): Effect of concentration in the photocatalytic degradation of alizarin yellow (AY). [pH: 6.0; Temperature 25±1 ^{0}C].

	% Removal				
	[Initial concentration of AY (mg/L)]				
	0.5	**1.0**	**5.0**	**10.0**	**15.0**
UV-A	13	11.1	4.5	0.2	0.1
Ce^{3+}/TiO_2(C1)	64.5	54	36.7	21.4	17
Ce^{3+}/TiO_2(C2)	67.9	57.07	38.56	25.65	18.98

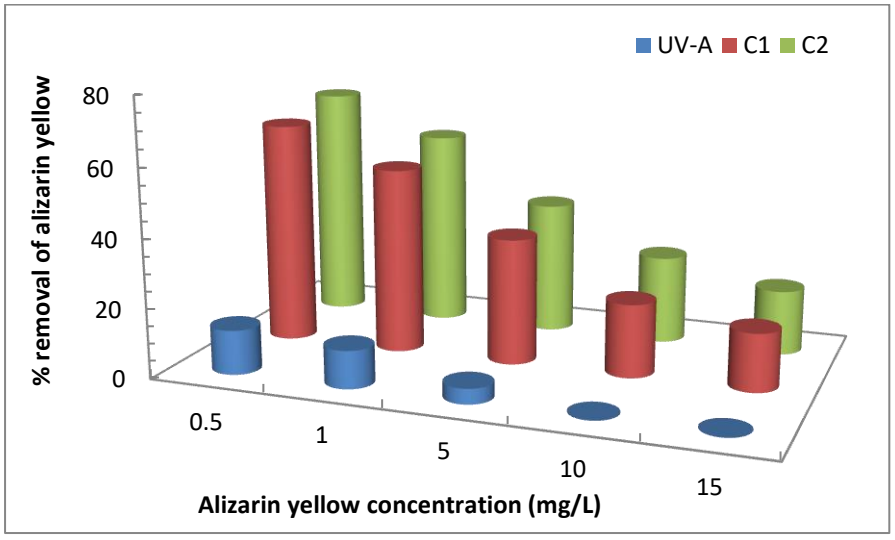

Figure 3.3.1.2(b): Effect of concentration in the photocatalytic degradation of alizarin yellow [C1: Ce^{3+}/TiO_2(C1); C2: Ce^{3+}/TiO_2(C;); pH: 6.0; Irradiation time: 2 hours; Temperature 25±1 ^{0}C].

3.3.1.3. Degradation Kinetics

The time dependent degradation of tetracycline and amoxicillin under photolysis and photocatalytic studies were conducted in order to deduce the reaction kinetics involved and to obtain apparent rate constant values. The kinetics was studied as a function of pollutant

concentration as well the solution pH. The value of C_t/C_0 was presented graphically in Figure 3.3.1.3(a) and 3.3.1.3(b), respectively, for the degradation of tetracycline and amoxicillin (initial concentration of TC and AMX: 1.0 mg/L at pH ~ 6.0) as a function of time (where C_0 is initial concentration of TC or AMX and C_t is the concentration of TC or AMX at time `t`). Figures 3.3.1.3(a) clearly exhibited that a sharp decrease of C_t/C_0 was occurred under the photocatalytic degradations of tetracycline or amoxicillin. A significant increase in the rate of degradation was observed with the thin film photocatalysts Ce^{3+}/TiO_2(C1) and Ce^{3+}/TiO_2(C2) compared to the UV-A photolysis process. Further, the thin film Ce^{3+}/TiO_2(C2) showed faster degradation kinetics compared to the thin film Ce^{3+}/TiO_2(C1). Quantitatively, the C_t/C_0 values for tetracycline at the end of 2 hours of UV-A irradiations were 0.72, 0.44 and 0.39 for the UV-A only, Ce^{3+}/TiO_2(C1) and Ce^{3+}/TiO_2(C2) samples, respectively. On the other hand, the C_t/C_0 values at the end of 2 hours of UV-A irradiations were 0.72, 0.50 and 0.39 for the UV-A only, Ce^{3+}/TiO_2(C1) and Ce^{3+}/TiO_2(C2) samples for degradation of amoxicillin, respectively.

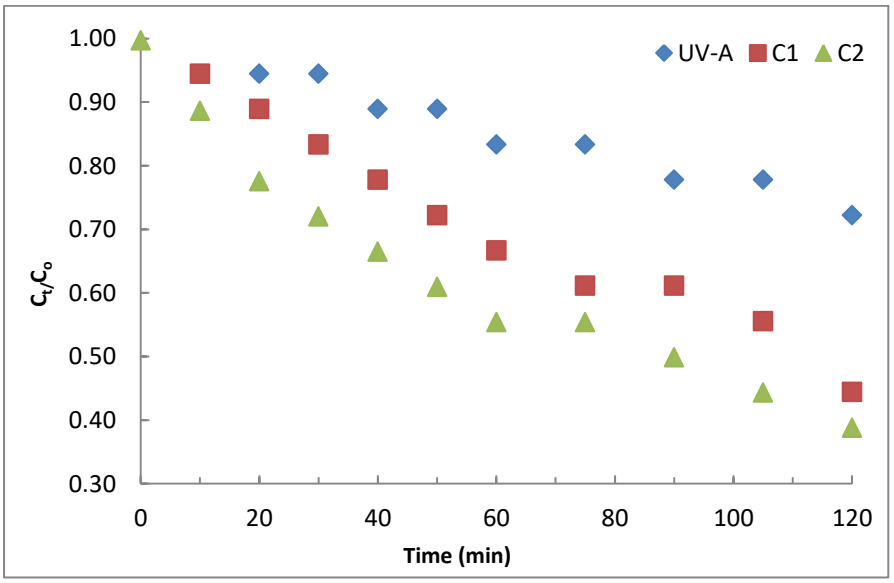

Figure 3.3.1.3(a): Photocatalytic degradation of tetracycline as a function of time using C1 (Ce^{3+}/TiO_2(C1)) and C2 (Ce^{3+}/TiO_2(C1)) thin film photocatalysts along with simple photolysis [TC concentration: 1.0 mg/L; pH: 6.0; Temperature: 25±1 ^{0}C].

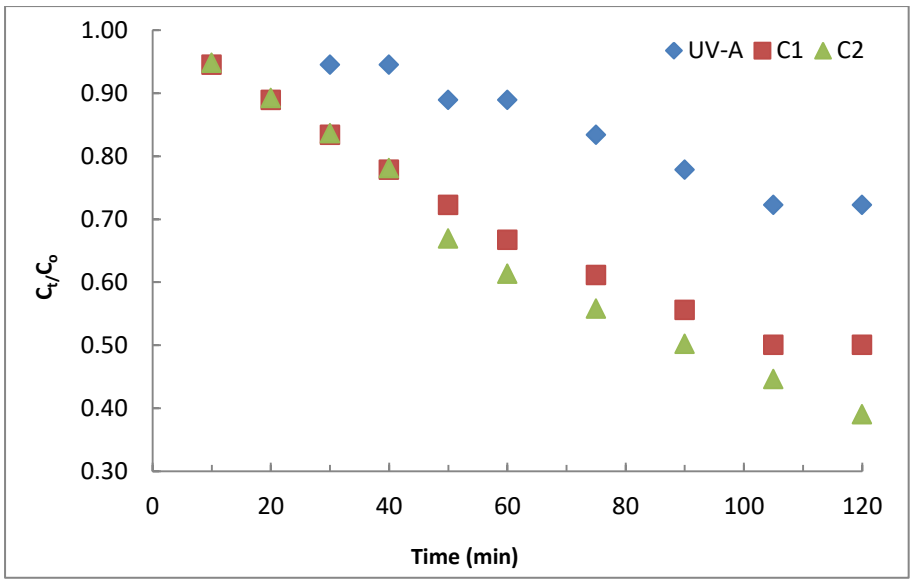

Figure 3.3.1.3(b). Photocatalytic degradation of amoxicillin as a function of time using C1 (Ce^{3+}/TiO_2(C1)) and C2 (Ce^{3+}/TiO_2(C1)) thin film photocatalysts along with simple photolysis [AMX concentration: 1.0 mg/L; pH: 6.0; Temperature: 25±1 ^{0}C].

The rate of elimination enabled to assess the overall efficacy of catalyst in reactor operations. The rate of degradation of antibiotic is presented by the pseudo-first order rate equation (Equation 3.3.1.3(i)):

$$r = -\frac{d[Antibiotic]}{dt} = k_{app}\left[k_{photolysis} + k_{photocatalysis}\right][Antibiotic]$$

$$= k_{app}\,[Antibiotic] \qquad \ldots (3.3.1.3(i))$$

where [Antibiotic] is used for the concentration of antibiotic and k_{app} is the pseudo-first-order rate constant. The above equation 3.3.1.3(i) is simplified to equation (3.3.1.3(ii)):

$$ln\left(\frac{C_0}{C_t}\right) = k_{app} \cdot t \qquad \ldots (3.3.1.3(ii))$$

where C_0 and C_t are the concentration of antibiotic at t = 0 and at time 't'. Therefore, plots were obtained between LN(C_0/C_t) *vs* the time `t` and shown in Figure 3.3.1.3(c)

(Insets). The k_{app} values were calculated for all the studied concentrations and presented in Figure 3.3.1.3(c) (both for amoxicillin (Primary axis) and tetracycline (Secondary axis) antibiotics) and Tables 3.3.1.3(a) & 3.3.1.3(b) (Initial concentration of antibiotics: 1.0 mg/L at pH: 6.0). A decrease in antibiotic concentrations had caused to increase the rate constant (k_{app}) values. Similarly, pseudo-first order rate kinetics were followed for the degradation of amoxicillin, ampicillin and cloxacillin in aqueous solutions under the UV/TiO_2 photocatalytic process (Elmolla and Chaudhuri, 2010i)

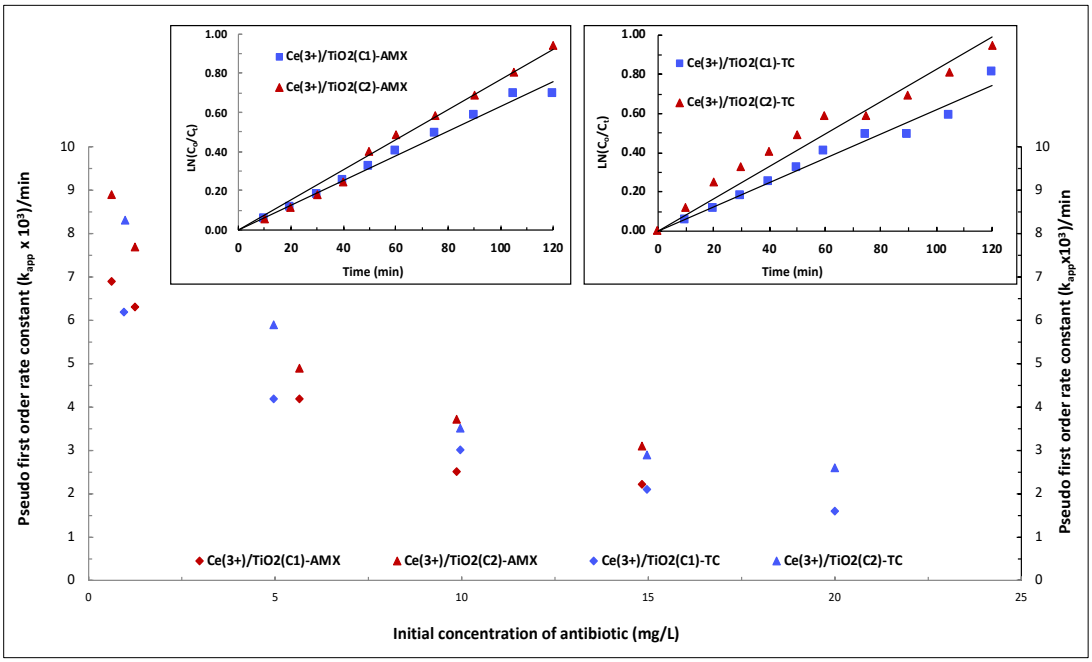

Figure 3.3.1.3(c). The pseudo-first order rate constant values for various concentrations of antibiotics (amoxicillin (Primary axis) and tetracycline (Secondary axis)) for photocatalytic degradation of antibiotics using the Ce^{3+}/TiO_2(C1) and Ce^{3+}/TiO_2(C2) photocatalysts. [Inset: Linear fitting of time dependence results for the pseudo-first-order rate kinetics; Initial concentration of antibiotics: 1.0 mg/L at pH: 6.0].

Table 3.3.1.3(a): Kinetic data obtained for the degradation of tetracycline using the thin film photocatalysts Ce^{3+}/TiO_2(C1) and Ce^{3+}/TiO_2(C2) and UV-A only irradiations.

	Pseudo-first order rate constant ($k_{app}x10^{-3}$)/min				
	[Initial concentration of tetracycline (mg/L)]				
	1.0	**5.0**	**10.0**	**15.0**	**20.0**
UV-A only	2.6 (0.972)	2.1 (0.955)	1.7 (0.984)	1.3 (0.983)	0.9 (0.983)
Ce^{3+}/TiO_2(C1)	6.2 (0.976)	4.2 (0.994)	3.0 (0.986)	2.1 (0.996)	1.6 (0.997)
Ce^{3+}/TiO_2(C2)	8.3 (0.946)	5.9 (0.995)	3.5 (0.994)	2.9 (0.978)	2.6 (0.985)

R^2 values are given in parenthesis.

Table 3.3.1.3(b). Kinetic data obtained for the degradation of amoxicillin using the thin film photocatalysts Ce^{3+}/TiO_2(C1), Ce^{3+}/TiO_2(C2) and UV-A only irradiations.

	Pseudo-first order rate constant ($k_{app}x10^{-3}$)/min				
	[Initial concentration of amoxicillin (mg/L)]				
	0.5	**1.0**	**5.0**	**10.0**	**15.0**
UV-A only	3.8 (0.930)	2.6 (0.929)	1.7 (0.971)	0.2 (0.776)	0 (0.706)
Ce^{3+}/TiO_2(C1)	6.9 (0.960)	6.3 (0.989)	4.2 (0.998)	2.5 (0.979)	2.2 (0.977)
Ce^{3+}/TiO_2(C2)	8.9 (0.953)	7.7 (0.990)	4.9 (0.994)	3.7 (0.968)	3.1 (0.983)

R^2 values are given in parenthesis.

Further, the photocatalytic elimination of amoxicillin and tetracycline was optimized to fit with the Langmuir-Hinshelwood (L-H) isotherm at various initial concentrations of each antibiotic to its linear form (Tiwari *et al*., 2018; Lalhriatpuia *et al*., 2015). The L-H adsorption constant '*K*' (L/mg) and the rate constant 'k_r' (mg/L/min) were estimated for the amoxicillin degradation (*cf.* Figure 3.3.1.3(d)) and found to be 0.174 and 0.044 (R^2: 0.998) and 0.168 and 0.058 (R^2: 998) for the Ce^{3+}/TiO_2(C1) and Ce^{3+}/TiO_2(C2) thin films, respectively. Similarly, the '*K*' and 'k_r' values obtained for the elimination of tetracycline (*cf.* Figure 3.3.1.3(e)) were found to be 0.153 and 0.046 (R^2: 0.998) and 0.144 and 0.065 (R^2: 0.998) for the Ce^{3+}/TiO_2(C1), and Ce^{3+}/TiO_2(C2) thin films, respectively.

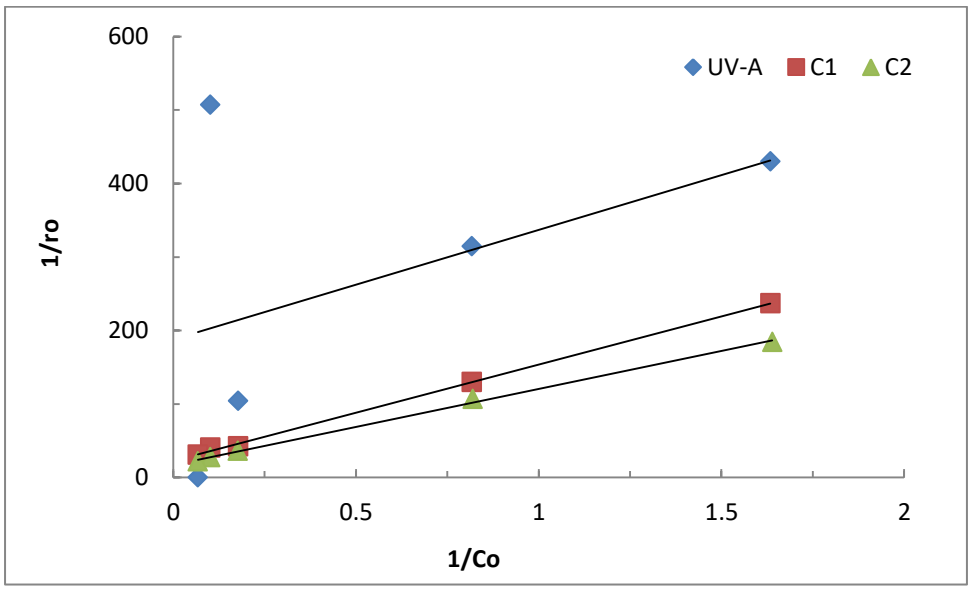

Figure 3.3.1.3(d): Langmuir-Hinselwood plot for the photocatalytic degradation of amoxicillin using using C1: Ce^{3+}/TiO_2(C1) and C2: Ce^{3+}/TiO_2(C2) thin film photocatalysts and UV-A only photolysis [AMX concentration: 0.5 – 15.0 mg/L; pH: 6.0; Temperature: 25±1 ^{0}C].

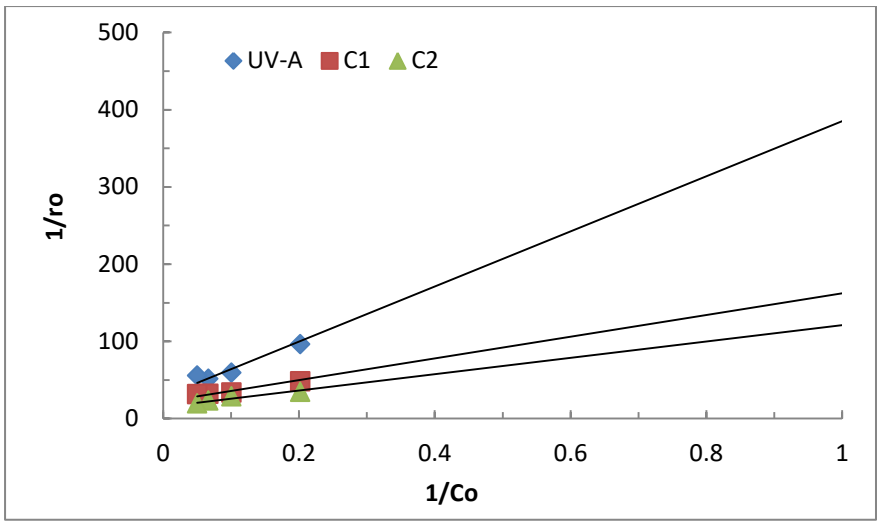

Figure 3.3.1.3(e): Langmuir-Hinshelwood plot for the photocatalytic degradation of tetracycline using C1: Ce^{3+}/TiO_2(C1) and C2: (Ce^{3+}/TiO_2(C2) thin film photocatalysts and UV-A only photolysis [TC concentration: 0.5 – 15.0 mg/L; pH: 6.0 at temperature: 25±1 ^{0}C].

The time dependent degradation of alizarin yellow enabled to deduce the kinetics of removal. The value of C_t/C_0 was presented graphically in Figure 3.3.1.3(f) for the degradation of alizarin yellow (initial concentration of AY: 1.0 mg/L at pH 6.0) as a function of time (where C_0 is initial concentration of AY and C_t is the concentration of AY at time 't'). The Figure 3.3.1.3(f) clearly showed that a sharp decrease of C_t/C_0 was occurred under the photocatalytic degradations of alizarin yellow whereas, the UV-A only irradiation showed almost no degradation of alizarin yellow within 2 hours of irradiation. Comparatively, the thin film Ce^{3+}/TiO_2(C2) showed faster degradation kinetics compared to the thin film Ce^{3+}/TiO_2(C1). This again indicated the higher efficiency of the PEG template thin films for the degradation of alizarin yellow from aqueous solution. Quantitatively, the calculated C_t/C_0 values at the end of 2 hours of UV-A irradiations were 0.89, 0.46 and 0.43 for the UV-A only, Ce^{3+}/TiO_2(C1) and Ce^{3+}/TiO_2(C2) samples, respectively.

Further, a linear relationship between the $LN(C_0/C_t)$ against time `t` were obtained and the results were presented in Figure 3.3.1.3(f) (inset) for the initial concentration of alizarin yellow as 1.0 mg/L at pH 6.0. The pseudo-first-order rate constants k_{app} and R^2 values were obtained for the Ce^{3+}/TiO_2(C1) and Ce^{3+}/TiO_2(C2) thin film photocatalysts along with the UV-A only treatment for all the concentrations of alizarin yellow at pH 6.0, the result has returned in Table 3.3.1.3(c). The time dependent kinetics was reasonably fitted well to the pseudo-first-order rate kinetics for the degradation of alizarin yellow at the studied concentrations using the UV-A only or photocatalyst thin films Ce^{3+}/TiO_2(C1) and Ce^{3+}/TiO_2(C2). Comparatively higher rate constant values were obtained for the photocatalytic degradation of alizarin yellow using Ce^{3+}/TiO_2(C1) and Ce^{3+}/TiO_2(C2) thin films compared to the UV-A photolysis. This again reaffirmed the utility of photocatalyst in the degradation of alizarin yellow from aqueous solutions. Similar pseudo-first-order rate kinetics was demonstrated for the degradation of alizarin yellow in aqueous solution by nano-TiO_2 thin films (Tiwari *et al*., 2015).

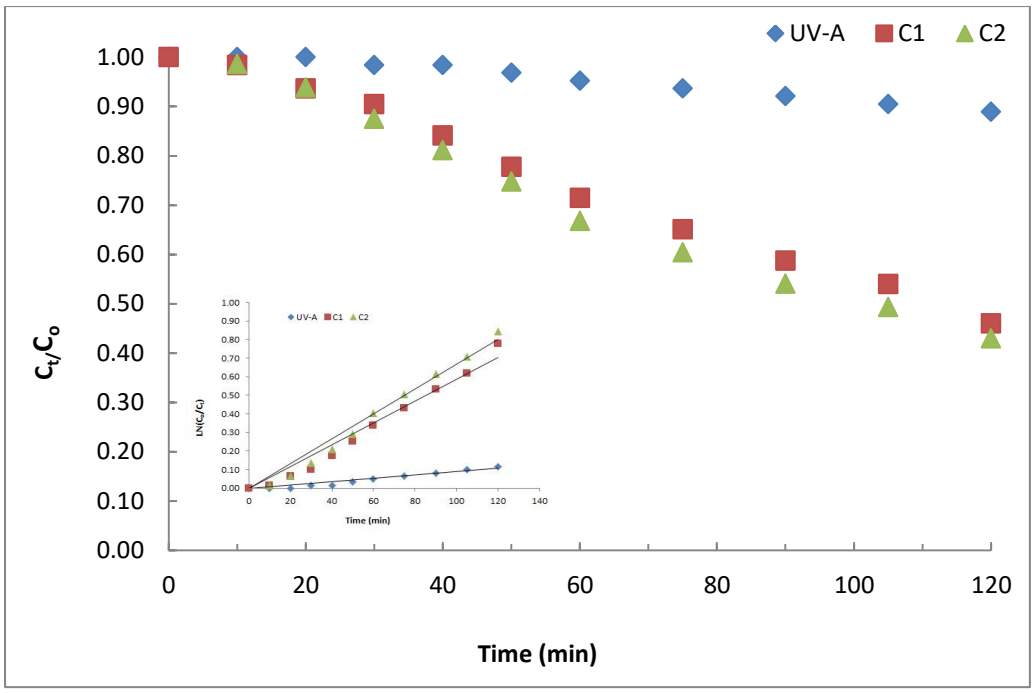

Figure 3.3.1.3(f). Photocatalytic degradation of alizarin yellow as a function of time using C1: Ce^{3+}/TiO_2(C1) and C2: Ce^{3+}/TiO_2(C2) thin film photocatalysts along with simple photolysis [AY concentration: 1.0 mg/L; pH: 6.0; Temperature: 25±1 ^{0}C].

Table 3.3.1.3(c). Kinetic data obtained for the degradation of alizarin yellow using the thin film photocatalysts Ce^{3+}/TiO_2(C1), Ce^{3+}/TiO_2(C2) and UV-A only irradiations.

	Pseudo-first order rate constant (k_{app}x10^{-3})/min				
	[Initial concentration of alizarin yellow (mg/L)]				
	0.5	**1.0**	**5.0**	**10.0**	**15.0**
UV-A only	1.3 (0.937)	0.9 (0.933)	0.4 (0.966)	0 (0.441)	0 (0.403)
Ce^{3+}/TiO_2(C1)	8.7 (0.989)	5.8 (0.969)	3.7 (0.997)	1.9 (0.991)	1.5 (0.982)
Ce^{3+}/TiO_2(C2)	8.8 (0.977)	6.7 (0.978)	4.1 (0.993)	2.4 (0.987)	1.6 (0.976)

R^2 values are given in parenthesis.

Further, using the L-H equation, the adsorption constant and the rate constant were evaluated while plotting $1/r_0$ against $1/C_0$ (Tiwari *et al*., 2018; Lalhriatpuia *et al*., 2015). The values of K and k_r were determined from the slope and intercept of these plots presented graphically in Figure 3.3.1.3(g). The results obtained for the k_r (mg/L/min) and K (L/mg) were 0.023 and 0.433 (R^2: 0.962 for Ce^{3+}/TiO_2(C1) sample) and 0.029 and 0.345 (R^2: 0.989 for Ce^{3+}/TiO_2(C2) sample), respectively, in the oxidation of alizarin yellow. Thus, the L-H kinetic was reasonably fitted well to the photocatalytic degradation of alizarin yellow using the thin film photocatalysts.

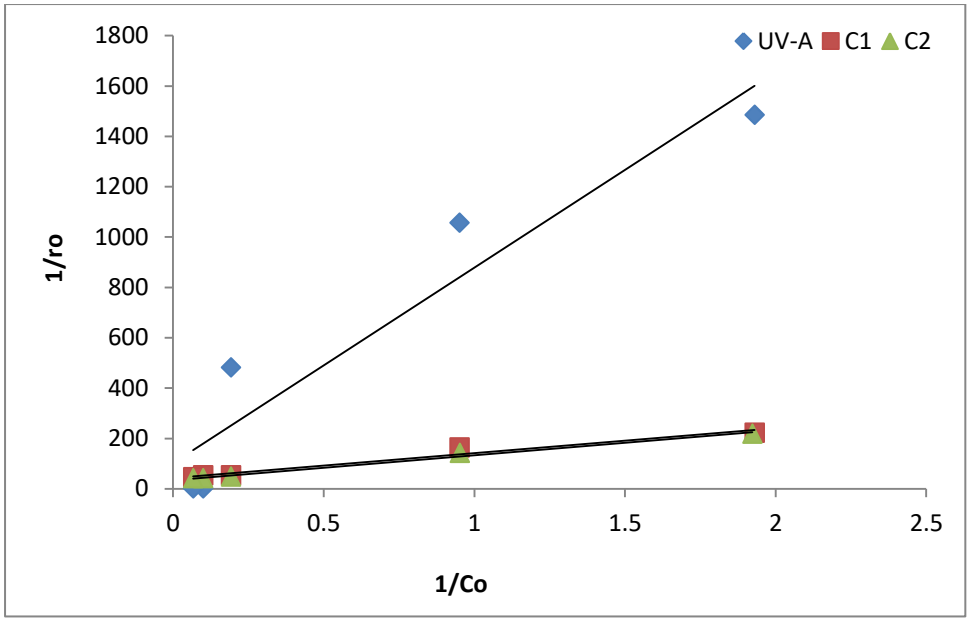

Figure 3.3.1.3(g): Langmuir-Hinshelwood plots for the photocatalytic degradation of alizarin yellow using C1: Ce^{3+}/TiO_2(C1) and C2: Ce^{3+}/TiO_2(C1) photocatalytic thin films and UV-A only photolysis [AY concentration: 0.5 – 15.0 mg/L; pH: 6.0; Temperature: 25±1 ^{0}C].

3.3.1.4. Effect of Co-existing ions on Tetracycline and Amoxicillin degradation

The assessment on the degradation of tetracycline or amoxicillin from aqueous solution by several interfering ions (50.0 mg/L), *viz.*, sodium chloride, sodium nitrate,

sodium nitrite, glycine, oxalic acid cadmium nitrate, copper sulphate and zinc chloride was done using the thin film Ce^{3+}/TiO_2(C2) photocatalyst. The samples were irradiated for 2 hours at pH 6.0 and the initial concentration of antibiotics was kept constant to 5.0 mg/L. The percent removal of tetracycline and amoxicillin was presented as a function of interfering ions and shown in Figures 3.3.1.4(a) and 3.3.1.4(b). The Figure clearly showed that the degradation of tetracycline or amoxicillin was inhibited to different extent in presence of different interfering ions. However, it was interesting to note that the presence of NaCl had caused to suppress significantly the degradation of tetracycline. Similar inhibition effect caused by chloride ion was also reported in the degradation of 4-fluorophenol using TiO_2 and ZnO_2 (Selvam *et al.,* 2007). It was mentioned that the scavenging property of Cl^- was to remove the hydroxyl radicals ($^{\bullet}OH$) thereby decreasing the degradation of the pollutant as given in the equation (1):

$$Cl^- + {}^{\bullet}OH \longrightarrow Cl^{\bullet} + OH^- \qquad \ldots (1)$$

The presence of other ions affected to a lesser extent in the photocatalytic degradation of tetracycline. The order of inhibition caused by the these interfering ions were found to be NaCl > $NaNO_3$ > oxalic acid > $CuSO_4$ > $Cd(NO_3)_2$ > $NaNO_2$ > glycine > $ZnCl_2$ for tetracycline degradation. On the other hand, the presence of several co-existing ions affected the degradation of amoxicillin. It was noted that the presence of $CuSO_4$ had caused to suppress significantly the degradation of amoxicillin. A major decrease in the degradation of amoxicillin in presence of $CuSO_4$ was probably due to the competitive adsorption of $CuSO_4$ onto the catalyst surface. The order of inhibition caused by the these interfering ions for the photocatalytic degradation of amoxicillin was found to be $CuSO_4$ > $NaNO_3$ > NaCl > $Cd(NO_3)_2$ > glycine > oxalic acid > $ZnCl_2$ > $NaNO_2$.

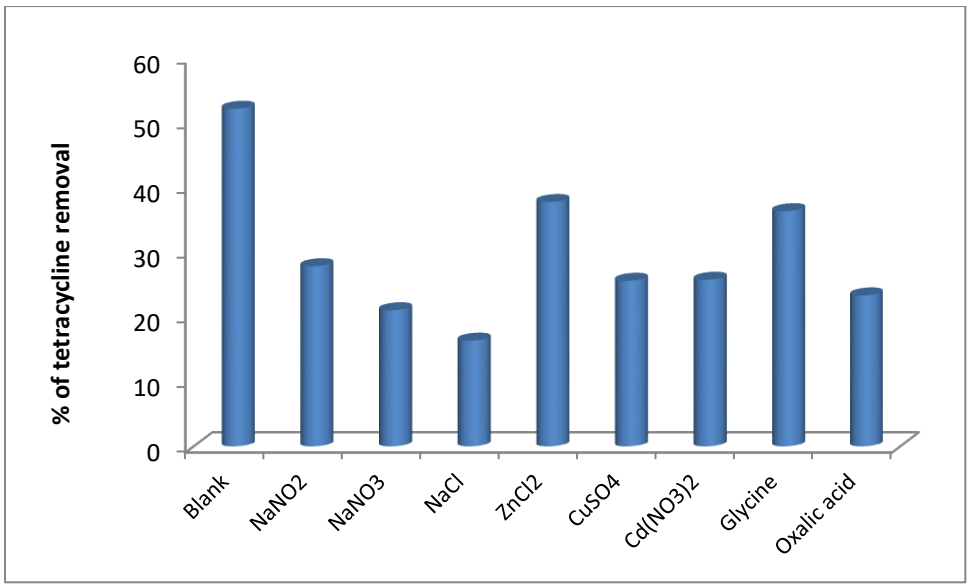

Figure 3.3.1.4(a): Photocatalytic degradation of tetracycline in presence of co-existing ions using Ce^{3+}/TiO_2(C2) thin film catalyst [TC concentration: 5.0 mg/L; Co-existing ion concentration: 50.0 mg/L; pH: 6.0; Temperature: 25±1 ^{0}C].

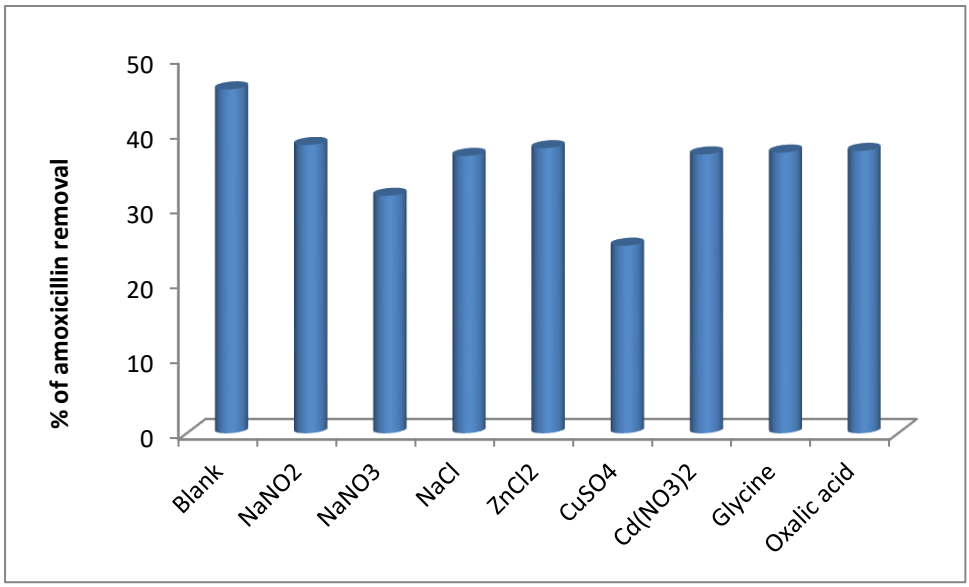

Figure 3.3.1.4(b): Photocatalytic degradation of amoxicillin in presence of several co-exiting ions using Ce^{3+}/TiO_2(C2) thin film catalyst [AMX concentration: 5.0 mg/L; Co-existing ion concentration: 50.0 mg/L; pH: 6.0; Temperature: 25±1 ^{0}C].

3.3.1.5 Mechanism of antibiotic removal

The present research work was extensively studied to propose a plausible mechanism of antibiotic removal using the Ce^{3+}/TiO_2(C2) thin film photocatalyst. The 2-propanol or HCO_3^- were potential scavengers of $^{\bullet}OH$ radicals (Lalhriatpuia *et al*., 2015; Xu *et al*., 2015). EDTA molecule suppressed significantly the photogenerated hole in the photoexcited titanium dioxide semiconductor (Jia *et al*., 2017i). On the other hand, the sodium azide (NaN_3) inhibited the singlet oxygen generated by combining the superoxide radical and photo generated h^+ (Barka *et al*., 2010). Therefore, the elimination of these antibiotics, *viz.*, amoxicillin and tetracycline was carried out in presence of scavengers. The antibiotic concentration taken was 5.0 mg/L at pH 6.0 and the scavenger concentration 1000.0 mg/L. The Ce^{3+}/TiO_2(C2) thin film photocatalyst was utilized in the photocatalytic reactor operations. The elimination efficiency of amoxicillin and tetracycline using the Ce^{3+}/TiO_2(C2) photocatalyst in presence of scavengers was shown in Figure 3.3.1.5. The results showed that the presence of these scavengers greatly suppressed the degradation efficacy of these two antibiotics. Moreover, among these scavengers, the 2-propanol and sodium azide suppressed significantly the tetracycline removal. Therefore, it implied that the $^{\bullet}OH$ radicals along with the superoxide radicals generated through the excited holes were responsible for the degradation of these antibiotics. It was reported that the doping of the cerium played an important role to enhance and stabilize the catalytic activity of TiO_2. The excitation of electron/hole pairs by the UV-A light was likely to be trapped by the doped cerium, followed by it moved to the adsorbed O_2 and ^-OH molecules on the catalyst surface (Tbessi *et al*., 2019). This resulted the formation of hydroxyl and superoxide radicals:

$$Ce^{3+} + O_2 \rightarrow Ce^{4+} + O^{\bullet}_2 \quad \ldots 3.3.1.5(i)$$

$$Ce^{3+} + h^+ \rightarrow Ce^{4+} \quad \ldots 3.3.1.5(ii)$$

$$Ce^{4+} + e^{-} \rightarrow Ce^{3+} \quad \ldots 3.3.1.5(iii)$$

$$Ce^{4+} + OH^{-} \rightarrow Ce^{3+} + {}^{\bullet}OH \quad \ldots 3.3.1.5(iv)$$

The Ce^{4+} ions reduced to Ce^{3+} at the potential of 1.61 V (vs NHE) and similarly, the reverse was at the potential of −1.61 V (vs NHE). Moreover, the conduction band of TiO_2 was having the potential of −0.29V. This potential was significantly lower than that of cerium reduction potential. This reaffirmed that electrons at conduction band able to reduce the Ce^{4+} to Ce^{3+}. On the other hand, the valence band (VB) of TiO_2 showed potential of +2.91V. This was more positive than the Ce^{3+} to Ce^{4+} oxidation potential. Therefore, the hole oxidized the Ce^{3+} to Ce^{4+}. Nevertheless, these cerium species (i.e., Ce^{3+}, Ce^{4+}) were primarily the charge carriers on the catalyst surface which effectively trapped the e^{-}/h^{+} pairs (Matejova *et al*., 2014; Xie *et al*., 2005).

On the other hand, the water molecule or the hydroxyl ions interacted with the hole and resulted with the hydroxyl radical species:

$$H_2O + h^{+} \rightarrow H^{+} + {}^{\bullet}OH \quad \ldots 3.3.1.5(v)$$

$$OH^{-} + h^{+} \rightarrow {}^{\bullet}OH \quad \ldots 3.3.1.5(vi)$$

These reactions showed that the presence of Ce^{3+} greatly restricted the recombination of electron hole pairs in the photoexcited TiO_2 semiconductor. Hence, it showed enhanced photocatalytic degradation of two antibiotics in aqueous solutions.

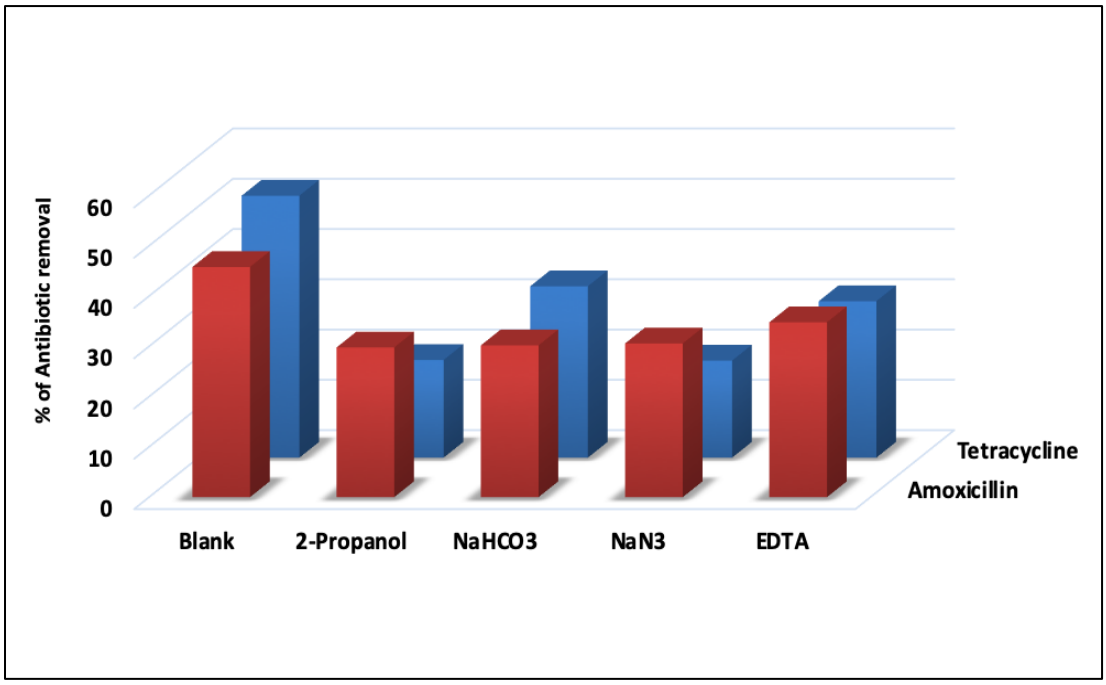

Figure 3.3.1.5. Photocatalytic removal of amoxicillin and tetracycline in presence of several scavengers using the Ce^{3+}/TiO_2(C2) thin film catalyst [TC/AMX concentration: 5.0 mg/L; Scavenger concentration: 1000.0 mg/L; pH: 6.0; Temperature: 25±1 ^{0}C].

3.3.1.6. Effect of Co-existing ions on Alizarin Yellow degradation

Similarly, the presence several anions and cations in the solution matrix could either inhibited or accelerated the degradation of the target pollutants in heterogeneous photocatalysis. Therefore, the efficiency of the thin film photocatalyst Ce^{3+}/TiO_2(C2) was examined in the photocatalytic degradation of alizarin yellow in presence of several co-existing ions (50.0 mg/L) including sodium nitrite, glycine, cadmium nitrate, copper sulphate, zinc chloride, sodium chloride, sodium nitrate, oxalic acid and EDTA. The samples were irradiated for 2 hours at pH 6.0 and the initial concentration of alizarin yellow was kept constant to 5.0 mg/L. The percent removal of alizarin yellow was presented as a function of interfering ions and presented in Figure 3.3.1.6(a). The Figure clearly showed that the degradation of alizarin yellow was inhibited to varied extent in presence of these co-

existing ions. However, it was observed that the presence of $CuSO_4$ and glycine had caused to suppress significantly the degradation of alizarin yellow. The order of inhibition caused by the these interfering ions were found to be $CuSO_4$ > glycine > EDTA > NaCl > $NaNO_3$ > $ZnCl_2$ > $NaNO_2$ > oxalic acid > $Cd(NO_3)_2$.

On the other hand the percentage removal of alizarin yellow in presence of scavengers, *viz.*, 2-propanol, sodium azide and sodium biocarbonate was shown in Figure 3.3.1.6(b). The scavenger sodium bicarbonate significantly suppressed the catalytic activity of the thin film Ce^{3+}/TiO_2(C2) since a marked decrease in percent removal of alizarin yellow was recorded. It was reported that HCO_3^- was a good scavenger of the $^{\bullet}OH_{bulk}$ ($^{\bullet}OH$ in aqueous medium) or surface $^{\bullet}OH$ radicals (Chang *et al.*, 2013). This indicated that the $^{\bullet}OH$ radicals predominantly attributing the degradation of alizarin yellow from aqueous solutions.

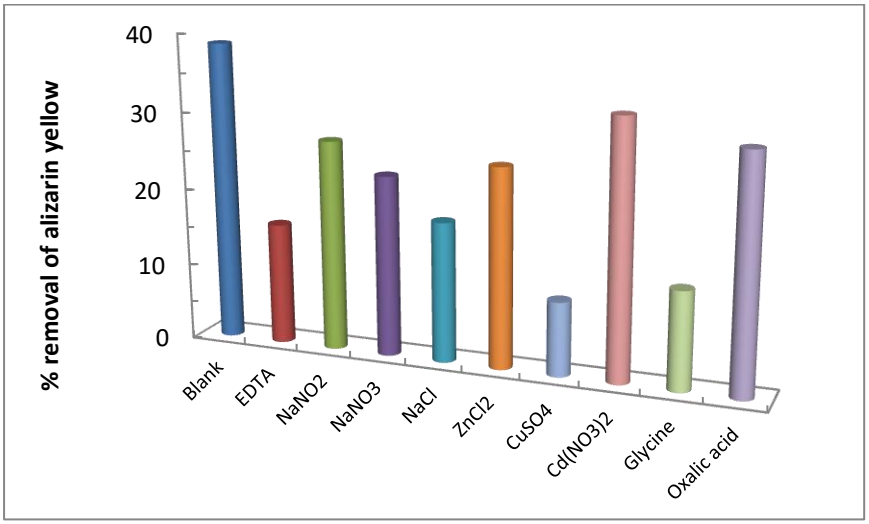

Figure 3.3.1.6(a): Photocatalytic degradation of alizarin yellow in presence of interfering ions using Ce^{3+}/TiO_2(C2) thin film catalyst [AY concentration: 5.0 mg/L; Co-existing ion concentration: 50.0 mg/L; pH: 6.0; Temperature: 25±1 ^{0}C].

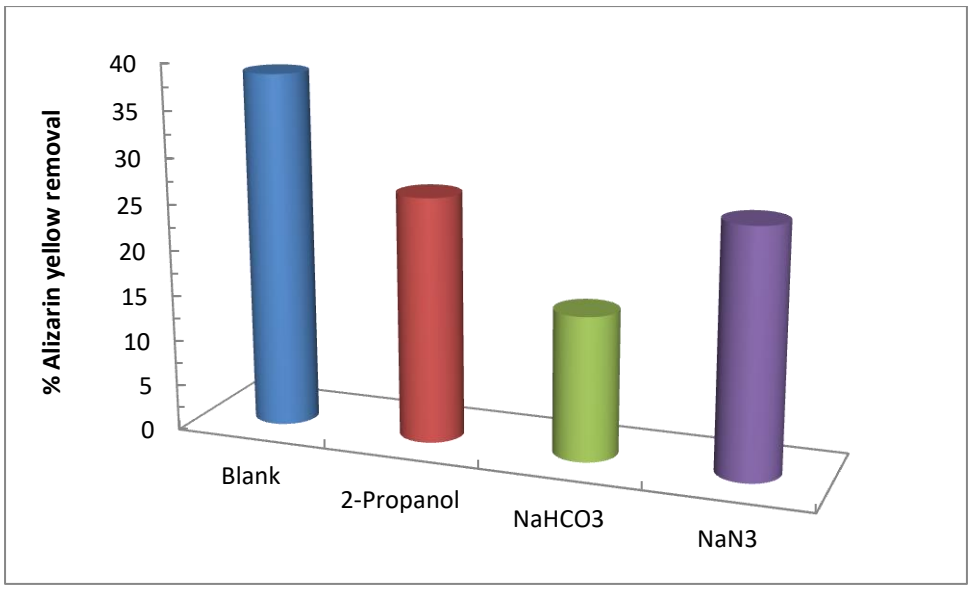

Figure 3.3.1.6(b): Effect of scavengers in the photocatalytic degradation of alizarin yellow using the Ce^{3+}/TiO_2(C2) thin film catalyst [AY concentration: 5.0mg/L; Scavenger concentration: 1000.0 mg/L; pH: 6.0; Temperature: 25±1 ^{0}C].

3.3.1.7. Mineralization Study

The mineralization of tetracycline was studied varying the tetracycline concentration from 1.0 to 20.0 mg/L at constant pH 6.0 employing the UV-A only, Ce^{3+}/TiO_2(C1) and Ce^{3+}/TiO_2(C2) samples. The results were obtained at the end of 2 hours of photo-irradiation. Percent of NPOC removal as a function of tetracycline concentration was computed and presented in Figure 3.3.1.7(a) and also shown in Table 3.3.1.7(a). The results clearly showed that increasing the concentration of tetracycline a sharp decrease in NPOC was observed. Quantitatively, increasing the concentration of tetracycline from 1.0 to 20.0 mg/L the percent of NPOC was decreased from 34.0 to 11.0% (using Ce^{3+}/TiO_2(C2) thin film); 29.67 to 7.4% (using Ce^{3+}/TiO_2(C1) thin film) and 21.27 to 3.17% (using UV-A only). The increase in concentration greatly suppressed the percentage mineralization of tetracycline. It was again observed that similar to the concentration dependence study, the Ce^{3+}/TiO_2(C1)

and Ce^{3+}/TiO_2(C2) thin films showed relatively higher efficiency in the mineralization of tetracycline compared to the UV-A photolysis.

On the other hand, the percent NPOC removal was studied as a function of pH. This enabled to optimise the best possible pH of treatment to achieve maximum mineralization of the tetracycline in the photocatalytic treatment. The tetracycline solutions ([TC]: 5.0 mg/L) was treated at different pH values (pH 4.0 to 10.00) for 2 hours using the UV-A only, Ce^{3+}/TiO_2(C1) and Ce^{3+}/TiO_2(C2) thin film catalysts. The percent of NPOC removal was presented as a function of pH (*cf.* Figure 3.3.1.7(b) and Table 3.3.1.7(b)). It was apparent from the Figure that the maximum NPOC removal was achieved at pH 10.0 using the UV-A only, Ce^{3+}/TiO_2(C1) and Ce^{3+}/TiO_2(C2) thin films. Quantitatively, at pH 10.0, 33.0, 23.0 and 17.2% NPOC removal was obtained using the Ce^{3+}/TiO_2(C2), Ce^{3+}/TiO_2(C1) and UV-A only treatment, respectively.

Table 3.3.1.7: Percentage removal of NPOC for tetracycline as a function of **(a)** concentration: **(b)** pH [C1: Ce^{3+}/TiO_2(C1); C2: Ce^{3+}/TiO_2(C2)].

(a)	**% Removal of NPOC**				
	TC concentration (mg/L)				
	1.0	**5.0**	**10.0**	**15.0**	**20.0**
UV-A	21.27	14.1	9.7	7.4	3.17
C1	29.67	21.6	18.9	12.9	7.4
C2	34.0	28.5	24.7	15.5	11.0

(b)	**% Removal of NPOC**			
	pH			
	4.0	**6.0**	**8.0**	**10.0**
UV-A	6.2	14.1	16.0	17.2
C1	20.0	22.0	25.0	23.0
C2	27.0	28.0	31.0	33.0

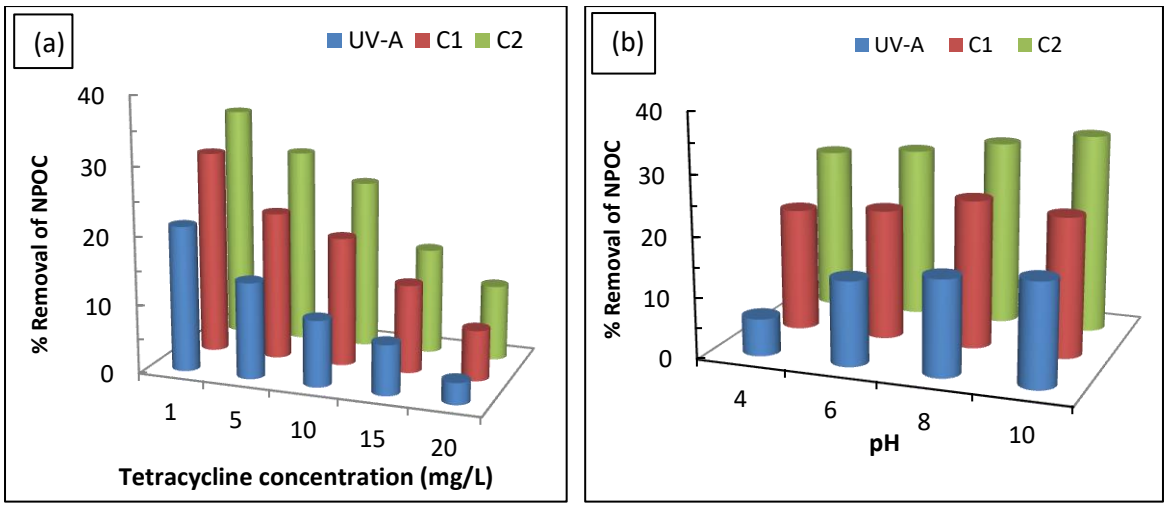

Figure 3.3.1.7: Percent mineralization of tetracycline (a) as a function of initial tetracycline concentration and (b) as a function of pH in the photolytic and photocatalytic degradations of tetracycline [C1: Ce^{3+}/TiO_2(C1); C2: Ce^{3+}/TiO_2(C2)].

Similarly, the percentage NPOC removal was obtained for the degradation of amoxicillin from aqueous solutions. The results were presented graphically in Figure 3.3.1.7(c) and in Table 3.3.1.7(c). The concentration of amoxicillin was increased from 0.5 to 15.0 mg/L and solution pH was kept constant pH 6.0 employing the UV-A only, Ce^{3+}/TiO_2(C1) and Ce^{3+}/TiO_2(C2) samples. The results were obtained at the end of 2 hours of photo-irradiation. It was obvious from the Figure that increasing the concentration of amoxicillin, a sharp decrease in NPOC was observed. Quantitatively, increasing the concentration of amoxicillin from 0.5 to 15.0 mg/L the percent of NPOC removal was decreased from 63.4 to 40.9% (using the Ce^{3+}/TiO_2(C2) thin film); from 54.0 to 35.4% (using Ce^{3+}/TiO_2(C1) thin film) and from 35.2 to 20.3 % (with UV-A only), respectively. It was again interesting to note that a significant mineralization was achieved using the thin films. However, the prolonged irradiation with the thin films might enable to enhance significantly the NPOC removal or to mineralize the amoxicillin significantly. Besides, similar to the concentration dependence study, the Ce^{3+}/TiO_2(C1) thin film showed

relatively lower efficiency in the mineralization of amoxicillin compared to the Ce^{3+}/TiO_2(C2) thin film. Similarly, the UV-A photolysis showed significantly lower NPOC removal compared to the photocatalytic treatments using the Ce^{3+}/TiO_2(C1) and Ce^{3+}/TiO_2(C2) thin films catalysts.

The pH dependence mineralization of amoxicillin was studied using the initial amoxicillin concentration (1.0 mg/L). The solutions were treated at different pH values (pH 4.0 to 10.0) for 2 hours using the UV-A only, Ce^{3+}/TiO_2(C1) and Ce^{3+}/TiO_2(C2) thin films and the percent of NPOC removal was presented as a function of pH in Figure 3.3.1.7(d) and in Table 3.3.1.7(d), respectively. It was evident from the Figure that the maximum NPOC removal was obtained at pH 6.0 using the UV-A only, Ce^{3+}/TiO_2(C1) and Ce^{3+}/TiO_2(C2) thin films. Quantitatively, at pH 6.0, the percentage of NPOC removal was achieved as 60.0, 50.0 and 26.6% using the thin film catalysts Ce^{3+}/TiO_2(C2), Ce^{3+}/TiO_2(C1) and UV-A only treatment, respectively. It was evident from the results that basic conditions slightly hindered the percent NPOC removal of amoxicillin from aqueous solutions. These results were again in agreement with the pH dependence removal of amoxicillin in the photocatalytic degradation.

Table 3.3.1.7: Percent removal of NPOC for amoxicillin as a function of **(c)** concentration: **(d)** pH [C1: Ce^{3+}/TiO_2(C1); C2: Ce^{3+}/TiO_2(C2)].

(c)	**% Removal of NPOC**				
	AMX concentration (mg/L)				
	0.5	**1.0**	**5.0**	**10.0**	**15.0**
UV-A	35.2	26.6	24.4	21.1	20.3
C1	54.0	49.9	45.3	40.0	35.4
C2	63.4	59.7	48.7	45.8	40.9

(d)	**% Removal of NPOC**			
	pH			
	4.0	**6.0**	**8.0**	**10.0**
UV-A	19.5	26.6	25.6	21.5
C1	41.0	50.0	47.0	40.0
C2	51.0	60.0	56.0	49.0

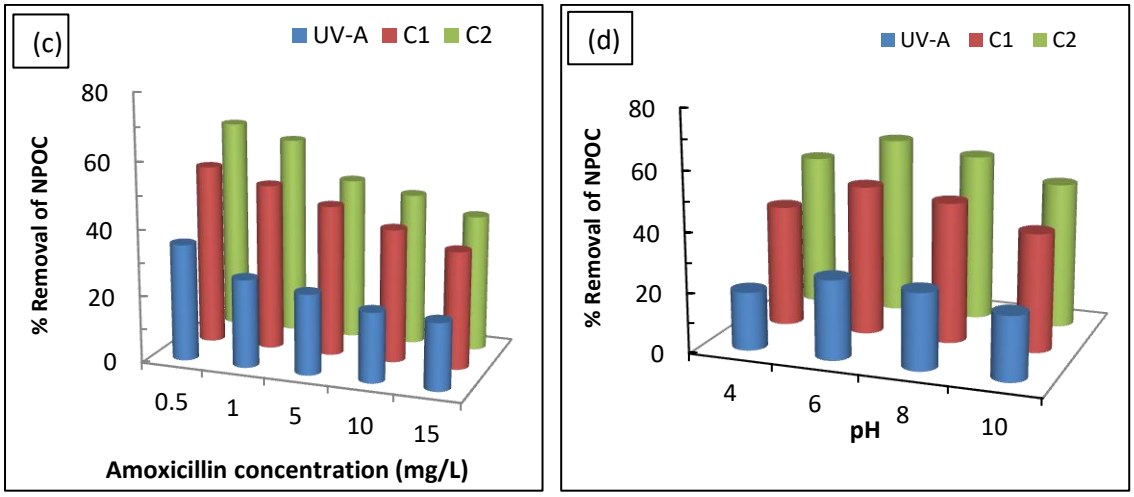

Figure 3.3.1.7: Percent mineralization of AMX (c) as a function of initial AMX concentration and (d) as a function of pH in the photolytic and photocatalytic degradations of AMX [C1: Ce^{3+}/TiO_2(C1); C2: Ce^{3+}/TiO_2(C2)].

The mineralization of alizarin yellow was also studied by varying the alizarin yellow concentration from 0.5 to 15.0 mg/L at constant pH 6.0 employing the UV-A only, Ce^{3+}/TiO_2(C1) and Ce^{3+}/TiO_2(C2) thin film samples. The results were obtained at the end of 2 hours of photo-irradiation. Percent of NPOC removal as a function of alizarin yellow concentration was computed and presented in Figure 3.3.1.7(e) and also shown in Table

3.3.1.7(e). The results clearly showed that increasing the concentration of alizarin yellow a sharp decrease in NPOC was observed. Quantitatively, increasing the concentration of alizarin yellow from 0.5 to 15.0 mg/L the percent of NPOC removal was decreased from 65.0 to 21.2% (using Ce^{3+}/TiO_2(C2) thin films); 62.8 to 19.8% (using Ce^{3+}/TiO_2(C1) thin films) and 10.7 to 3.8% (using UV-A only). The increase in concentration greatly suppressed the percentage mineralization of alizarin yellow. It was again observed that similar to the concentration dependence study, the Ce^{3+}/TiO_2(C1) and Ce^{3+}/TiO_2(C2) thin films showed relatively higher efficiency in the mineralization of alizarin yellow compared to the UV-A photolysis.

On the other hand, the percent NPOC removal as a function of pH was also studied and the results were shown in Figure 3.3.1.7(f) and in Table 3.3.1.7(f). The initial alizarin yellow concentration taken was 1.0 mg/L and the samples were treated at different pH values (pH 4.0 to 10.0) for 2 hours using the UV-A only, Ce^{3+}/TiO_2(C1) and Ce^{3+}/TiO_2(C2) thin film catalysts. It was evident from the results that the maximum NPOC removal was achieved at pH 6.0 using the UV-A only, Ce^{3+}/TiO_2(C1) and Ce^{3+}/TiO_2(C2) thin films. Quantitatively, at pH 6 the percentage removal of NPOC was found to be 54.0%, 51.0% and 10.2% using the Ce^{3+}/TiO_2(C2), Ce^{3+}/TiO_2(C1) and UV-A only treatment, respectively. These results were again in conformity with the pH dependence removal of alizarin yellow in the photocatalytic degradation. This clearly revealed that the thin films greatly favoured an enhanced NPOC removal, i.e., greater mineralization of alizarin yellow was attained using the photocatalyst thin films compared to the only photolysis treatment, i.e., UV-A illumination. Despite of partial mineralization of these pollutants as obtained by the photocatalytic treatment, however, a complete mineralization could be achieved with repeated treatment or even prolonged treatment of the samples.

Table 3.3.1.7: Percent removal of NPOC for alizarin yellow as a function of **(e)** concentration: **(f)** pH [C1: Ce^{3+}/TiO_2(C1); C2: Ce^{3+}/TiO_2(C2)].

(e)	**% NPOC Removal**				
	AY concentration (mg/L)				
	0.5	**1.0**	**5.0**	**10.0**	**15.0**
UV-A	10.7	10.2	5.5	4.8	3.8
C1	62.8	50.9	34.6	23.9	19.8
C2	65.0	54.1	38.2	26.6	21.2

(f)	**% NPOC Removal**			
	pH			
	4.0	**6.0**	**8.0**	**10.0**
UV-A	8.1	10.2	7.2	6.8
C1	47.0	51.0	39.0	36.0
C2	49.0	54.0	47.0	44.0

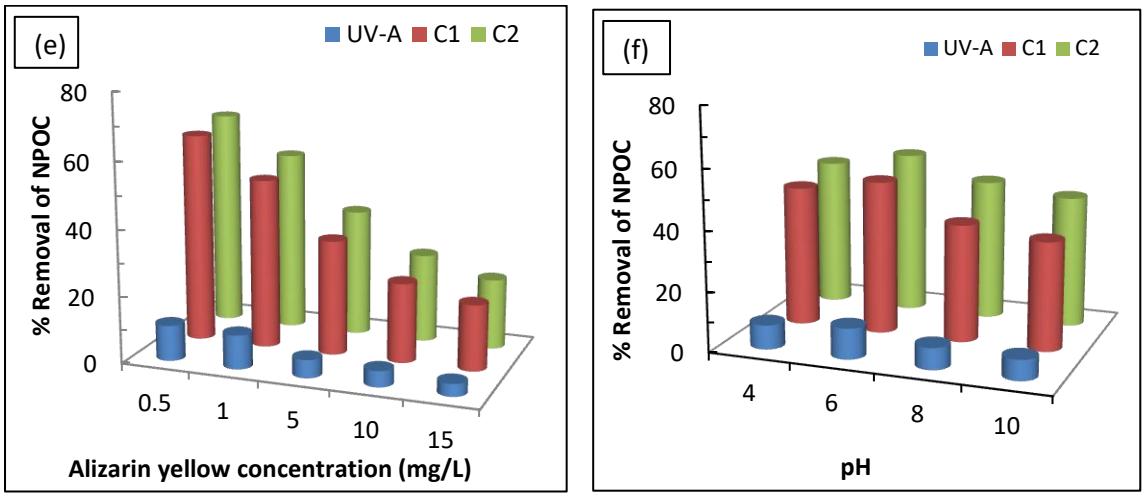

Figure 3.3.1.7: Percent mineralization of alizarin yellow (e) as a function of initial alizarin yellow concentration and (f) as a function of pH in the photolytic and photocatalytic degradations of alizarin yellow [C1: Ce^{3+}/TiO_2(C1) C2: Ce^{3+}/TiO_2(C2)].

3.3.2. Stability of Thin Film Photocatalyst

The photocatalytic stability of the catalyst Ce^{3+}/TiO_2(C2) thin film was assessed in the repeated reactor operations. The repeated use of photocatalyst impacted the long term implication of catalyst and eventually could show the cost effectiveness of the overall process. Threfore, the six cycles of photocatalytic operations were conducted using the Ce^{3+}/TiO_2(C2) thin film photocatalyst. In order to perform the stability tests, the initial concentration of amoxicillin or tetracycline or alizarin yellow taken was 5.0 mg/L at pH 6.0. Once after completion of reactor operation, the catalyst disk was washed with purified water and dried at 105 ^{0}C and again employed for next reactor operation. The results of efficiency test of the Ce^{3+}/TiO_2(C2) thin film for tetracycline and amoxicillin were illustrated in Figure 3.3.2(a). It was evident from the Figure that even at the completion of six cycles of reactor operations the photocaatlytic activity of the Ce^{3+}/TiO_2(C2) thin film photocatalyst was not affected at least in the elimination of amoxicillin and tetracycline. Quantitatively, the removal efficiency of catalyst was decreased from 48.8% to 43.4% (for amoxicillin) and from 52.1% to 51.1% (for tetracycline) at the end of sixth reactor operation. Similarly, at the end of six repeated cycles had caused a decrease in alizarin yellow removal efficiency from 45.78% to 43.37% (i.e., a decrease of 2.41%) using the Ce^{3+}/TiO_2(C2) (*cf.* Figure 3.3.2(b)). The results clearly revealed that very minimal decrease in efficiency of Ce^{3+}/TiO_2(C2) photocatalyst was recorded for these antibiotics/dye removal. This implied the potential use of photocatalyst in the reactor operations. On the other hand, it was reported that the TiO_2 powder showed marked decrease in catalytic efficiency for dye removal (Saggioro *et al*., 2011). However, similar excellent stability of 1%Ce – 0.6%Mn/TiO_2 was obtained in the four cycle of operations in the removal of diclofenac (Tbessi *et al*., 2019).

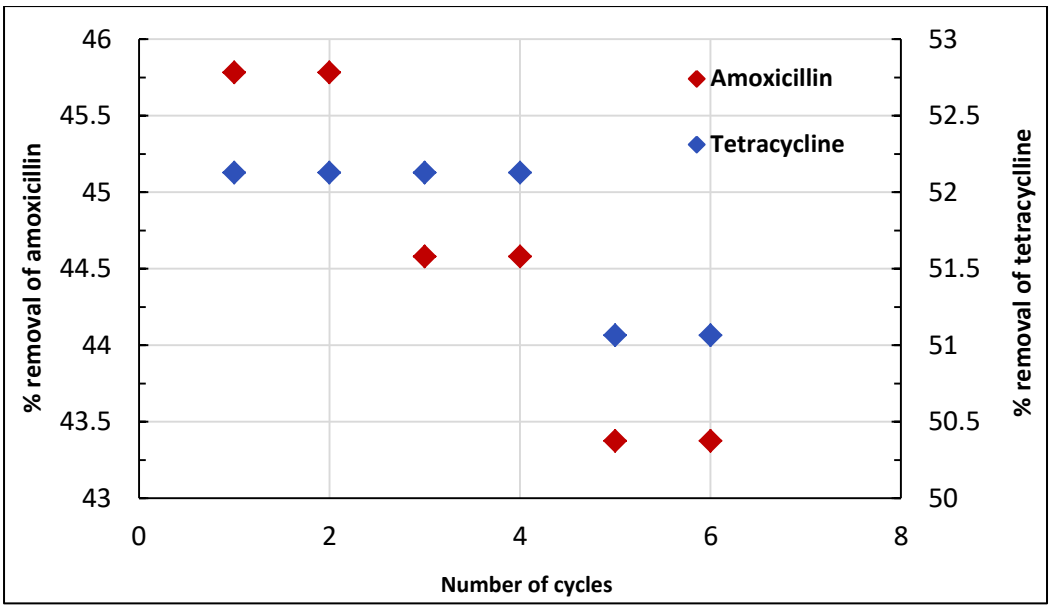

Figure 3.3.2(a). Cycling runs for photocatalytic degradation of amoxicillin and tetracycline using the Ce^{3+}/TiO_2(C2) thin film photocatalyst ([AMX and TC] = 5.0 mg/L, pH: 6).

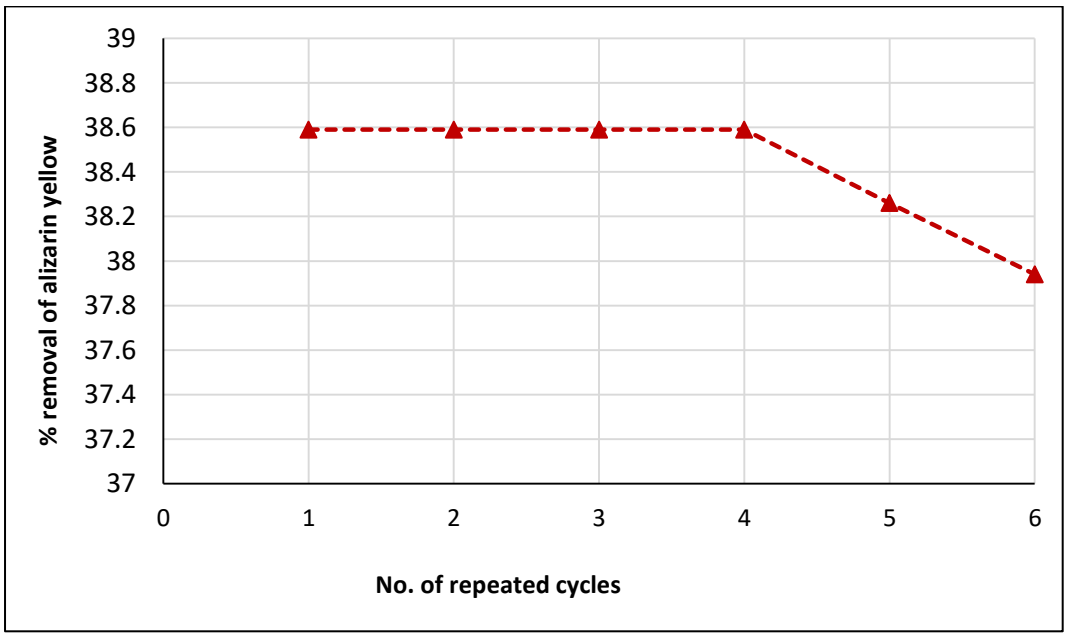

Figure 3.3.2(b). Cycling runs for photocatalytic degradation of alizarin yellow using the Ce^{3+}/TiO_2(C2) thin film photocatalyst ([Alizarin Yellow]= 5.0 mg/L, pH: 6).

4. CONCLUSIONS

Zerovalent Ag-nanoparticles doped TiO_2 thin films were synthesized by the template method using polyethylene glycol as filler medium. The materials were characterized by the advanced analytical methods. SEM (Scanning electron microscopy) images showed that the grains of TiO_2 were evenly distributed and forming uniform surface morphology on the borosilicate glass substrate. The TEM (Transmission electron microscopy) images showed that the Ag(NPs) were distributed within the titania network and the particles were in the range of 10 – 15 nm for the solids i.e., Ag^0(NP)/TiO_2(A1) (non-template) and Ag^0(NP)/TiO_2(A2) (template) samples. Moreover, the interplanar distance of the Ag-nanoparticles were obtained to be 0.20 and 0.17 nm for the Ag^0(NP)/TiO_2(A1) and Ag^0(NP)/TiO_2(A2) solids, respectively. EDX elemental mapping enabled to ascertained the doping of Ag(NPs) with titania network. AFM images confirmed the pillar formation of TiO_2 onto the glass substrate and the pillar height was found to be *Ca*. 35 and 250 nm for the thin films Ag^0(NP)/TiO_2(A1) and Ag^0(NP)/TiO_2(A2), respectively. XRD (X-Ray diffraction) data showed that the thin films were predominantly amorphous in nature. However, a distinct peak observed at 2θ value 25.39 confirmed the anatase phase of TiO_2 in both the solids. BET analytical results indicated that nanocomposite materials were having the H2 type of hysteresis loops and the BET specific surface area and pore sizes were found to be 5.61 nm and 49.55 m^2/g (for Ag^0(NP)/TiO_2(A1)); 5.67 nm and 12.02 m^2/g (for Ag^0(NP)/TiO_2(A2)) solids, respectively. Further, the DRS analysis showed that the band gap energies were found to be 3.12, 2.88 and 2.89 eV respectively for the bare TiO_2, Ag^0(NP)/TiO_2(A1) and Ag^0(NP)/TiO_2(A2) solids.

Similarly, the thin films of TiO_2 were prepared using the polyethylene glycol (PEG) as template medium and the Au-nanoparticles were doped *in situ* in the sol-gel preparation

method. The surface morphology of thin films were obtained by the SEM and TEM/EDX imaging that indicated nanoparticles of TiO_2 were evenly distributed within the thin film Au^0(NP)/TiO_2(B1) (prepared without PEG) and some crack were visible with the PEG template thin film Au^0(NP)/TiO_2(B2). The Au-nanoparticles were clearly visible at places with TEM images of these films. Moreover, EDX elemental mapping indicated that Au-nanoparticles were very evenly distributed within the titania network. AFM images showed that TiO_2 were forming pillars onto the borosilicate glass substrate and pillar height was found to be *Ca*. 50 and 300 nm for the thin films Au^0(NP)/TiO_2(B1) and Au^0(NP)/TiO_2(B2), respectively. XRD data showed that the thin films were amorphous in nature. However, a peak was clearly visible at 2θ of around 25 indicated the anatase phase of TiO_2. N_2 adsorption and desorption data indicated that the materials showed H2 type of hysteresis loops and the BET specific area and pore sizes were found to be 5.27 nm and 41.47 m^2/g (for Au^0(NP)/TiO_2(B1)); 5.59 nm and 19.91 m^2/g (for Au^0(NP)/TiO_2(B2)) thin films, respectively. The band gap energies were found to be 2.86 and 2.87 eV respectively for the Au^0(NP)/TiO_2(B1) and Au^0(NP)/TiO_2(B2) solids.

Further, The Ce^{3+} doped titanium dioxide thin film was synthesized by one step facile template method. The Ce^{3+}/TiO_2(C1) (non-template) and Ce^{3+}/TiO_2(C2) (template) thin films showed anatase TiO_2 mineral phase. The XPS analysis showed that cerium (Ce) was predominantly doped in its Ce^{3+} oxidation state. SEM images showed that both the thin films possessed with heterogeneous surface structure. Moreover, the fine particles of TiO_2 were evenly distributed on the substrate surface. The Ce-particles were clearly visible at places with TEM images of these materials. The interplanar distances of the Ce-particles within the solids were found to be 0.29 and 0.33 nm for the Ce^{3+}/TiO_2(C1) and Ce^{3+}/TiO_2(C2) solids. 3D-AFM images showed maximum surface roughness (R_{max}) values

of 30.1 nm and 18.2 nm for the Ce^{3+}/TiO_2(C1) and Ce^{3+}/TiO_2(C2) thin films, respectively. Further, the thin film catalysts were fully employed in the photocatalytic degradation of several micropollutants and dye *viz.*, triclosan (TCS) (using Ag^0(NP)/TiO_2(A1) and Ag^0(NP)/TiO_2(A2)), alizarin yellow (AY) (using Ag^0(NP)/TiO_2(A1), Ag^0(NP)/TiO_2(A2), Au^0(NP)/TiO_2(B1), Au^0(NP)/TiO_2(B2), Ce^{3+}/TiO_2(C1) and Ce^{3+}/TiO_2(C2)), tetracycline (TC) (using Ce^{3+}/TiO_2(C1) and Ce^{3+}/TiO_2(C2)) and amoxicillin (AMX) (using Ce^{3+}/TiO_2(C1) and Ce^{3+}/TiO_2(C2)) under the reactor operations.

Various physico-chemical parametric studies revealed that triclosan showed highest degradation at pH ~ 4.0. Alizarin yellow and amoxicillin showed highest degradation at pH ~ 6.0 whereas tetracycline showed highest degradation at pH ~ 10. The effect of pollutant concentration studies showed that decreasing the pollutant concentration favoured greatly the percent degradation of these pollutants. The results suggested that these thin films could be employed effectively at a wide range of solution pH and concentration for the pollutant degradations. The thin film photocatalysts were found to be potential in the removal of these residual pollutants from aquatic environment. The total organic carbon measurement using TOC analyser was used to further study the apparent mineralization of these pollutants. The results clearly showed that the mineralization of these pollutants increased with decreasing the micropollutants/dye concentrations.

The time dependence photocatalytic degradation of micropollutants/dye was further utilized to deduce the kinetics of degradation. The kinetic data was obtained for the degradation of triclosan, alizarin yellow, tetracycline and amoxicillin which were found to be pseudo-first-order rate kinetics and the degradation rate was applicable with Langmuir-Hinshelwood isotherm. The L-H isotherm fitted reasonably well to the photocatalytic degradations of triclosan, alizarin yellow, tetracycline and amoxicillin.

Besides, the scavengers effects in the photocatalytic degradation processes of triclosan, alizarin yellow, tetracycline and amoxicillin were studied using several scavengers to trap the radical species, *viz.*, $^{\bullet}OH$ or $O_2^{\bullet-}$ or singlet oxygen species. The scavengers studies inferred that $^{\bullet}OH$ radicals were greatly taking part in the degradation of these pollutants when using $Ag^0(NP)/TiO_2(A1)$, $Ag^0(NP)/TiO_2(A2)$, $Au^0(NP)/TiO_2(B1)$, $Au^0(NP)/TiO_2(B2)$, $Ce^{3+}/TiO_2(C1)$ and $Ce^{3+}/TiO_2(C2)$ thin films. The presence of several cations and anions affected the photocatalytic degradation of these pollutants at varied level. The presence of EDTA, sodium azide and HCO_3^- inhibited significantly the percentage degradation of alizarin yellow which clearly indicated that the $^{\bullet}OH$ radicals, holes and the singlet oxygen was involved in the alizarin yellow degradation. Besides, the presence of 2-propanol, EDTA, sodium azide or HCO_3^- also inhibited significantly the percentage degradation of triclosan which clearly inferred that the $^{\bullet}OH$ radicals and holes were predominantly involved in the degradation process. Additionally, the singlet oxygen was also involved in the triclosan degradation mechanism. Moreover, presence of these scavengers greatly suppressed the degradation efficacy of tetracycline and amoxicillin. Moreover, among these scavengers, the 2-propanol and sodium azide suppressed significantly the tetracycline removal. Therefore, it implied that the $^{\bullet}OH$ radicals along with the superoxide radicals generated through the excited holes were responsible for the degradation of tetracycline and amoxicillin.

The repeated use of thin films, *viz.*, $Ag^0(NP)/TiO_2(A1)$, $Ag^0(NP)/TiO_2(A2)$, $Au^0(NP)/TiO_2(B1)$, $Au^0(NP)/TiO_2(B2)$, $Ce^{3+}/TiO_2(C1)$ and $Ce^{3+}/TiO_2(C2)$ showed no significant decrease in percentage degradation of these micropollutants/dye from aqueous solutions which inferred that the thin films were fairly stable at least for six photocatalytic operations. Overall, the template synthesized photocatalysts $Ag^0(NP)/TiO_2(A2)$,

Au^0(NP)/TiO_2(B2) and Ce^{3+}/TiO_2(C2) showed significantly enhanced catalytic activity than the corresponding non-template synthesized photocatalysts Ag^0(NP)/TiO_2(A1), Au^0(NP)/TiO_2(B1) and Ce^{3+}/TiO_2(C1). The photocatalytic efficiencies were found remarkably higher than the photolytic degradations of triclosan, alizarin yellow, tetracycline and amoxicillin. This pointed further the greater applicability of thin film photocatalysts without much decline in activity which conveyed the cost effectiveness and makes it potential practical applications in real wastewater treatment. The overall treatment process was found to be "greener" and showed greater applicability of the photocatalysts (*viz.*, Ag^0(NP)/TiO_2(A1), Ag^0(NP)/TiO_2(A2), Au^0(NP)/TiO_2(B1), Au^0(NP)/TiO_2(B2), Ce^{3+}/TiO_2(C1) and Ce^{3+}/TiO_2(C2)) in the advanced treatment technologies.

4.1. Future Scope of Present Work

The present research works deals with efficient, cost-effective studies for the remediation of aquatic environment contaminated with the emerging micropollutants/dye, *viz.*, triclosan, alizarin yellow, tetracycline and amoxicillin. The photocatalyst thin films, *viz.*, Ag^0(NP)/TiO_2(A1), Ag^0(NP)/TiO_2(A2), Au^0(NP)/TiO_2(B1), Au^0(NP)/TiO_2(B2), Ce^{3+}/TiO_2(C1) and Ce^{3+}/TiO_2(C2) were successfully applied for the photocatalytic degradation of these contaminants from aqueous solutions in the laboratory reactor processes. The promising laboratory experiments could be, perhaps, employed for its further implications at the larger scale treatment under the pilot plant level for real wastewater treatment. The input research data perhaps implied for scaling the unit operations for the technology development.

The research studies may further be extended for academic development for finding the insights of oxidation process by unveiling the oxidation pathways; conducting the

experiments with the mass-spectrometry to identify the by-products and involvement of specific radicals using the fast analytical techniques.

The fabrication of photocatalysts could possibly be employed using the natural clay support media which eventually make the materials more indigenous and profitable. Also, the production of Ag or Au or Ce nanoparticles could be obtained using the plant extracts which make the fabrication process greener and environment benign.

REFERENCES

Aazam, E.S., (2014). Photocatalytic oxidation of cyanide under visible light by Pt doped $AgInS_2$ nanoparticles. *J. Ind. Eng. Chem*., **20**: 4008–4013.

Abdi, J., Vossoughi, M., Mahmoodi, N.M., Alemzadeh, I., (2017). Synthesis of metal-organic framework hybrid nanocomposites based on GO and CNT with high adsorption capacity for dye removal. *Chem. Eng. J*., **326**: 1145–1158.

Abrahart, E.N., (1977). Dyes and Their Intermediates, Chemical Publishing, New York.

Adolfsson–Erici, M., Pettersson, M., Parkkonen, J., Sturve, J., (2002). Triclosan, a commonly used bactericide found in human milk and in the aquatic environment in Sweden. *Chemosphere*, **46**: 1485–1489.

Ahmed. S., Rasul. M.G., Wayde. N.M., Brown. R., Hashib. M.A., (2010). Heterogeneous photocatalytic degradation of phenols in wastewater: A review on current status and developments. *Desalination*, **261**: 3–18.

Aksu, Z., Balibek, E., (2010). Effect of salinity on metal-complex dye biosorption by Rhizopus arrhizus. *J. Environ. Manage*., **91**: 1546–1555.

Aksu, Z., Tunc, O.D., (2005). Application of biosorption for penicillin G removal: comparison with activated carbon. *Process. Biochem*., **40 (2)**: 831–847.

Alwani, M.A.M.A., Norasikin, A.L., Mohamad, A.B., Kadhum, A.A.H., Mukhlus, A., (2018). Application of dyes extracted from Alternanthera Dentata leaves and Musa Acuminata Bracts as natural sensitizers for dye-sensitized solar cells, *Spectrochim. Acta. A: Mol. Biomol. Spectrosc*., **192**: 487–498.

Ameen, S., Akhtar, M.S., Seo, H.-K., Shin, H.-S., (2014). Solution-processed CeO_2/TiO_2 nanocomposite as potent visible light photocatalyst for the degradation of bromophenol dye. *Chem. Eng. J*., **247**: 193–198.

Anderson, R.J., Bendell, D.J., Groundwater, P.W., (2004). Organic Spectroscopic Analysis. *The Royal Society of Chemistry*, **22**: 7–23.

Andreozzi, R., Canterino, M., Marotta, R., Paxeus, N., (2005). Antibiotic removal from wastewaters: the ozonation of amoxicillin. J. *Hazard. Mater*., **122 (3)**: 243–250.

Andreozzi, R., Caprio, V., Ciniglia, C., de Champdor e, M., Giudice, R.L., Marotta, R., Zuccato, E., (2004). Antibiotics in the environment: occurrence in Italian STPs, fate, and preliminary assessment on algal toxicity of amoxicillin. *Environ. Sci. Tech*., **38 (24)**: 6832–6838.

Andreozzi, R., Caprio, V., Insola, A., Marotta, R., (1999). Advanced oxidation processes (AOP) for water purification and recovery. *Catal. Today*, **53**: 51–59.

Andreu, V., Vazquez-Roig, P., Blasco, C., Pico, Y., (2009). Determination of tetracycline residues in soil by pressurized liquid extraction and liquid chromatography tandem mass spectrometry. *Anal. Bioanal. Chem*., **394**: 1329–1339.

Angadi, S.C., Manjeshwar, L.S., Aminabhavi, T.M., (2012). Novel composite blend microbeads of sodium alginate coated with chitosan for controlled release of amoxicillin. *Int. J. Biol. Macromol.*, **51(1- 2)**: 45–55.

Anpo, M., Aikawa, N., Kodama, S., Kubokawa, Y., (1984). Photocatalytic hydrogenation of alkynes and alkenes with water over titanium dioxide. Hydrogenation accompanied by bond fission. *J. Phys. Chem*., **88**: 2569–2572.

Anpo, M., Shima, T., Kodama, S., Kubokawa, Y., (1987). Photocatalytic hydrogenation of propyne with water on small–particle titania: size quantization effects and reaction intermediates. *J. Phys. Chem*., **91**: 4305–4310.

Aranami, K., Readman, J.W., (2007). Photolytic degradation of triclosan in freshwater and seawater. *Chemosphere*, **66**: 1052–1056.

Arikan, O.A., Mulbry, W., Rice, C., (2009). Management of antibiotic residues from agricultural sources: use of composting to reduce chlortetracycline residues in beef manure from treated animals. *J. Hazard. Mater*., **164**: 483–489.

Asha, K.K., Sankar, T.V., Nair, P.G., (2007). Effect of tetracycline on pancreas and liver function of adult male albino rats. *J. Pharm. Pharmacol*., **59**: 1241–1248.

Avinash Shivajirao, P., (2012). Treatment of distillery wastewater using membrane

technologies. *Int. J. Adv. Eng. Res. Stud.,* **1 (3)**: 275–283.

Aysin, B., Ozturk, A., Park, J., (2013). Silver–loaded TiO_2 powders prepared through mechanical ball milling. *Ceram. Int*., **39**: 7119–7126.

Babic, S., Curkovic, L., Ljubas, D., Cizmic, M., (2017). TiO_2 assisted photocatalytic degradation of macrolide antibiotics. *Curr. Opin. Green Sustain. Chem.,* **6**: 34–41.

Bacsa, R.R., Kiwi, J., (1998). Effect of rutile phase on the photocatalytic properties of nanocrystalline titania during the degradation of p–coumaric acid. *Appl. Catal. B, Environ.*, **16**: 19–29.

Bae, E., Choi, W., (2003). Highly enhanced photoreductive degradation of perchlorinated compounds on dye-sensitized metal/TiO_2 under visible light. *Environ. Sci. Technol*., **37**: 147–152.

Bafana, A., Devi, S.S., Chakrabarti, T., (2011). Azo dyes: past, present and the future. *Environ. Rev*., **19**: 350–371

Bahnemann, D., Henglein, A., Lilie, J., Spanhel, L., (1984). Flash photolysis observation of the absorption spectra of trapped positive holes and electrons in colloidal titanium dioxide. *J. Phys. Chem*., **88**: 709–711.

Bai, Z.Y., Yang, Q., Wang, J.L., (2016a). Catalytic ozonation of sulfamethazine using $Ce_{0.1}Fe_{0.9}OOH$ as catalyst: mineralization and catalytic mechanisms. *Chem. Eng. J*., **300**: 169–176.

Bai, Z.Y., Yang, Q., Wang, J.L., (2016b). Fe_3O_4/multi–walled carbon nanotubes as an efficient catalyst for catalytic ozonation of p–hydroxybenzoic acid. *Int. J. Environ. Sci. Technol*., **13**: 483–492.

Ball, P., (2007). The clinical development and launch of amoxicillin/clavulanate for the treatment of a range of community-acquired infections. *Int. J. Antimicrob. Agents*, **30S**: S113-S117.

Barka, N., Qourzal, S., Assabbane, A., Nounah, A., Ait-Ichou, Y., (2010). Photocatalytic degradation of an azo reactive dye, Reactive Yellow 84, in water using an industrial titanium dioxide coated media. *Arab. J. Chem*., **3**: 279–283.

Bartelt-Hunt, S,L., Snow, D.D., Damon, T., Shockley, J., Hoagland, K., (2009). The occurrence of illicit and therapeutic pharmaceuticals in wastewater effluent and surface waters in Nebraska. *Environ. Pollut*., **157**: 786–791.

Bebu, A., Szabo, L., Leopold, N., Berindean, C., David, L., (2011). IR, Raman, SERS and DFT study of amoxicillin. *J. Mol. Struct*., **993**: 52–56.

Bedoux, G., Roig, B., Thomas, O., Dupont, V., Le Bot, B., (2012). Occurrence and toxicity of antimicrobial triclosan and by–products in the environment. *Environ. Sci. Pollut. Res*., **19 (4)**: 1044–1065.

Benitez, F.J., Real, F.J., Acero, J.L., Garcia. C., Llanos, E.M., (2007). Kinetics of phenylurea herbicides oxidation by Fenton and photo–Fenton processes. *J. Chem. Technol. Biot*., **82**: 65–73.

Berghe, H.V.D., Garric, X., Vert, M., Coudane, J., (2011). New amoxicillin–poly(lactic acid) –based conjugates: synthesis and in vitro release of amoxicillin. *J. Polym. Int*., **60**: 398.

Beshkar, F., Zinatloo-Ajabshir, S., Bagheri, S., Salavati-Niasari, S., (2017). Novel preparation of highly photocatalytically active copper chromite nanostructured material via a simple hydrothermal route. PLOS One.

Bharatvaj, J., Preethi, V., Kanmani, S., (2018). Hydrogen production from sulphide wastewater using Ce^{3+}–TiO_2 photocatalysis. *Int. J. Hydrog. Energy*, **43**: 3935–3945.

Bhatkhande, D.S., Kamble, S.P., Sawant, S.B., Pangarkar, V.G., (2004). Photocatalytic and photochemical degradation of nitrobenzeneusing artificial ultraviolet light. *Chem. Eng. J*., **102**: 283–290.

Bicchi, C., Schilirò, T., Pignata, C., Fea, E., Cordero, C., Canale, F., Gilli, G., (2009). Analysis of environmental endocrine disrupting chemicals using the E–screen method and stir bar sorptive extraction in wastewater treatment plant effluents. *Sci. Total Environ*., **407**: 1842–1851.

Bokare, A.D., Choi, W., (2014). Review of iron–free Fenton-like systems for activating H_2O_2 in advanced oxidation processes. *J. Hazard. Mater*., **275**: 121–135.

Bolong, N., Ismail, A.F., Salim, M.R., Matsuura, T., (2009). A review of the effects of emerging contaminants in wastewater and options for their removal. *Desalination*, **239**: 229–246.

Borthakur, P., Boruah, P.K., Hussain, N., Silla, Y., Das, M.R., (2017). Specific ion effect on the surface properties of Ag/reduced graphene oxide nanocomposite and its influence on photocatalytic efficiency towards azo dye degradation. *Appl. Surf. Sci*., **423**: 752–761.

Borujeni, F.G., Mahvi, A.H., Naseri, S., Faramarzi, M.A., Nabizadeh, R., Alimohammadi, M., (2011). Application of immobilized horseradish peroxidase for removal and detoxification of azo dye from aqueous solution. *Res. J. of Chem. Environ*., **15 (2)**: 217–222.

Bowman, J.C., Zhou, J.L., Readman, J.W., (2002). Sediment–water interactions of natural oestrogens under estuarine conditions. *Marine Chem*., **77**: 263–276.

Brausch, J.M., Rand, G.M., (2011). A review of personal care products in the aquatic environment: environmental concentrations and toxicity. *Chemosphere*, **82 (11)**: 1518–1532.

Bu, S., Jin, Z., Liu, X., Du, H., Cheng, Z., (2004). Preparation and Formation Mechanism of Porous TiO_2 Films Using PEG and Alcohol Solvent as Double–Templates. *J. Solgel Sci. Technol.*, **30**: 239–248.

Bu, S., Jin, Z., Liu, X., Yin, T., Cheng, Z., (2006). Preparation of nanocrystalline TiO_2 porous films from terpineol–ethanol–PEG system. *J. Mater. Sci*., 41: 2067–2073.

Bunch, A., Bernot, M., (2010). Distribution of nonprescription pharmaceuticals in central Indiana streams and effects on sediment microbial activity. *Ecotoxicology*, **20**: 97–109.

Buxton, G.V., Greenstock, C.L., Helman, W.P., Ross, A.B., (1988). Critical review of rate constants for reactions of hydrated electrons, hydrogen atoms and hydroxyl radicals (·OH/·O− in Aqueous Solution, *J. Phys. Chem. Ref. Data*, **17**: 513–886.

Caliskan, Y., Yatmaz, H.C., Bektas, N., (2017). Photocatalytic oxidation of high concentrated dye solutions enhanced by hydrodynamic cavitation in a pilot reactor, *Process Saf. Environ. Prot.*, **111**: 428–438.

Canizares, P., Martinez, F., Jimenez, C., Lobato, J., Rodrigo, M.A., (2006). Coagulation and electrocoagulation of wastes polluted with dyes. *Environ. Sci. Technol*., **40 (20)**: 6418–6424.

Cao, M., Wang, P., Ao, Y., Wang, C., Hou, J., Qian, J., (2016). Visible light activated photocatalytic degradation of tetracycline by a magnetically separable composite photocatalyst: Graphene oxide/magnetite/cerium-doped titania. *J. Colloid Interface Sci*., **467**: 129–139.

Carballa, M., Omil, F., Lema, J.M., Lompart, M., García-Jares, C., Rodríguez, I., Gómez, M., Ternes, T., (2004). Behavior of pharmaceuticals, cosmetics and hormones in a sewage treatment plant. *Water Res*., **38**: 2918–2926.

Carless, J.E., (1996). Remington's pharmaceutical sciences. *J. Pharm. Pharmacol*., **18 (7)**: 479–480.

Carp, O., Huisman, C.L., Reller, A., (2004). Photoinduced reactivity of titanium dioxide. *Prog. Solid State Chem*., **32**: 33–177.

Cassano, A.E., Alfano, O.M., (2000). Reaction engineering of suspended solid heterogeneous photocatalytic reactors. *Catal. Today*, **58**: 167–197.

Causanilles, A., Ruepert, C., Ibanez, M., Emke, E., Hern andez, F., de Voogt, P., (2017). Occurrence and fate of illicit drugs and pharmaceuticals in wastewater from two wastewater treatment plants in Costa Rica. *Sci. Total. Environ*., **599–600**: 98–107.

Cernigoj, U., Stangar, U.L., Trebse, P., Krasovec, U.O., Gross, S., (2006). Photocatalytically active TiO_2 thin films produced by surfactant–assisted sol–gel processing. *Thin Solid Films*, **495**: 327–332.

Cha, J., Cupples, A.M., (2009). Detection of the antimicrobials triclocarban and triclosan in agricultural soils following land application of municipal biosolids. *Water Res*., **43**: 2522–2530.

Chacko, J.T., Subramaniam, K., (2011). Enzymatic degradation of azo dyes–a review. *Int. J. Environ. Sci*. **1 (6)**: 1250–1260.

Chai, Y., Ding, H., Zhang, Z., Xian, Y., Pan, P., Jin, L., (2006). Study on photocatalytic oxidation for determination of the low chemical oxygen demand using a nano–TiO_2–$Ce(SO_4)_2$ coexisted system. *Talanta*. **68**: 610–615.

Chang, C., Zhu, L., Fu, Y., Chu, X., (2013). Highly active Bi/BiOI composite synthesized by one–step reaction and its capacity to degrade bisphenol A under simulated solar light irradiation. *Chem. Eng. J.*, **233:** 305–314.

Chao, H.E., Yun, Y.U., Xingfang, H.U., Larbot, A., (2003). Effect of silver doping on the phase transformation and grain growth of sol–gel titania powder. *J. Eur. Ceram. Soc*., **23**: 1457–1464.

Chee-Sanford, J.C., Aminov, R.I., Krapac, I.J., Garrigues-Jeanjean, N., Mackie, R.I., (2001). Occurrence and diversity of tetracycline resistance genes in lagoons and groundwater underlying two swine production facilities. *Appl. Environ. Microbiol*., **67**: 1494–1502.

Chemie, V.F., (2005). New methods for determination of β-lactam antibiotics by means of diffuse reflectance spectroscopy using polyurethane foam as sorbent, PhD thesis, Duisburg University, Germany.

Chen, F., Ho, P., Ran, R., Chen, W., Si, Z., Wu, X., Weng, D., Huang, Z., Lee, C., (2017). Synergistic effect of CeO_2 modified TiO_2 photocatalyst on the enhancement of visible light photocatalytic performance. *J. Alloys Compd*., **714**: 560–566.

Chen, J.–Q., Wang, D., Zhu, M.–X., Gao, C.–J., (2007). Photocatalytic degradation of dimethoate using nanosized TiO_2 powder. *Desalination*, **207**: 87–94.

Chen, W.S., Huang, Y.L., (2011). Removal of dinitrotoluenes and trinitrotoluene from industrial wastewater by ultrasound enhanced with titanium dioxide. *Ultrason. Sonochem.*,**18**: 1232–1240.

Chen, X., Nielsen, J.L., Furgal, K., Liu, Y., Lolas, I.B., Bester, K., (2011a). Biodegradation of triclosan and formation of methyl-triclosan in activated sludge under aerobic conditions. *Chemosphere*, **84**: 452–456.

Chen, Y., Stathatos, E., Dionysiou, D.D., (2008). Microstructure characterization and photocatalytic activity of mesoporous TiO_2 films with ultrafine anatase nanocrystallites. *Surf. Coat. Technol.*, **202**: 1944–1950.

Chen, Z., Wang, H., Chen, Z., Ren, N., Wang, A., Shi, Y., et al., (2011). Performance and model of a full-scale up-flow anaerobic sludge blanket (UASB) to treat the pharmaceutical wastewater containing 6-APA and amoxicillin. *J. Hazard. Mater.*, **185(2-3)**: 905–913.

Chen, Z.F., Ying, G.G., Liu, Y.S., Zhang, Q.Q., Zhao, J.L., Liu, S.S., Pan, C.G., (2014). Triclosan as a surrogate for household biocides: an investigation into biocides in aquatic environments of a highly urbanized region. *Water Res.*, **58**: 269–279.

Cheng, G., (2005). Interaction of tetracycline with aluminum and iron hydrous oxides. *Environ. Sci. Technol.*, **39**: 2660–2667.

Cheng, H., Ma, J., Zhao Z., Qi, L., (1995). Hydrothermal Preparation of Uniform Nanosize Rutile and Anatase Particles. *Chem. Mater.*, **7**: 663–671.

Cherednichenko, G., Zhang, R., Bannister, R.A., Timofeyev, V., Li, N., Fritsch, E.B., Feng, W., Barrientos, G.C., Schebb, N.H., Hammock, B.D., Beam, K.G., Chiamvimonvat, N., Pessah, I.N., (2012). Triclosan impairs excitation–contraction coupling and Ca^{2+} dynamics in striated muscle. *Proc. Natl. Acad. Sci*., **109**: 14158–14163.

Cho, H.H., Huang, H., Schwab, K., (2011). Effects of solution chemistry on the adsorption of ibuprofen and triclosan onto carbon nanotubes. *Langmuir*, **27 (21)**: 12960–12967.

Choi, W., Termin, A., Hoffmann, M.R., (1994). The Role of Metal Ion Dopants in Quantum-Sized TiO_2: Correlation between Photoreactivity and Charge Carrier Recombination Dynamics. *J. Phys. Chem.*, **98**: 13669–13679

Chong, M.N., Jin, B., Chow, C.W.K., Saint, C., (2010). Recent developments in photocatalytic water treatment technology: a review. *Water Res.*, **44**: 2997–3027.

Chowdhury, I.H., Ghosh, S., Naskar, M.K., (2015). Aqueous–based synthesis of mesoporous TiO_2 and Ag–TiO_2 nanopowders for efficient photodegradation of methylene blue. *Ceram. Int.*, **42**: 2488–2496.

Chung, W.J., Chun, S.Y., Kim, S.S., Chang, S.W., (2016). Photocatalytic removal of tetracycline using TiO_2/Ge composite optimized by response surface methodology (RSM). *J. Ind. Eng. Chem.*, **36**: 320–325.

Clara, M., Strenn, B., Kreuzinger, N., Kroiss, H., Gans, O., Martinez, E., (2005). Removal of selected pharmaceuticals, fragrances and endocrine disrupting compounds in a membrane bioreactor and conventional wastewater treatment plants. *Water Res*., **39**: 4797–4807.

Clescerl, L.S., Greenberg, A.E., Eaton, A.D., (1999). Standard Methods for Examination of Water and Wastewater (20th ed.). Washington, DC: American Public Health Association, ISBN 0–87553–235–7. Method 5310A.

Colombo, D.P., Bowman, R.M., (1996). Does Interfacial Charge Transfer Compete with Charge Carrier Recombination? A Femtosecond Diffuse Reflectance Investigation of TiO_2 Nanoparticles. *J. Phys. Chem*., **100**: 18445–18449.

Constantin, L.A., Nitoi, I., Cristea, N.I., Constantin, M.A., (2018). Possible degradation pathways of triclosan from aqueous systems via TiO_2 assisted photocatalyis. *J. Ind. Eng. Chem.*, **58:** 155–162.

Couto, S.R., Osma, J.F., Herrera, J.L.T., (2009). Removal of synthetic dyes by an eco-friendly strategy. *Eng. Life Sci*., **9 (2)**: 116–123.

Cozzoli, P.D., Comparelli, R., Fanizza, E., Curri, M.L., Agostiano, A., Laub, D., (2004). Photocatalytic synthesis of silver nanoparticles stabilized by TiO2 nanorods: a semiconductor/metal nanocomposite in homogeneous nonpolar solution. *J. Am. Chem. Soc*., **126**: 3868–3879.

Curco, D., Gimenez, J., Addardak, A., Cervera-March, S., Esplugas, S., (2002).. Effects of radiation absorption and catalyst concentration on thephotocatalytic degradation of pollutants. *Catal. Today,* **76**: 177–188.

da Silva, B.F., Jelic, A., López-Serna, R., Mozeto, A.A., Petrovic, M., Barceló, D., (2011). Occurrence and distribution of pharmaceuticals in surface water, suspended solids and sediments of the Ebro river basin, Spain. *Chemosphere*, **85**: 1331–1339.

Dai C.M., Geissen S.U., Zhang Y.L., Zhang Y.J., Zhou X.F., (2011). Selective removal of diclofenac from contaminated water using molecularly imprinted polymer microspheres. *Environ. Pollut*., **159**: 1660−1666.

Dalrymple, O.K., Yeh, D.H., Trotz, M.A., (2007). Removing pharmaceuticals and endocrine disrupting compounds from wastewater by photocatalysis. *J. Chem. Technol. Biotechnol*., **82**: 121–1134.

Damas, S. B., Miranda, M.I.A., Clar, M.I.I., Pia, A.B., Roca, J.A.M., Clar, A.I., (2006). Study of the UF process as pretreatment of NF membranes for textile wastewater reuse. *Desalination*, **200**: 745–747.

Dann, A.B., Hontela, A., (2011). Triclosan: environmental exposure, toxicity and mechanisms of action. *J. Appl. Toxicol*., **31 (4)**: 285–311.

Daughton, C.G., Ternes, T.A., (1999). Pharmaceuticals and personal care products in the environment: agents of subtle change. *Environ. Health Persp*., **107**: 907–938.

Dawson, A., Kamat, P.V., (2001). Semiconductor–metal nanocomposites. Photoinduced fusion and photocatalysis of gold-capped TiO_2 (TiO_2/Gold) nanoparticles. *J. Phys. Chem. B,* 105: 960–966.

Dayan, A.D., (2007). Risk assessment of triclosan [Irgasan®] in human breast milk. *Food Chem. Toxicol*., **45 (1)**: 125–129.

De Almeida, M.F., Bellato, C.R., Mounteer, A.H., Ferreira, S.O., Milagres, J.L., Miranda, L.D.L., (2015). Enhanced photocatalytic activity of TiO_2–impregnated with MgZnAl mixed oxides obtained from layered double hydroxides for phenol degradation. *Appl. Surf. Sci*., **357**: 1765–1775.

De Bel, E., Janssen, C., De Smet, S., Van Langenhove, H., Dewulf, J., (2011). Sonolysis of ciprofloxacin in aqueous solution: influence of operational parameters. *Ultrason. Sonochem*., **18**: 184–189.

De Gusseme, B, Vanhaecke, L., Verstraete, W., Boon, N., (2011). Degradation of acetaminophen by Delftia tsuruhatensis and Pseudomonas aeruginosa in a membrane bioreactor. *Water Res*., **45 (4)**: 1829–1837.

De la Cruz, N., Esquius, L., Grandjean, D., Magnet, A., Tungler, A., de Alencastro, L.F., Pulgarín, C., (2013). Degradation of emergent contaminants by UV, UV/H_2O_2 and neutral photo-Fenton at pilot scale in a domestic wastewater treatment plant. *Water Res*., **47**: 5836–5845.

De la Cruz, N., Giménez, J., Esplugas, S., Grandjean, D., de Alencastro, L.F., Pulgarín, C., (2012). Degradation of 32 emergent contaminants by UV and neutral photo–fenton in domestic wastewater effluent previously treated by activated sludge. *Water Res*., **46**: 1947–1957.

de Souza, M.L., Corio, P., (2013). Effect of silver nanoparticles on TiO_2-mediated photodegradation of Alizarin Red S. *Appl. Catal. B Environ*., **136–137**: 325–333.

Deblonde, T., Cossu-Leguille, C., Hartemann, P., (2011). Emerging pollutants in wastewater: a review of the literature. *Int. J. Hyg. Environ. Health*, **214**: 442–448.

Demeestere, K., Visscher, A.D., Dewulf, J., Leeuwen, M.V., Langenhove, H.V., (2004). A new kinetic model for titanium dioxide mediated heterogeneous photocatalytic degradation of trichloroethylene in gas–phase. *Appl. Catal. B, Environ.*, **49**: 1–14.

Denoncourt, J.M., Martyniuk, C.J., de Solla, S.R., Balakrishnan, V.K., Langlois, V.S., (2014). Sediment contaminated with the Azo dye disperse yellow 7 alters cellular stress and androgen–related transcription in silurana tropicalis larvae. *Environ. Sci. Technol*., **48**: 2952–2961.

Destrieux, D., Laurent, F., Budzinski, H., Pedelucq, J., Vervier, P., Gerino, M., (2017). Drug residues in urban water: a database for ecotoxicological risk management. *Sci. Total. Environ*., **609**: 927–941.

Dhillon, G., Kaur, S., Pulicharla, R., Brar, S., Cledón, M., Verma, M., Surampalli, R., (2015). Triclosan: current status, occurrence, environmental risks and bioaccumulation potential. *Int. J. Environ. Res. Public Health*, **12**: 5657–5684.

Diebold, U., (2003). The surface science of titanium dioxide. *Surf. Sci. Rep*., **48**: 53–229.

Dijkstra, M.F.J., Michorius, A., Buwalda, H., Panneman, H.J., Winkelman, J.G.M., Beenackers, A.A.C.M., (2001). Comparison of the efficiency of immobilized and suspended systems in photocatalytic degradation. *Catal. Today*, **66**: 487–494.

Ding, H., Sun, H., Shan, Y., (2005). Preparation and characterization of mesoporous SBA–15 supported dye–sensitized TiO_2 photocatalyst. *J. Photochem. Photobiol. A*, **169**: 101–107.

Ding, R., Zhang, P., Seredych, M., Bandosz, T.J., (2012). Removal of antibiotics from water using sewage sludge and waste oil sludge–derived adsorbents. *Water Res.,* **46 (13)**: 4081–4090.

Domen, K., Naito, S., Soma, M., Onishi, T., Tamaru, K., (1982). Photocatalytic decomposition of water vapour on an NiO–$SrTiO_3$ catalyst. *Chem. Phys. Lett..,* **92**: 543–544.

Dung, N.T., Khoa, N.V., Herrmann, J.–M., (2005). Photocatalytic degradation of reactive dye RED–3BA in aqueous TiO_2 suspension under UV–visible light. *Int. J. Photoenergy*, **7**: 11–15.

Elmolla, E.S., Chaudhuri, M., (2009). Improvement of biodegradability of synthetic amoxicillin wastewater by photo-Fenton process. *World Appl. Sci. J*., **5**: 53–58.

Elmolla, E.S., Chaudhuri, M., (2010). Degradation of amoxicillin, ampicillin and cloxacillin antibiotics in aqueous solution by the UV/ZnO photocatalytic process. *J. Hazard. Mater*., **173**: 445–449.

Elmolla, E.S., Chaudhuri, M., (2010i). Photocatalytic degradation of amoxicillin, ampicillin and cloxacillin antibiotics in aqueous solution using UV/TiO_2 and UV/H_2O_2/TiO_2 photocatalysis. *Desalination,* **252**: 46–52.

Eloirdi, R., Cakir, P., Huber, F., Seibert, A., Konings, R., Gouder, T., (2018). X-ray photoelectron spectroscopy study of the reduction and oxidation of uranium and cerium single oxide compared to (U-Ce) mixed oxide films. *Appl. Surf. Sci*., **457**: 566–571.

El–Sayed M.A., (2001). Some interesting properties of metals confined in time and nanometer space of different shapes. *Acc. Chem. Res*., **34**: 257–264.

Elsherif, K.M., El–hashani, A., El–dali, A., Dakhil, O., Najar, A., Algeriani, M., (2014). Absorption Spectral Studies on Naphthyl Pyridyl Pyrazole (NPP) in Mixed Solvent Systems. *Chem. Sci. Trans*., **3(3)**: 1221–1227.

EU, (2016). Commission Implementing Decision (EU) 2016/110: Not Approving Triclosan as an Existing Active Substance for Use in Biocidal Products for Product Type1.

European Commission (EC), (1991). Directive of the European Communities and the council 91/271/EEC concerning urban wastewater treatment. *Offic. J. L*., 135, 30/05/1991.

European Commission (EC), (2000). Directive of the European Parliament and of the Council 2000/60/EC establishing a framework for community action in the field of water policy. *Offic. J.,* C513, 23/10/2000.

European Commission (EC), (2004). Report from the Commission on the Implementation of Council Directive 91/271/EEC Concerning Urban Wastewater Treatment. COM, Brussels, p. 248.

European Commission (EC), (2008). Directive 2008/105/EC of the European Parliament and of the Council of 16 December 2008 on environmental quality standards in the field of water policy, amending and subsequently repealing Council Directives 82/176/EEC, 83/513/EEC, 84/156/EEC, 84/491/EEC, 86/491/EEC, 86/280/EEC and amending Directive 2000/60/EC of the European Parliament and of the Council.

Evgenidou, E., Fytianos, K., Poulios, I., (2005). Semiconductor–sensitized photodegradation of dichlorvos in water using TiO_2 and ZnO as catalysts. *Appl. Catal. B, Environ*., **59**: 81–89.

Fair, P.A., Lee, H., Adams, J., Darling, C., Pacepavicius, G., Alaee, M., Bossart, G.D., Henry, N., Muir, D., (2009). Occurrence of triclosan in plasma of wild Atlantic bottlenose dolphins (*Tursiops truncatus*) and in their environment. *Environ. Pollut*., **157**: 2248–2254.

Fan, X., Wan, J., Liu, E., Sun, L., Hu, Y., Li, H., Hu, X., Fan, J., (2015). High–efficiency photoelectrocatalytic hydrogen generation enabled by Ag deposited and Ce doped TiO_2 nanotube arrays. *Ceram. Int*., **41**: 5107–5116.

Farombi, E.O., Ugwuezunmba, M.C., Ezenwadu, T.T., Oyeyemi, M.O., Ekor, M., (2008). Tetracycline–induced reproductive toxicity in male rats: Effects of vitamin C and *N*–acetylcysteine. *Experim. Toxicol. Pathol*., **60**: 77–85.

Fatta, D., Achilleos, A., Nikolaou, A., Meric, S., (2007). Analytical methods for tracing pharmaceutical residues in water and wastewater. *TrAC Trend. Anal. Chem.,* **26 (6)**: 515–533.

Fazelirad, H., Ranjbar, M., Taher, M.A., Sargazi, G., (2015). Preparation of magnetic multi-walled carbon nanotubes for an efficient adsorption and spectrophotometric determination of amoxicillin. *J. Ind. Eng. Chem*., **21**: 889–892.

Feizpoor, S., Habibi-Yangjeh, A., Yubuta, K., (2018). Integration of carbon dots and polyaniline with TiO_2 nanoparticles: Substantially enhanced photocatalytic activity to removal various pollutants under visible light. *J. Photochem. Photobiol. A: Chem.*, **367**: 94–104.

Feldstein, M.J., Keating, C.D., Liau, Y.H., Natan, M.J., Scherer, N.F., (1997). Electronic relaxation dynamics in coupled metal nanoparticles. *J. Am. Chem. Soc*., **119**: 6638–6647.

Feng, L., van Hullebusch, E.D., Rodrigo, M.A., Esposito, G., Oturan, M.A., (2013). Removal of residual anti-inflammatory and analgesic pharmaceuticals from aqueous systems by electrochemical advanced oxidation processes. *A Rev. Chem. Eng. J*., **228**: 944–964.

Feng, X., Sloppy, J.D., LaTempa, T.J., Paulose, M., Komarneni, S., Bao, N., Grimes, C.A., (2011). Synthesis and deposition of ultrafine Pt nanoparticles within high aspect ratio TiO_2 nanotube arrays: application to the photocatalytic reduction of carbon dioxide. *J. Mater. Chem*., **21**: 13429–13433.

Fent, K., Weston, A.A., Caminada, D., (2006). Ecotoxicology of human pharmaceuticals. *Aquat. Toxicol*., **76**: 122–159.

Fiorenza, R., Bellardita, M., Barakat, T., Scire, S., Palmisano, L., (2018). Visible light photocatalytic activity of macro-mesoporous TiO_2-CeO_2 inverse opals. *J. Photoch. Photobio. A*, **352**: 25–34.

Forgacs, E., Cserhati, T., Oros, G., (2004). Removal of synthetic dyes from wastewaters: a review. *Environ. Int*., **30 (7)**: 953–971.

Frimmel, F.H., (1994). Photochemical aspects related to humic substances. *Environ. Int*., **20**: 373–385.

Fritsch, E.B., Connon, R.E., Werner, I., Davies, R.E., Beggel, S., Feng, W., Pessah, I.N., (2013). Triclosan impairs swimming behavior and alters expression of excitation–contraction coupling proteins in fathead minnow (Pimephales promelas). *Environ. Sci. Technol*., **47**: 2008–2017.

Fujishima, A., Hashimoto, K., Watanabe, T., (1999). TiO_2 photocatalysis: fundamentals and applications. Tokyo: BKC, Inc.

Fujishima, A., Honda, K., (1972). Electrochemical photolysis of water at a semiconductor electrode. *Nature*, **238**: 37–38.

Fujishima, A., Honda, K., Kikuchi, S., (1969). Photosensitized electrolytic oxidation on TiO_2 semiconductor electrode. *J. Chem. Soc. Japan,* **72**:108–113.

Fujishima, A., Rao, T.N., Tryk, D.A., (2000). Titanium dioxide photocatalysis. *J. Photochem. Photobiol. C,* **1**: 1–21.

Fujishima, A., Zhang, X., (2006). TiO_2 photocatalysis: present situation and future perspectives. *C. R. Chim*., **9**: 750–760.

Furube, A., Asahi, T., Masuhara, H., Yamashita, H., Anpo, M., (1999). Charge Carrier Dynamics of Standard TiO_2 Catalysts Revealed by Femtosecond Diffuse Reflectance Spectroscopy. *J. Phys. Chem. B,* **103**: 3120–3127.

Gao, Y., Ji, Y., Li, G., An, T., (2014). Mechanism, kinetics and toxicity assessment of OH-initiated transformation of triclosan in aquatic environments. *Water Res*., **49**: 360–370.

Gao, Y., Liu, H., (2005). Preparation and catalytic property study of a novel kind of suspended photocatalyst of TiO_2–activated carbon immobilized on silicone rubber film. *Mater. Chem. Phys*., **92**: 604–608.

Garcia, G., Buonsanti, R., Runnerstrom, E.L., Mendelsberg, R.J., Llordes, A., Anders, A., Richardson, T.J., Milliron, D.J., (2011). Dynamically modulating the surface plasmon resonance of doped semiconductor nanocrystals. *Nano Lett*., **11**: 4415–4420.

García–Espinoza, J.D., Mijaylova–Nacheva, P., Avil es–Flores, M., (2018). Electrochemical carbamazepine degradation: effect of the generated active chlorine, transformation pathways and toxicity. *Chemosphere*, **192**: 142–51.

Garcia–Segura, S., Ocon, J.D., Chong, M.N., (2018). Electrochemical oxidation remediation of real wastewater effluents – a review. *Process. Saf. Environ. Prot*., **113**: 48–67.

Gaya, U.I., Abdullah, A.H., (2008). Heterogeneous photocatalytic degradation of organic contaminants over titanium dioxide: A review of fundamentals, progress and problems. *J. Photochem. Photobiol. C,* **9:** 1–12.

Gee, R.H., Charles, A., Taylor, N., Darbre, P.D., (2008). Oestrogenic and androgenic activity of triclosan in breast cancer cells. *J. Appl. Toxicol*., **28**: 78–91.

Gelband, H., Miller-Petrie, M., Pant, S., Gandra, S., Levinson, J., Barter, D., White, A., Laximinarayan, R., (2015). The State of the World's Antibiotics (Washington D.C.).

Geng, Q.J., Wang, X.K., Tang, S.F., (2008). Heterogeneous photocatalytic degradation kinetic of gaseous ammonia over nano–TiO_2 supported on latex paint film, *Biomed. Environ. Sci*., **21**: 118–123.

George, D.K., Crawford, D.H., (1996). Antibacterial-induced hepatotoxicity. Incidence, prevention and management. *Drug Saf*., **15**: 79–85.

Geundi, M.S.E., Ismail, H.M., Attyia, K.M.E., (1995). Activated clay as an adsorbent for cationic dyestuffs. *Adsorpt. Sci. Technol*., **12 (2)**: 109–117.

Gharagozlou, M., Bayati, R., (2014). Photocatalytic activity and formation of oxygen vacancies in cation doped anatase TiO_2 nanoparticles. *Ceram. Int*., 40: 10247–10253.

Ghosh, S.K., Pal, T., (2007). Interparticle coupling effect on the surface plasmon resonance of gold nanoparticles: From theory to applications. *Chem. Rev*., **107**: 4797–4862.

Giraldo–Aguirre, A.L., Serna–Galvis, E.A., Erazo–Erazo, E.D., Silva–Agredo, J., Giraldo–Ospina, H., Florez–Acosta, O.A., Torres–Palma, R.A., (2017). Removal of β–lactam antibiotics from pharmaceutical wastewaters using photo–Fenton process at near–neutral pH. *Environ. Sci. Pollut. Res*., **25 (21)**: 20293–20303.

Gjessing, E.T., Kallqvist, T., (1991). Algicidal and chemical effect of UV–radiation of water containing humic substances. *Water Res*., **25**: 491–494.

Gleick, P.H., (1993). *Water in Crisis: A Guide to the World's Freshwater Resources*. Oxford University Press Inc., 198 Madison Avenue, New York.

Gozmen, B., Turabik, M., Hesenov, A., (2009). Photocatalytic degradation of Basic Red 46 and Basic Yellow 28 in single and binary mixture by UV/TiO_2/periodate system. *J. Hazard. Mater*., **164**: 1487–95.

Guillard, C., Disdier, J., Herrmann, J.M., Lehaut, C., Chopin, T., Malato, S., Blanco, J., (1999). *Catal. Today*, **54**: 217.

Guillard, C., Lachheb, H., Houas, A., Ksibi, M., Elaloui, E., Herrmann, J.–M., (2003). Influence of chemical structure of dyes, of pH and of inorganic salts on their photocatalytic degradation by TiO_2 comparison of the efficiency of powder and supported TiO_2. *J. Photochem. Photobiol. A*, **158:** 27–36.

Guo, H., Zheng, Z., Chen, J., Weng, W., Huang, M., (2016). Facile template–free one–pot fabrication of TiO_2@C microspheres with high visible–light photocatalytic degradation activity. *J. Ind. Eng. Chem*., **36**: 306–313.

Gurses, A., Açıkyıldız, M., Güne , K., Gurses, M.S., (2016). Dyes and pigments: their structure and properties. *Dyes and Pigments*.

Guyer, G.T., Ince, N.H., (2011). Degradation of diclofenac in water by homogeneous and heterogeneous sonolysis. *Ultrason. Sonochem*., **18**: 114–119.

Guzmana, C., del Angel, G., Gomez, R., Galindo-Hernandez, F., Angeles-Chavez, C., (2011). Degradation of the herbicide 2,4-dichlorophenoxyacetic acid over Au/TiO_2–CeO_2 photocatalysts: Effect of the CeO_2 content on the photoactivity. *Catal. Today*, **166**: 146–151.

Halden, R.U., Paull, D.H., (2005). Co-occurrence of triclocarban and triclosan in US water resources. *Environ. Sci. Technol*., **39 (6)**: 1420–1426.

Halling-Sorensen, B., (2001). Inhibition of aerobic growth and nitrification of bacteria in sewage sludge by antibacterial agents. *Arch. Environ. Contam. Toxicol*., **40**: 451–460.

Halling-Sørensen, B., Nors Nielsen, S., Lanzky, P.F., Ingerslev, F., Holten Lützhøft, H.C., et al., (1988). Occurrence, fate and effects of pharmaceutical substances in the environment–a review. *Chemosphere*, **36**: 357–393.

Hamscher, G., (2009). Veterinary drugs in the environment: current knowledge and challenges for the future. *J. Vet. Pharmacol. Ther*., **32**: 24–25.

Han, B., Liu, W., Li, J., Wang, J., Zhao, D., Xu, R., Lin, Z., (2017). Catalytic hydrodechlorination of triclosan using a new class of anion exchange-resin supported palladium catalysts. *Water Res*., **120**: 199–210.

Hao, O.J., Kim, H., Chiang, P.C., (2000). Decolorization of wastewater. *Crit. Rev. Environ. Sci. Technol*., **30**: 449–505.

Haque, M.M., Muneer, M., Bahnemann, D.W., (2006). Semiconductor–mediated photocatalyzed degradation of a herbicide derivative, chlorotoluron, in aqueous suspensions. *Environ. Sci. Technol*., **40**: 4765–4770.

He, Y., Gao, J.F., Feng, F.Q., Liu, C., Peng, Y.Z., Wang, S.Y., (2012). The comparative study on the rapid decolorization of azo, anthraquinone and triphenylmethane dyes by zero–valent iron. *Chem. Eng. J*., **179**: 8–18.

Heberer T., (2002). Occurrence, fate, and removal of pharmaceutical residues in the aquatic environment: a review of recent research data. Toxicol. Lett., **131**: 5−17.

Heidler, J., Halden, R.U., (2007). Mass balance assessment of triclosan removal during conventional sewage treatment. *Chemosphere*, **66**: 362–369.

Herrmann, J.–M., Tahiri, H., Ait–Ichou, Y., Lassaletta, G., Gonzalez–Elipe,A.R., Fernandez, A., (1997). Characterization and photocatalytic activity in aqueous medium of TiO_2 and Ag–TiO_2 coatings on quartz. *Appl. Catal. B, Environ.*, **13**: 219–228.

Herrmann, J.–M., (1999). Heterogeneous photocatalysis: fundamentals and applications to the removal of various types of aqueous pollutants. *Catal. Today*, **53**: 115–129.

Hirsch, R., Ternes, T.A., Haberer, K., Kratz, K.L., (1999). Occurrence of antibiotics in the aquatic environment. *Sci. Total Environ*., **225 (1–2)**: 109–118.

Hoffmann, M.R., Martin, S.T., Choi, W., Bahnemann, D.W., (1995). Environmental applications of semiconductor photocatalysis. *Chem. Rev*., **95**: 69–96.

Homem, V., Alves, A., Santos, L., (2013). Microwave-assisted Fenton's oxidation of amoxicillin. *Chem. Eng. J*., **220**: 35–44.

Homem, V., Santos, L., (2011). Degradation and removal methods of antibiotics from aqueous matrices–a review. *J. Environ. Manage*., **92 (10)**: 2304–2347.

Horvath, I.T., (2003). Encyclopedia Catalysis. *Wiley-Interscience*, **5**: 577.

Hou, J.P., Poole, J.W., (1971). Beta-lactam antibiotics, their physico chemical properties and biological activity in relation to structure. *J. Pharm. Sci*., **60**: 503–509.

Hou, W., Hung, W.H., Pavaskar, P., Goeppert, A., Aykol, M., Cronin, S.B., (2011). Photocatalytic conversion of CO_2 to hydrocarbon fuels via plasmon-enhanced absorption and metallic interband transitions. *ACS Catal*., **1**: 929–936.

Huerta-Fontela, M., Galceran, M.T., Ventura, F., (2011). Occurrence and removal of pharmaceuticals and hormones through drinking water treatment. *Water Res*., **45**: 1432–1442.

Hugul. M., Ercag, E., Apak, R., (2002). Kinetic studies on UV–photodegradation of some chlorophenols using TiO_2 catalyst. *J. Environ. Sci. Health, A, Tox. Hazard. Subst. Environ. Eng*., **37:** 365–83.

Huo, P., Guan, J., Zhou, M., Ma, C., Liu, X., Yan, Y., Yuan, S., (2017). Carbon quantum dots modified CdSe loaded reduced graphene oxide for enhancing photocatalytic activity. *J. Ind. Eng. Chem.,* **50**: 147–154.

Ihara, M., Tanaka, K., Sakaki, K., Honma, I., Yamada, K., (1997). Enhancement of the absorption coefficient of cis–(NCS)2 Bis(2,2'–bipyridyl–4,4'-dicarboxylate)ruthenium (II) dye in dye–sensitized solar cells by a silver Island film. *J. Phys. Chem. B*, **101**: 5153–5157.

Ikehata, K., Naghashkar, N.J., Ei-Din, M.G., (2006). Degradation of aqueous pharmaceuticals by ozonation and advanced oxidation processes: a review. *Ozone Sci. Eng*., **28**: 353–414.

Iliev, V., Tomova, D., Bilyarska, L., Eliyas, A., Petrov, L., (2006). Photocatalytic properties of TiO_2 modified with platinum and silver nanoparticles in the degradation of oxalic acid in aqueous solution. *Appl. Catal. B, Environ*., **63**: 266–271.

Ilisz, I., Dombi, A., (1999). Investigation of the photodecomposition of phenol in near–UV–irradiated aqueous TiO_2 suspensions. II. Effect of charge–trapping species on product distribution. *Appl. Catal. A, Gen*., **180**: 35–45.

Ince, N.H., (2018). Ultrasound–assisted advanced oxidation processes for water decontamination. *Ultrason. Sonochem*., **40**: 97–103.

Jabeen, U., Shah, S.M., Khan, S.U., (2017). Photo catalytic degradation of Alizarin red S using ZnS and cadmium doped ZnS nanoparticles under unfiltered sunlight. *Surf. Interfaces*, **6**: 40–49.

Jafari, M., Abdollahzadeh, A.A., Aghababaei, F., (2017). Copper Ion Recovery from Mine Water by Ion Flotation. *Mine Water Environ*., **36**: 323–327.

Ji, L., Chen, W., Zheng, S., Xu, Z., Zhu, D., (2009). Adsorption of sulfonamide antibiotics to multiwalled carbon nanotubes. *Langmuir*, **25 (19)**: 11608–11613.

Jia, Y., Liu, J., Cha, S., Choi, S., Park, Y.C., Liu, C., (2017). Magnetically separable Au–TiO_2/nanocube $ZnFe_2O_4$ composite for chlortetracycline removal in wastewater under visible light. *J. Ind. Eng. Chem*., **47**: 303–314.

Jia, Y., Wu, C., Lee, B.W., Liu, C., Kang, S., Lee, T., Park, Y.C., Yoo, R., Lee, W., (2017i). Magnetically separable sulfur-doped $SnFe_2O_4$/graphene nanohybrids for effective photocatalytic purification of wastewater under visible light. *J. Hazard. Mater*., **338**: 447–457.

Jing, L.Q., Sun, X.J., Cai, W.M., Li, X.Q., Fu, H.G., Hou, H.G., Fan, N.Y., (2003). Photoluminescence of Ce doped TiO_2 nanoparticles and their photocatalytic activity. *Acta Chim. Sin*., **61**: 1241–1245.

Jjemba, P.K., (2006). Excretion and ecotoxicity of pharmaceutical and personal care products in the environment. *Ecotoxicol. Environ. Saf*., **63**: 113–130.

Jones, O.A., Vouvoulis, N., Lester, J.N., (2002). Aquatic environmental assessment of the top 25 English prescription pharmaceuticals. *Water Res.*, 36: 5013–5022.

Jovic, V., Chen, W.-T., Sun-Waterhouse, D., Blackford, M.G., Idriss, H., Waterhouse, G.I.N., (2013). Effect of gold loading and TiO_2 support composition on the activity of Au/TiO_2 photocatalysts for H_2 production from ethanol–water mixtures. J. Catal., **305**: 307–317.

Jung, C., Son, A., Her, N., Zoh, K.-D., Cho, J., Yoon, Y., (2015). Removal of endocrine disrupting compounds, pharmaceuticals, and personal care products in water using carbon nanotubes: a review. *J. Indus. Eng. Chem.*, **27**: 1–11.

Kabra, K., Chaudhary, R., Sawhney, R.L., (2004). Treatment of Hazardous Organic and Inorganic Compounds through Aqueous–Phase Photocatalysis: A Review. *Ind. Eng. Chem. Res.*, **43**: 7683–7696.

Kajihara, K., Nakanishi, K., Tanaka, K., Hirao, K., Soga, N., (2005). Preparation of Macroporous Titania Films by a Sol–Gel Dip-Coating Method from the System Containing Poly(ethylene glycol). *J. Am. Ceram. Soc.*, **81**: 2670–2676.

Kalsi, P.S., (1995). Spectroscopy of Organic Compounds. Second edition. New Age International Limited, Publishers, New Delhi, India.

Kalsi, P.S., (2004). Spectroscopy of Organic Compounds. Sixth edition. New Age International Limited, Publishers, New Delhi, India.

Kamat, P.V., (2002). Photophysical, Photochemical and Photocatalytic Aspects of Metal Nanoparticles. *J. Phys. Chem. B*, **106**: 7729–7744.

Kanakaraju, D., Glass, B.D., Oelgemoller, M., (2018). Advanced oxidation process–mediated removal of pharmaceuticals from water: A review. *J. Environ. Manage.*, **219**: 189–207.

Kanakaraju, D., Kockler, J., Motti, C.A., Glass, B.D., Oelgemoller, M., (2015). Titanium dioxide/zeolite integrated photocatalytic adsorbents for the degradation of amoxicillin. *Appl. Catal. B, Environ.*, **166–167**: 45–55.

Kanetoshi, A., Katsura, E., Ogawa, H., Ohyama, T., Kaneshima, H., Miura, T., (1992). Acute toxicity, percutaneous absorption and effects on hepatic mixed function oxidase activities of 2,4,4'–Trichloro–2'–hydroxydiphenyi ether (Irgasan ® DP300) and its chlorinated derivatives. *Arch. Environ. Contam. Toxicol*., **23**: 91–98.

Kansal, S.K., Singh, M., Sud, D., (2007). Studies on photodegradation of two commercial dyes in aqueous phase using different photocatalysts. *J. Hazard. Mater*., **141**: 581–590.

Kant, R., (2012). Textile dyeing industry an environmental hazard. *J. Nat. Sci*., **04 (01)**: 22–26.

Karthikeyan, K.G., Meyer, M.T., (2006). Occurrence of antibiotics in wastewater treatment facilities in Wisconsin, USA. *Sci. Total Environ*., **361**: 196–207.

Kasik, J.E., Thompson, J.S., (1970). Allergic reactions to antibiotics. *Med. Clin. North Am*., **54**: 59–73.

Kassinos, D.F., Meric, S., Nikolaou, A., (2011a). Pharmaceutical residues in environmental waters and wastewater: current state of knowledge and future research. *Anal. Bioanal. Chem*., **399**: 251–275.

Kaur, S.P., Rao, R., Nanda, S., (2011). Amoxicillin: a broad spectrum antibiotic. *Int. J. Pharm. Pharm. Sci*., **3 (3)**: 30–37.

Kidak, R., Dogan, S., (2018). Medium–high frequency ultrasound and ozone based advanced oxidation for amoxicillin removal in water. *Ultrason. Sonochem*., **40**: 131–139.

Kilinc, N., Sennik, E., Isika, M., Ahsena, A.S., Ozturka, O., Ozturka, Z.Z., (2014). Fabrication and gas sensing properties of C–doped and un–doped TiO_2 nanotubes. *Ceram. Int*., **40**: 109–115.

Kim, H., Lee, S., Han, Y., Park, J., (2005). Preparation of dip–coated TiO_2 photocatalyst on ceramic foam pellets. *J. Mater. Sci*., **40**: 5295–5298.

Kim, I., Naoyuki, Y., Hiroaki, T., (2009). Performance of UV and UV/H_2O_2 processes for the removal of pharmaceuticals detected in secondary effluent of a sewage treatment plant in Japan. *J. Hazard. Mater*., **166 (2)**: 1134–1140.

Kim, S.-E., Woo, J.-Y., Kang, S.-Y., Min, B.K., Lee, J.K., Lee, S.-W., (2016). A facile general route for ternary Fe_2O_3@TiO_2@nanometal (Au,Ag) composite as a high-performance and recyclable photocatalyst. *J. Ind. Eng. Chem*., **43**: 142–149.

Kiruthigaa, G., Manoharan, C., Bououdina, M., Ramalingam, S., Raju, C., (2015). Structural, optical and photocatalytic properties of Ce–doped SnS_2 nanoflakes. *Solid State Sci*., **44**: 32–38.

Ko, S., Banerjee, C.K., Sankar, J., (2011). Photochemical synthesis and photocatalytic activity in simulated solar light of nanosized Ag doped TiO_2 nanoparticle composite. *Composites Part B–Eng*., **42**: 579–583.

Koepke, C., Wiśniewski, K., Sikorski, L., Piątkowski, D., Kowalska, K., Naftaly, M., (2006). Upconverted Luminescence under 800 nm Laser Diode Excitation in Nd^{3+}–Activated Fluoroaluminate Glass. *Opt. Mater*., **28**: 129–136.

Kogo, K., Yoneyama, H., Tamura, H., (1980). Photocatalytic oxidation of cyanide on platinized titanium dioxide. J. Phys. Chem., **84**: 1705–1710.

Kolpin, D.W., Furlong, E.T., Meyer, M.T., Thurman, E.M., Zaugg, S.D., Barber, L.B., Buxton, H.T., (2002). Pharmaceuticals, hormones, and other organic wastewater contaminants in U.S. streams, 1999–2000: a national reconnaissance. *Environ. Sci. Technol*., **36**: 1202–1211.

Konstantinou, I.K., Albanis, T.A., (2004). TiO_2–assisted photocatalytic degradation of azo dyes in aqueous solution: kinetic and mechanistic investigations. *Appl. Catal. B, Environ*., **49**: 1–14.

Kosera, V.S., Cruz, T.M., Chaves, E.S., Tiburtius, E.R.L., (2017). Triclosan degradation by heterogeneous photocatalysis using ZnO immobilized in biopolymer as catalyst. *J. Photochem. Photobiol. A,* **344**: 184–191.

Kosmulski, M., (2006). pH–dependent surface charging and points of zero charge. III. Update. *J. Colloid Interface Sci*., **298**: 730–741.

Kosmulski, M., (2009). pH–dependent surface charging and points of zero charge. IV. Update and new approach. *J. Colloid Interface Sci*., **337**: 439–448.

Kowalska, E., Mahaney, O.O.P., Abe, R., Ohtani, B., (2010). Visible–light–induced photocatalysis through surface plasmon excitation of gold on titania surfaces. *Phys. Chem. Chem. Phys.*, 12: 2344–2355.

Kyzas, G.Z., Koltsakidou, A., Nanaki, S.G., Bikiaris, D.N., Lambropoulou, D.A., (2015). Removal of beta-blockers from aqueous media by adsorption onto graphene oxide. *Sci. Total Environ.*, **537**: 411–420.

Labbe, G., Fromenty, B., Freneaux, E., Morzelle, V., Letteron, P., Berson, A., Pessayre, D., (1991). Effects of various tetracycline derivatives on in vitro and in vivo beta-oxidation of fatty acids, egress of triglycerides from the liver, accumulation of hepatic triglycerides, and mortality in mice. *Biochem. Pharmacol*., **41 (4)**: 638–641.

Lade, H.S., Waghmode, T.R., Kadam, A.A., Govindwar, S.P., (2012). Enhanced biodegradation and detoxification of disperse azo dye Rubine GFL and textile industry effluent by defined fungal–bacterial consortium. Int. Biodeterior. Biodegrad., **72**: 94–107.

Lalhmunsiama, Lalchhingpuii, Nautiyal, B.P., Tiwari, D., Choi, S.I., Kong, S.-H., Lee, S.M., (2016). Silane grafted chitosan for the efficient remediation of aquatic environment contaminated with arsenic(V). *J. Colloid Interface Sci*., **467**: 203–212.

Lalhriatpuia, C., Tiwari, A., Shukla, A., Tiwari, D., Lee, S.M., (2016). Nanopillars TiO_2 thin film photocatalyst application in the remediation of aquatic environment, *Korean J. Chem. Eng*., **33**: 3367–3373.

Lalhriatpuia, C., Tiwari, D., Tiwari, A., Lee, S.M., (2015). Immobilized Nanopillars–TiO_2 in the efficient removal of micro–pollutants from aqueous solutions: Physico–chemical studies, *Chem. Eng. J*., **281**: 782–792.

Lalliansanga, N., Tiwari, A., Shukla, A., Tiwari, D., Lee, S.M., (2018). Nanocomposite Au NP/TiO_2 thin film in the efficient remediationof aqueous solutions contaminated with emerging micro-pollutants. *Environ. Sci. Pollut. Res.*, **25**: 20125–20140.

Lalliansanga, Tiwari, A., Shukla, A., Kim, D.J., Lee, S.M., (2019). Facile synthesis and characterization of nanocomposite Au^0(NPs)/titanium dioxide: Photocatalytic degradation of Alizarin Yellow. *J. Ind. Eng. Chem.,* **In Press**.

Latch, D.E., Packer, J.L., Arnold, W.A., McNeill, K., (2003). Photochemical conversion of triclosan to 2,8–dichlorodibenzo-p-dioxin in aqueous solution. *J. Photochem. Photobiol. A*, **158**: 63–66.

Latch, D.E., Packer, J.L., Stender, B.L., Vanoverbeke, J., Arnold, W.A., McNeill, K., (2005). Aqueous photochemistry of triclosan: formation of 2,4–dichlorophenpl, 2,8–dichlorodibenzo–p–dioxin, and oligomerization products. *Environ. Toxicol. Chem*., **24**: 517–525.

Lee, C.M., Palaniandy, P., Dahlan, I., (2017). Pharmaceutical residues in aquatic environment and water remediation by TiO_2 heterogeneous photocatalysis: a review. *Environ. Earth. Sci*., **76**: 611.

Lee, J., Choi, W., Yoon, J., (2005). Photocatalytic degradation of N–nitrosodi–methylamine: mechanism, product distribution and TiO_2 surface modification. *Environ. Sci. Technol*., **39**: 6800–6807.

Lee, Y.J., Lee, S.E., Lee, D.S., Kim, Y.H., (2008). Risk assessment of human antibiotics in Korean aquatic environment. *Environ. Toxicol. Pharm*., **26**: 216–221.

Legrini, O., Oliveros, E., Braun, A.M., (1993). Photochemical processes for water–treatment. *Chem. Rev*., **93**: 671–698.

Leofanti, G., Padovan, M., Tozzola, G., Venturelli, B., (1998). Surface area and pore texture of catalysts. *Catal. Today*, **41**: 207–219.

Letteron, P., Fromenty, B., Terris, B., Degott, C., Pessayre, D., (1996). Acute and chronic hepatic steatosis lead to in vivo lipid peroxidation in mice. *J. Hepatol*., **24 (2)**: 200–208.

Letteron, P., Sutton, A., Mansouri, A., Fromenty, B., Pessayre, D., (2003). Inhibition of microsomal triglyceride transfer protein: another mechanism for drug-induced steatosis in mice. *Hepatology*, **38 (1)**: 133–140.

Li, F.B., Li, X.Z., Hou, M.F., Cheah, K.W., Choy, W.C.H., (2005). Enhanced photocatalytic activity of Ce^{3+}–TiO_2 for 2-mercaptobenzothiazole degradation in aqueous suspension for odour control. *Appl. Catal., A: Gen*., **285**: 181–189.

Li, W., Nanaboina, V., Chen, F., Korshin, G.V., (2016). Removal of polycyclic synthetic musks and antineoplastic drugs in ozonated wastewater: quantitation based on the data of differential spectroscopy. *J. Hazard. Mater*., **304**: 242–250.

Li, Y.Y., Wang, J.S., Liu, B., Dang, L.Y., Yao, H.C., Li, Z.J., (2011). BiOI–sensitized TiO_2 in phenol degradation: A novel efficient semiconductor sensitizer.*Chem. Phys. Lett.*, **508:** 102–106.

Li, Z.H., Schulz, L., Ackley, C., Fenske, N., (2010). Adsorption of tetracycline on kaolinite with pH-dependent surface charges. *J. Colloid Interface Sci*., **351**: 254–260.

Liang, J., Komarow, S., Hayashi, N., Kasai, E., (2007). Improvement in sonochemical degradation of 4–chlorophenol by combined use of Fenton–like reagents, *Ultrason. Sonochem*., **14**: 201–207.

Lin, H., Li, H., Chen, L., Li, L., Yin, L., Lee, H., Yang, Z., (2018). Mass loading and emission of thirty–seven pharmaceuticals in a typical municipal wastewater treatment plant in Hunan Province, Southern China. *Ecotox. Environ. Safe*., **147**: 530–536.

Linic, S., Christopher, P., Ingram, D.B., (2011). Plasmonic-metal nanostructures for efficient conversion of solar to chemical energy. *Nat. Mater*.,**10**: 911–921.

Liu, C., Tang, X., Mo, C., Qiang, Z., (2008). Characterization and activity of visible–light–driven TiO_2 photocatalyst codoped with nitrogen and cerium. *J. Solid State Chem*., **181**: 913–919.

Liu, F.-F., Zhao, J., Wang, S., Du, P., Xing, B., (2014a). Effects of solution chemistry on adsorption of selected pharmaceuticals and personal care products (PPCPs) by graphenes and carbon nanotubes. *Environ. Sci. Technol*., **48 (22)**: 13197–13206.

Liu, H., Zhang, G.P., Liu, C.Q., Li, L., Xiang, M., (2009a). The occurrence of chloramphenicol and tetracyclines in municipal sewage and the Nanming River, Guiyang City, China. *J. Environ. Monitor*., **11**: 1199–1205.

Liu, M., Hou, L., Yu, S., Xi, B., Zhao, Y., Xia, X., (2013a). MCM-41 impregnated with A zeolite precursor: synthesis, characterization and tetracycline antibiotics removal from aqueous solution. *Chem. Eng. J*. **223**: 678–687.

Liu, P., Zhang, H., Feng, Y., Yang, F., Zhang, J., (2014). Removal of trace antibiotics from wastewater: a systematic study of nanofiltration combined with ozone-based advanced oxidation processes. *Chem. Eng. J*., **240**: 211–220.

Liu, S., Wang, N., Zhang, Y., Li, Y., Han, Z., Na, P., (2015). Efficient removal of radioactive iodide ions from water by three–dimensional Ag_2O–Ag/TiO_2 composites under visible light irradiation. *J. Hazard. Mater*., **284**: 171–181.

Liu, S., Zhao, X.-R., Sun, H.-Y., Li, R.-P., Fang, Y.-F., Huang, Y.-P., (2013). The degradation of tetracycline in a photo-electro-Fenton system. *Chem. Eng. J*. **231**: 441–448.

Liu, X., Yang, Y., Shi, X., Li, K., (2015i). Fast photocatalytic degradation of methylene blue dye using a low–power diode laser. *J. Haz. Mater.*, **283:** 267–275.

Liu, Y.K., Hu, J., Wang, J.L., (2014b). Fe^{2+} enhancing sulfamethazine degradation in aqueous solution by gamma irradiation. *Radiat. Phys. Chem*., **96**: 81–87.

Liu, Z.H., Kanjo, Y., Mizutani, S., (2009). Removal mechanisms for endocrine disrupting compounds (EDCs) in wastewater treatment-physical means, biodegradation, and chemical advanced oxidation: a review. *Sci. Total Environ*., **407**: 731–748.

Locatelli, M.A.F., Sodré, F.F., Jardim, W.F., (2011). Determination of antibiotics in Brazilian surface waters using liquid chromatography-electrospray tandem mass spectrometry. *Arch. Environ. Contam. Toxicol*., **60**: 385–393.

Logonathan, K., Bommusamy, P., Muthaiahpillai, P., Velayutham, M., (2011). The syntheses, characterizations, and photocatalytic activities of silver, platinum, and gold doped TiO_2 nanoparticles. *Environ. Eng. Res*., **16**: 81–90.

Lores, M., Llompart, M., Sanchez-Prado, L., Garcia-Jares, G., Cela, R., (2005). Confirmation of the formation of dichlorodibenzo–p–dioxin in the photodegradation of triclosan by photo-SPME. *Anal. Bioanal. Chem*., **381**: 1294–1298.

Lozano, N., Rice, C.P., Ramirez, M., Torrents, A., (2013). Fate of Triclocarban, Triclosan and Methyltriclosan during wastewater and biosolids treatment processes. *Water Res*., **47**: 4519–4527.

Lu, Y., Yu, H., Chen, S., Quan, X., Zhao, H., (2012). Integrating Plasmonic Nanoparticles with TiO_2 Photonic Crystal for Enhancement of Visible-Light-Driven Photocatalysis. *Environ. Sci. Technol*., **46**: 1724–1730.

Luna, L.A.V.D, da Silva, T.H.G., Nogueira, R.F.P., Kummrow, F., Umbuzeiro, G.A., (2014). Aquatic toxicity of dyes before and after photo–Fenton treatment, *J. Hazard. Mater*., **276**: 332–338.

Luo, Y., Guo, W., Ngo, H.H., Nghiem, L.D., Hai, F.I., Zhang, J., Liang, S., Wang, X.C., (2014). A review on the occurrence of micropollutants in the aquatic environment and their fate and removal during wastewater treatment. *Sci. Total. Environ*., **473–474**: 619–641.

Luo, Y., Xu, L., Rysz, M., Wang, Y., Zhang, H., Alvarez, P.J.J., (2011). Occurrence and transport of tetracycline, sulfonamide, quinolone, and macrolide antibiotics in the Haihe river Basin, China. *Environ. Sci. Technol*., **45**: 1827–1833.

Machida, M., Norimoto, K., Kimura, T., (2004). Antibacterial Activity of Photocatalytic Titanium Dioxide Thin Films with Photodeposited Silver on the Surface of Sanitary Ware. *J. Am. Ceram. Soc*., **88 (1)**: 95–100.

Magesh, G., Viswanathan, B., Viswanath, R.P., Varadarajan, T.K., (2009). Photocatalytic behavior of CeO_2–TiO_2 system for the degradation of methylene blue. *Indian J. Chem*., 4**8A**: 480–488.

Mailler, R., Gasperi, J., Coquet, Y., Deshayes, S., Zedek, S., Cren-Olive , C., Cartiser, N., Eudes, V., Bressy, A., Caupos, E., Moilleron, R., (2015). Study of a large scale powdered activated carbon pilot: removals of a wide range of emerging and priority micropollutants from wastewater treatment plant effluents. *Water Res*., **72**: 315–330.

Maira, A.J., Yeung, K.L., Soria, J., Coronado, J.M., Belver, C., Lee, C.Y., Augugliaro, V., (2001). Gas–phase photo–oxidation of toluene using nanometer–size TiO_2 catalysts. *Appl. Catal. B, Environ*., **29**: 327–336.

Makdee, A., Unwiset, P., Chanapattharapol, K.C., Kidkhunthod. P., (2018). Effects of Ce addition on the properties and photocatalytic activity of TiO_2, investigated by X–ray absorption spectroscopy. *Mater. Chem. Phys.*, **213**: 431–443.

Malakootian. M., Moridi. A. Efficiency of electro-Fenton process in removing Acid Red 18 dye from aqueous solutions, Process Saf. Environ. Prot. 111 (2017) 138–147.

Malato, S., Blanco, J., Vidal, A., Richter, C., (2002). Photocatalysis with solar energy at a pilot–plant scale: an overview. *Appl. Catal. B, Environ*., **37**: 1–15 .

Mansilla, H.D., Bravo, C., Ferreyra, R., Litter, M.I., Jardim, W.F., Lizama, C., Freer, J., Fernandez, J., (2006). Photocatalytic EDTA degradation on suspended and immobilized TiO_2. *J. Photochem. Photobiol. A*, **181**: 188–194.

Mansour, H.B., Houas, I., Montassar, F., Ghedira, K., Barillier, D., Mosrati, R., Chekir-Ghedira, L., (2012). Alteration of in vitro and acute in vivo toxicity of textile dyeing wastewater after chemical and biological remediation. *Environ. Sci. Pollut. Res*., **19**: 2634–2643.

Marques, I., Magalhâes-Mota, G., Pires, F., Sério, S., Ribeiro, P.A., Raposo, M., (2017). Detection of traces of triclosan in water. *Appl. Surf. Sci*., **421**: 142–147.

Martinez, J.L., (2009). Environmental pollution by antibiotics and by antibiotic resistance determinants. *Environ. Pollut*., **157**: 2893–2902.

Matejova, L., Koci, K., Reli, M., Capek, L., Hospodkova, A., Peikertova, P., Matej, Z., Obalova, L., Wach, A., Kustrowski, P., Kotarba, A., (2014). Preparation, characterization and photocatalytic properties of cerium doped TiO_2: On the effect of Ce loading on the photocatalytic reduction of carbon dioxide. *Appl. Cat. B: Environ*., **152-153**: 172–183.

McFarland, A.D., Haynes, C.L., Mirkin, C. A., Duyne, R.P.V., Godwin, H.A., (2004). Color my nanoworld. *J. Chem. Educ*., **81**: 544A.

Meinel, F., Ruhl, A.S., Sperlich, A., Zietzschmann, F., Jekel, M., (2015). Pilot–scale investigation of micropollutant removal with granular and powdered activated carbon. *Water Air Soil Pollut*., **226 (1)**: 1–10.

Mendioroz, S., Pajares, J.A., Benito, I., Pesquera, C., Gonzalez, F., Blanco, C., (1987). Texture evolution of montmorillonite under progressive acid treatment: change from H3 to H2 type of hysteresis. *Langmuir*, **3**: 676–681.

Mestre, A., Pires, J., Nogueira, J., Carvalho, A., (2007). Activated carbons for the adsorption of ibuprofen. Carbon **45 (10)**: 1979–1988.

Mezcua, M., Gomez, M.J., Ferrer, I., Aguera, A., Hernando, M.D., Fernandez-Alba, A.R., (2004). Evidence of 2,7/2,8–dibenzodichloro–p–dioxin as a photodegradation product of triclosan in water and wastewater samples. *Anal. Chim. Acta*, **524**: 241–247.

Miao, X.S., Bishay, F., Chen, M., Metcalfe, C.D., (2004). Occurrence of antimicrobials in the final effluents of wastewater treatment plants in Canada. *Environ. Sci. Technol*. **38 (13)**: 3533–3541.

Michael, I., Rizzo, L., McArdell, C.S., Manaia, C.M., Merlin, C., Schwartz, T., Dagot, C., Fatta-Kassinos, D., (2013). Urban wastewater treatment plants as hotspots for the release of antibiotics in the environment: a review. *Water Res*., **47**: 957–995.

Michalova, E., Novotna, P., Schlegelova, J., (2004). Tetracyclines in veterinary medicine and bacterial resistance to them. *Vet. Med*., **49 (3)**: 79–100.

Miege, C., Choubert, J.M., Ribeiro, L., Euse be, M., Coquery, M., (2009). Fate of pharmaceuticals and personal care products in wastewater treatment plantseconception of a database and first results. *Environ. Pollut*.. **157**: 1721–1726.

Mills, A., Hunte, S.L., (1997). An overview of semiconductor photocatalysis. *J. Photochem. Photobiol. A*, **108**: 1–35.

Miranda, R.C., Gomes, E.B., Pereira J.N., Marin-Morales, M.A., Machado, K.M., Gusmào, N.B., (2013). Bio–treatment of textile effluent in static bioreactor by *Curvularia lunata* URM 6179 and *Phanerochaete chrysosporium* URM 6181. *Bioresour. Technol*., 142: 361–367.

Modirshahla, N., Hassani, A., Behnajady, M.A., Rahbarfam, R., (2011). Effect of operational parameters on decolorization of Acid Yellow 23 from wastewater by UV irradiation using ZnO and ZnO/SnO_2 photocatalysts. *Desalination*, **271**: 187–192.

Moellering, R.C., (1979). Special consideration of the use of antimicrobial agents during pregnancy, post-partum, and in the newborn. *Clin. Obstet. Gynecol*., **22**: 373–378.

Mohamed, R.M., Mkhalid, I.A., (2015). Visible light photocatalytic degradation of cyanide using Au–TiO_2/multi-walled carbon nanotube nanocomposites. *J. Ind. Eng. Chem*., **22**: 390–395.

Mohammadi, M.R., Cordero-Cabrera, M.C., Fray, D.J., Ghorbani, M., (2006). Preparation of high surface area titania (TiO_2) films and powders using particulate sol–gel route aided by polymeric fugitive agents. *Sensor Actuat. B–Chem*., **120**: 86–95.

Mompelat, S., Le Bot, B., Thomas, O.. (2009). Occurrence and fate of pharmaceutical products and by-products, from resource to drinking water. *Environ. Int*., **35**: 803–814.

Morrall, D., McAvoy, D., Schatowitz, B., Inauen, J., Jacob, M., Hauk, A., Eckhoff, W., (2004). A field study of triclosan loss rates in river water (Cibolo Creek, TX). *Chemosphere*, **54**: 653–660.

Moyo, M., Florence, L.R., Okonkwo, J.O., (2015). Improved electro–oxidation of triclosan at nano-zinc oxide-multiwalled carbon nanotube modified glassy carbon electrode. *Sens. Actuat. B-Chem.*, **209**: 898–905.

Mu, Y., Rabaey, K., Rozendal, R.A., Yuan, Z.G., Keller, J., (2009). Decolorization of azo dyes in bioelectrochemical systems. *Environ. Sci. Technol*., **43 (13)**: 5137–5143.

Muzvidziwa, T., Moyo, M., Okonkwo, O., et al., (2017). Electrodeposition of zinc oxide nanoparticles on multiwalled carbon nanotube–modified electrode for determination of caffeine in wastewater effluent. *Int. J. Environ. Anal. Chem*., **97**: 1–14.

Naddeo, V., Belgiorno, V., Kassinos, D., Mantzavinos, D., Meric, S., (2010). Ultrasonic degradation, mineralization and detoxification of diclofenac in water: optimization of operating parameters. *Ultrason. Sonochem*., **17**: 179–185.

Nagele, E., Moritz, R., (2005). Structure elucidation of degradation products of the antibiotic amoxicillin with ion trap MSn and accurate mass determination by ESI TOF. *J. Am. Soc. Mass. Spectrom*., **16 (10):** 1670–1676.

Nam, S.-W., Choi, D.-J., Kim, S.-K., Her, N., Zoh, K.-D., (2014). Adsorption characteristics of selected hydrophilic and hydrophobic micropollutants in water using activated carbon. *J. Hazard. Mater*., 270, 144–152.

Narmadha, D., Selvam Kavitha, V.M., (2012). Treatment of domestic waste water using natural flocculants. *Int. J. Life Sci. Biotechnol. Pharm. Res*., **1 (3)**: 206–2013.

Narumiya, M., Nakada, N., Yamashita, N., Tanaka, H., (2013). Phase distribution and removal of pharmaceuticals and personal care products during anaerobic sludge digestion. *J. Hazard. Mater*., **260**: 305–312.

Nassef, M., Matsumoto, S., Seki, M., Khalil, F., Kang, I.J., Shimasaki, Y., Oshima, Y., Honjo, T., (2010). Acute effects of triclosan, diclofenac and carbamazepine on feeding performance of Japanese medaka fish (Oryzias latipes). *Chemosphere*, **80**: 1095–1100.

Nasseri, S., Mahvi, A.H., Seyedsalehi, M., Yaghmaeian, K., Nabizadeh, R., Alimohammadi, M., Safari, G.H., (2017). Degradation kinetics of tetracycline in aqueous solutions using peroxydisulfate activated by ultrasound irradiation: Effect of radical scavenger and water matrix. *J. Mol. Liq*., **241**: 704–714.

Navaro, V.J., Senior, J.R., (2006). Drug-related hepatotoxicity. *N Engl. J. Med*., **354**: 731–739.

Naya, S.-I., Inoue, A., Tada, H., (2010). Self-assembled heterosupramolecular visible light photocatalyst consisting of gold nanoparticle-loaded titanium(IV) dioxide and surfactant. *J. Am. Chem. Soc.*, **132:** 6292–6293.

Nazar, M.F., Shah. S.S., Khosa. M.A., (2010). Interaction of Azo Dye with Cationic Surfactant Under Different pH Conditions. *J. Surfactants Deterg*., **13**: 529–537.

Nguyen, T.A., Juang, R. –S., (2013). Treatment of waters and wastewaters containing sulfur dyes: a review. *Chem. Eng. J*., **219**: 109–117.

Ni, M., Leung, M.K., Leung, D.Y., Sumathy, K., (2007). A review and recent developments in photocatalytic water-splitting using TiO_2 for hydrogen production. *Renew. Sustain. Energy Rev*., **11**: 401–425.

Nikl, M., Jary, V., Havlak, L., Barta, J., Buryi, M., Mihokova, E., Rejman, M., Laguta, V., (2015). Optical, structural and paramagnetic properties of Eu–doped ternary sulfides $ALnS_2$ (A = Na, K, Rb; Ln = La, Gd, Lu, Y). *Materials*, **8**: 6978–6998.

Nishi, I., Kawakami, T., Onodera, S., 2008. Monitoring of triclosan in the surface water of the tone canal, Japan. *B. Environ. Contam. Tox.,* **80**: 163–166.

Nitoi, N., Oancea, P., Raileanu, M., Crisan, M., Constantin, L., Cristea, I., (2015). UV–VIS photocatalytic degradation of nitrobenzene from water using heavy metal doped titania. *J. Ind. Eng. Chem*., **21**: 677–682.

Nogawa, T., Isobe, T., Matsushita, S., Nakajima, A., (2012). Preparation and visible-light photocatalytic activity of Au- and Cu-modified TiO_2 powders. *Mater. Lett*., **82**: 174–177.

Novo, A., Andre , S., Viana, P., Nunes, O.C., Manaia, C.M., (2013). Antibiotic resistance, antimicrobial residues and bacterial community composition in urban wastewater. *Water Res*., **47 (5)**: 1875–1887.

O'Regan, B., Gratzel, M., (1991). A low cost high–efficiency solar cell based on dye–sensitized colloidal TiO_2 films. *Nature*, **353**: 737–739.

Ohe, P.C.V.D., Schmitt–Jansen, M., Slobodnik, J., Brack, W., (2012). Triclosan– the forgotten priority substance? *Environ. Sci. Pollut. Res*., **19**: 585–591.

Ohno, T., (2004). Preparation of visible light active S–doped TiO_2 photocatalysts and their photocatalytic activities, *Water Sci. Technol*., **49**: 159–163.

Oka, H., Ito, Y., Matsumoto, H.. (2000). Chromatographic analysis of tetracycline antibiotics in foods. *J. Chromatogr. A*.. **882**: 109–133.

Ollis, D.F., Pelizzetti, E., Serpone, N., (1991). Photocatalyzed destruction of water contaminants. *Environ. Sci. Technol*., **25**: 1522–1529.

O'Neill, C., Hawkes, F.R., Hawkes, D.L., Laurenco, N.D., Pinheiro, H.M., Delee, W., (1999). Color in textile effluents sources, measurement, discharge consents and simulation: a review. *J. Chem. Technol. Biotechnol*., **74**: 1009–1018.

Pal, A., Gin, K.Y.–H., Lin, A.Y.–C., (2010). Reinhard, M., Impacts of emerging organic con- taminants on freshwater resources: review of recent occurrences, sources, fate and effects. *Sci. Total Environ*., **408**: 6062–6069.

Palmisano, G., Addamo, M., Augugliaro, V., Caronna, T., Paola, A.D., Lopez, E.G., Loddo, V., Marci, G., Palmisano, L., Schiavello, M., (2007). Selectivity of hydroxyl radical in the partial oxidation of aromaticcompounds in heterogeneous photocatalysis. *Catal. Today,* **122**: 118–127.

Pan, X., Deng, C., Zhang, D., Wang, J., Mu, G., Chen, Y., (2008). Toxic effects of amoxicillin on the photosystem II of Synechocystis sp. characterized by a variety of in vivo chlorophyll fluorescence tests. *Aquat. Toxicol.,* **89**: 207–213.

Pan, Y., Wang, Y., Zhou, A., Wang, A., Wu, Z., Liting, L., Li, X., Zhang, K., Zhu, T., (2017). Removal of azo dye in an up-flow membrane-less bioelectrochemical system integrated with bio-contact oxidation reactor. *Chem. Eng. J*., **326**: 454–461.

Pandey, A., Singh, P., Iyengar, L., (2007). Bacterial decolorization and degradation of azo dyes– a Review. *Int. Biodeterior. Biodegrad*., **59**: 73–84.

Pareek, V., Chong, S., Tade, M., Adesina, A., (2008). Light intensity distribution in heterogeneous photocatalytic reactors. *Asia-Pac. J. Chem. Eng*., **3**: 171–201.

Park, S., Selvaraj, R., Meetani, M.A., Kim, Y., (2017). Enhancement of visible-light-driven photocatalytic reduction of aqueous Cr(VI) with flower-like In3+-doped SnS_2. *J. Ind. Eng. Chem*., **45**: 206–214.

Passos, M.L.C., Saraiva, M.L.M.F.S., (2019). Detection in UV-visible spectrophotometry: Detectors, detection systems, and detection strategies. *Measurement,* **135**: 896−904.

Patil, S.B., Basavarajappa, P.S., Ganganagappa, N., Jyothi, M.S., Raghu, A.V., Reddy, K.R., (2019). Recent advances in non-metals-doped TiO_2 nanostructured photocatalysts for visible-light driven hydrogen production, CO_2 reduction and air purification. *Int. J. Hydrog. Energy*, **44**: 13022–13039.

Pelizzetti, E., Minero, C., (1993). Mechanism of the photo–oxidative degradation of organic pollutants over TiO_2 particles. *Electrochim. Acta*, **38**: 47–55.

Pena, A., Paulo, M., Silva, L., Seifrtová, M., Lino, C., Solich, P., (2010). Tetracycline antibiotics in hospital and municipal wastewaters: a pilot study in Portugal. *Anal. Bioanal. Chem*., **396**: 2929–2936.

Peng, X.Z., Xiong, S.S., Qu, W.H., Wang, Z.F., Tan, J.H., Jin, J.B., Tang, C.M., Liu, J., Fan, (2017). Persistence, temporal and spatial profiles of ultraviolet absorbents and phenolic personal care products in riverine and estuarine sediment of the Pearl River catchment. China. *J. Hazard. Mater*., **323 (Part A)**: 139–146.

Peng, Y., Zhang, Y., Huang, H., Zhong, C., (2018). Flexibility induced high–performance MOF–based adsorbent for nitroimidazole antibiotics capture. *Chem. Eng. J*., **333**: 678–685.

Perez, J.F., Llanos, J., Saez, C., Lopez, C., Canizares, P., Rodrigo, M.A., (2017). Treatment of real effluents from the pharmaceutical industry: a comparison between Fenton oxidation and conductive-diamond electro-oxidation. *J. Environ. Manag*., **195**: 216–223.

Perini, J.A.L., Tonetti, A.L., Vidal, C., Montagner, C.C., Nogueira, R.F.P., (2018). Simultaneous degradation of ciprofloxacin, amoxicillin, sulfathiazole and sulfamethazine, and disinfection of hospital effluent after biological treatment via photo–Fenton process under ultraviolet germicidal irradiation. *Appl. Catal. B, Environ*., **224**: 761–771.

Pico, Y., Andreu, V., (2007). Fluoroquinolones in soil-risks and challenges. *Anal. Bioanal .Chem*., **387**: 1287–1299.

Pintado-Herrera, M.G., Gonza lez-Mazo, E., Lara-Martín, P.A., (2014). Determining the distribution of triclosan and methyl triclosan in estuarine settings. *Chemosphere*, **95**: 478–485.

Pouran, S.R., Aziz, A.R.A., Daud, W.M.A.W., (2015). Review on the main advances in photo–Fenton oxidation system for recalcitrant wastewaters. *J. Ind. Eng. Chem.*, **21:** 53–69.

Prado, N., Renault, E., Ochoa, J., Amrane, A., (2009). Development and validation of a rapid method for the determination of tetracycline in activated sludge by SPE clean-up and HPLC–UV detection. *Environ. Technol*., **30**: 469–476.

Putra, E.K., Pranowo, R., Sunarso, J., Indraswati, N., Ismadji, S., (2009). Performance of activated carbon and bentonite for adsorption of amoxicillin from wastewater: mechanisms, isotherms and kinetics. *Water Res*., **43**: 2419–2430.

Qamar, M., Muneer, M., Bahnemann, D., (2006). Heterogeneous photocatalysed degradation of two selected pesticide derivatives, triclopyr and daminozid in aqueous suspensions of titanium dioxide. *J. Environ. Manage*., **80**: 99–106.

Qu, Y.–Z., Yao, M.–M., Li, F., Sun, X.–H., (2011). Microstructures and photocatalytic properties of Fe^{3+} /Ce^{3+} codoped nanocrystalline TiO_2 films. *Water, Air, Soil Pollut*., **221**: 13–21.

Radjenovic , J., Petrovic , M., Barcelo´, D., (2007a). Advanced mass spectrometric methods applied to the study of fate and removal of pharmaceuticals in wastewater treatment. *Trends Anal. Chem*., **26**: 1132–1144.

Rafqah, S., Chung, P.W.–W., Nelieu, S., Einhorn, J., Sarakha, M., (2006). Phototransformation of triclosan in the presence of TiO2 in aqueous suspension: Mechanistic approach. *Appl. Catal. B, Environ.*, **66**: 119–125.

Raghuvanshi, S., Bhakar, V., Sowmya, C., Sangwan, K.S., (2017). Waste Water treatment plant life cycle assessment: treatment process to reuse water. *Procedia CIRP*, **61**: 761–766.

Rahman, M.F., Yanful, E.K., Jasim, S.Y., (2009). Occurrences of endocrine disrupting compounds and pharmaceuticals in the aquatic environment and their removal from drinking water: challenges in the context of the developing world. *Desalination*, **248**: 578–585.

Ramaswamy, B.R., Shanmugam, G., Velu, G., Rengarajan, B., Larsson, D.G.J., (2011). GC–MS analysis and ecotoxicological risk assessment of triclosan, carbamazepine and parabens in Indian rivers. *J. Hazard Mater*., **186**: 1586–1593.

Ranjit, K. T., Willner, I., Bossmann, S.H., Braun, A.M., (2001). Lanthanide Oxide Doped Titanium Dioxide Photocatalysts: Effective Photocatalysts for the Enhanced Degradationof Salicylic Acid and t–Cinnamic Acid. *J. Catal*., **204**: 305–313.

Rashid, M.U., Bhuiyan, M.K.H., Quayum, M.E., (2013). Synthesis of silver nano particles (Ag-NPs) and their uses for quantitative analysis of vitamin C tablets. Dhaka Univ. *J. Pharm. Sci*. **12**: 29–33.

Rayaroth, M.P., Aravind, U.K., Aravindakumar, C.T., (2016). Degradation of pharmaceuticals by ultrasound–based advanced oxidation process. *Environ. Chem. Lett*., **14**: 259–290.

Reda, S.M., Khairy, M., Mousa, M.A., (2017). Photocatalytic activity of nitrogen and copper doped TiO_2 nanoparticles prepared by microwave–assisted sol–gel process, *U. A. R. J. Chem*., (2017) in press.

Reemtsma, T., Weiss, S., Mueller, J., Petrovic , M., Gonzalez, S., Barcelo´, D., Ventura, F., Knepper, T., (2006). Polar pollutants entry into the water cycle by municipal wastewater: a European perspective. *Environ. Sci. Technol*., **40**: 5451–5458.

Reiss, R., Mackay, N., Habig, C., Griffin, J., (2002). An ecological risk assessment for triclosan in lotic systems following discharge from wastewater treatment plants in the United States. *Environ. Toxicol. Chem*., **21 (11)**: 2483–2492.

Rivera-Utrilla, J., Sánchez–Polo, M., Ferro–García, M. A., Prados–Joya, G., Ocampo–Pérez, R., (2013). Pharmaceuticals as emerging contaminants and their removal from water. A review. *Chemosphere*, **93:** 1268–1287.

Roberts, J., Kumar, A., Du, J., Hepplewhite, C., Ellis, D.J., Christy, A.G., Beavis, S.G., (2016). Pharmaceuticals and personal care products (PPCPs) in Australia's largest inland sewage treatment plant, and its contribution to a major Australian river during high and low flow. *Sci. Total Environ*., **541**: 1625–1637.

Robinson, T., McMullan, G., Marchant, R., Nigam, P., (2001). Remediation of dyes in textile effluent: a critical review on current treatment technologies with a proposed alternative. *Bioresour. Technol*., **77 (3)**: 247–255.

Rodriguez, E., Campinas, M., Acero, J.L., Rosa, M.J., (2016). Investigating PPCP removal from wastewater by powdered activated carbon/ultrafiltration. *Water, Air, & Soil Pollut*., **227**: 1–4.

Rodriguez-Mozaz, S., Chamorro, S., Marti, E., Huerta, B., Gros, M., Sànchez-Melsiò, A.,

Borrego, C.M., Barcelò, D., Balcàzar, J.L., (2015). Occurrence of antibiotics and antibiotic resistance genes in hospital and urban wastewaters and their impact on the receiving river. *Water Res*., **69**: 234–242.

Rosu, M.-C., Coros, M., Pogacean, F.et al., (2017). Azo dyes degradation using TiO_2 M.-C.Pt/graphene oxide and TiO_2 M.-C.Pt/reduced graphene oxide photocatalysts under UV and natural sunlight irradiation. *Solid State Sci*., **70**: 13–20.

Roushani, M., Saedi, Z., Musa beygi, T., (2016). Anionic dyes removal from aqueous solution using TMU-16 and TMU-16-NH_2 as isoreticular nanoporous metal organic frameworks. *J. Taiwan Inst. Chem. E*., **66**: 164–171.

Saggioro, E.M., Oliveira, A.S., Pavesi, T., Maia, C.G., Ferreira, L.F.V., Moreira, J.C., (2011). Use of Titanium Dioxide Photocatalysis on the Remediation of Model Textile Wastewaters Containing Azo Dyes. *Molecules*, **16**: 10370–10386.

Saien, J., Khezrianjoo, S., (2008). Degradation of the fungicide carbendazim in aqueous solutions with UV/TiO_2 process: optimization, kinetics and toxicity studies. *J. Hazard. Mater*., **157**: 269–276.

Salavati-Niasari, M., Soofivand, F., Sobhani-Nasab, A., Shakouri-Arani, M., Yeganeh Faal, A., Bagheri, S., (2016). Synthesis, characterization, and morphological control of ZnTiO3 nanoparticles through sol-gel processes and its photocatalyst application. *Advanced Powd. Technol*., **27**: 2066–2075.

Saleh, T.A., (2015). Isotherm, kinetic, and thermodynamic studies on Hg(II) adsorption from aqueous solution by silica- multiwall carbon nanotubes. *Environ. Sci. Pollut. Res.*, **22**: 16721–16731.

Saleh, T.A., Tuzen, M., Sari, A., (2018). Polyamide magnetic palygorskite for the simultaneous removal of Hg(II) and methyl mercury; with factorial design analysis. *J. Environ. Manage*., **211**: 323–333.

Santos, A.B.D., Cervantes, F.J., Lier, J.B.V., (2007). Review paper on current technologies for decolourisation of textile wastewaters: perspectives for anaerobic biotechnology. *Bioresour. Technol*., **98 (12)**: 2369–2385.

Saquib, M., Muneer, M., (2003). TiO_2-mediated photocatalytic degradation of a triphenylmethane dye (gentian violet), in aqueous suspensions. *Dyes and Pigments,* **56:** 37–49.

Sarmah, A.K., Meyer, M.T., Boxall, A.B., (2006). A global perspective on the use, sales, exposure pathways, occurrence, fate and effects of veterinary antibiotics (VAs) in the environment. Chemosphere, **65**: 725–759.

Sassman, S.A., Lee, L.S., (2005). Sorption of three tetracyclines by several soils: assessing the role of pH and cation exchange. *Environ. Sci. Technol*., **39 (19)**: 7452−7459.

Schattka, J.H., Wong, E.H.–M., Antonietti, M., and Caruso, R.A., (2006). Sol–gel templating of membranes to form thick, porous titania, titania/zirconia and titania/silica films. *J. Mater. Chem.,* **16**: 1414–1420.

Sclafani, A., Herrmann, J.M., (1998). Influence of metallic silver and of platinum–silver bimetallic deposits on the photocatalytic activity of titania (anatase and rutile) in organic and aqueous media. *J. Photochem. Photobiol. A,* **113**: 181–188.

Seaton, N.A., (1991). Determination of the connectivity of porous solids from nitrogen sorption measurements. *Chem. Eng. Sci.***46**: 1895–1909.

Seery, M.K., George. R., Floris, P., Pillai, S.C., (2007). Silver doped titanium dioxide nanomaterials for enhanced visible light photocatalysis. *J Photochem. Photobiol. Chem*., **189**: 258–263.

Selvam, K., Muruganandham, M., Muthuvel, I., Swaminathan, M., (2007). The influence of inorganic oxidants and metal ions on semiconductor sensitized photodegradation of 4–fluorophenol. *Chem. Eng. J.,* **128:** 51–57.

Sen, S.K., Raut, S., Bandyopadhyay, P., Raut, S., (2016). Fungal decolouration and degradation of azo dyes: a review. *Fungal Biol. Rev*., **30**: 112–133.

Silva, C.G., Juá rez, R., Marino, T., Molinari, R., García, H., (2011). Influence of excitation wavelength (UV or visible light) on the photocatalytic activity of titania containing gold nanoparticles for the generation of hydrogen or oxygen from water. *J. Am. Chem. Soc.,* **133**: 595–602.

Simon, N.S., (2005). Loosely bound oxytetracycline in riverine sediments from two tributaries of the Chesapeake Bay. *Environ. Sci. Technol*., **39**: 3480–3487.

Singer, H., Müller, S., Tixier, C., Pillonel, L., (2002). Triclosan: occurrence and fate of a widely used biocide in the aquatic environment: field measurements in wastewater treatment plants, surface waters, and lake sediments. *Environ. Sci. Technol*., **36 (23)**: 4998–5004.

Singh, H.K., Saquib, M., Haque, M., Muneera, M., Bahnemann, D., (2007). Titanium dioxide mediated photocatalysed degradation of phenoxyacetic acid and 2,4,5–trichlorophenoxyacetic acid, in aqueous suspension. *J. Mol. Catal. A–Chem*., **264**: 66–72.

Singh, R.P., Singh, P.K., Singh, R.L., (2014). Bacterial decolorization of textile azo dye Acid Orange by *Staphylococcus hominis* RMLRT03. *Toxicol. Int*., **21**: 160–166.

Sires, I., Brillas, E., (2012). Remediation of water pollution caused by pharmaceutical residues based on electrochemical separation and degradation technologies: a review. *Environ. Int*., **40**: 212–229.

Sires, I., Oturan, N., Oturan, M.A., et al., (2007). Electro–Fenton degradation of antimicrobials triclosan and triclocarban. *Electrochim. Acta*, **52:** 5493–5503.

Soleymani, A.R., Chahardoli, R., Kaykhaii, M., (2016). Development of UV/H_2O_2/TiO_2–LECA hybrid process based on operating cost: Application of an effective fixed bed photo-catalytic recycled reactor. *J. Ind. Eng. Chem*., **44**: 90–98.

Solis, M., Solis, A., Perez, H.I., Manjarrez, N., Flores, M., (2012). Microbial decolouration of azo dyes: a review. *Process Biochem*., **47 (12)**: 1723–1748.

Sommer, L., (1989). *Studies in Analytical Chemistry, Elsevier*, Amsterdam.

Sorensen, J.P.R., Lapworth, D.J., Nkhuwa, D.C.W., Stuart, M.E., Gooddy, D.C., Bell, R.A., Chirwa, M., Kabika, J., Liemisa, M., Chibesa, M., Pedley, S., (2015). Emerging contaminants in urban groundwater sources in Africa. *Water Res*., **72**: 51–63.

Sousa, M.A., Gonçalves, C., Vilar, V.J.P., Boaventura, R.A.R., Alpendurada, M.F., (2012). Suspended TiO_2-assisted photocatalytic degradation of emerging contaminants in a

municipal WWTP effluent using a solar pilot plant with CPCs. *Chem. Eng. J*., **198–199**: 301–309.

Stamatelatou, K., Pakou. C., Lyberatos, G., (2011). Occurrence, Toxicity, and Biodegradation of Selected Emerging Priority Pollutants in Municipal Sewage Sludge. *Comprehensive biotechnology*, **2011**: 473–484.

Stathatos, E., Petrova, T., Lianos, P., (2001). Study of the Efficiency of Visible–Light Photocatalytic Degradation of Basic Blue Adsorbed on Pure and Doped Mesoporous Titania Films. *Langmuir*, 17: 5025–5030

Stengl, V., Bakardjieva, S., Murafa, N., (2009). Preparation and photocatalytic activity of rare earth doped TiO_2 nanoparticles. *Mater. Chem. Phys*., **114**: 217–226.

Storozhuk, P.G., Shamsutdinova, V.V., (1976). Effect of certain antibiotics of tetracycline series on the level of blood sugar and the role of insulin in the mechanism of its regulation. *Probl. Endokrinol (Mosk)*., **22**: 106–10.

Strenn, B., Clara, M., Gans, O., Kreuzinger, N., (2004). Carbamazepine, diclofenac, ibuprofen and bezafibrate – investigations on the behaviour of selected pharmaceuticals during wastewater treatment. *Water Sci. Technol*., **50**: 269–276.

Stylidi, M., Kondarides, D.I., Verykios, X.E., (2004). Visible light–induced photocatalytic degradation of Acid Orange 7 in aqueous TiO_2 suspensions. *Appl. Catal. B, Environ.*, **47**: 189–201.

Sun, J., Li, W., Zheng, P., Zhu, J., (2012). Toxicity evaluation of antibiotics in piggery wastewater by luminescent bacteria. *Pol. J. Environ.*, **21**: 741–747.

Sun, J., Wang, X., Sun, J., Sun, R., Sun, S., Qiao, L., (2006). Photocatalytic degradation and kinetics of Orange G using nano–sized Sn(IV)/TiO_2/AC photocatalyst. *J. Mol. Catal. A, Chem.*, **260:** 241–246.

Sun, X., Li, C., Ruan, L., Peng, Z., Zhang, J., Zhao, J., Li, Y., (2014). Ce-doped SiO_2@TiO_2 nanocomposite as an effective visible light photocatalyst. *J. Alloys Compd*., **585**: 800–804.

Svorc, L., Borovska, K., Cinkova, K., Stankovic, D.M., Plankova, A., (2017). Advanced electrochemical platform for determination of cytostatic drug flutamide in various matrices using a boron–doped diamond electrode. *Electrochim. Acta*, **251**: 621–630.

Tahir, K., Ahmad, A., Li, B., Khan, A.U., Nazir, S., Khan, S., Khan, Z.U.H., Khan, S.U., (2016). Preparation, characterization and an efficient photocatalytic activity of Au/TiO_2 nanocomposite prepared by green deposition method. *Mater. Lett*., **178**: 56–59.

Tang, W.Z., Huang, C.P., (1996). 2,4–Dichlorophenol oxidation kinetics by Fenton's reagent, *Environ. Technol*., **17**: 1371–1378.

Tao, Y., Mai, W., (2002). Present status of biological chemical industry and pollution treatment, *Henan Chem. Ind*., **2002**: 4–7.

Tariq, M.A., Faisal, M., Muneer, M., Bahnemann, D., (2007). Photochemical reactions of a few selected pesticide derivatives and other priority organic pollutants in aqueous suspensions of titanium dioxide. *J. Mol. Catal. A*, **265:** 231–236.

Tbessi, I., Benito, M., Molins, E., LIorca, J., Touati, A., Sayadi, S., Najjar, W., (2019). Effect of Ce and Mn co-doping on photocatalytic performance of sol-gel TiO_2. *Solid State Sci*., **88**: 20–28.

Ternes, T.A., (1998). Occurrence of drugs in german sewage treatment plants and rivers. *Water Res*., **32**: 3245–3260.

Thanhmingliana, Lee, S.M., Tiwari, D., Prasad, S.K., (2015). Efficient attenuation of 17α-ethynylestradiol (EE2) and tetracycline using novel hybrid materials: batch and column reactor studies. *RSC Adv.*, **5**: 46834–46842.

Thevenon, F., Adatte, T., Wildi, W., Poté, J., (2012). Antibiotic resistant bacteria/genes dissemination in lacustrine sediments highly increased following cultural eutrophication of Lake Geneva (Switzerland). *Chemosphere*, **86**: 468–476.

Thrile–Bruhn, S., (2003). Pharmaceutical antibiotics compounds in soils–a review. *J. Plant Nutr. Soil Sci.*, **166**: 145–167.

Tissue, B.M., (2012). Characterization of Materials. *John Wiley & Sons, Inc.*

Tiwari, A., Shukla, A., Lalliansanga, Tiwari, D., Lee, S.M., (2018). Nanocomposite thin films Ag^0(NP)/TiO_2 in the efficient removal of micropollutants from aqueous solutions: A case study of tetracycline and sulfamethoxazole removal. *J. Environ. Manag*., **220**: 96−108.

Tiwari, A., Shukla, A., Lalliansanga, Tiwari, D., Lee, S.M., (2019a). Synthesis and characterization of Ag^0(NPs)/TiO_2 nanocomposite: insight studies of triclosan removal from aqueous solutions. *Environ. Technol*., **22**: 1–15.

Tiwari, A., Shukla, A., Lalliansanga, Tiwari, D., Lee, S.M., (2019b). Au-nanoparticle/nanopillars TiO_2 meso-porous thin films in the degradation of tetracycline using UV-A light. *J. Ind. Eng. Chem*., **69**: 141–152.

Tiwari, D., Lalhriatpuia, C., Lalhmunsiama, Lee. S.M., Kong, S.H., (2015). Efficient application of nano–TiO_2 thin films in the photocatalytic removal of Alizarin Yellow from aqueous solutions, *Appl. Surf. Sci*. **353:** 275–283.

Tolls, J., (2001). Sorption of veterinary pharmaceuticals in soils: a review. *Environ. Sci. Technol*., **35**: 3397–3406.

Touati, A., Hammedi, T., Najjar, W., Ksibi, Z., Sayadi, S., (2016). Photocatalytic degradation of textile wastewater in presence of hydrogen peroxide: Effect of cerium doping titania. *J. Ind. Eng. Chem*., **35**: 36–44.

Tunesi, S., Anderson, M.A., (1987). Photocatalysis of 3,4–DCB in TiO_2 aqueous suspensions; effects of temperature and light intensity; CIR–FTIR interfacial analysis. *Chemosphere*, **16**: 1447–1456.

Turchi, C.S., Ollis, D.F., (1990). Photocatalytic Degradation of Organic Water Contaminants: Mechanisms Involving Hydroxyl Radical Attack. J. *Catal*., **122**: 178–192.

Tuzen, M., Sarı, A., Saleh, T.A., (2018). Response surface optimization, kinetic and thermodynamic studies for effective removal of rhodamine B by magnetic AC/CeO_2 nanocomposite. *J. Environ. Manage*., **206**: 170–177.

Valente, J.P.S., Padilha, P.M., Florentino, A.O., (2006). Studies on the adsorption and kinetics of photodegradation of a model compound for heterogeneous photocatalysis onto TiO_2. *Chemosphere*, **64**: 1128–1133.

Van Boeckel, T.P., Brower, C., Gilbert, M., Grenfell, B.T., Levin, S.A., (2015). Global trends in antimicrobial use in food animals. *Proc. Natl. Acad. Sci. U.S.A.*, 5649– 5654

Vaz-Moreira, I., Nunes, O.C., Manaia, C.M., (2014). Bacterial diversity and antibiotic resistance in water habitats: searching the links with the human microbiome. *FEMS Microbiol. Rev.*, **38 (4)**: 761–778.

Verlicchi, P., Al Aukidy, M., Zambello, E., (2012). Occurrence of pharmaceutical compounds in urban wastewater: removal, mass load and environmental risk after a secondary treatment–a review. *Sci. Total Environ.*, **429**: 123–155.

Verstraeten, I.M., Heberr, T., Vogel, J.R., Speth, T., Zuehlke, T., Duennbier, U., (2003). Occurrence of endocrine-disrupting and other wastewater compounds during water treatment with case studies from Lincoln, Nebraska and Berlin, Germany. *Pract. period. hazard., toxic, radioact. waste manag.*, **7**: 253–263.

Vieira, G.B., Jose, H.J., Peterson, M., Baldissarelli, V.Z., Alvarez, P., Moreira, R. F. P. M., (2018). CeO_2/TiO_2 nanostructures enhance adsorption and photocatalytic degradation of organic compounds in aqueous suspension. *J. Photoch. Photobio. A*, **353**: 325–336.

Vogna, D., Marotta, R., Napolitano, A., Andreozzi, R., d'Ischia, M., (2004). Advanced oxidation of the pharmaceutical drug diclofenac with UV/H_2O_2 and ozone. *Water Res.*, **38 (2)**: 414–422.

Wan, Z., Hu, J., Wang, J., (2016). Removal of sulfamethazine antibiotics using Ce–Fe–grapheme nanocomposite as catalyst by Fenton–like process. *J. Environ. Manag.*, **182**: 284–291.

Wang, C.–C., Lee, C.–K., Lyu, M.–D., Juang, L.–C., (2008). Photocatalytic degradation of C.I. Basic Violet 10 using TiO_2 catalysts supported by Y zeolite: an investigation of the effects of operational parameters. *Dyes and Pigments,* **76:** 817–824.

Wang, J., Wang, S., (2016). Removal of pharmaceuticals and personal care products (PPCPs) from wastewater: A review. *J. Environ. Manag.*, **182**: 620–640.

Wang, J.L., Xu, L.J., (2012). Advanced oxidation processes for wastewater treatment: formation of hydroxyl radical and application. Crit. Rev. *Environ. Sci. Technol*., 42: 251–325.

Wang, L., Zhao, Y., Zhang, J., (2017). Electrospun cerium-based TiO_2 nanofibers for photocatalytic oxidation of elemental mercury in coal combustion flue gas. *Chemosphere*, **185**: 690–698.

Wang, P., Huang, B., Dai, Y., Whangbo, M.-H., (2012). Plasmonic photocatalysts: Harvesting visible light with noble metal nanoparticles. *Phys. Chem. Chem. Phys.*, **14**: 9813–9825.

Wang, Y., Cheng, H., Hao, Y., Ma, J., Li, W., Cai, S., (1999). Photoelectrochemical properties of metal–ion–doped TiO_2 nanocrystalline electrodes. *Thin Solid Films*, **349**: 120–125.

Wang, Y., Ma, J., Zhu, J., Ye, N., Zhang, X., Huang, H., (2016a). Multi–walled carbon nanotubes with selected properties for dynamic filtration of pharmaceuticals and personal care products. *Water Res*., **92**: 104–112.

Watkinson, A.J., Murby, E.J., Kolpin, D.W., Costanzo, S.D., (2009). The occurrence of antibiotics in an urban watershed: from wastewater to drinking water. *Sci. Total Environ*., **407**: 2711–2723.

Weerachawanasak, P., Mekasuwandumrong, O., Arai, M., Fujita, S.-I., Praserthdam, P., Panpranot, J., (2009). Effect of strong metal–support interaction on the catalytic performance of Pd/TiO_2 in the liquid–phase semihydro- genation of phenylacetylene. *J. Catal*., **262**: 199–205.

Weisburger, J.H., (2002). Comments on the history and importance of aromatic and heterocyclic amines in public health. *Mutat. Res. Fund. Mol*., **506–507**: 9–20.

Wilke, K., Breuer, H.D., (1999). The influence of transition metal doping on the physical and photocatalytic properties of titania. *J. Photochem. Photobiol. A*, **121:** 49–53.

Windholz, M., Budavari, S., Stroumtsos, L.Y., Fertig, M.N., (1976). *The Merck index. An encyclopedia of chemicals and drugs.* Merck & Co.

Wu, Q., Shi, H., Adams, C.D., Timmons, T., Ma, Y., (2012). Oxidative removal of selected endocrine-disruptors and pharmaceuticals in drinking water treatment systems, and identification of degradation products of triclosan. *Sci. Total Environ*., **439**: 18–25.

Xie, X., Zhou, Q., He, Z., Bao, Y., (2010). Physiological and potential genetic toxicity of chlortetracycline as an emerging pollutant in wheat (Triticum aestivum L.). *Environ. Toxicol. Chem*., **29**: 922–928.

Xie, Y., Yuan, C., Li, X., (2005). Photosensitized and photocatalyzed degradation of azo dye using Ln^{n+}–TiO_2 sol in aqueous solution under visible light irradiation. *Mater. Sci. Eng. B,* **117**: 325–333.

Xiu, Z., Xing, Z., Li, Z., Wu, X., Yan, X., Hu, M., Cao, Y., Yang, S., Zhou, W., (2018). Ti^{3+}-TiO_2/Ce^{3+}-CeO_2 Nanosheet heterojunctions as efficient visible-light driven photocatalysts. *Mater. Res*., **100**: 191–197.

Xu, C., Rangaiah, G.P., Zhao, X.S., (2014). Photocatalytic degradation of methylene blue by titanium dioxide: Experimental and modeling study. *Ind. Eng. Chem. Res*., **53**: 14641–14649.

Xu, D., Liu, K., Shi, W., et al., (2015), Ag–decorated $K_2Ta_2O_6$ nanocomposite photocatalysts with enhanced visible-light-driven degradation activities of tetracycline (TC). *Ceram. Int*., **3**: 4444–4451.

Xu, H., Heinze, T.M., Chen, S., Cerniglia, C.E., Chen, H., (2007). Anaerobic metabolism of 1–2amino–2–naphthol–based azo dyes (Sudan dyes) by human intestinal microflora. *Appl. Environ. Microbiol*., **73**: 7759–7762.

Xu, J.J., Ao, Y.H., Fu, D.G., (2009). Study on photocatalytic performance and degradation kinetics of X–3B with lanthanide–modified titanium dioxide under solar and UV illumination. *J. Hazard. Mater*., **164**: 762–768.

Xu, L.J., Wang, J.L., (2012). Magnetic Nanoscaled Fe_3O_4/CeO_2 composite as an efficient Fenton–like heterogeneous catalyst for degradation of 4–chlorophenol. *Environ. Sci. Technol*., **46 (18)**: 10145–10153.

Yagub, M.T., Sen, T.K., Afroze, S., Ang, H.M., (2014). Dye and its removal from aqueous solution by adsorption: a review. *Adv. Colloid Interface Sci*., **209**: 172–184.

Yang, B., Ying, G.–G., Zhao, J.–L., Zhang, L.–J., Fang, Y.–X., Nghiem, L.D., (2011). Oxidation of triclosan by ferrate: Reaction kinetics, products identification andtoxicity evaluation. *J. Hazard. Mater*., **186**: 227–235.

Yang, G.C., Tang, P.-L., (2016). Removal of phthalates and pharmaceuticals from municipal wastewater by graphene adsorption process. *Water Sci. Technol*., **73 (9)**: 2268–2274.

Yang, L., Liu, Z., (2007). Study on light intensity in the process of photocatalytic degradation of indoor gaseous formaldehyde for saving energy. *Energ. Convers. Manage*., **48**: 882–889.

Yang, S.F., Hai, F.I., Price, W.E., McDonald, J., Khan, S.J., Nghiem, L.D., (2016a). Occurrence of trace organic contaminants in wastewater sludge and their removals by anaerobic digestion. *Bioresour. Technol*., **210**: 153–159.

Yap, P.–S., Lim, T.–T., (2011). Effect of aqueous matrix species on synergistic removal of bisphenol–A under solar irradiation using nitrogen–doped TiO_2/AC composite. *Appl. Catal. B, Environ.,* **101:** 709–717.

Yin, H., Wada, Y., Kitamura, T., Kambe, S., Murasawa, S., Mori, H., Sakata, T., Yanagida, S., (2001). *J. Mater. Chem*., **11**: 1694–1703.

Ying, G.G., Kookana, R.S., (2007). Triclosan in wastewaters and biosolids from Australian wastewater treatment plants. *Environ. Int*., **33**: 199–205.

You, S.J., Damodar, R.A., Hou, S.C., (2010). Degradation of Reactive Black 5 dye using anaerobic/aerobic membrane bioreactor (MBR) and photochemical membrane reactor. *J. Hazard. Mater*., **177**: 1112–1118.

Young, T.A., Heidler, J., Matos-Pe rez, C.R., Sapkota, A., Toler, T., Gibson, K.E., Schwab, K.J., Halden, R.U., (2008). Ab initio and in situ comparison of caffeine, triclosan, and triclocarban as indicators of sewage-derived microbes in surface waters. *Environ. Sci. Technol*., **42 (9)**: 3335–3340.

Yu, J., Zhao, X., Du, J., Chen, W., (2000). Preparation, Microstructure and Photocatalytic Activity of the Porous TiO_2 Anatase Coating by Sol–Gel Processing. *J. Solgel Sci. Technol.,* **17**: 163–171.

Yu, J.C., Kwong, T.Y., Luo, Q., Cai, Z., (2006). Photocatalytic oxidation of triclosan. *Chemosphere*, **65**: 390–399.

Yuan, F., Hu, C., Hu, X., Wei, D., Chen, Y., Qu, J., (2011). Photodegradation and toxicity changes of antibiotics in UV and UV/H_2O_2 proces. *J. Hazard. Mater*., 185 (2), 1256–1263.

Zang, Y., Farnood, R., (2005). Photocatalytic decomposition of methyltert-butyl etherin aqueous slurry of titanium dioxide. *Appl. Catal. B, Environ.*, **57**: 275–282.

Zeltner, W.A., Tompkins, D.T., (2005). Applications of UV Photocatalysis for Gaseous Contaminants: Shedding Light on Photocatalysis. ASHRAE., **3**: 532.

Zeng, G., Ye, Z., He, Y., Yang, X., Ma, J., Shi, H., Feng, Z., (2017). Application of dopamine–modified halloysite nanotubes/PVDF blend membranes for direct dyes removal from wastewater. *Chem. Eng. J*., **323**: 572–583,

Zhan, F., Liu, W., Li, H., Yang, Y., Wang, M., (2018). Ce–doped CdS quantum dot sensitized TiO_2 nanorod films with enhanced visible–light photoelectrochemical properties. *Appl. Surf. Sci*., **455**: 476–483.

Zhang, Q.-Q., Ying, G.-G., Pan, C.-G., Liu, Y.-S., Zhao, J.-L., (2015). Comprehensive evaluation of antibiotics emission and fate in the river basins of China: source analysis, multimedia modeling, and linkage to bacterial resistance, Environ. Sci. Technol., **49**: 6772–6782.

Zhao, G., Kozuka, H., Yoko, T., (1996). Sol–gel preparation and photoelectrochemical properties of TiO_2 films containing Au and Ag metal particles. *Thin Solid Films*, **277**: 147–154.

Zhao, J., Yang, X., (2003). Photocatalytic oxidation for indoor air purification: a literature review. *Build. Environ*., **38**: 645–654.

Zhao, J., Ying, G., Liu, Y., Chen, F., Yang, J., Wang, L., (2010). Occurrence and risks of triclosan and triclocarban in the Pearl River system, South China: from source to the receiving environment. *J. Hazard Mater*., **179**: 215–222.

Zhu, J., Zhu, K., Chen, L., (2006). Influence of gold nanoparticles on the up–conversion fluorescence in Sm^{3+}. *J. Non-Cryst. Solids*, **352**: 150–154.

Zia, H., Shalchian, N., Borhanian, F., (1977). Kinetics of amoxicillin degradation in aqueous solutions. *Can. J. Pharm. Sci*., **12**: 80–83.

Zinatloo–Ajabshir, S., Morassaei, M.S., Salavati–Niasari, M., (2018). $Nd_2Sn_2O_7$ nanostructures as highly efficient visible light photocatalyst: Green synthesis using pomegranate juice and characterization. *J. Clean. Prod.*, **198**: 11–18.

Zorrilla, L.M., Gibson, E.K., Jeffay, S.C., Crofton, K.M., Setzer, W.R., Cooper, R.L.,. Stoker, T.E., (2009). The effects of triclosan on puberty and thyroid hormones in male wistar rats. *Toxicol. Sci*., **107**: 56–64.

Zucca, P., Vinci, C., Sollai. F., Rescigno, A., Sanjust, E., (2008). Degradation of Alizarin Red S under mild experimental conditions by immobilized 5,10,15,20–tetrakis(4–sulfonatophenyl)porphine–Mn(III) as a biomimetic peroxidase–like catalyst. *J. Mol. Catal. Chem*., **288**: 97–102.

Zuccato, E., Castiglioni, S., Bagnati, R., Melis, M., Fanelli, R., (2010). Source, occurrence and fate of antibiotics in the Italian aquatic environment. *J. Hazard Mater*., **179**: 1042–1048.

List of Publications

A. Journals

International Journals

1. **Lalliansanga**, Alka Tiwari, Alok Shukla, Diwakar Tiwari, Seung Mok Lee. Nanocomposite Au NP/TiO_2 thin film in the efficient remediation of aqueous solutions contaminated with emerging micro-pollutants. *Environ. Sci. Pollut. R*., 25 (2018) 20125–20140.

2. Alka Tiwari, Alok Shukla, **Lalliansanga**, Diwakar Tiwari, Seung Mok Lee. Nanocomposite thin films Ag^0(NP)/TiO_2 in the efficient removal of micropollutants from aqueous solutions: A case study of tetracycline and sulfamethoxazole removal. *J. Environ. Manage*., 220 (2018) 96–108.

3. Alka Tiwari, Alok Shukla, **Lalliansanga**, Diwakar Tiwari, Seung-Mok Lee. Au-nanoparticle/nanopillars TiO_2 meso-porous thin films in the degradation of tetracycline using UV-A light. *J. Ind. Eng. Chem*., 69 (2019) 141–152.

4. Alka Tiwari, Alok Shukla, **Lalliansanga**, Diwakar Tiwari, Seung-Mok Lee. Nano structured TiO_2 thin films in the efficient removal of b-estradiol from aqueous solution: physico-chemical studies. *Desalin. Water Treat*., 150 (2019) 263–273.

5. Alka Tiwari, Alok Shukla, **Lalliansanga**, Diwakar Tiwari, Seung Mok Lee. Synthesis and characterization of Ag^0(NPs)/TiO_2 nanocomposite: insight studies of triclosan removal from aqueous solutions. *Environ. Technol*., (2019).

6. **Lalliansanga**, Diwakar Tiwari, Alka Tiwari, Alok Shukla, Dong-Jin Kim, Yi-Yong Yoon, Seung-Mok Lee. Facile synthesis and characterization of nanocomposite Au^0 (NPs)/titanium dioxide: Photocatalytic degradation of Alizarin Yellow. *J. Ind. Eng. Chem*., 82 (2020) 153–163.

B. Paper presented in Conferences / Symposia

1. Paper entitled "Au-nanoparticle/TiO_2 meso-porous thin films in the degradation of Tetracycline using UV-A light" presented in International Conference on *Emerging Trends in Chemical Sciences (ETCS-2018),* 26-28 February, 2018. Department of Chemistry, Dibrugarh University, Dibrugarh, Assam, India.

2. Paper entitled **"**Au-nanoparticle/TiO_2 meso-porous thin films in the degradation of Alizarin Yellow using UV-A light" presented in National Conference of *Mizoram Science Congress (MSC-2018).* 4-5 October, 2018. Department of Chemistry, Pachhunga University College, Aizawl, Mizoram, India.

3. Paper entitled **"**Triclosan degradation by heterogeneous photocatalysis using Ag-nanoparticle/TiO_2 mesoporous thin films" presented in *International Conference on Chemistry & Environmental Sustainability (ICCES-2019),* 19-22 February, 2019. Department of Chemistry, School of Physical Sciences, Mizoram University, Aizawl, Mizoram, India.

4. Paper entitled **"**Photocatalytic degradation of Alizarin Yellow using Ce-nanoparticle/TiO_2 thin films" presented in *National Conference on Emerging Trends in Environmental Research (NACETER-2019),* 31 October - 2 November, 2019. Department of Environmental Science, Pachhunga University College, Aizawl, Mizoram, India.

5. Paper entitled **"**Efficient Degradative Removal of Amoxicillin using Heterogeneous Photocatalyst Ce^{3+}/TiO_2" presented in *National Conference on Functional Materials and Applications (NCFMA-2019),* 22-23 November, 2019. Department of Physics, NIT Mizoram, Chaltlang, Aizawl, India.

Particulars of the candidate

Name of candidate	: Lalliansanga
Degree	: Ph.D
Department	: Chemistry
Title of thesis	: Photocatalytic applications of nano-structured Ag or Au/TiO_2 thin films in the efficient removal of micro-pollutants from aqueous solutions
Date of admission	: 11.08.2014

Approval of research proposal

1. B.O.S.	:
2. SCHOOL BOARD	: 11.05.2015
3. REGISTRATION NO. & DATE	: MZU/Ph.D/731 of 11.05.2015
Extension (if any)	: NIL

Head

Department of Chemistry

Bio-Data

Name of candidate : Lalliansanga

Designation : Research scholar

Department : Chemistry

Adress : C-13, Aizawl Venglai, Aizawl, 796007

Email : ls_avl@yahoo.co.uk

Educational

Degree	**Institution**	**Year**	**Details**
B.Sc.	Mizoram University	2007	1st Division
M.Sc.	Mizoram University	2013	1st Division

Publication

Year	Title	Publisher/Journal
2018	Nanocomposite Au NP/TiO_2 thin film in the efficient remediation of aqueous solutions contaminated with emerging micro-pollutants.	Environmental Science and Pollution Research. 25(2018), 20125–20140.
2018	Nanocomposite thin films Ag^0(NP)/TiO_2 in the efficient removal of micro-pollutants from aqueous solutions: A case study of tetracycline and sulfamethoxazole removal.	Journal of environmental management. 220(2018), 96–108.
2019	Au-nanoparticle/nanopillars TiO_2 meso-porous thin films in the degradation of tetracycline using UV-A light.	Journal of Industrial and Engineering Chemistry. 69(2019), 141–152.
2019	Nano structured TiO_2 thin films in the efficient removal of b-estradiol from aqueous solution: physico-chemical studies.	Desalination and Water Treatment. 150(2019), 263–273.
2019	Synthesis and characterization of Ag^0(NPs)/TiO_2 nanocomposite: insight studies of triclosan removal from aqueous solutions.	Environmental Technology. (2019).
2020	Facile synthesis and characterization of nanocomposite Au^0 (NPs)/titanium dioxide: Photocatalytic degradation of Alizarin Yellow.	Journal of Industrial and Engineering Chemistry. 82 (2020) 153–163.

Conference attended/Paper presented

Year	Name of paper/Conference	Organizer
2018	Paper presented entitled "Au-nanoparticle/TiO_2 meso-porous thin films in the degradation of Tetracycline using UV-A light". International Conference on Emerging Trends in Chemical Sciences (ETCS-2018).	Department of Chemistry, Dibrugarh University, Dibrugarh, Assam.
2018	Paper presented entitled **"**Au-nanoparticle/TiO_2 meso-porous thin films in the degradation of Alizarin Yellow using UV-A light". National Conference of Mizoram Science Congress (MSC-2018)	Department of Chemistry, Pachhunga University College, Aizawl, Mizoram
2019	Paper presented entitled **"**Triclosan degradation by heterogeneous photocatalysis using Ag-nanoparticle/TiO_2 mesoporous thin films". International Conference on Chemistry & Environmental Sustainability (ICCES-2019)	Department of Chemistry, School of Physical Sciences, Mizoram University, Aizawl, Mizoram.
2019	Paper presented entitled **"**Photocatalytic degradation of Alizarin Yellow using Ce-nanoparticle/TiO_2 thin films". National Conference on Emerging Trends in Environmental Research (NACETER-2019)	Department of Environmental Science, Pachhunga University College, Aizawl, Mizoram.
2019	Paper presented entitled **"**Efficient Degradative Removal of Amoxicillin using Heterogeneous Photocatalyst Ce^{3+}/TiO_2" National Conference on Functional Materials and Applications (NCFMA-2019).	Department of Physics, NIT Mizoram, Chaltlang, Aizawl.

Journal of Industrial and Engineering Chemistry 82 (2020) 153–163

Contents lists available at ScienceDirect

Journal of Industrial and Engineering Chemistry

journal homepage: www.elsevier.com/locate/jiec

Facile synthesis and characterization of nanocomposite Au^0(NPs)/titanium dioxide: Photocatalytic degradation of Alizarin Yellow

Lalliansanga[a], Diwakar Tiwari[a], Alka Tiwari[b], Alok Shukla[b], Dong-Jin Kim[c], Yi-Yong Yoon[d,*], Seung-Mok Lee[d,*]

[a] Department of Chemistry, School of Physical Sciences, Mizoram University, Aizawl 796004, India
[b] Department of Physics, National Institute of Technology, Aizawl 796001, India
[c] Department of Environmental Science & Biotechnology, Hallym University, Chuncheon 24252, Republic of Korea
[d] Department of Health and Environment Catholic Kwandong University, Gangneung 25601, Republic of Korea

ARTICLE INFO

Article history:
Received 25 March 2019
Received in revised form 11 September 2019
Accepted 4 October 2019
Available online 15 October 2019

Keywords:
Nanocomposite
Plasmonic material
Alizarin yellow
Mineralization
Interplanar distance
Kinetics of degradation

ABSTRACT

The present communication aims to synthesise the plasmonic nanocomposite Au^0(NPs)/TiO_2 by a facile route and to utilize material in the efficient removal of Alizarin Yellow in aqueous solutions using the UV-A light. Au^0-nanoparticles were *in situ* doped with titania network using template method. Polyethylene glycol was employed as filler media. The nanocomposites Au^0(NPs)/TiO_2 (non-template) and Au^0(NPs)/TiO_2(T) (template) were characterized by the XRD and DRS (Diffuse Reflection Spectroscopy) methods. Surface characteristics were discussed by the SEM and TEM pictures of these materials. The interplanar distance of Au(NPs) were found to be 0.14 nm and 0.20 nm for the materials Au^0(NPs)/TiO_2 and Au^0(NPs)/TiO_2(T), respectively. The Atomic Force Microscopy (AFM) analysis showed heterogeneous surface structure and TiO_2 were pillared on the surface. Physico-chemical studies deduced the mechanistic pathways of removal. The pseudo-first order rate constant values were decreased with the increase in dye concentrations. Further, mineralization of Alizarin Yellow was obtained at wide range of pH (pH 4.0–8.0). The nanocomposite thin films showed fairly a good stability for repeated cycle of operations in removal of Alizarin Yellow. The photocatalyst shown greater applicability in the real matrix treatment using Tlwang river water.

Introduction

Synthetic dyes are known to be complex organic compounds and widely used in various modern industries including textile, leather, food, paper production, cosmetics, pharmaceuticals, hair colourings, photoelectrochemical cells etc. A rough estimate states that every year *Ca* 2.8×10^5 tons of textile dyes seemingly discharged through the industrial effluents only [1–3]. Moreover, during the synthesis and processing of dyes it releases *Ca.* 15% of total dyes to the terrestrial environment [4]. Dye compounds are potential recalcitrant in nature since these are insignificantly biodegradable and found fairly stable towards several oxidizing agents [5]. Therefore, the dye compounds easily escaped through the existing wastewater treatment plants and caused serious impact on the aquatic ecosystem as entered into the waterbodies [6]. The water contaminated with dyes therefore; experiences a reduced transmission of solar radiation. This causes reduced or complete inhibition of photosynthesis. Further, several dyes are reported to be bio-accumulative, toxic and potentially causes skin diseases or even found to be carcinogenic and teratogenic [7–9].

Among the variety of synthetic dyes, the azo dyes constitute *Ca* 80% of all reactive dyes which contains the azo chromogen [10–12]. Azo dyes are found highly toxic and showed the carcinogenic/mutagenic activities [9,13]. Therefore, a complete elimination of dyes from the aqueous effluents is required as to maintain the stringent water standards as prescribed by the regulatory bodies. There are several conventional methods implied and demonstrated in the removal of dyes from water bodies [14–16]. However, several methods have shown limitations in required efficiency, high energy requirement or huge sludge formation that further creates additional environmental burden to be dealt amicably. Additionally, literature reveals that several advanced or hybrid

* Corresponding authors.
E-mail addresses: yoonyy@cku.ac.kr (Y.-Y. Yoon), leesm@cku.ac.kr (S.-M. Lee).

https://doi.org/10.1016/j.jiec.2019.10.008
1226-086X/

treatment methods are proposed for the effective degradation of azo dyes. Hollow cobalt nanoparticles are obtained by a galvanic replacement reaction using Al-nanoparticles template. The hollow Co(NPs) showed efficient in the degradation of methyl orange from aqueous solutions having the degradation rate constant 2.444 min^{-1} [17]. Similarly, palladium nanoparticles (PdNPs) were obtained by using the cellulose (CMC) and palladium chloride in an aqueous solution which was stable for years and showed good catalytic activity towards the removal of several azo dyes *viz.*, p-aminoazobenzene, acid red 66, acid orange 7, scarlet 3 G and Reactive Yellow 17 by sodium borohydride [18]. A hybrid system contained with the hydrodynamic cavitation along with the photo catalyst TiO_2 or ZnO showed promising treatment process, at the pilot plant level, in the decolourization of Reactive red 180 dye [16]. CdS loaded Ag–ZnO catalysts were obtained by the precipitation and thermal decomposition process. The composite material was intended to utilize in the efficient removal of azo dyes RR 120, RO 4 and RY 84 from aqueous solutions using the solar radiations. Moreover, the composite material has shown fair stability in the repeated operations [19]. Similarly, composite materials *viz.*, TiO_2-Pt(NP)/graphene oxide and TiO_2-Pt(NP)/reduced graphene oxide were utilized in the degradation of several azo dyes under UV and natural sunlight. Results indicated that the removal efficiencies were found to be 99.56%, 99.15%, and 96.23%, respectively for the amaranth, sunset yellow and tartrazine using the photocatalyst TiO_2-Pt(NP)/graphene oxide [12]. ZnO nanostructures were obtained by the sodium dodecylsulfate (SDS) or polyvinyl alcohol (PVA) as templating materials in a low temperature precipitation process. ZnO possessed predominantly wurtzite hexagonal phase and showed good catalytic activity in the degradation of reactive red (RR141) [4]. Bio-electrochemical degradation processes were shown enhanced oxidative removal of azo dyes. The method is integrated with bio-contact oxidation in the efficient performance of this hybrid system [20,21]. $Dy_2Sn_2O_7$-SnO_2 ternary nanocomposites were synthesized using propane-1,2-diol as novel polymerizing agent and trimesic acid as stabilizing agent. The nanocomposite was employed for the photocatalytic degradation of several dyes including the eosin Y, eriochrome black T, erythrosine and methyl orange [22]. Erichrome black T was efficiently degraded using the nanostructured ZrO_2 photocatalyst. The precursors were employed as zirconyl nitrate and ethylene diamine [23]. An interesting study was conducted using the bimematic photocatalyst *i.e.*, 2D nanostructured Bi_2WO_6 impregnated with the monomeric hemin (HBWO). The hemin take part as electron shuttle along with play important role in efficient oxygen transfer which results an efficient photocatalytic behaviour of catalyst [24]. Similarly, the HBWO is employed in the Fenton-like process in the degradation of organic pollutants [25].

On the other hand, the semiconductor TiO_2 showed useful applications in the advanced oxidation processes in removal of several persistent pollutants from aqueous media. The widespread use of TiO_2 is because of its high photocatalytic efficiency, stability and biologically not active [16,26–30]. However, the wide energy band gap *i.e.*, 3.05 eV for rutile and 3.2 eV for anatase phase of TiO_2 restrict it to employ with UV light only. Moreover, the solar light contribute only 5% of UV-radiations and as well known fact that UV-radiations are associated with serious harmful effects towards human being [31]. However, the impregnation of noble metals *viz.*, Au, Ag, Pt nanoparticles with the titania network facilitate greatly to overcome the problems associated with large band gap [32–35]. These nanoparticles reduce significantly fast recombination of the photogenerated e^-/h^+ pairs since it retains electrons and behaves like sink for interfacial charge transfer reactions [36,24]. Therefore, the photo-excitation of nanoparticles enhances markedly the photocatalytic efficiency of titanium dioxide. The presence of these NPs with the titania enables to reduce the band gap energy of the titanium dioxide, that results an enhanced interaction between the NPs and titania [37]. Additionally, the Ag or Au nanoparticles decorated TiO_2 absorbs the light in the visible region and undergoes with the surface plasmon resonance that stimulates the localized electric field around titanium dioxide and resulted the facile generation of charge carriers at the surface of titanium dioxide [38]. Similarly, the NPs on titanium dioxide surface behaves like a co-catalyst which enhances the e^-/h^+ separations [39,40]. On the other hand, the novel magnetic ternary nanocomposites $TiO_2/Fe_3O_4/CoWO_4$ were found to be useful photocatalytic materials for the enhanced photocatalytic activity through the p-n heterojunction [41]. Nanostructured praseodymium oxide was synthesized by simple facile and solvent less method employing the praseodymium nitrate and triethylenetetramine (Trien) or the Schiff base ligand as precursor materials. The materials were shown an enhanced photocatalytic activity for several persistent water pollutants [42,43]. Integration of carbon dots and polyaniline with titanium dioxide resulted ternary nanocomposite. The visible light driven materials have shown enhanced photocatalytic activity in the removal of several water pollutants [44]. The other studies showed that the morphological control was obtained in the sol-gel synthesis of $ZnTiO_3$ nanoparticles and the material was employed in the efficient photocatalytic removal of methyl orange [45]. The ZnS nanoclusters were synthesized by the hydrothermal processing using the [bis (salicylidene)zinc(II)] [46]. Sonochemical method was employed to synthesize the nanorods of $NiMoO_4$. The shape and size of the nanorods or nanoparticles of $NiMoO_4$ was greatly controlled with the irradiation power, concentration of initial precursors, sonication time, pH etc. [47]. Highly photocatalytic active CuInZnS nanoporous structure was theoretically and experimentally studied for the removal of atmospheric NO gas [48].

Therefore, the advanced nanocomposite materials showed enhance use in advanced oxidation processes (AOP) in particular with visible light driven, however, the use of solid powders in unit operations showed several limitations including with difficult phase separation, shadowing effect etc. This restricts the wider applications of solid samples in AOPs. However, on the other hand, the titanium dioxide thin films which alternately used as photo catalyst showed greater applicability in AOPs. This provides an easy removal from the reactor therefore; shows enhanced applicability for successive operations. However, doping of NPs with titanium dioxide network with thin film is found to be daunting task [49]. Our previous attempt intended to impregnate the Au(0) (NPs) with the titania network and fabricated the thin film samples. The thin film photocatalyst were employed in the degradation of some of micro-pollutants *viz.*, tetracycline, sulfamethoxazole and triclosan in aqueous solutions [50,51]. Therefore, the present study is eventually the extension of previous studies to provide facile synthesis of plasmonic nanocomposite Au^0(NPs)/TiO_2 thin films with the template synthetic method. The Au^0(NPs) were impregnated *in situ* to obtain even and fine distribution of Au^0(NPs) within the titania network. Further, the nanocomposite materials are intended to utilize for the decontamination of aquatic environment contaminated by one of potentially important azo dye Alizarin Yellow from aqueous solutions. The detailed physicochemical studies contributed to devise the mechanistic aspects of the degradation process.

Materials and methods

Chemicals and instruments

Titanium(IV) isopropoxide (≥97.0%), gold chloride (≥99.9%) and Alizarin Yellow (50%) were obtained from the Sigma Aldrich. Co., USA and were utilized without further purification. Polyethylene

glycol (mol. weight 2000) was obtained from Samchun Pure Chemical Co. Ltd., Korea. $NaNO_3$ (99.0%), EDTA (98%) and CH_3COOH (glacial) (99.9%) were procured from Loba Chemicals, India. Ethanol (anhydrous) (99.9%) was procured from Daejung Chemicals & Metals Co. Ltd., Korea. Sodium chloride (99.0%), sodium azide (≥99%), oxalic acid dihydrate (≥99%), sodium hydrogen carbonate (99.0%), 2-propanol (99.7%), zinc chloride dry, (≥95%), cadmium nitrate tetrahydrate (99%), copper (II) sulphate pentahydrate (≥99%), glycine (99.0%) and acetonitrile (99.7%) were procured from Merck India Ltd., India. Water was purified by using the Sartorius water Purification System (model: arium Mini Plus UV Lab., SterilePlus, Sartopore 2150, Germany; Pore Size of 0.45 + 0.2 μm). The river water sample was collected from the local river Tlawng, Aizawl (India). The river water sample was analysed for and the analytical results are reported elsewhere [52].

Spectrophotometer (Shimadzu Model: UV 1800, Japan) was used for quantitative estimation of Alizarin Yellow at the λ_{max} of 372 nm. The standard solutions of Alizarin Yellow were prepared having the concentrations 0.5, 1.0, 5.0, 10.0 and 15.0 mg/L. Calibration curve was obtained and utilized for the determination of unknown concentration of Alizarin Yellow. The TOC (Total Organic Carbon) Analyser (Shimadzu, Japan; Model: TOC-VCPH/CPN) was used for NPOC (Non-Purgeable Organic Carbon) measurement of the solutions. This data, perhaps, provides the mineralization of Alizarin Yellow. A UV-A lamp, wavelength (λ_{max}) = 360 nm (Model: 9W, PLS9 W BLB/2P 1CT, Philips) was procured from Hansung UV Pvt. Co. Ltd., Korea. SEM (Scanning Electron Microscope) machine (Model FE-SEM SU-70, Hitachi, Japan) was used for surface characterization. TEM (Transmission Electron Microscopic) analysis was performed using the TEM/EDX Analyser (Tecnai F20 Transmission Electron Microscope, FEI, USA). AFM (Atomic Force Microscope) images of the solids were obtained using the AFM machine (XE-100 apparatus from Park Systems, Korea) having sharp tips (>8 nm tip radius; PPP-NCHR type from Nano sensors™). The X-ray diffraction (XRD) data was collected using XRD machine (*i.e.*, PANalytical, Netherland; Model X'Pert PRO MPD). The X-ray diffraction pattern was obtained at the scan rate of 0.033 of 2θ illumination.

Methodology

Synthesis of nanocomposite materials

Gold (NPs) are obtained by previously described process [53]. Further, the TiO_2 was synthesized by sol-gel synthetic route. The polyethylene glycol is used as modifier in sol gel process. Titanium (IV) isopropoxide (28 g) along with polyethylene glycol (2 g) was introduced and dissolved in acetyl-acetone (13 g). 25 mL of Au(0)-nanoparticle solution was immediately introduced. Moreover, ethanol (184 g), acetic acid (5.8 g) and distilled water (22.5 g) was carefully introduced with the titanium solution. This mixture was stirred continuously for 2 h at room temperature. Then it was sonicated for 30 min. A transparent sol solution of Au^0(NPs)/TiO_2(T) is obtained. This was aged *Ca.* 24 h and this was then utilized for the coating of glass disks. Similarly, the Au^0(NPs)/TiO_2 was prepared without introducing the filler media polyethylene glycol.

Nanocomposite thin films

Thoroughly cleaned and dried circular glass disk (1.15 cm radius and 0.05 cm thickness) was utilized for the thin film coatings. The detailed procedure of fabrication is demonstrated elsewhere [51]. The two thin films are obtained and are named as Au^0(NPs)/TiO_2 and Au^0(NPs)/TiO_2(T). The disks were kept safely for further use in photocatalytic reactor operations.

The sol solutions were then used to obtain the powder of the precursors [51]. The powder samples were employed for some characterizations of these materials.

Characterization of nanocomposite thin films

Au^0(NPs)/TiO_2 or Au^0(NPs)/TiO_2(T) nanocomposite disks were exposed to obtain SEM images of thin films. Nanocomposite powder materials were utilized for obtaining the TEM images of these solids. Nanocomposite Au^0(NPs)/TiO_2 or Au^0(NPs)/TiO_2(T) thin films were subjected for obtaining the topographical 3D images using the AFM. XRD pattern of powder samples (Au^0(NPs)/TiO_2 or Au^0(NPs)/TiO_2(T)) was recorded and presented.

Further, the diffuse reflection spectra (DRS) was obtained for the solids *viz.*, Ag^0(NPs)/TiO_2/or Ag^0(NPs)/TiO_2(T) along with the nano TiO_2 prepared with template method using the UV–VISNIR spectrophotometer (DS104 Optical Spectrometer, Varian/Model Cary 5G, USA). The optical band gap of these solids was then estimated. The equipment was employed using the diffuse reflectance spectra (DRA) having the absorbance conversion and F(R) conversion. The data was collected in the wave length range of 200–1000 nm having the bandwidth of 1 nm.

Reactor operations

A standard bulk solution of Alizarin Yellow (40.0 mg/L) was prepared by direct weighing of dye. This solution was appropriately diluted to obtain the required experimental concentrations of Alizarin Yellow. Solution pH was maintained by drop-wise addition of conc. HCl/NaOH. The concentration effect in the degradation of dye was studied varying the Alizarin Yellow concentrations from 0.5 to 15.0 mg/L.

The reactor operations were conducted for the photolytic and photocatalytic degradation of Alizarin Yellow in the self-assembled

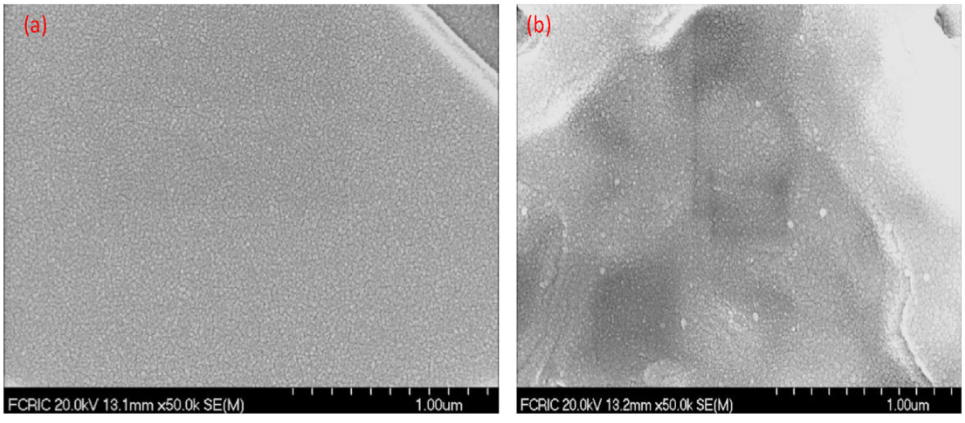

Fig. 1. SEM images of the nanocomposites (a) Au^0(NPs)/TiO_2 and Au^0(NPs)/TiO_2(T) thin films.

reactor. 50.0 mL solution of Alizarin Yellow was taken in a beaker and placed inside the black box. Further, cautiously, thin film disk (Au^0(NPs)/TiO_2 or Au^0(NPs)/TiO_2(T)) was placed horizontally inside the reactor. The UV-A light source was mounted about 10 cm above to the reactor vessel. This ensures the photocatalytic process to take place on the surface of photocatalysts. Reactor temperature was maintained to $25 \pm 1\,^{\circ}C$ by water-bath. The pH dependence degradation of Alizarin Yellow was conducted taking the Alizarin Yellow Solutions (1.0 mg/L) having pH values (4.0, 6.0, 8.0 and 10.0). In order to perform the kinetics of degradation, the sample of Alizarin Yellow solution was withdrawn from the reactor at definite but constant time intervals and dye concentration was analysed using the UV–vis Spectrophotometer. The photolytic operation was conducted by the UV-A irradiation only and the results were compared with the photocatalytic removal of Alizarin Yellow. The real matrix treatment was conducted employing the Tlwang river water. The Alizarin Yellow solutions (1.0 mg/L) were prepared having different pH values using the river water. The samples were treated using the photocatalyst thin film Au^0(NPs)/TiO_2(T). The percentage removal of Alizarin Yellow was obtained and compared with the distilled water samples removal.

Results and discussion

Characterization of nanocomposite thin films

SEM pictures of Au^0(NPs)/TiO_2 and Au^0(NPs)/TiO_2(T) nanocomposite coated disks are shown in Fig. 1. Fig. 1 illustrated that the small sized particles of titanium dioxide are uniformly dispersed on to substrate surface for both the samples. It is further noted that the titanium dioxide is forming a heterogeneous surface structures on the surface with no aggregation of titanium dioxide particles. The Au^0(NPs)/TiO_2(T) thin film showed some cracks on the surface. Moreover, the white reflections seen on the surface is, possibly, because of the Au^0(NPs) which are orderly distributed within the titania network. Moreover, the Au^0(NPs) are not aggregated or clustered to form bulk gold particles. Similar results shown elsewhere where gold nanoparticles are doped with TiO_2 nanotubes by two-step anodization process [53]. Moreover, the Au-nanoparticles having the size of 15–20 nm in diameter were obtained on the surface of TiO_2/Preyssler composite and the gold nanoparticles were well dispersed on the surface of the titania [36].

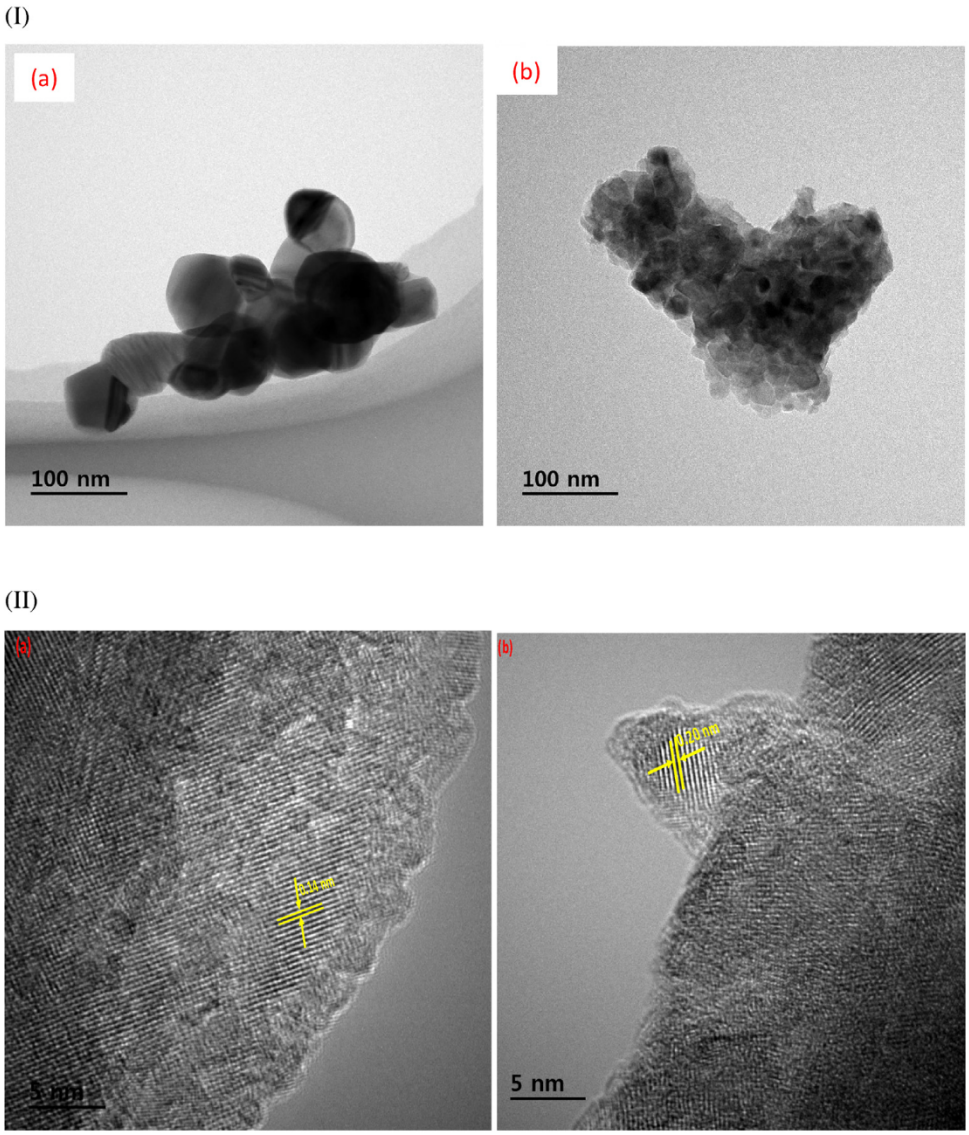

Fig. 2. TEM images of nanocomposite materials having different resolutions (a) Au^0(NPs)/TiO_2; and (b) Au^0(NPs)/TiO_2(T) [50].

TEM pictures of nanocomposite Au^0(NPs)/TiO_2 and Au^0(NPs)/TiO_2(T) materials were obtained and shown in Fig. 2(I & II). TEM images showed that Au-Nanoparticles are rather uniformly distributed within titanium dioxide network and particles were ranged within 20–25 nm (Fig. 2(I)). It is also observed that at places the Au (NPs) are clustered and forming relatively bigger sized particles in both the samples. Fairly a good heterogeneous and disordered structure was obtained. Further, the profile analysis of these solids indicated that the average interplanar distance of the Au-nanoparticles are found to be 0.14 nm and 0.20 nm for the solids Au^0(NPs)/TiO_2 and Au^0(NPs)/TiO_2(T), respectively. The other studies showed that Ti doped with MCSM-41 (silica) found a lattice distance 3.98 nm [54]. The other studies indicated that the 4-amino-3-hydrazino-5-mercapto-1, 2, 4-triazole (AHMT) was functionalized with gold nanoparticles (AuNPs) and the TEM images showed that nanoparticles of gold are well dispersed in the AHMT [55]. Further, the TEM-EDX elemental mapping was conducted and results were shown elsewhere [50]. It is evident from the figure that the Au(NPs) are intimately distributed with the titania network.

The 3D-AFM images of nanocomposite Au^0(NP)/TiO_2 and Au^0(NP)/TiO_2(T) coated disks are obtained and presented previously [50,51], however, it is worth to include the brief description. TiO_2 is forming relatively more disordered and heterogeneous surface structure with the Au^0(NP)/TiO_2(T) thin film sample compared to Au^0(NP)/TiO_2 thin film. This indicated that template synthesis of titanium dioxide provided an enhanced heterogeneity. Further, the titanium dioxide is pillared on the substrate surface. The pillar height is estimated to be 300 and 600 nm respectively for the nanocomposite Au^0(NP)/TiO_2, Au^0(NP)/TiO_2(T) coated disks. Similarly, root mean square roughness (Rq) and mean roughness (Ra) were found to be 7.314 nm and 1.333 nm (for Au^0(NP)/TiO_2); 124.330 nm and 94.659 nm (for Au^0(NP)/TiO_2(T)), respectively. This concludes that template process enabled to synthesize a good heterogeneous surface structure having with increased pillar height of TiO_2. However, the non-template titanium dioxide solid showed more smooth surface than the template synthesized titanium dioxide.

The XRD patterns of two nanomaterials *viz.*, Au^0(NPs)/TiO_2 and Au^0(NPs)/TiO_2 (T) were obtained and presented previously [50]. It is evident from the XRD patterns that the TiO_2 in both the samples possessed predominantly the amorphous mineral phase. However, a distorted peak at the 2θ value of 25.27 is due to the anatase mineral phase of TiO_2 [56]. The materials are annealed at moderate temperature hence, it was devoid with crystallinity. However, the powder sample was annealed at 800 °C and the results are shown in Fig. 3. The TiO_2 annealed at this temperature, showed a good crystalline structure however, it is predominantly converted in to rutile phase. In order to reveal the silver nanoparticles, the intensity was further resolved using the Au^0(NPs)/TiO_2 nanocomposite and interesting to note that (Fig. 3 (Inset)), a clear reflections are observed at the 2θ values of 39.27, 44.25, 64.29 which are characteristic diffraction peaks of the gold nanoparticles [57].

Further, the spectral analysis based on the diffuse reflectance spectroscopy was conducted to estimate the band gap of these solids. The Kubelka Munk theory as elaborated by the Tauc mathematical equation was utilized in deducing the band gap energy [58]. The band gap energies were found to be 3.12, 2.86 and 2.87 eV respectively for the bare TiO_2(T) Au^0(NPs)/TiO_2 and Au^0(NPs)/TiO_2(T) solids. The silver nanoparticles doping greatly decreases the band gap energy of these solids. Similar results were obtained in the copper chromite nanostructured material prepared hydrothermally and shown the Eg value 3.38 eV [59]. On the other

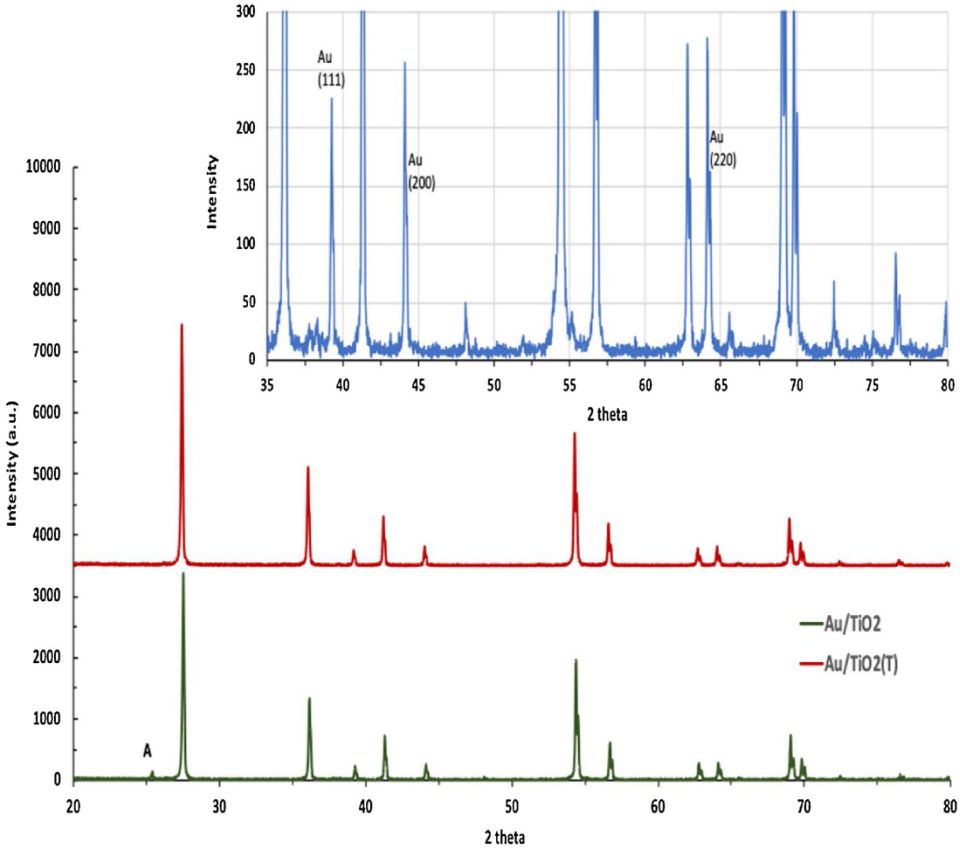

Fig. 3. X-ray diffraction pattern of nanocomposite Au^0(NPs)/TiO_2 and Au^0(NPs)/TiO_2(T) materials annealed at 800 °C.

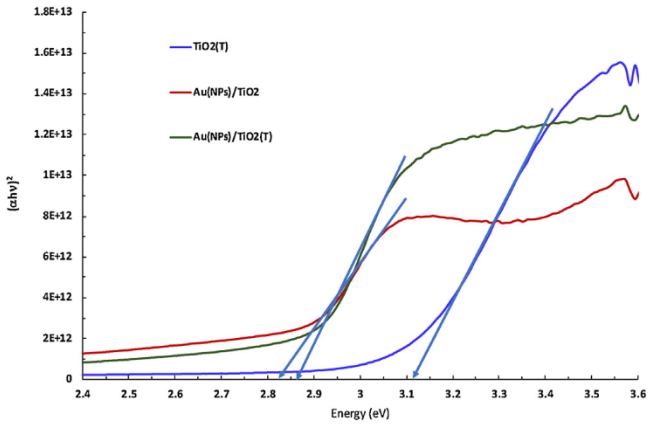

Fig. 4. Plots between hν (Energy) *vs* $(\alpha h\nu)^2$ for the bare TiO_2, $Au^0(NPs)/TiO_2(A)$ and $Au^0(NPs)/TiO_2(B)$ solids.

hand the Nanostructured $Nd_2Sn_2O_7$ was obtained using the pomegranate juice at low temperature. The solid showed the band gap of 2.8 eV and was efficiently employed as visible light driven photocatalyst [60] (Fig. 4).

Reactor operations

pH dependence removal

The solution pH is an important parameter that affects greatly the removal of Alizarin Yellow from aqueous solutions since the physico-chemical properties of dye and catalyst both are changed significantly with the variation of pH [61,62]. Moreover, the photo induced radicals generated also showed varied reactivity with the change in pH [63]. Therefore, to demonstrate the insight of degradation mechanism of Alizarin Yellow, a systematic study was carried out varying the solution pH from 4.0 to 10.0. The percentage removal of Alizarin Yellow as a function of solution pH is obtained and illustrated in Fig. 5 (Secondary axis). The concentration of Alizarin Yellow is taken 1.0 mg/L and the UV-A illumination was given 2 h. Fig. 5 shows that photocatalytic removal of Alizarin Yellow was increased by increase in pH from 4.0 6.0 however; further increase in pH *i.e.*, pH 6.0 to 10.0 had caused to decrease the percentage degradation of Alizarin Yellow. Moreover, the percentage of Alizarin Yellow removal was increased from 53.12 to 59.38% with increase in pH from 4.0 to 6.0 employing the nanocomposite $Au^0(NPs)/TiO_2(T)$ thin film. However, further increase in pH 6.0–10.0 had suppressed the removal efficiency of Alizarin Yellow from 59.38 to 40.63%, respectively. A similar removal trend was obtained for the photocatalyst $Au^0(NPs)/TiO_2$ thin film.

The pH dependence removal of Alizarin Yellow using the nanocomposite photocatalysts could be, explicitly, demonstrated by the speciation studies of Alizarin Yellow and the surface behaviour of nanocomposite in aqueous solutions at varied pH conditions. Hence, a systematic speciation studies of Alizarin Yellow was conducted separately at wide range of pH *i.e.*, pH 2.0–10.0. Alizarin Yellow molecule that contains invariably two dissociable hydrogens (*i.e.*, attached with the phenolic and carboxylic groups (*cf* Scheme 1)). The values of pk_a^1 and pk_a^2 were reported to be 5.0 and 11.0, respectively [64]. Therefore, the speciation studies indicated that the mono-anionic species of Alizarin Yellow is dominantly present within the pH region 6.0–10.0 (*cf* Fig. 5 (Primary axis)). However, it the mono-ionic species exists in equilibrium with the non-ionic species as resulted with the hydrogen bonding between the two phenolic and carboxylic oxygen atoms (*cf* Scheme 1) [64]. Further increase in pH > 10.0, due to the dissociation of the phenolic hydrogen, the Alizarin Yellow turned to di-anionic species that eventually carried net negative charge density. On the other hand, titanium dioxide possessed point of zero charge pH_{PZC} 5.9 [65]. This suggests, titanium dioxide possessed net positive charge density at pH < 5.9 which turns to negatively charged at pH > 5.9. Therefore, it is evident that at higher pH conditions (pH 6–10) both the nanocomposite and Alizarin Yellow are carrying the net negative charges which causes to repel each other. Hence, this greatly hinders the electrostatic attraction of Alizarin Yellow by the nanocomposite materials. Therefore, this restricted the sorption of Alizarin Yellow by the surface active sites of nanocomposites or even it restricted the sorbing species to enter within the Stern plane to enable it for a chemisorption of Alizarin Yellow at the solid surface. This led to a mark decrease in removal of Alizarin Yellow at high pH values. Moreover, relatively high percentage removal of Alizarin Yellow at pH 6.0 is explicable by the fact that at this pH the anionic species of Alizarin Yellow is seemingly attracted by the positively charged surface of nanocomposite which enabled an

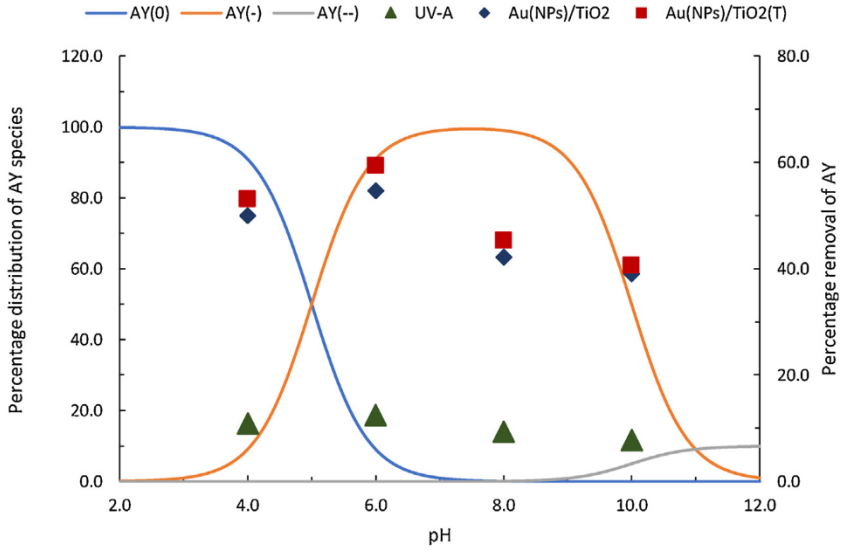

Fig. 5. Percentage distribution of Alizarin Yellow species as a function of pH (Smooth Line) and percentage removal of Alizarin Yellow at various pH values (Scattered Points) for catalytic and photolytic treatments [Initial concentration of Alizarin Yellow: 1.0 mg/L].

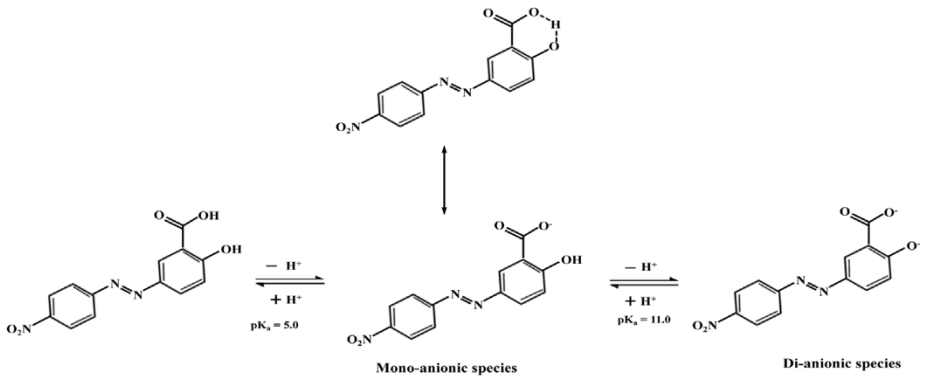

Scheme 1. pH dependence dissociation of Alizarin Yellow in aqueous solution.

enhanced sorption of Alizarin Yellow species on to the surface of catalyst and hence; undergo with an enhanced catalytic degradation of Alizarin Yellow. A similar very high sorptive removal of several anionic dyes was recorded at pH *Ca* 5 which was significantly decreased at pH 10.0 using the isorecticular nanoporous Zn(II)-MOFs (metal oxide framework) known as TMU-16 and TMU-16-NH_2 [66]. The enhanced removal of Alizarin Yellow at pH 6.0 was also supported with the fact that the hydroxyl ions were readily oxidized to the $^{\bullet}OH$ at the catalyst surface and are found to be predominant and stable at the neutral pH conditions [67] which further synergised the removal of Alizarin Yellow. However, the photocatalytic degradation of Congo red was decreased by increasing the pH from 3.0 to 10.0 whereas the dye Bismarck brown removal was increased by increasing the similar pH *i.e.*, 3.0 to 10.0 using the Ag/reduced graphene oxide nanocomposite [68].

However, at lower pH conditions the percentage removal of Alizarin Yellow is obtained relatively less. This is due to the reason that the Alizarin Yellow species are predominantly present to its un-dissociated species and the surface of nanocomposite also contained with high positive charge density. Therefore, relatively less sorption of Alizarin Yellow is occurred onto the solid surface which caused to decrease in percentage removal of Alizarin Yellow. Moreover, at low pH conditions the hydroxyl species are also readily reduced as associated with the H^+ ions which then suppressed the $^{\bullet}OH$ induced degradation of Alizarin Yellow Eq. (1) [69,70,44,45].

$$^{\bullet}OH + H^+ + e^- \rightarrow H_2O \quad (1)$$

Similar degradation trend was shown for the oxidative removal of Alizarin Yellow by the nanopillar-TiO_2 using the UV irradiation [71]. Relatively high percentage removal of Alizarin Red S is obtained at pH 7.0 using the biomimetic peroxidase-like photocatalyst 5,10,15,20-tetrakis(4-sulfonatophenyl)porphine–Mn(III) [63].

Fig. 5 further indicated that the percentage efficiency of Alizarin Yellow is markedly higher using the nanocomposite Au^0(NP)/TiO_2 or Au^0(NPs)/TiO_2(T) photocatalysts than the corresponding blank process using UV-A illumination. Therefore, it again demonstrated that nanocomposite thin films possesses an enhanced catalytic activity, at least, in the degradation of Alizarin Yellow in aqueous media. Moreover, the template synthesized photocatalyst Au^0(NPs)/TiO_2(T) showed relatively higher removal efficiency of Alizarin Yellow than the non-template nanocomposite Au^0(NPs)/TiO_2. This indicates that templated synthesized TiO_2 with *in situ* impregnation of Au-nanoparticles resulted a dense titania network which showed an enhanced photocatalytic efficiency.

Change in Alizarin Yellow concentration

Alizarin Yellow dye concentration is varied from 0.5 mg/L to 15.0 mg/L at pH 6.0. The Alizarin Yellow solution was irradiated for a period of 2 h. Further, the degradation efficiency of Alizarin Yellow with reference to dye concentration was obtained and illustrated in Fig. 6. Fig. 6 shows that increasing the concentration of Alizarin Yellow had suppressed significantly the percentage removal of Alizarin Yellow for both photolytic and photocatalytic treatment. Quantitatively, the percentage efficiency of Alizarin Yellow was decreased from 71.88 to 24.27% increasing the pollutant concentration from 0.5 mg/L to 15.0 mg/L, respectively using the nanocomposite Au^0(NPs)/TiO_2(T) catalyst. This decrease in degradation efficiency of Alizarin Yellow at increased dye

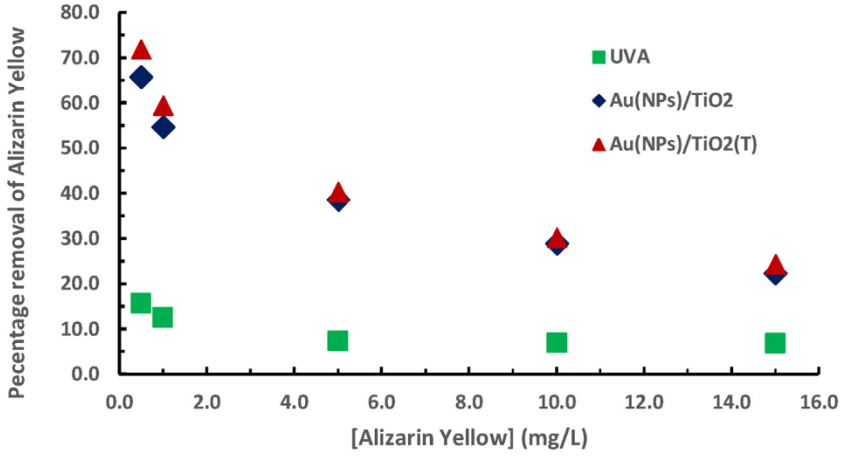

Fig. 6. Removal efficiency of Alizarin Yellow at different concentrations of Alizarin Yellow for photolytic and photocatalytic operations [pH: 6.0].

concentration is due to the reason; at higher concentration of dye molecules have relatively less contact possibilities to the catalyst surface. Previous study indicated that increasing the pollutant concentration causing to scavenge the surface active sites which suppressed significantly the removal efficiency [72,73]. A similar decolourization rate (%) was observed in the removal of Acid Brilliant Scarlet GR using the bio-AuNPs (bio: strain *Trichoderma sp.* WL-Go) [74]. The other study showed a similar decrease in percentage removal of Reactive Red 180-RR180 in a hybrid process contained with UV + ZnO + HC (HC: hydrodynamic). It was further demonstrated that the content of free radicals that take part in decomposing the organic molecules are constant however; the pollutant molecules are increased significantly at higher initial concentration this eventually reduced the percent degradation of dye at higher initial concentration of dye [16].

Kinetic studies

Kinetics of dye removal under the photolytic or photocatalytic treatments are conducted using the time dependence data. The rate of degradation enables eventually the overall efficiency of catalyst. The rate of degradation of Alizarin Yellow was presented by pseudo-first order rate equation Eq. (2):

$$r = -\frac{d[Dye]}{dt} = k_{app}\ [k_{photolysis} + k_{photocatalysis}][Dye] = k_{app}\ [Dye] \quad (2)$$

where [Dye] is used for the concentration of Alizarin Yellow and k_{app} is the pseudo-first-order rate constant. The above Eq. (2) is simplified to Eq. (3):

$$ln\left(\frac{C_0}{C_t}\right) = k_{app} \cdot t \quad (3)$$

where C_0 and C_t are the concentration of Alizarin Yellow at t = 0 and at time 't'. Therefore, plots were obtained between $\ln(C_0/C_t)$ vs the time `t` and shown in Fig. 8 (Insets) (Initial concentration of Alizarin Yellow: 1.0 mg/L at pH: 6.0). The k_{app} values were calculated for all the studied concentrations and presented in Fig. 7. A decrease in Alizarin Yellow concentration greatly enhanced the k_{app} values. Further, interesting to observe that the k_{app} value for the catalytic removal of Alizarin Yellow was found readily higher than photolytic process carried out in UV-A light only. This further confirms the greater applicability of catalyst in the oxidative removal of Alizarin Yellow. The other studies showed that the removal of methylene blue using P25 titanium dioxide catalyst followed pseudo-first-order kinetics [75]. Similarly, the degradation of several dyes *viz.*, amaranth, sunset yellow and tartrazine in the photocatalytic processes using the catalysts TPt, TPt-GO and TPt-rGO catalysts (T: Titanium, Pt: Platinum Nnao-particles; GO: Graphene oxide; and rGO: reduced graphene oxide) are followed pseudo-first order rate law. It was further indicated that rate constant values were significantly increased for the

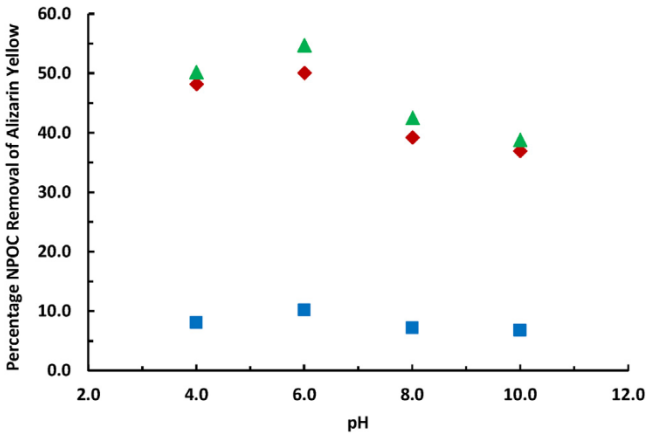

Fig. 8. Perecntange removal of NPOC of Alizarin Yellow at different pH values for photolytic and photocatalytic processes ([Alizarin Yellow]: 1.0 mg/L).

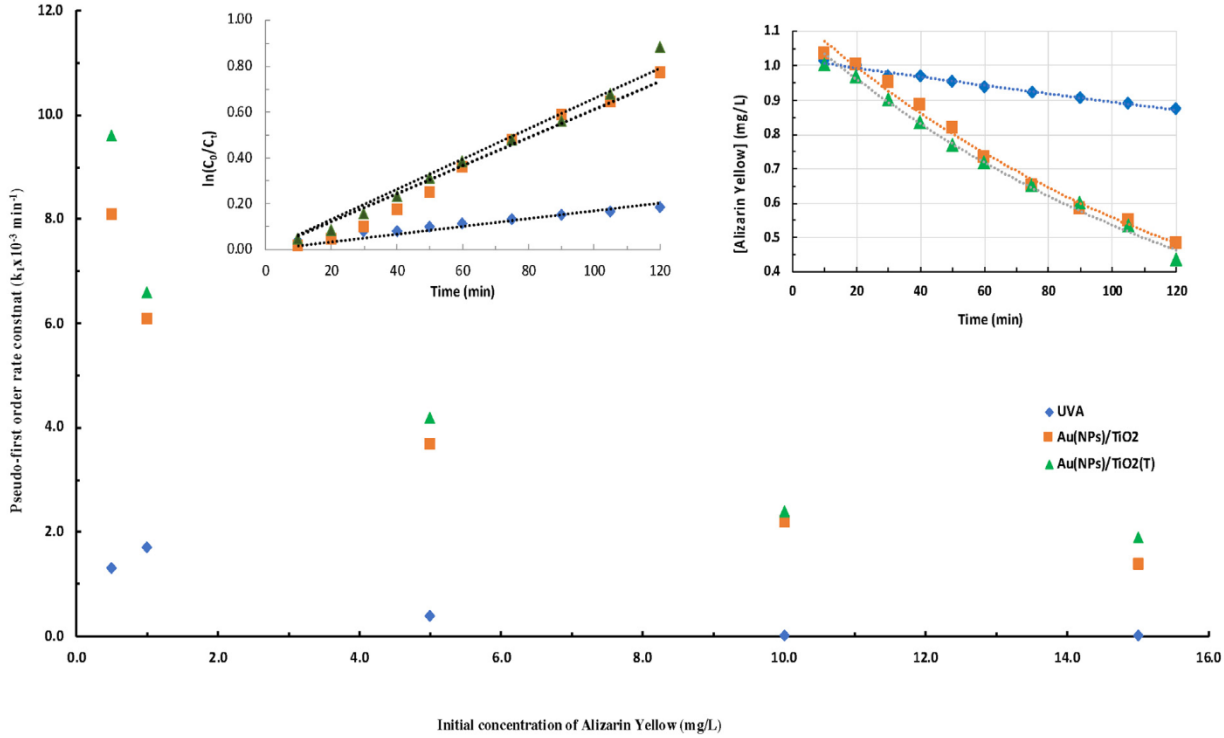

Fig. 7. The pseudo-first order rate constant values for various concentrations of Alizarin Yellow for photolytic and photocatalytic operations [Inset: Linear and Non-linear fitting of time dependence results for the pseudo-first order rate kinetics; Initial concentration of Alizarin Yellow: 1.0 mg/L and pH:6.0].

photocatalyzed processes compared to the photolytic processes [12].

Further, the photocatalytic degradation of Alizarin Yellow was modelled with the Langmuir–Hinshelwood (L–H) isotherm at varied concentrations of Alizarin Yellow to its linear form [76]. The L–H adsorption constant 'K' (L/mg) and the rate constant 'k_r' (mg/L/min) values are found to be 0.362 and 0.026 (R^2: 0.987; for nanocomposite Au^0(NPs)/TiO_2); 0.372 and 0.029 (R^2: 0.968; for nanocomposite Au^0(NPs)/TiO_2(T)) thin films, respectively.

NPOC removal of Alizarin Yellow

Further, percent mineralization of dye in the degradation process is an important aspect of this study. Hence, NPOC results were obtained for treated and untreated Alizarin Yellow samples. The percentage of NPOC removal was shown at varied pH (*cf* Fig. 8). The Alizarin Yellow concentration was taken 1.0 mg/L and the solution was illuminated for a period of 2 h. Fig. 8 clearly indicated that initially the percentage of NPOC removal was increased with increase in pH 4.0–6.0. However, further increase in pH from 6.0 to 10.0, the removal efficiency of NPOC was suppressed to a greater extent. Moreover, NPOC removal was increased from 50.26 to 54.73% with the increase in pH from 4.0 to 6.0 using nanocomposite Au^0(NPs)/TiO_2(T) photocatalyst. However, further increase in pH from 6.0 to 10.0 had caused to decrease the mineralization of Alizarin Yellow from 54.73% to 38.89%, respectively using the Au^0(NPs)/TiO_2(T) photocatalyst. Similar trend was observed for the other photocatalyst Au^0(NPs)/TiO_2. The percent mineralization of Alizarin Yellow was found relatively high using the template synthesized nanocomposite Ag^0(NPs)/TiO_2(T) compared to the non-template synthesized material Ag^0(NPs)/TiO_2. This again showed the greater utility of template synthesized material. On the other hand, the photolysis process showed insignificant percentage removal of NPOC (*cf* Fig. 8). Overall, it was noted that a single photocatalytic operation could enable to mineralize a significant percentage of Alizarin Yellow in aqueous solutions.

Stability of thin film catalyst

Stability of nanocomposite coated disk is important for prolonged and continued use of catalyst in wastewater treatment plants. Nevertheless, it demonstrates the long term use of catalyst. Threfore, the nanocomposite Au^0(NPs)/TiO_2(T) thin film was intended to employ in the six cycle of operations using the same disk. The results of six operations are shown in Fig. 9. The initial conecntration of Alizarin Yellow was used 5.0 mg/L at pH 6.0. The disk was cleaned with purified water at the end of each reactor operation. After washing of disk it was dried at 105 °C in drying oven. The dried disk was again employed for the next cycle of treatment. Fig. 9 clearly showed that even after six cycles of treatmnet the Nanocomposite Ag^0(NPs)/TiO_2(T) thin film possessed fairly high stability since the degradation efficiency of Alizarin Yellow was not affected significantly. Quantitatively, at the end of sixth repeated operation, the percentage degrdation of Alizarin Yellow was decreased from 38.58% to 37.30% only (*i.e.*, a decrease of 1.28%) or otherwise the C_0/C_t value was increased from 0.614 to 0.640. This indicated that the nanocomposite thin film is fairly stable at least for the long term photocatalytic implication. These studies further demonstrated the applicability of nanocomposite coated disk for efficient and prolonged treatment of wastewater. However, the use of TiO_2 catalyst powder for repeated operations showed marked decrease in catalytic efficiency. This was due to the aggregation of dye particles around the TiO_2 particles which substancially caused to decrease the efficiency of catalyst [77]. Similarly, the use of Ag/rGO nanocomposite photocatalyst showed *Ca* 10% decrease in the removal efficiency of azo dyes *viz.*, Congo red and Bismarck brown for repeated use [68]. However, use of nanocomposite thin film could enable to provide a prolonged catalytic operations. Similar stability was reported previously using the catalyst 6 wt% MWCNT/Au–TiO_2 in oxidative removal of cyanide for 5 repeated operations [78] or the molecular oxygen activation using the boron nitride quantum dots decorated ultrathin porous graphitic carbon nitride (g-C_3N_4) [79]. Further, the SEM images and the XRD data was collected for the six cycles used Ag^0(NPs)/TiO_2(T) thin film. The results are shown in Supplementary Figures S1 and S2 respectively for SEM image and XRD patterns. Figure clearly revealed that the surface structure of the nanocomposite Ag^0(NPs)/TiO_2(T) thin film was slightly changed and in addition to the fine grains of the TiO_2 the aggregated particles are visible. This is, perhaps, because of the presence of the pollutant particles on the TiO_2 surface. On the other hand, the XRD

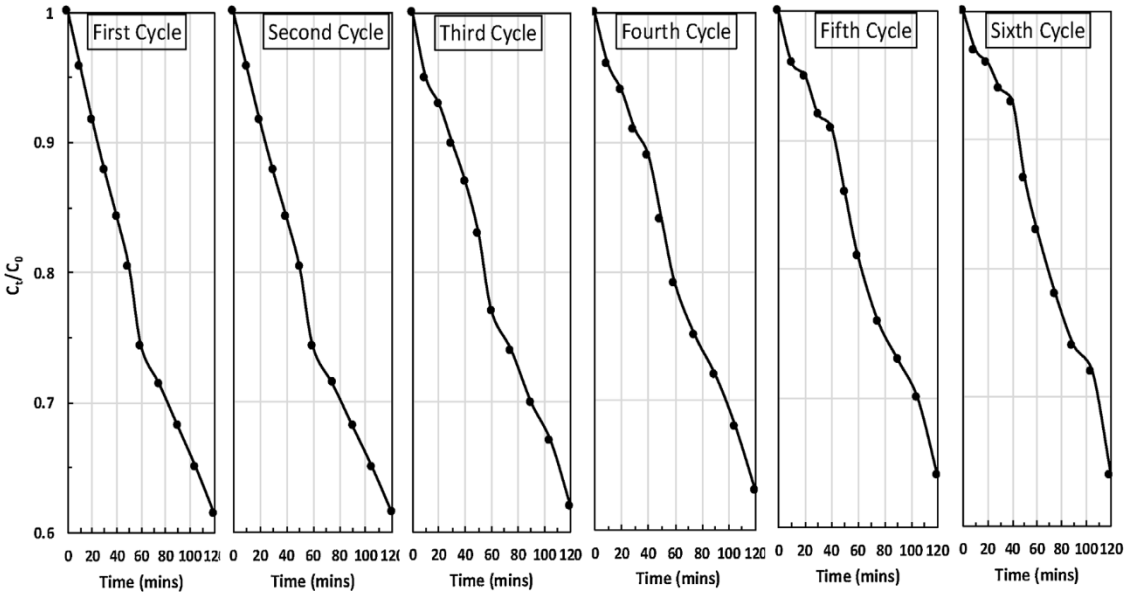

Fig. 9. Repeated cycle of photocatalytic operations using the Au^0(NPs)/TiO_2(T) nanocomposite thin film for the degradation of Alizarin Yellow ([Alizarin Yellow]: 5.0 mg/L; pH: 6.0).

pattern of the thin film showed similar amporphous nature of solid contained with chracteristic peak of anatase phase of TiO_2 which is very distortly observed at the 2θ of 25.27. These results further, evidenced the stability of thin films to be employed for successive reator operations.

Real matrix treatment

The study was further intended to implement for the real water samples. The water from the local river Tlawng was collected. The water sample was analysed for various physico/chemical parameters and reported elsewhere [52]. The analytical results indicated that the water is having relatively high concentrations of Ca, Zn and Fe along with high value of inorganic carbon and some NPOC. The solutions of Alizarin Yellow were prepared in this water having different concentrations at constant pH 6.0. The photocatalytic treatment of Alizarin Yellow was conducted using the Au^0(NPs)/TiO_2(T) catalyst. The total duration of UV-A irradiation was kept constant to 2.0 h. The percentage removal of Alizarin Yellow was obtained and compared with the purified water removal (*Cf* Fig. 10). It is indeed to observe that the removal of Alizarin Yellow was not significantly affected even in river water samples which pointed greater applicability of catalyst in the degradation of Alizarin Yellow.

Degradation mechanism

The radical scavengers *viz.*, 2-propanol or HCO_3^- are known to scavenge the $^{\bullet}OH$ radicals [80,81]. Similarly, the EDTA inhibits significantly the formation of hole in titanium dioxide [82]. Sodium azide (NaN_3) suppresses singlet oxygen which is generated with combining the superoxide radical and photo generated h^+ [83]. Therefore, photocatalytic removal of Alizarin Yellow was studied in presence of these scavengers each having 1000 mg/L employing the nanocomposite Ag^0(NPs)/TiO_2(T) coated disk. Percentage removal of Alizarin Yellow is illustrated in Fig. 11. Figure indicated that the presence of these scavengers affected significantly the percentage removal of Alizarin Yellow. Among these scavengers, EDTA and NaN_3 suppressed significantly the degradation of Alizarin Yellow. These results, therefore, inferred that the holes were involved in generating the $^{\bullet}OH$ radicals that caused to oxidize the Alizarin Yellow. Similarly, the singlet oxygen is partly taking part in the degradation pathway. Additionally, the decrease in percentage removal of Alizarin Yellow in presence of 2-propanol or HCO_3^- indicated the direct involvement of $^{\bullet}OH$ radical in the degradation of Alizarin Yellow.

Therefore, photocatalytic removal of Alizarin Yellow by nanocomposite Au^0(NPs)/TiO_2(T) thin film is to be proposed in possible

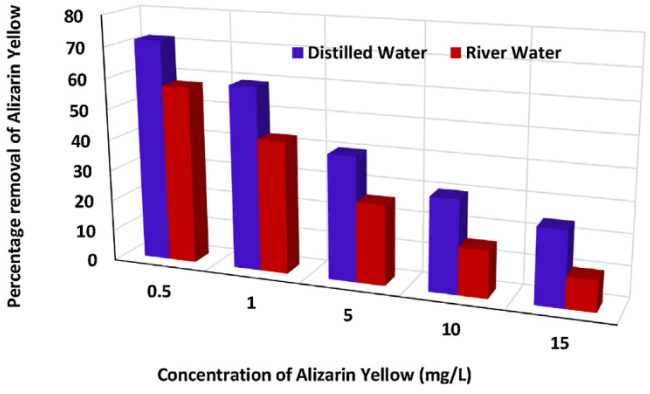

Fig. 10. Comparison of photocatalytic degradation of Alizarin Yellow in distilled water and Tlwang river water using the Ag^0(NPs)/TiO_2(T) thin film catalyst [pH: 6.0 and irradiation time: 2 h].

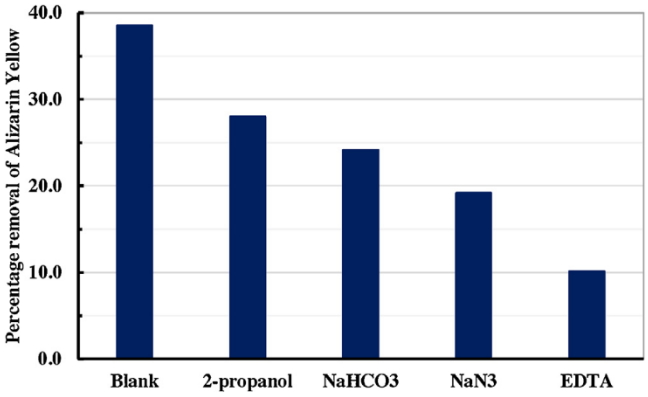

Fig. 11. Photocatalytic degradation of Alizarin Yellow in presence of several scavengers using the nanocomposite Au^0(NPs)/TiO_2(T) thin film.

two different mechanistic pathways. The UV-A (λ = 360 nm) photons excites the electrons from valance band to conduction band in titanium dioxide. The Au(NPs) traps the excited electron around conduction band. Then, this restricts the possibility of recombination of e^-/h^+ in TiO_2. Electron that trapped undergoes to form superoxide radical and hence the generation of $^{\bullet}OH$. On the other hand, h^+ which is formed in the valance band, combined with the O_2 and generates the $O_2^{\bullet}$. This again produces the $^{\bullet}OH$. Therefore, the reactive $^{\bullet}OH$ radicals are, perhaps, involved in the degradation of Alizarin Yellow. Moreover, the Au^0(NPs) absorbs photons energy in the UV-A region that generates local electromagnetic field. This causes local excitation of electrons in semiconductor titanium dioxide and hence, the formation of e^-/h^+ pairs. This further generates hydroxyl radicals and simultaneously involved in the oxidative degradation of Alizarin Yellow.

Conclusion

A newer facile synthesis was adopted to obtain the plasmonic nanocomposite Au^0(NPs)/TiO_2 materials. The *in situ* impregnation of Au^0-Nanoparticles with the titania network was proceeded by template process and polyethylene glycol was employed as filler media. X-ray pattern showed that both the solids Au^0(NPs)/TiO_2 (non-template) and Au^0(NPs)/TiO_2(T) (template) possessed predominantly the amorphous in nature. However, the annealed powder at 800 °C showed a good crystalline structure and diffraction peaks of Au(NPs) are occurred. The SEM images indicated that the TiO_2 grains were distributed uniformly onto the borosilicate substrate surface. TEM images showed that Au(NPs) are spatially distributed within titanium dioxide network having the sizes of 20–25 nm. The average interplanar distance of the Au(NPs) were found to be 0.14 nm and 0.20 nm for the solids Au^0(NPs)/TiO_2 and Au^0(NPs)/TiO_2(T), respectively. AFM images of these nanocomposite thin films showed that titanium dioxide was pillared onto the substrate and forming very hetrerogeneous surface structure. Au(0)(NPs) doping with TiO_2 caused to decrease the band gap energies from 3.12 eV to 2.86 and 2.87 eV respectively for the Au^0(NPs)/TiO_2 and Au^0(NPs)/TiO_2(T) solids. The photocatalytic degradation of Alizarin Yellow was favored at pH 6.0 and at lower concentration of Alizarin Yellow. Pseudo-first order rate law was followed the degrdation and pseudo-first order rate constnts were increased with a decrease in Alizarin Yellow concentration 15.0 to 0.5 mg/L. The proposed treatment was enabled to mineralize the significant amount of Alizarin Yellow. Additionally, the scavengers studies inferred that $^{\bullet}OH$ radicals were greatly took part in the degradation of AlizarinYellow. The thin film photocatalyst was found to be fairly stable for successive photocatalytic operations since the catalytic efficiency of catalyst was not affected in the repeated operations.

Moreover, the real matrix treatment of Alizarin Yellow using the Tlwang river water indicated that no significant change in removal efficiency was occurred compred to the purified water treatment. The study showed that the template synthesized photocatalyst Au^0(NPs)/TiO_2(T) possessed relatively higher removal efficiency than non-template synthesized nanocomposite Au^0(NPs)/TiO_2 thin film. The Nanocomposite thin film materials therefore; showed potential applicability in a large scale treatment of waste waters contaminated with Alizarin Yellow.

Acknowledgement

"This research was supported by Basic Science Research Program through the National Research Foundation of Korea (NRF) funded by the Ministry of Education (NRF-2019R1I1A3A01062424)".

Appendix A. Supplementary data

Supplementary material related to this article can be found, in the online version, at doi:https://doi.org/10.1016/j.jiec.2019.10.008.

References

[1] Decolorization of a dye industry effluent by Aspergillus fumigatus XC6 | SpringerLink, (n.d.). https://link.springer.com/article/10.1007%2Fs00253-006-0658-1.
[2] H. Safajou, H. Khojasteh, M. Salavati-Niasari, S. Mortazavi-Derazkola, J. Colloid Interf. Sci. 498 (2017) 423.
[3] A. Sadeghzadeh-Attar, Solar Energy Mater. Solar Cells 183 (2018) 16.
[4] S. Kakarndee, S. Nanan, J. Environ. Chem. Eng. 6 (2018) 74.
[5] K.-W. Jung, B.H. Choi, C.M. Dao, Y.J. Lee, J.-W. Choi, K.-H. Ahn, S.-H. Lee, J. Ind. Eng. Chem. 59 (2018) 149.
[6] K.-W. Jung, B.H. Choi, M.-J. Hwang, T.-U. Jeong, K.-H. Ahn, Bioresour. Technol. 219 (2016) 185.
[7] R.O. Alves de Lima, A.P. Bazo, D.M.F. Salvadori, C.M. Rech, D. de Palma Oliveira, G. de Aragão Umbuzeiro, Mutat. Res. Toxicol. Environ. Mutagen. 626 (2007) 53.
[8] K.L. Hatch, H.I. Maibach, J. Am. Acad. Dermatol. 32 (1995) 631.
[9] M.T. Yagub, T.K. Sen, S. Afroze, H.M. Ang, Adv. Colloid Interface Sci. 209 (2014) 172.
[10] C.-C. Su, M. Pukdee-Asa, C. Ratanatamskul, M.-C. Lu, Desalination 278 (2011) 211.
[11] N. Muhd Julkapli, S. Bagheri, S. Bee Abd Hamid, Sci. World J. 2014 (2014).
[12] M.-C. Rosu, M. Coros, F. Pogacean, L. Magerusan, C. Socaci, A. Turza, S. Pruneanu, Solid State Sci. 70 (2017) 13.
[13] K.B. Tan, M. Vakili, B.A. Horri, P.E. Poh, A.Z. Abdullah, B. Salamatinia, Sep. Purif. Technol. 150 (2015) 229.
[14] A.B. dos Santos, F.J. Cervantes, J.B. van Lier, Bioresour. Technol. 98 (2007) 2369.
[15] C.R. Holkar, A.J. Jadhav, D.V. Pinjari, N.M. Mahamuni, A.B. Pandit, J. Environ. Manage. 182 (2016) 351.
[16] Y. Çalışkan, H.C. Yatmaz, N. Bektaş, Process Saf. Environ. Prot. 111 (2017) 428.
[17] Y. Sha, I. Mathew, Q. Cui, M. Clay, F. Gao, X.J. Zhang, Z. Gu, Chemosphere 144 (2016) 1530.
[18] G. Li, Y. Li, Z. Wang, H. Liu, Mater. Chem. Phys. 187 (2017) 133.
[19] B. Subash, B. Krishnakumar, A.J.F.N. Sobral, C. Surya, N.A.A. John, A. Senthilraja, M. Swaminathan, M. Shanthi, Sep. Purif. Technol. 164 (2016) 170.
[20] Y.-Z. Wang, A.-J. Wang, W.-Z. Liu, Q. Sun, Bioresour. Technol. 142 (2013) 688.
[21] Y. Pan, Y. Wang, A. Zhou, A. Wang, Z. Wu, L. Lv, X. Li, K. Zhang, T. Zhu, Chem. Eng. J. 326 (2017) 454.
[22] Sahar Zinatloo-Ajabshir, Maryam Sadat Morassaei, Masoud Salavati- Niasari, J. Colloid Interf. Sci. 497 (2017) 298.
[23] S. Zinatloo-Ajabshir, M. Salavati-Niasari, J. Mol. Liq. 216 (2016) 545.
[24] H. Yi, M. Yan, D. Huang, G. Zeng, C. Lai, M. Li, X. Huo, L. Qin, S. Liu, X. Liu, B. Li, H. Wang, M. Shen, Y. Fu, X. Guo, Appl. Cat. B: Environ. 250 (2019) 52.
[25] H. Yi, M. Jiang, D. Huang, G. Zeng, C. Lai, L. Qin, C. Zhou, B. Li, X. Liu, M. Cheng, W. Xue, P. Xu, Chen Zhang, J. Taiwan Inst. Chem. Eng. 93 (2018) 184.
[26] Y. Liao, C. Xie, Y. Liu, H. Chen, H. Li, J. Wu, Ceram. Int. 38 (2012) 4437.
[27] H. Yi, D. Huang, L. Qin, G. Zeng, C. Lai, M. Cheng, S. Ye, B. Song, X. Ren, X. Guo, Appl. Cat. B: Environ. 239 (2018) 408.
[28] H. Yi, L. Qin, D. Huang, G. Zeng, C. Lai, X. Liu, B. Li, H. Wang, C. Zhou, F. Huang, S. Liu, X. Guo, Chem. Eng, J. 358 (2019) 480.
[29] M. Mousavi, A. Habibi-Yangjeh, S.R. Pouran, J Mater Sci: Mater. Electron. 29 (2018) 1719.
[30] M. Shakofteh-Gohari, A. Habibi-Yangjeh, M. Abitorabi, A. Rouhi, Cri. Rev. Environ. Sci. Technol. 48 (2018) 806.
[31] K. Hashimoto, H. Irie, A. Fujishima, Jpn. J. Appl. Phys. 44 (2005) 8269.
[32] S.G. Kumar, L.G. Devi, J. Phys. Chem. A. 115 (2011) 13211.
[33] H. Tada, T. Kiyonaga, S. Naya, Chem. Soc. Rev. 38 (2009) 1849.
[34] S. Feizpoor, A. Habibi-Yangjeh, Mater. Res. Bull. 99 (2018) 93.
[35] E. Abroshan, S. Farhadi, A. Zabardasti, Solar Energy Mater. Solar Cells 178 (2018) 154.
[36] A. Ayati, A. Ahmadpour, F.F. Bamoharram, B. Tanhaei, M. Mänttäri, M. Lahtinen, M. Sillanpää, Sep. Purif. Technol. 133 (2014) 415.
[37] M.A. Debeila, M.C. Raphulu, E. Mokoena, M. Avalos, V. Petranovskii, N.J. Coville, M.S. Scurrell, Mater. Sci. Eng. A. 396 (2005) 70.
[38] M. Ihara, K. Tanaka, K. Sakaki, I. Honma, K. Yamada, J. Phys. Chem. B. 101 (1997) 5153.
[39] M.K. Seery, R. George, P. Floris, S.C. Pillai, J. Photochem. Photobiol. Chem. 189 (2007) 258.
[40] M.A. El-Sayed, Acc. Chem. Res. 34 (2001) 257.
[41] S. Feizpoor, A. Habibi-Yangjeh, J. Colloid Interf. Sci. 524 (2018) 325.
[42] S. Zinatloo-Ajabshira, M. Salavati-Niasari, New J. Chem. 39 (2015) 3948.
[43] S. Zinatloo-Ajabshir, M. Salavati-Niasari, M. Hamadanian, RSC Adv. 5 (2015) 33792.
[44] S. Feizpoor, A. Habibi-Yangjeh, K. Yubuta, J. Photochem. Photobiol. A: Chem. 367 (2018) 94.
[45] M. Salavati-Niasari, F. Soofivand, A. Sobhani-Nasab, M. Shakouri-Arani, A. Yeganeh Faal, S. Bagheri, Adv. Powd. Technol. 27 (2016) 2066.
[46] M. Salavati-Niasari, F. Davar, M. Mazaheri, J. Alloys Compd. 470 (2009) 502.
[47] G. Kianpour, M. Salavati-Niasari, H. Emadi, Ultrasonics Sonochem. 20 (2013) 418.
[48] Y. Ye, Z. Zang, T. Zhou, F. Dong, S. Lu, X. Tang, W. Wei, Y. Zhang, J. Cat. 357 (2018) 100.
[49] M. Maham, M. Nasrollahzadeh, S.M. Sajadi, M. Nekoei, J. Colloid Interface Sci. 497 (2017) 33.
[50] A. Tiwari, A. Shukla, Lalliansanga, D. Tiwari, S.-M. Lee, J. Ind. Eng. Chem. 69 (2019) 141.
[51] A. Lalliansanga, A. Tiwari, D. Shukla, Tiwari, S.M. Lee, Environ. Sci. Pollut. Res. 25 (2018) 20125.
[52] J. Lalmalsawmi, D. Zirlianngura, Tiwari, S.-M. Lee, Environ. Eng. Res. (2019) Paper Accepted.
[53] S. Noothongkaew, J.K. Han, Y.B. Lee, O. Thumthan, K.-S. An, Prog. Nat. Sci. Mater. Int. 27 (2017) 641.
[54] K. Zhou, X.-D. Xie, C.-T. Chang, Appl. Surf. Sci. 416 (2017) 248.
[55] L. Qin, G. Zeng, C. Lai, D. Huang, C. Zhang, P. Xu, T. Hu, X. Liu, M. Cheng, Y. Liu, L. Hu, Y. Zhou, Sen. Actuators B 243 (2017) 946.
[56] B.S. Shorke, P.V. Korake, P.P. Hankare, S.R. Bamane, K.M. Garadkar, J. Mater. Sci. Mater. Electron. 22 (2018) 821.
[57] S. Aswathy Aromal, K.V. Dinesh Babu, D. Philip, Spectrochim. Acta Part A: Mol. Biomol. Spectr. 96 (2012) 1025.
[58] N. Sangiorgi, L. Aversa, R. Tatti, R. Verucchi, A. Sanson, Opt. Mater. 64 (2017) 18.
[59] F. Beshkar, S. Zinatloo-Ajabshir, S. Bagheri, M. Salavati-Niasari, PLOS One (2017), doi:http://dx.doi.org/10.1371/journal.pone.0158549.
[60] S. Zinatloo-Ajabshir, M.S. Morassaei, M. Salavati-Niasari, J. Cleaner Prod. 198 (2018) 11.
[61] N.A. Seaton, Chem. Eng. Sci. 46 (1991) 1895.
[62] G. Leofanti, M. Padovan, G. Tozzola, B. Venturelli, Catal. Today 41 (1998) 207.
[63] P. Zucca, C. Vinci, F. Sollai, A. Rescigno, E. Sanjust, J. Mol. Catal. Chem. 288 (2008) 97.
[64] M.F. Nazar, S.S. Shah, M.A. Khosa, J. Surfact. Deterg. 13 (2010) 529.
[65] M. Kosmulski, J. Colloid Interface Sci. 337 (2009) 439.
[66] M. Roushani, Z. Saedi, T. Musa beygi, J. Taiwan Inst. Chem. Eng. 66 (2016) 164.
[67] G.V. Buxton, C.L. Greenstock, W.P. Helman, A.B. Ross, J. Phys. Chem. Ref. Data 17 (1988) 513.
[68] P. Borthakur, P.K. Boruah, N. Hussain, Y. Silla, M.R. Das, Appl. Surf. Sci. 423 (2017) 752.
[69] W.Z. Tang, C.P. Huang, Environ. Technol. 17 (1996) 1371.
[70] F.J. Benitez, F.J. Real, J.L. Acero, C. Garcia, E.M. Llanos, J. Chem. Technol. Biotechnol. 82 (2007) 65.
[71] D. Tiwari, C. Lalhriatpuia, Lalhmunsiama, S.-M. Lee, S.-H. Kong, Appl. Surf. Sci. 353 (2015) 275.
[72] C. Lalhriatpuia, A. Tiwari, A. Shukla, D. Tiwari, S.M. Lee, Korean J. Chem. Eng. 33 (2016) 3367.
[73] S. Nasseri, A.H. Mahvi, M. Seyedsalehi, K. Yaghmaeian, R. Nabizadeh, M. Alimohammadi, G.H. Safari, J. Mol. Liq. 241 (2017) 704.
[74] Y. Qu, W. Shen, X. Pei, F. Ma, S. You, S. Li, J. Wang, J. Zhou, J. Environ. Sci. 56 (2017) 79.
[75] C. Xu, G.P. Rangaiah, X.S. Zhao, Ind. Eng. Chem. Res. 53 (2014) 14641.
[76] I.K. Konstantinou, T.A. Albanis, Appl. Catal. B Environ. 49 (2004) 1.
[77] E.M. Saggioro, A.S. Oliveira, T. Pavesi, C.G. Maia, L.F.V. Ferreira, J.C. Moreira, 16 (2011) 10370.
[78] R.M. Mohamed, I.A. Mkhalid, J. Ind. Eng. Chem. 22 (2015) 390.
[79] Y. Yang, C. Zhang, D. Huang, G. Zeng, J. Huang, C. Lai, C. Zhou, W. Wang, H. Guo, W. Xue, R. Deng, M. Cheng, W. Xiong, Appl. Cat. B: Environ. 245 (2019) 87.
[80] C. Lalhriatpuia, D. Tiwari, A. Tiwari, S.M. Lee, Chem. Eng. J. 281 (2015) 782.
[81] D. Xu, K. Liu, W. Shi, M. Chen, B. Luo, L. Xiao, W. Gu, Ceram. Int. 41 (2015) 4444.
[82] Y. Jia, C. Wu, B.W. Lee, C. Liu, S. Kang, T. Lee, Y.C. Park, R. Yoo, W. Lee, J. Hazard. Mater. 338 (2017) 447.
[83] N. Barka, S. Qourzal, A. Assabbane, A. Nounah, Y. Ait-Ichou, Arab. J. Chem. 3 (2010) 279.

Environmental Science and Pollution Research (2018) 25:20125–20140
https://doi.org/10.1007/s11356-018-2215-8

RESEARCH ARTICLE

Nanocomposite Au NP/TiO_2 thin film in the efficient remediation of aqueous solutions contaminated with emerging micro-pollutants

Lalliansanga Nil[1] · Alka Tiwari[2] · Alok Shukla[2] · Diwakar Tiwari[1] · Seung Mok Lee[3]

Received: 12 February 2018 / Accepted: 1 May 2018 / Published online: 10 May 2018

Abstract

The present communication specifically aims to synthesize novel nanocomposite material Au NPs/TiO_2 in a simple template process using the polyethylene glycol as filler media. The thin film of the nanocomposite material was characterized by the advanced analytical tools. The surface morphology was obtained by the scanning electron microscopic (SEM) and transmission electron microscopic (TEM) images of solids. Similarly, the surface topography and roughness of solid were obtained by the atomic force microscopic (AFM) image of thin film. X-ray diffraction (XRD) data enabled to confirm that the TiO_2 was predominantly present with its anatase phase. The specific surface area and pore size of the solid were obtained using the N_2 adsorption/desorption data. Nanocomposite Au NP/TiO_2 thin film was employed in the photocatalytic removal of sulfamethoxazole and triclosan from aqueous solutions using less harmful UV-A light (λ_{max} = 330 nm). Various physicochemical parametric studies enabled to deduce the mechanism involved in the degradation process. The degradation kinetics as a function of pH (pH 4.0–10.0) and micro-pollutant concentrations (0.5–15.0 mg/L) was extensively studied. The mineralization of these pollutants was obtained using the non-purgeable organic carbon (NPOC) data. The stability of thin film was assessed by the repeated operations, and presence of several co-existing ions simulates the studies to real matrix treatment. Further, the presence of scavengers enabled to pin point the radical-induced degradation of sulfamethoxazole and triclosan from aqueous solutions.

Keywords Emerging water pollutants · Nanocomposite Au NPs/TiO_2 · Degradation kinetics · Mineralization · Stability of catalysts

Introduction

The detection of several pharmaceuticals and personal care products (PCPs) in water bodies is found ubiquitous and widespread (Mompelat et al. 2009; da Silva et al. 2011; Wu et al. 2012). These water contaminants are persistent and found difficult to eliminate completely in the existing biological or physicochemical wastewater treatment plants. Hence, they are eventually escaped through the wastewater treatment plants (WWTPs), at low level, and subsequently enter into the fresh water system, contaminating the water bodies, viz., drinking water, surface water, or even the river/lake waters. Based on its toxicity or prevalence to drug resistance in the environment and human commensal microbes or due to persistence in nature, these compounds are known as emerging water pollutants (Constantin et al. 2018; Han et al. 2017). Although the regulatory bodies have not prescribed the permissible limit of these emerging pollutants in the water bodies, however, based on its potential risk towards the human being, animals or aquatic life, it is important to eliminate effectively from aqueous solutions (Kosera et al. 2017).

Sulfamethoxazole is one of widely used antibiotics which belongs to the sulfonamide group of antibiotics. This is included with the other antibiotics sulfadiazine, sulfamerazine, sulfamethazine sulfathiazole, and sulfapyridine (Kolpin et al. 2002a; Cheng et al. 2017). It was most detected (100%) water contaminants as monitored in 139 streams in the USA from

Responsible editor: Suresh Pillai

✉ Diwakar Tiwari
diw_tiwari@yahoo.com

[1] Department of Chemistry, School of Physical Sciences, Mizoram University, Aizawl 796004, India

[2] Department of Physics, National Institute of Technology, Aizawl 796001, India

[3] Department of Health and Environment, Catholic Kwandong University, 24, Beomil-ro 579beon-gil, Gangneung 210-701, South Korea

1999 to 2000 (Ahmed et al. 2015; Kang et al. 2018). Sulfamethoxazole possesses the log K_{ow} and pK_a values of 0.89 and 1.6/5.7, respectively. This antibiotic is widely used as bacteriostatic agent and frequently supplemented in human and veterinary medicines (Hu et al. 2007; Wang et al. 2018b). This is also prescribed as a synergistic additive with trimethoprim to treat urinary tract infections (Dias et al. 2014). The contamination of aquatic environment by the pharmaceuticals, in general, is mainly due to the wastewaters that originate from the hospitals, veterinary clinics, households, pharmaceutical manufacturing facilities, etc. Similarly, a large and significant contribution is from the wastes originating from the livestock as the feces and urine of animals contained with significant load of antibiotics (Behera et al. 2011). A report suggested that about 29.9 million pounds of antibiotics were used on farm animals (Leavey-Roback et al. 2016; Wang and Wang 2016). Since, only part of it is metabolized and *Ca* 70–90% is excreted through feces and urines as such or its metabolite forms (Massé et al. 2014). This subsequently enters as influent of WWTPs and eventually contaminates the water bodies.

On the other hand, the triclosan (5-Chloro-2-(2,4-dichlorophenoxy)phenol) is polychlorinated aromatic antimicrobial drug. It effectively inhibits the *enoyl-acyl* carrier protein reductase for fatty acid synthesis in bacteria, blocking lipid biosynthesis in *Escherichia coli* and promoting a mutation in a *FabI* gene (Heath et al. 2000; Heath and Rock 2000; Jones et al. 2000). It is often included as an additive for many health and personal care products (Sivaraman et al. 2003). Triclosan is introduced as a preservative or as an antiseptic agent for several consumer products of daily use, viz., hand soaps, skin creams, toothpastes, and household cleaners or even in textiles (Singer et al. 2002; Yang et al. 2011). It is reported that triclosan is less toxic, hence less health concerns; however, triclosan is readily photo-transformed in aqueous media and generating 2,8-dichloro-dibenzo 1,4-dioxincompounds which are potential carcinogens (Aranami and Readman 2007; Sanchez-Prado et al. 2006). Similarly, it was pointed that methyl triclosan occurred through the biological methylation was known to be more lipophilic and bioaccumulative than the parent triclosan compound (Lindström et al. 2002). The acidic dissociation constant (pK_a) of triclosan is ranged between 7.9 and 8.1; hence, the solubility of triclosan increases with the increase in pH (Grove et al. 2003). The octanol-water partition coefficient (log K_{ow}) was reported to be 5.4 that indicates the compound is a stable lipophilic (Hart 1999). Therefore, triclosan feebly accumulates in aquatic and terrestrial organisms (Son et al. 2009). Triclosan is one of abundantly detected contaminants in the aquatic environment (Huang et al. 2016; Thomaidi et al. 2017) and reported to be 57.6% in US streams and 62.7% in Elbe River water samples (Kolpin et al. 2002a). It is often detected in the human urine, plasma, breast milk, etc. samples (Adolfsson-Erici et al. 2002; Allmyr et al. 2006; Arbuckle et al. 2015). Triclosan is reported to be geno- and cytotoxic compound studied for the aquatic organisms and species such as algae and fish (Kolpin et al. 2002b). Another report indicated that triclosan itself shows weak androgenic activity towards aquatic life (Foran et al. 2000) and, hence, the estrogenic and androgenic responses in human breast cancer cells (Gee et al. 2008). These studies further demonstrated that triclosan is a potential endocrine-disrupting compound.

Therefore, the widespread and ubiquitous presence of these emerging water contaminants poses a serious environmental challenge to tune better the existing wastewater treatment technologies to eliminate these contaminants effectively. The role of advanced hybrid materials or metamaterials showed widespread applications in the area of electronics (Srinivasarao et al.; Guslienko 2008; Shankar et al. 2018; Sun et al. 2018), enhanced interfacial shear strength (IFSS) and tensile strength materials (Wang et al. 2017), mechanical properties (Liu et al. 2017), and electrically conducting thermoplastic materials (Liu et al. 2015, 2016, a; Hu et al. 2018; Li et al. 2018) or even in several environmental remediation strategies (Song et al. 2012; Ahmed et al. 2015). Similarly, the 2D photocatalysts were employed in the efficient water splitting process (Su et al. 2018). The composite materials based on titania were used for an enhanced catalytic activity or even in self-cleansing titania mesh membrane for efficient oil/water separation process (Zhang et al. 2017b; Kang et al. 2018). The antibacterial and bacterially adhesive cotton fabrics coated with cationic fluorinated polymer materials were synthesized by co-polymerization process (Lin et al. 2018). An interesting computer simulation study was overviewed to study the physical properties of several nanocomposite materials (Zhao et al. 2017). In a line, the advanced oxidation process integrated with the TiO_2 or titania-based photocatalysts is found to be an effective method to degrade the stable and potentially emerging micro-pollutants (Zhang et al. 2017a). The process includes with in situ generation of highly reactive hydroxyl radicals (rate constants in the order of 10^6 to 10^9 M^{-1} s^{-1}) that are predominantly responsible for the degradation/or even mineralization of micro-pollutants from wastewaters (Buxton et al. 1988; Zhang et al. 2017a, b). The variety of template materials were introduced in literature to synthesize several nanocomposites that include acrylonitrile-butadiene-styrene, polydimethylsiloxane, poly(acrylic acid), polyacrylonitrile, and poly(vinyl alcohol) (Li et al. 2017; Sun et al. 2017a; Ma et al. 2017; Wang et al. 2018a; X. Cui et al.). Literature survey further reveals that the graphene-based titanium oxide composite materials were found useful in the removal of antibiotics, viz., sulfamethoxazole (SMX), erythromycin (ERY), and clarithromycin (CLA), antibiotic-resistant bacteria, and their associated genes using the solar radiation. The results indicated that the composite materials could degrade ERY (84 ± 2%), CLA (86 ± 5%), and SMX (87

±4%) which were slightly higher than the pristine TiO_2 photocatalyst (Karaolia et al. 2018). Iron phthalocyanine is supported with activated carbon fiber (FeMATNPc) to enhance the catalytic degradation of sulfamethoxazole from aqueous solutions. The EPR results demonstrated that the radical species and the higher valent iron (Fe(IV)) were dominantly involved in the degradation of sulfamethoxazole (Wang et al. 2018b). Similarly, several photo-Fenton or Fenton-like processes were demonstrated in the removal of sulfamethoxazole using the materials Ce-Fe-graphene nanocomposite (Wan et al. 2016) or ferrioxalate complexes (Dias et al. 2014). On the other hand, a photoelectrocatalytic (PEC) process along with the UV illumination showed to achieve 78.7% removal of triclosan; however, the harmful intermediate 2,7-dichlorodibenzodioxin (DCDD) was formed in the degradation process (Liu et al. 2013). The TiO_2-based photocatalytic degradation of triclosan using the UV-A illumination showed a high percentage removal, and the kinetic studies showed that the degradation process followed the Langmuir–Hinshelwood model ($b = 27.99\ mM^{-1}$, $K_{triclosan} = 9.49\ mM^{-1}$) (Son et al. 2009). A CPC reactor (packed bed reactor type CPC) was packed with the TiO_2-impregnated tezontle stones, and it was then operated for the removal of triclosan using the solar radiations. This could achieve a removal efficiency of 74% in presence of persulfate as an effective electron acceptor (Martínez et al. 2014). TiO_2 (Degussa) photocatalyst was employed in the degradation of triclosan from aqueous solutions using the UV light ($\lambda < 365$), and it is interesting to observe that no dichlorophenol intermediate was formed in the photocatalytic degradation process (Yu et al. 2006). The heterogeneous zinc oxide (ZnO: crystal phase wurtzite) immobilized with sodium alginate showed fairly a high removal efficiency of triclosan within 20 min of contact whereas solar-irradiated sample required 90 min of contact to achieve the degradation efficiency 90% (Kosera et al. 2017). Similarly, the Fenton-like processes using the $BiFeO_3$ magnetic nanoparticles ($BiFeO_3$ MNPs) (Song et al. 2012) or ferric ion (Munoz et al. 2012) were introduced to achieve a high degradation efficiency of triclosan from aqueous solutions.

The TiO_2 catalyst decorated with the noble metal nanoparticles (NPs), viz., NPs of Ag or Au could absorb the photon in the visible region since these NPs enable to cause the surface plasmon resonance effect and stimulate the localized electric field in the vicinity of TiO_2 that results in facile generation of e^-/h^+ pairs at the surface of TiO_2 (Ihara et al. 1997). Additionally, the NPs on TiO_2 act as co-catalysts which promote the e^-/h^+ separations (Seery et al. 2007). The catalytic activity of TiO_2 largely depends upon the particle size, geometry, and the type of noble metal NPs doped in its sphere (El-Sayed 2001). Previously, the $BaTiO_3$ nanoparticles were synthesized by the thermohydrolysis route which provides a novel low-temperature route in the synthesis of perovskite films. The films possessed with a stable dielectric constant of 30 having the frequency ranged from 0 Hz to 1 MHz (Sun et al. 2017b). Similarly, the enhanced lithium ion batteries were obtained using the nanocomposites of $TiNb_2O_7$/carbon nanotubes or nanoparticles of $FeNb_{11}O_{29}$ as anode materials (Lou et al. 2017; Hou Qinzhi et al. 2018). In a line, the TiO_2 thin films are a viable option of utilizing the photocatalysts in the treatment of wastewater treatment plants that makes the phase separation easy and possesses greater applicability in the repeated catalytic operations. However, the impregnation of NPs with TiO_2 network in thin film is a challenging objective. A simple deposition of NPs is found unstable under reaction conditions, and it readily migrates and aggregates to the larger particles. This causes the loss of its unique properties (Huang et al. 2017). Therefore, present communication aims to synthesize a Au NP/TiO_2 nanocomposite thin film with the template synthetic method. Further, the nanocomposite material was employed in the remediation of aqueous solutions contaminated with emerging water pollutants, viz., sulfamethoxazole and triclosan. The detailed physicochemical parametric studies enabled to deduce the mechanism of degradation, and kinetic studies revealed the efficiency of nanocomposite materials in the degradation process.

Materials and methods

Chemical and materials

Gold(III) chloride hydrate, triclosan (99.999%), sulfamethoxazole, acetic acid (99%), and sodium borohydride (98%) were obtained from the Sigma-Aldrich. Co., USA. Titanium (IV) isopropoxide (99%) and polyethylene glycol (average molecular weight 800) were obtained from the Samchun Pure Chemical Co. Ltd., Korea. Sodium nitrate and ethylenediaminetetraacetic acid disodium salt was obtained from Loba Chemicals, India. Ethanol anhydrous was obtained from the Daejung Chemicals & Metals Co. Ltd., Korea. Sodium chloride, sodium azide, oxalic acid dihydrate, sodium hydrogen carbonate, 2-propanol, zinc chloride dry, cadmium nitrate tetrahydrate, copper (II) sulfate pentahydrate, glycine, and acetonitrile (HPLC grade) were obtained from the Merck India Ltd., India. Purified water (18.2 MΩ cm at 25 °C) was collected from the Millipore Water Purification system (model: Elix 3).

UV-visible spectrophotometer (Thermo Fisher Evolution Model-220, UK) was employed for the spectrophotometric determination of sulfamethoxazole or triclosan in aqueous solutions. The sulfamethoxazole and triclosan give the distinct absorption peaks at the wavelength (λ_{max}) 360 and 254 nm, respectively. The standard solutions of sulfamethoxazole or triclosan were prepared having the micro-pollutant concentrations 0.5, 1.0, 5.0, 10.0, and 15.0 mg/L. Calibration lines were drawn between the concentrations of these standard solutions

and its corresponding measured absorbance (correlation coefficient $R^2 = 0.999$). The total organic carbon (TOC) analyzer (Shimadzu, Japan; model: TOC-VCPH/CPN) was employed to measure the non-purgeable organic carbon (NPOC) values to study the, possible, mineralization of sulfamethoxazole or triclosan from aqueous solutions by the photolytic/or photocatalytic treatments. A UV-A lamp, wavelength (λ_{max}) = 360 nm (model: 9W, PLS9W BLB/2P 1CT, Philips), was obtained from the Hansung UV Pvt. Co. Ltd., Korea.

Methodology

Synthesis of gold nanoparticles

Nanoparticles of gold were obtained by using previously described method (McFarland et al. 2004). Briefly, 0.1 mmol/L of gold(III) chloride solution was prepared in distilled water. Fifty-milliliter gold(III) solution was taken into a conical flask and was heated up to its boiling. Then slowly, under the stirred conditions, 2-mL 1% trisodium citrate solution was added quickly to the gold(III) solution. The solution was taken off from the hot plate. The gold(III) rapidly reduces to Au(0) and the color of the solution was quickly changed to deep red. The gold nanoparticles were formed and it was found stable for hours.

Synthesis of Au/titania sol

A template synthesis of TiO_2 was carried out using the titanium alkoxide precursor. The polyethylene glycol was introduced as a template to generate titania network. Titanium(IV) isopropoxide 28 g was mixed with 13 g of acetylacetone and 2 g of polyethylene glycol was dissolved in it. Simultaneously, freshly prepared 10 mL of Au(0) nanoparticle suspension was mixed. Further, a solution mixture of ethanol (184 g), acetic acid (5.8 g), and distilled water (22.5 g) was mixed slowly to the titanium solution. The solution mixture was stirred vigorously for 2 h followed by sonication for 30 min in a sonication bath. A clear sol Au NP/TiO_2 was obtained which was aged for Ca. 24 h and employed for the fabrication of thin films.

Preparation of nanocomposite Au NP/TiO_2 thin film

Borosilicate glass disk (2.3 cm diameter and 0.5 mm thickness) was cleaned by 0.1 mol/L HNO_3 and washed repeatedly by the distilled water and dried in a drying oven. Further, the disk was taken slowly in the transparent solution of Au NPs/TiO_2 and placed vertically in the titania sol for 1 h. It was then taken out slowly using a forceps. The disk was kept in air for *Ca* 12 h and then dried first at 100 °C for 1 h followed by annealing at 500 °C for 3 h in an electric furnace (Nabertherm; model no. LT/15/12/P330, Germany). This results a very fine thin film formation of nanocomposite Au NPs/TiO_2 onto the substrate surface. Further, the process was repeated for another two times that enables to obtain a fine and smooth thin film formation onto the surface. The thin film samples were stored in a vacuum desiccator under dark conditions for its further use as photocatalyst.

Further, the solvents of sol solution Au NPs/TiO_2 were evaporated at 105 °C followed by annealing at 500 °C to obtain the nanocomposite Au NP/TiO_2 solid. The solid was crushed in a mortar to obtain the fine powder of material. It was kept in the airtight polyethylene bottle.

Morphological study of material

The surface morphology of thin film Au NPs/TiO_2 was obtained by the scanning electron microscope (SEM) machine (model FE-SEM SU-70, Hitachi, Japan). Similarly, the nanocomposite Au NP/TiO_2 powder was subjected for the transmission electron microscopic (TEM) analysis using the TEM analyzer (Tecnai F20 Transmission Electron Microscope, FEI, USA). The topographical 3D image of thin film was obtained by the atomic force microscope (AFM) machine (XE-100 apparatus from Park Systems, Korea) having sharp tips (>8 nm tip radius; PPP-NCHR type from Nanosensors™). The images were taken over the area of $10 \times 10\ \mu m^2$ and it was conducted in a non-contact mode. The 3D data clearly enabled the pillar height of TiO_2 along with the surface roughness.

Characterization of thin films

The X-ray diffraction (XRD) data of Au NP/TiO_2 thin film was collected using the X-ray diffraction machine (i.e., PANalytical, Netherland; model X'Pert PRO MPD). It was recorded at the scan rate of 0.033 of 2θ illumination and having the generator settings 30 mA, 40 kV. The $CuK_{\alpha 1}$ and $CuK_{\alpha 1}$ radiations were employed having wavelengths of 1.5406 and 1.54443 Å. The BET specific surface area was obtained using BET surface area analyzer (model ASAP 2020; Protech Korea) based on the liquid N_2 adsorption and desorption method.

Photocatalytic removal of micro-pollutants

Stock solutions of sulfamethoxazole or triclosan (each 20.0 mg/L) were prepared in a purified water. In order to increase the solubility of these micro-pollutants, the solutions were sonicated for 10 min in a sonication bath. Further, the required experimental concentrations of sulfamethoxazole or triclosan were obtained by the successive dilution of each stock solution. The pH of micro-pollutant solution was adjusted by the dropwise addition of conc. HCl/NaOH solutions. The concentration dependence data was collected by varying each micro-pollutant concentrations from 1.0 to 15.0 mg/L.

In order to conduct the photolytic or photocatalytic operations, a self-assembled photo reactor was used. A black box (dimension 60 × 45 × 45 cm) was made by cardboard and wrapped with black paper. A borosilicate glass beaker (100 mL) was contained with 50.0 mL of micro-pollutant solution and was placed inside the black box. Carefully, the nanocomposite Au NP/TiO_2 thin film disk was placed horizontally at the bottom of the reactor vessel. A UV-A lamp was mounted *Ca* 10 cm above to the micro-pollutant solution. The UV-A radiations enter the photocatalyst through the pollutant solution that enables the photocatalytic oxidation of micro-pollutants, i.e., sulfamethoxazole or triclosan. The temperature of reactor was maintained to 25 ± 1 °C using a self-assembled water bath. The sample solution was taken out from the reactor at definite time intervals in order to analyze the micro-pollutant concentrations using a UV-Vis spectrophotometer. Always a blank experiment was performed using only UV-A irradiation without the thin film photocatalyst for comparison of photocatalytic degradation of these micro-pollutants.

Results and discussion

Morphological study of thin films

The SEM image of Au NP/TiO_2 thin film is shown in Fig. 1a. Figure 1a clearly indicated that fine grains of TiO_2 are distributed on the surface of borosilicate glass-making thin film of composite material of Au NPs/TiO_2. Very heterogeneous surface structure is visible on the surface having some cracks at places. Moreover, some of the mesopores are also seen on the surface. Interesting to note that at places, the Au(0) nanoparticles are visible with the TiO_2 structure. A similar Au(NPs) were impregnated/decorated with the TiO_2 nanotubes using the two-step anodization method. The Au nanoparticles were clustered at the TiO_2 surface, and the density of gold clusters depends largely on the gold concentrations along with the bias voltages (Noothongkaew et al. 2017).

The TEM image of the powder nanocomposite Au NPs/TiO_2 was taken and presented in Fig. 1b. It is evident from the TEM image that the Au nanoparticles are distributed with the TiO_2 network. The particle size was ranged within 25–30 nm. Further, the interplanar distance of the Au Nanoparticles was estimated to be 0.25 nm for the solid sample of Au NPs/TiO_2. It was reported previously that Au (NPs) are well dispersed with the spherical surface of SiO_2 having a mean diameter of about 3–5 nm, and the interplanar distance of Au NP adjacent lattice planes was measured to be 0.32 (Huang et al. 2017). The other studies also indicated that the average Au particles were ranged between 3 and 5 nm on the TiO_2 catalyst surface (Nguyen et al. 2008).

Further, the TEM/EDX elemental mapping was conducted for the nanocomposite material Au NPs/TiO_2 and results are illustrated in Fig. 1c. The EDX mapping was recorded for the elements titanium (Ti), oxygen (O), and gold (Au). The figure clearly demonstrated that the oxygen is intimately associated with Ti that confirmed the presence of TiO_2 and forming a chemical bond between the titanium and oxygen (Ti-O). Moreover, it is evident from the figure that the Au

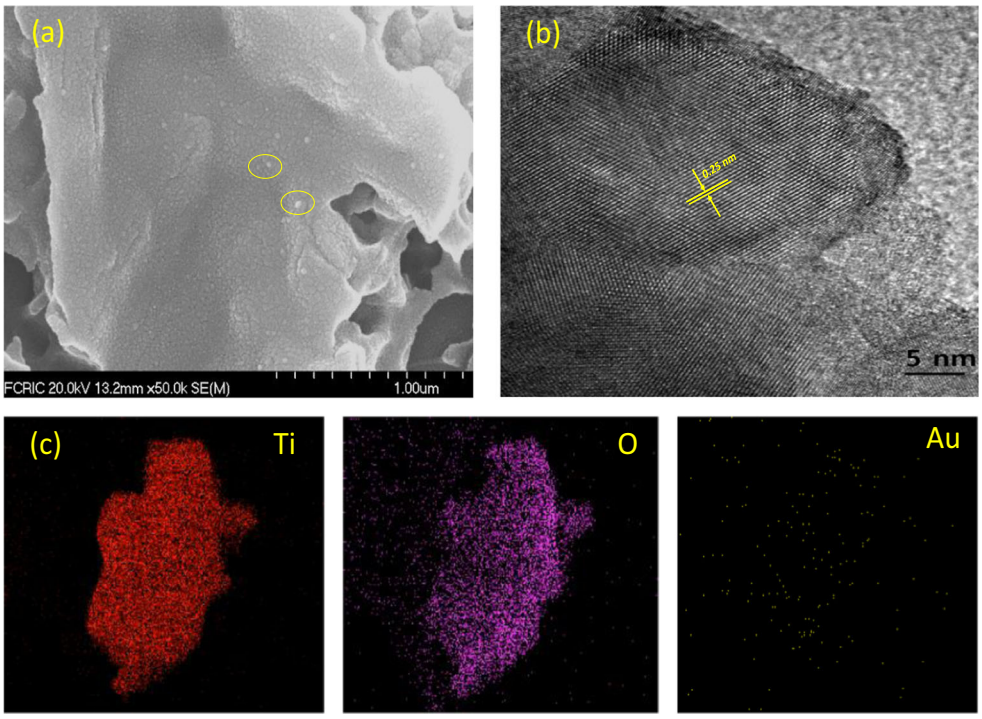

Fig. 1 **a** SEM image, **b** TEM image, and **c** TEM elemental mapping of the nanocomposite Au NPs/TiO_2

nanoparticles are very evenly and distinctly distributed within the titanium dioxide network. The Au^0 nanoparticles are not aggregated on the surface of titanium dioxide. Therefore, the in situ impregnation of Au nanoparticles enabled to distribute evenly within the titanium dioxide network. Similar EDX results were reported for the composite material TiO_2-Pt/graphene oxide solid that confirms the presence of Ti, O, Pt elements, and uniform distribution of Pt nanoparticles over the graphene sheets. The results further inferred that the intimate contact within these components has provided an enhanced photocatalytic activity of catalyst by the efficient carrier mobility (Rosu et al. 2017).

Further, a 3D atomic force microscopic image of nanocomposite Au NP /TiO_2 thin film is obtained and shown in Fig. 2. It is observed that TiO_2 is forming a very disordered heterogeneous structure on the surface. Moreover, it is pillared on the surface and the average pillar height was found to be *Ca* 600 nm. Further, the root mean square roughness (Rq) and mean roughness (Ra) were found to be 124.330 and 94.659 nm, respectively. It is evident again that the template synthesis enabled to synthesize a good heterogeneous surface structure with an enhanced pillar height of TiO_2.

Characterization of thin films

The X-ray diffraction data was collected for the nanocomposite Au NP/TiO_2 thin film. Results are shown in Fig. 3. The figure clearly reveals that the material is having predominantly amorphous in nature. This is because the material was not annealed at required high temperature. However, characteristic peak was observed around the 2θ value of 25.5 indicated the presence of anatase phase of TiO_2 (Shorke et al. 2018).

Further, the BET specific surface area, pore volume, and pore sizes of nanocomposite Au NPs/TiO_2 were obtained by the usual N_2 adsorption/desorption method. The N_2 adsorption/desorption curves are illustrated in Fig. 4. Adsorption/desorption isotherms revealed that it possessed the hysteresis loop of H2 type, which indicated the pores are having narrow mouths and cannel-like (Mendioroz et al. 1987; Seaton 1991). The pore size, pore volume, and the specific surface area of nanocomposite Au NPs/TiO_2 were found to be 5.60 nm, 0.034 cm^3/g, and 19.91 cm^2/g, respectively. Therefore, the material was possessed with good mesoporosity.

Photolytic and photocatalytic removal of triclosan and sulfamethoxazole

pH dependence study

The pH dependence degradation of sulfamethoxazole and triclosan was conducted as a function pH and illustrated in Fig. 5. Simultaneously, the speciation of sulfamethoxazole and triclosan was carried out and presented in Fig. 5. The pH dependence degradation of micro-pollutants greatly influenced with the species distribution of these micro-pollutants as well as the surface properties of solid catalyst. The photocatalytic processes largely depend upon the sorption of these species onto the catalyst surface. Figure 5 clearly demonstrated that the increase in pH caused for decrease in percentage removal of both the micro-pollutants from aqueous solutions. More quantitatively, increasing the pH from 4.0 to 10.0, the pollutant degradation was decreased from 64.45 to 55.18% (for sulfamethoxazole) and from 60.94 to 40.63% (for triclosan), respectively.

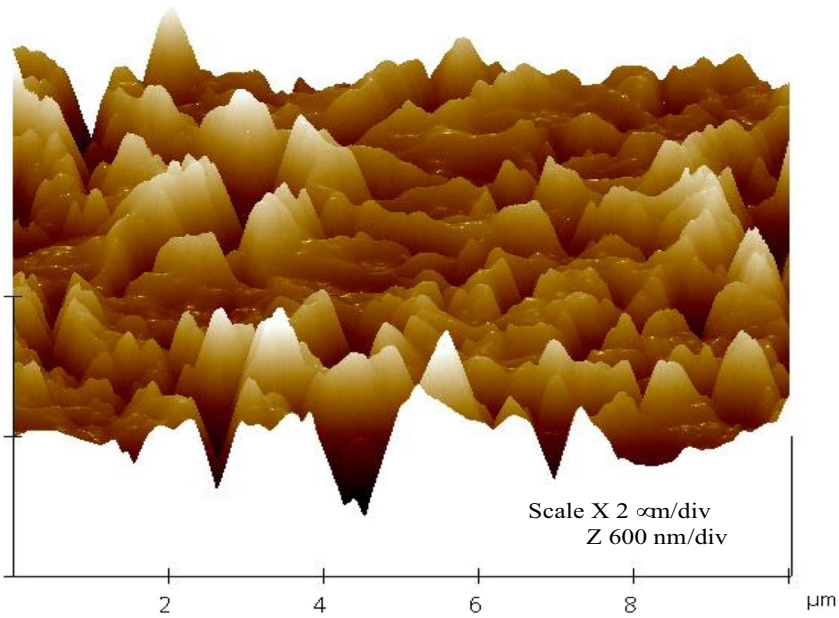

Fig. 2 Atomic force microscopic image of nanocomposite Au NP/TiO_2 thin film

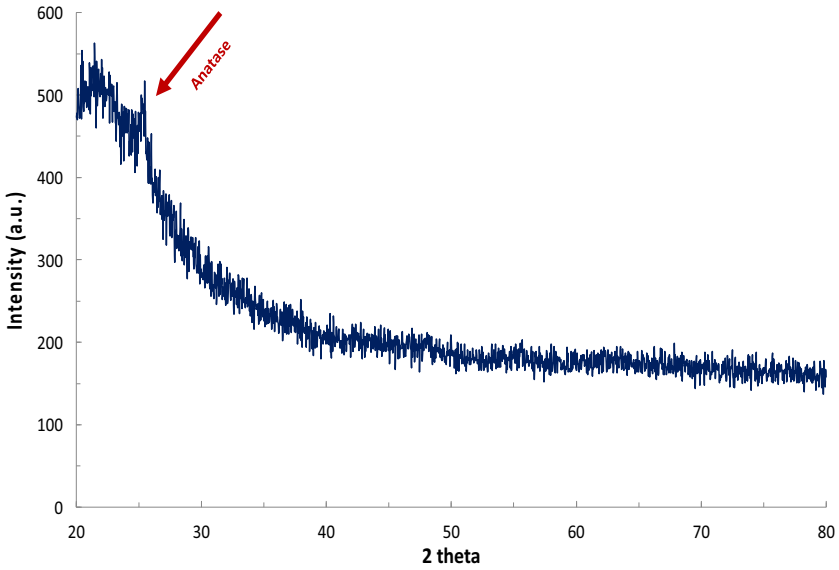

Fig. 3 X-ray diffraction pattern of nanocomposite Au NP/TiO_2 thin film

It was reported that the sulfamethoxazole (SMX) is having two dissociable hydrogens with the acid dissociation constant values pK_a^1 and pK_a^2, respectively 1.8 and 5.6 (Lucida et al. 2000). Therefore, the speciation studies revealed that above pH 3.6, the sulfamethoxazole is dominantly present with anionic species either SMX(-) or SMX(2-) (cf Fig. 5). Below pH 3.8, it partly exists as neutral sulfamethoxazole species of SMX(0). On the other hand, the pH_{PZC} (point of zero charge) values of anatase TiO_2 lie within the pH 4.8 to 6.5 with an accepted average value of 5.9. This indicated that the TiO_2 surface carries a net positive charge below pH 5.9, and eventually with the dissociation of proton, it turns to dissociated species and carries net negative charge above pH 5.9 as depicted in Eq. (1):

$$\equiv Ti{-}OH_2^{+} \leftrightarrow \underset{pH_{PZC}}{\equiv T{-}} OH^0 \leftrightarrow \equiv Ti{-}O^{-} \quad (1)$$

This indicates that at moderate to high pH values, i.e., pH > 5.9, both the surface and sulfamethoxazole species are negatively charged; hence, it electrostatically repels to each other. This causes less sorption of sulfamethoxazole onto the catalyst surface; therefore, a reduced degradation of sulfamethoxazole at high pH value is recorded. However, an increased degradation of sulfamethoxazole at low pH value, i.e., at pH 4.0, is due to the fact that the negatively charged sulfamethoxazole species are strongly sorbed onto the positively charged TiO_2 surface which favored the degradation of sulfamethoxazole.

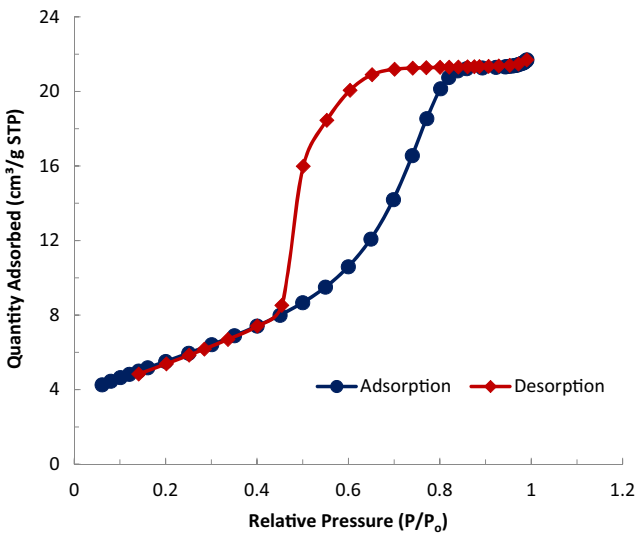

Fig. 4 BET adsorption/desorption isotherms of the nanocomposite Au NP/TiO_2 powder

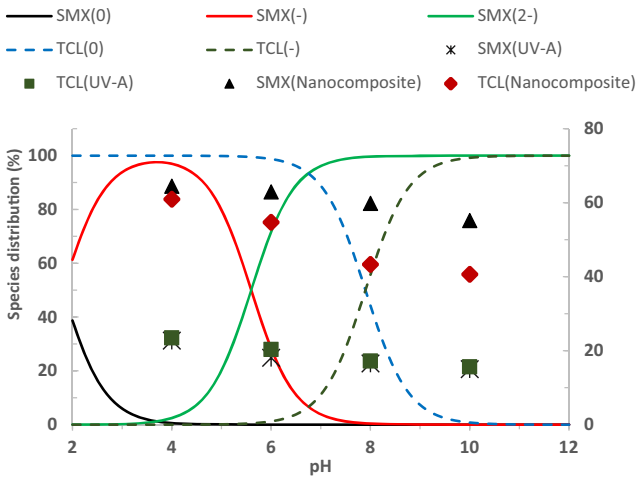

Fig. 5 Percentage distribution of species of sulfamethoxazole (smooth line) and triclosan (dotted lines) as a function of pH (Primary axis) and percentage removal of sulfamethoxazole and triclosan as a function of pH (Secondary axis) under the photolytic and photocatalytic operations [initial concentration of micro-pollutants, 1.0 mg/L]

Similarly, pH dependence sorption of sulfamethoxazole by the carbon nanotubes (CNT) was demonstrated under the fixed bed column reactor studies (Tian et al. 2013). It was pointed previously that the •OH radicals are having the same degradation tendency towards the anionic or neutral species of sulfamethoxazole; hence, a constant rate was obtained, i.e., $k_{SH,\bullet OH}$ and $k_{S^-,\bullet OH}$ having the value of $(7.63 \pm 0.85) \times 10^9$ M^{-1} s^{-1} (Yang et al. 2017). Other studies revealed that in a Fenton-like process, a similar less degradation of sulfamethoxazole was obtained at higher pH values employing the zero-valent iron under the oxic and anoxic environment (Kobayashi et al. 2017).

On the other hand, triclosan is a monoprotic acid and having the acid dissociation constant pK_a value 7.9 (Muzvidziwa et al. 2017). Hence, triclosan predominantly exists as a neutral species below pH 7.9 and pH > 7.9; it turns to the anionic species (cf Fig. 5). Therefore, increasing the pH causes a decrease in the sorption of triclosan by the TiO_2 surface; hence, a decreased degradation percentage of triclosan is obtained at high pH values, i.e., pH 8~10. These results further indicated that the neutral species of triclosan is readily degraded by the photocatalytic degradation. This is possibly due to the affinity of neutral triclosan species towards the TiO_2 surface, and the neutral species are less stable compared to the anionic species of triclosan. The results are in a line to the other reports indicated that a decrease in pH from 7.0 to 10.0 greatly decreased the pseudo-second-order rate constant (k_{app}) values in the degradation of triclosan by ferrate(VI) (Yuval et al. 2017). Moreover, the sorption of triclosan by the carbon nanotube (CNT) and functionalized CNT was decreased with the increase in pH (Li et al. 2017).

Further, it was noted that significantly less degradation of sulfamethoxazole or triclosan was obtained with the photolytic process at all studied pH compared to the photocatalytic process conducted with using the nanocomposite Au NP/TiO_2 thin film (cf Fig. 5). This clearly demonstrated that the thin film nanocomposite Au NPs/TiO_2 showed a greater catalytic activity that enabled to enhance the degradation percentage of sulfamethoxazole or triclosan from aqueous solutions. Moreover, increasing the pH from 4.0 to 10.0, a marked decrease in percentage degradation of these micro-pollutants is recorded. More quantitatively, increasing the pH from 4.0 to 10.0, the percentage degradation of sulfamethoxazole is decreased from 22.72 to 14.99, respectively. Similarly, the triclosan removal was decreased from 23.44 to 15.63% for the similar increase in pH. These results are pointed that the anionic species of sulfamethoxazole or triclosan are more stable than the neutral species of these micro-pollutants.

Concentration dependence removal of micro-pollutants

The initial concentration of sulfamethoxazole and triclosan was increased from 0.5 to 15.0 mg/L at constant pH 6.0. The micro-pollutants were treated for a constant time interval of 2 h using UV-A lamp. The percentage removal of sulfamethoxazole or triclosan was recorded and presented as a function of micro-pollutant concentration in Fig. 6. It is evident from the figure (Fig. 6) that increasing the micro-pollutant concentration significantly decreases the percentage removal of both the micro-pollutants, viz., sulfamethoxazole or triclosan, from aqueous solutions for the photolytic or photocatalytic processes. Increasing the concentration of micro-pollutant from 0.5 to 15.0 mg/L has caused to decrease the percentage removal of micro-pollutant from 75.27 to 35.60% (for sulfamethoxazole) and from 71.87 to 22.19% (for triclosan), respectively, using the nanocomposite Au NP/TiO_2 thin film. This decrease in percentage removal of micro-pollutants with the increase in initial concentration of micro-pollutant is explained with the fact that the contact possibilities of pollutants to the catalyst surface are relatively high at lower pollutant concentrations. Additionally, the catalyst surface contained with relatively higher percentage of surface active sites for lower number of total pollutant species present at lower concentration of pollutant (Lalhriatpuia et al. 2015). Moreover, the high concentration of pollutant species scavenges the catalyst activity; hence, a lower removal of pollutant was obtained at higher concentration of pollutants (Nasseri et al. 2017). Similarly, the results indicated that the photolytic degradation of sulfamethoxazole or triclosan is significantly less than the corresponding photocatalytic removal of these pollutants using the nanocomposite Au NP/TiO_2 thin film. This further inferred the potential catalytic activity of nanocomposite in the degradation of these emerging water contaminants.

Kinetic studies of micro-pollutant degradation

The time dependence photolysis or photocatalytic degradation of sulfamethoxazole and triclosan was carried out, and the observed values were modeled with a known pseudo-first-

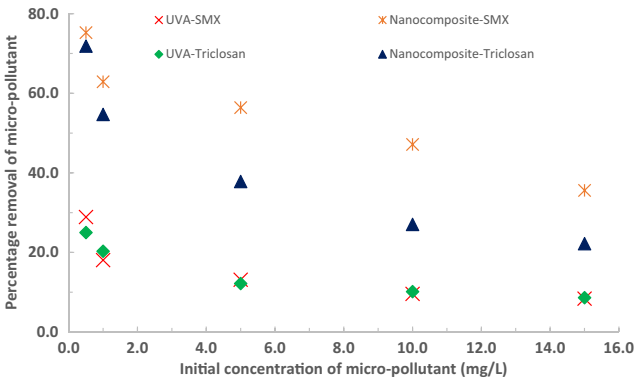

Fig. 6 Percentage removal of sulfamethoxazole and triclosan at various initial concentrations of micro-pollutants under the photolytic and photocatalytic processes using the nanocomposite Au NP/TiO_2 thin film photocatalyst [pH 6.0]

order rate equation (Tiwari et al. 2015). The kinetics was performed at all studied concentrations and at pH 6.0.

The pseudo-first-order rate constant (k_{app}) values were obtained at all the studied concentrations and presented in Fig. 7. The linear and non-linear (exponential) fitting for the pseudo-first-order rate equations was conducted to obtain the pseudo-first rate constant values for both the micro-pollutants, viz., sulfamethoxazole and triclosan, and the fitting data is shown in insets of Fig. 7. It is evident from Fig. 7 that a decrease in micro-pollutant concentration from 15.0 to 0.5 mg/L was apparently favored the rate constant values. More quantitatively, decreasing the concentration of sulfamethoxazole from 15.0 to 0.5 mg/L had caused to increase the pseudo-first-order rate constant values from 2.9×10^{-3} to 9.7×10^{-3} min^{-1}, respectively, using the nanocomposite Au NP/TiO_2 thin film. Similarly, for a similar decrease in triclosan concentration, the rate constant value was decreased from 1.7×10^{-3} to 8.8×10^{-3} min^{-1}, respectively, using the photocatalyst thin film. On the other hand, the pseudo-first-order rate constant values obtained for the photolytic degradation of sulfamethoxazole or triclosan are significantly lower than the corresponding rate constant values obtained for the photocatalytic degradation of these micro-pollutants (cf Fig. 7). This again reaffirmed the utility of nanocomposite Au NP/TiO_2 thin film photocatalyst in the removal of sulfamethoxazole or triclosan in aqueous solutions. A similar pseudo-first-order kinetics was obtained for the photocatalytic degradation of dyes (methylene blue, rhodamine B, eosin Y, and Congo red) from aqueous solutions using the CuS (NPs) photocatalyst (Ayodhya et al. 2016). Similarly, the triclosan degradation by the electro-Fenton process showed to be the pseudo-first-order rate kinetics (Sirés et al. 2007).

Further, it is interesting to find that the photocatalytic degradation of sulfamethoxazole and triclosan followed the known Langmuir–Hinshelwood (L-H) isotherm to its linear form at the studied concentrations (Lalhriatpuia et al. 2015). The L-H adsorption constant "K" (L/mg) and the rate constant "k_r" (mg/L/min) values were estimated and found to be 0.167 and 6.02×10^{-2} (R^2 0.979; for sulfamethoxazole) and 0.384 and 2.64×10^{-2} (R^2 0.984; for triclosan), respectively, using the nanocomposite Ag NPs/TiO_2 thin film. These results inferred that the photocatalytic degradation of these micro-pollutants fairly well demonstrated with the L-H kinetic modeling.

NPOC removal of micro-pollutants

The removal of micro-pollutants was intended to its mineralization, and the percentage mineralization of sulfamethoxazole or triclosan was obtained for the photolysis or photocatalytic processes. Therefore, the non-purgeable organic carbon (NPOC) data was collected for the treated aqueous samples. Using the initial NPOC values of micro-pollutants, the percentage mineralization was obtained at different pH values. The initial concentration of these micro-pollutants was kept constant 1.0 mg/L and the total illumination time was 2 h. The results were presented in Fig. 8. Figure 8 clearly demonstrated that increasing the solution pH, i.e., pH 4.0–10.0, had caused to decrease significantly the percent mineralization of these two pollutants. Quantitatively, increasing the pH from 4.0 to 10.0 the respective decrease in percentage NPOC removal was decreased from 54.30 to 39.49% (for sulfamethoxazole) and from 32.29 to 26.84% (for triclosan), respectively, using the nanocomposite Au NP/TiO_2 thin film photocatalyst. On the other hand, the photolytic mineralization of these two pollutants was obtained significantly less than the corresponding photocatalytic degradation. Although, a partial but significant amount of the micro-pollutants was mineralized in the photocatalytic process, however, a complete mineralization could be achieved with a prolonged or multiple operations of the process. The NPOC removal results were quite in a line to the results obtained for the degradation of pollutants in the concentration dependence studies.

Repeated use of thin film catalyst

The nanocomposite Au NP/TiO_2 thin film was subjected for the repeated photocatalytic operations, i.e., at least six-cycle operations, and results are presented in Fig. 9. The thin film was washed with distilled water and dried in a drying oven at 105 °C for 3 h and again was used for the next cycle of operation. The initial concentration of micro-pollutant was taken 5.0 mg/L with a constant pH 6.0. The results clearly demonstrated (Fig. 9) that even at the end of six cycle of operations, the percentage efficiency of photocatalyst was not hampered and almost an identical removal of sulfamethoxazole or triclosan was obtained. More quantitatively, at the completion of six cycles, the percentage removal of sulfamethoxazole was decreased from 55.24 to 54.60% (i.e., a decrease of 0.64%). Similarly, the triclosan percentage removal was decreased from 36.22 to 35.26% only (i.e., a decrease of 0.96%) at the end of six cycles of operations. These results showed that fairly a good stability of nanocomposite Au NP/TiO_2 thin film was achieved at least in successive operations of photocatalytic treatment. This eventually enhanced the applicability of the nanocomposite thin film in the wastewater treatment. It was reported previously that methyl orange removal using the TiO_2 supported on spherical activated carbon (TiO_2/SAC) was significantly decreased even at the completion of five cycles of operations (Yoon et al. 2012).

Presence of co-existing ions

Further, the presence of several co-exiting ions in the removal of micro-pollutants is an important parameter which simulates the study to the real matrix treatment. Therefore, the study was

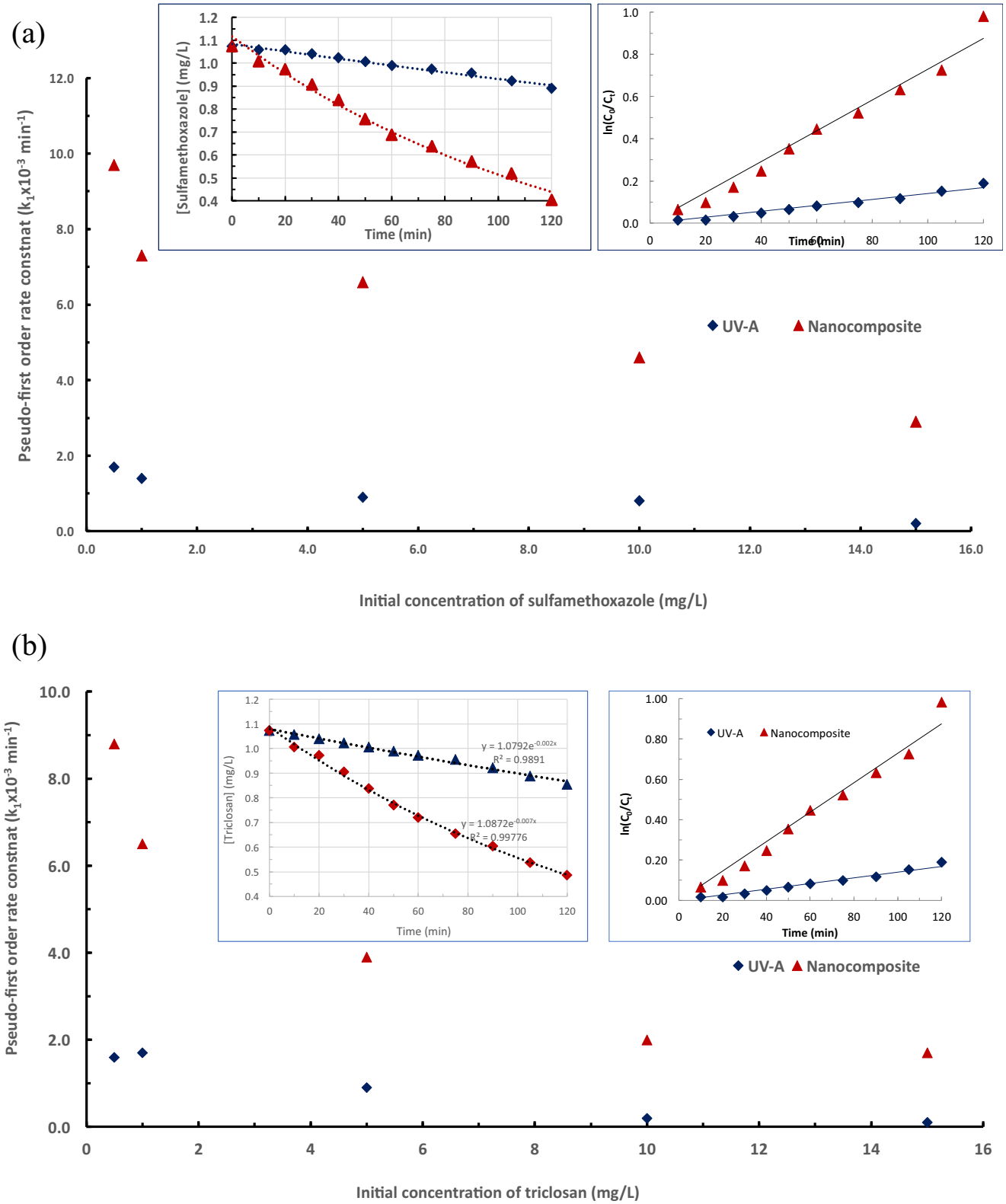

Fig. 7 The pseudo-first-order rate constant at varied concentrations of **a** sulfamethoxazole and **b** triclosan under the photolytic and photocatalytic processes [insets, linear and non-linear fitting of data for the pseudo-first-order rate kinetics; initial concentration of micro-pollutants 1.0 mg/L and pH 6.0]

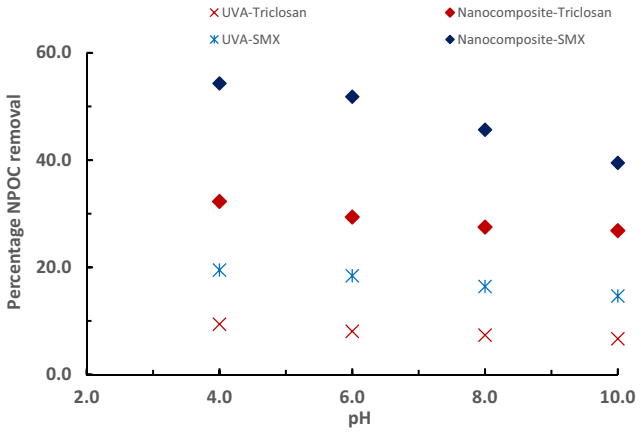

Fig. 8 Percentage removal of total NPOC of sulfamethoxazole and triclosan as a function of pH under the photolytic and photocatalytic degradation processes [initial concentration of micro-pollutant 1.0 mg/L]

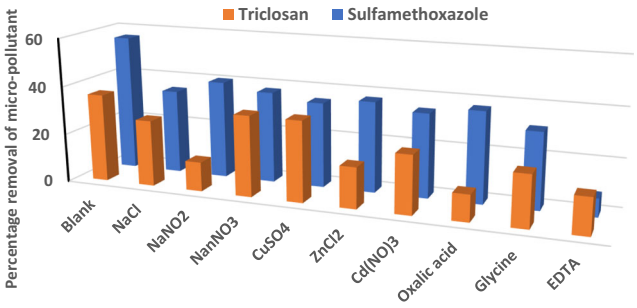

Fig. 10 Photocatalytic removal of sulfamethoxazole and triclosan in presence of several co-existing ions using the nanocomposite Au NP/TiO_2 thin film photocatalyst ([micro-pollutant] 5.0 mg/L; [co-ions] 50.0 mg/L; pH 6.0)

extended to assess the photocatalytic degradation of sulfamethoxazole and triclosan from aqueous solutions in presence of several co-existing cations and anions, viz., NaCl, $NaNO_3$, $NaNO_2$, $CuSO_4$, $Cd(NO_3)_2$, $ZnCl_2$, glycine, oxalic acid, and EDTA using the Au NP/TiO_2 photocatalyst. The initial concentration of sulfamethoxazole and triclosan was taken 5.0 mg/L and pH 6.0. The total illumination time was provided 2 h. Moreover, the co-existing ion concentration was taken 50.0 mg/L. The percentage of degradation of these micro-pollutants in presence of co-existing ions is presented in Fig. 10. The figure clearly revealed that the presence of these ions affected to a greater or lesser extent the degradation of sulfamethoxazole or triclosan. However, it is interesting to note that the presence of EDTA, $NaNO_2$, and oxalic acid had caused to suppress significantly the degradation of triclosan. Similarly, the presence of EDTA affected the degradation of sulfamethoxazole in the photocatalytic degradation process. The presence of other ions was affected to a lesser extent in the photocatalytic degradation of these two micro-pollutants.

Radical scavenger study

The 2-propanol and HCO_3^- molecules readily scavenge the •OH radicals in aqueous solutions (Xu et al. 2015; Lalhriatpuia et al. 2015). Similarly, the EDTA could scavenge the h^+ in TiO_2 semiconductor (Jia et al. 2017), and sodium azide (NaN_3) suppresses the singlet oxygen that occurred by the interaction of superoxide radical and photogenerated holes. The singlet oxygen readily degrades the organic compounds in aqueous media (Barka et al. 2010). Therefore, the photocatalytic degradation of sulfamethoxazole and triclosan (initial concentration of each pollutant 5.0 mg/L and pH 6.0) in presence of 2-propanol, HCO_3^-, and sodium azide (each one is having 1000 mg/L) was carried out using the nanocomposite Au NP/TiO_2 thin film photocatalyst. The percentage removal of sulfamethoxazole or triclosan in presence of these

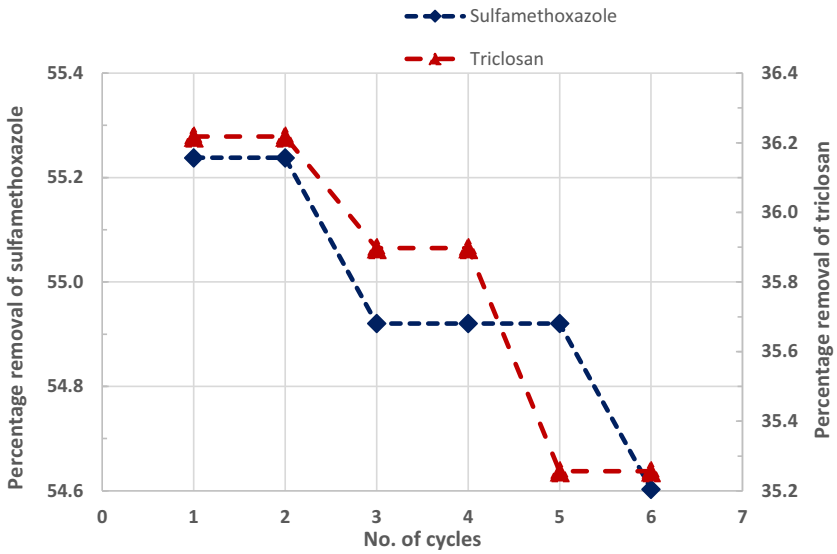

Fig. 9 Repeated use of nanocomposite Au NP/TiO_2 photocatalyst in the photocatalytic removal of sulfamethoxazole and triclosan using the UV-A illumination [initial concentration of micro-pollutant 5.0 mg/L; pH 6.0]

radical scavengers is shown in Fig. 11. The presence of these scavengers, viz., 2-propanol, sodium azide, and sodium biocarbonate, along with the EDTA (shown before) showed a significant decrease in percentage removal of sulfamethoxazole or triclosan from aqueous solutions. This indicated that these radicals are scavenging greatly the involved radical species; therefore, the removal of these pollutants was greatly inhibited. It was therefore affirmed that the •OH radicals were predominantly taking part in the photocatalytic degradation of triclosan. Moreover, the hole was involved to produce the •OH radicals that also degrade the micro-pollutants from aqueous solutions. Similarly, the presence of sodium azide that inhibited the removal of these pollutants showed that the singlet oxygen, possibly, induces the oxidation of triclosan.

Overall the study therefore demonstrates that the absorption of UV-A radiations ($\lambda = 360$ nm) by the nanocomposite Ag NPs/TiO_2 thin film catalyst induces the photocatalytic degradation of sulfamethoxazole or triclosan by the two different mechanistic pathways. UV-A photons cause to excite the electrons from the VB to CB in the TiO_2 semiconductor where the Au(NPs) traps efficiently the excited electrons at the CB. This eventually restricts the recombination of electron/hole pairs in TiO_2 catalyst. The trapped electrons are able to generate the superoxide radical followed by the formation of •OH radicals. On the other hand, the hole that is created in the VB interacts with the O_2 molecule and produces the O_2• radical species. This results the formation of •OH radicals. Therefore, the reactive radical species are predominantly involved in the degradation of micro-pollutants. Similarly, the other possible pathway of degradation is due to the localized surface plasmon resonance effect which produces the electromagnetic field created by the absorption of photon energy by the Au NPs. This electromagnetic field causes the local excitation of the TiO_2 with the generation of electron/hole pairs. Therefore, it again enables the formation of •OH radical, which simultaneously takes part in the degradation of sulfamethoxazole or triclosan from aqueous solutions.

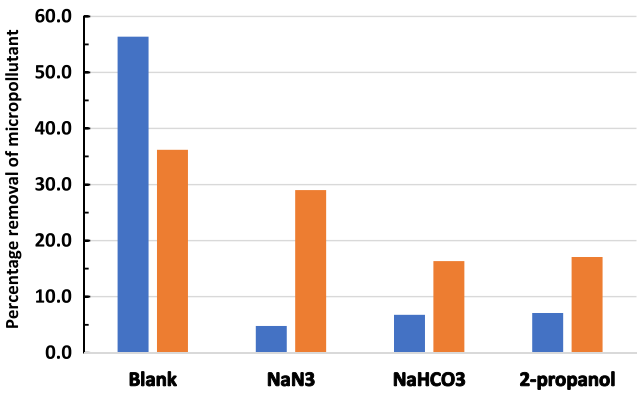

Fig. 11 Photocatalytic degradation of sulfamethoxazole and triclosan in presence of scavengers using the nanocomposite Au NP/TiO_2 thin film photocatalyst ([micro-pollutant] 5.0 mg/L; [scavengers] 1000.0 mg/L; pH 6.0)

Conclusion

Nanocomposite material Au NPs/TiO_2 was synthesized by the template method. SEM image of nanocomposite thin film showed fine grains of TiO_2 were distributed on the surface of borosilicate glass and a heterogeneous structure was obtained. Similarly, the TEM image of nanocomposite powder showed the distribution of gold nanoparticles having the particle size in the range of 25–30 nm and the interplanar distance of the Au nanoparticles 0.25 nm. AFM image of nanocomposite thin film showed that the TiO_2 was making a heterogeneous surface structure on the surface and the root mean square roughness (Rq) and mean roughness (Ra) were found to be 124.33 and 94.66 nm, respectively. The TiO_2 was predominantly possessed the anatase phase with the thin film material. Moreover, the liquid N_2 adsorption/desorption results indicated that the solid was having the H_2 type of hysteresis loop and the pore size, pore volume, and the specific surface area of nanocomposite Au NPs/TiO_2 were found to be 5.60 nm, 0.034 cm^3/g, and 19.91 cm^2/g, respectively. The thin film nanocomposite materials were then successfully utilized in the photocatalytic degradation of emerging micropolltants, viz., sulfamethoxazole and triclosan, from aqueous solutions using the less harmful UV-A light (λ_{max} 360 nm). Increase in solution pH (pH 4.0–8.0) and initial micro-pollutant concentrations (0.5–15.0 mg/L) greatly hampered the percentage removal of these two pollutants both in the photolytic and photocatalytic processes. The kinetic studies showed that the degradation of sulfamethoxazole or triclosan was followed by the pseudo-first-order rate kinetics and increase in concentration from 0.5 to 15.0 mg/L caused to decrease the pseudo-first-order rate constant values from 9.7×10^{-3} to 2.9×10^{-3} min^{-1} (for sulfamethoxazole) and from 8.8×10^{-3} to 1.7×10^{-3} min^{-1} (for triclosan), respectively. Moreover, the degradation of these micro-pollutants followed reasonably well the Langmuir–Hinshelwood isotherm. A significant decrease in percentage of non-purgeable organic carbon (NPOC) was achieved in the photocatalytic degradation of sulfamethoxazole and triclosan. The simultaneous presence of several co-existing ions was tended to affect the removal of these micro-pollutants. Moreover, the presence of 2-propanol, sodium azide, HCO_3^-, and EDTA inhibited significantly the percentage removal of sulfamethoxazole and triclosan from aqueous solutions. This confirmed the active •OH radicals were involved in the degradation process. The stability of nanocomposite thin film was reassessed with the repeated use of catalyst which showed

that no significant decrease in photocatalytic degradation efficiency of these two micro-pollutants from aqueous solutions. Overall, the template-synthesized photocatalyst Au NP/TiO_2 possessed an improved and enhanced catalytic activity in the degradation of emerging micro-pollutants. Moreover, the photocatalytic efficiency was found to be remarkably higher than the photolytic degradation efficiency at least for the removal of sulfamethoxazole and triclosan.

References

Adolfsson-Erici M, Pettersson M, Parkkonen J, Sturve J (2002) Triclosan, a commonly used bactericide found in human milk and in the aquatic environment in Sweden. Chemosphere 46:1485–1489. https://doi.org/10.1016/S0045-6535(01)00255-7

Ahmed MB, Zhou JL, Ngo HH, Guo W (2015) Adsorptive removal of antibiotics from water and wastewater: progress and challenges. Sci Total Environ 532:112–126. https://doi.org/10.1016/j.scitotenv.2015.05.130

Allmyr M, Adolfsson-Erici M, McLachlan MS, Sandborgh-Englund G (2006) Triclosan in plasma and milk from Swedish nursing mothers and their exposure via personal care products. Sci Total Environ 372:87–93. https://doi.org/10.1016/j.scitotenv.2006.08.007

Aranami K, Readman JW (2007) Photolytic degradation of triclosan in freshwater and seawater. Chemosphere 66:1052–1056. https://doi.org/10.1016/j.chemosphere.2006.07.010

Arbuckle TE, Weiss L, Fisher M, Hauser R, Dumas P, Bérubé R, Neisa A, LeBlanc A, Lang C, Ayotte P, Walker M, Feeley M, Koniecki D, Tawagi G (2015) Maternal and infant exposure to environmental phenols as measured in multiple biological matrices. Sci Total Environ 508:575–584. https://doi.org/10.1016/j.scitotenv.2014.10.107

Ayodhya D, Venkatesham M, kumari AS et al (2016) Photocatalytic degradation of dye pollutants under solar, visible and UV lights using green synthesised CuS nanoparticles. J Exp Nanosci 11:418–432. https://doi.org/10.1080/17458080.2015.1070312

Barka N, Qourzal S, Assabbane A, Nounah A, Ait-Ichou Y (2010) Photocatalytic degradation of an azo reactive dye, Reactive Yellow 84, in water using an industrial titanium dioxide coated media. Arab J Chem 3:279–283. https://doi.org/10.1016/j.arabjc.2010.06.016

Behera SK, Kim HW, Oh J-E, Park H-S (2011) Occurrence and removal of antibiotics, hormones and several other pharmaceuticals in wastewater treatment plants of the largest industrial city of Korea. Sci Total Environ 409:4351–4360. https://doi.org/10.1016/j.scitotenv.2011.07.015

Buxton GV, Greenstock CL, Helman WP, Ross AB (1988) Critical review of rate constants for reactions of hydrated electrons, hydrogen atoms and hydroxyl radicals (·OH/·O−) in aqueous solution. J Phys Chem Ref Data 17:513–886. https://doi.org/10.1063/1.555805

Cheng DL, Ngo HH, Guo WS, Liu YW, Zhou JL, Chang SW, Nguyen DD, Bui XT, Zhang XB (2017) Bioprocessing for elimination antibiotics and hormones from swine wastewater. Sci Total Environ 621:1664–1682. https://doi.org/10.1016/j.scitotenv.2017.10.059

Constantin LA, Nitoi I, Cristea NI, Constantin MA (2018) Possible degradation pathways of triclosan from aqueous systems via TiO2 assisted photocatalyis. J Ind Eng Chem 58:155–162. https://doi.org/10.1016/j.jiec.2017.09.020

da Silva BF, Jelic A, López-Serna R et al (2011) Occurrence and distribution of pharmaceuticals in surface water, suspended solids and sediments of the Ebro river basin, Spain. Chemosphere 85:1331–1339. https://doi.org/10.1016/j.chemosphere.2011.07.051

Dias IN, Souza BS, Pereira JHOS, Moreira FC, Dezotti M, Boaventura RAR, Vilar VJP (2014) Enhancement of the photo-Fenton reaction at near neutral pH through the use of ferrioxalate complexes: a case study on trimethoprim and sulfamethoxazole antibiotics removal from aqueous solutions. Chem Eng J 247:302–313. https://doi.org/10.1016/j.cej.2014.03.020

El-Sayed MA (2001) Some interesting properties of metals confined in time and nanometer space of different shapes. Acc Chem Res 34:257–264. https://doi.org/10.1021/ar960016n

Foran CM, Bennett ER, Benson WH (2000) Developmental evaluation of a potential non-steroidal estrogen: triclosan. Mar Environ Res 50:153–156. https://doi.org/10.1016/S0141-1136(00)00080-5

Gee RH, Charles A, Taylor N, Darbre PD (2008) Oestrogenic and androgenic activity of triclosan in breast cancer cells. J Appl Toxicol 28:78–91. https://doi.org/10.1002/jat.1316

Grove C, Liebenberg W, Du JP et al (2003) Improving the aqueous solubility of triclosan by solubilization, complexation, and in situ salt formation. J Cosmet Sci 54:537–550

Guslienko KY (2008) Magnetic vortex state stability, reversal and dynamics in restricted geometries. J Nanosci Nanotechnol 8:2745–2760. https://doi.org/10.1166/jnn.2008.003

Han B, Liu W, Li J, Wang J, Zhao D, Xu R, Lin Z (2017) Catalytic hydrodechlorination of triclosan using a new class of anion-exchange-resin supported palladium catalysts. Water Res 120:199–210. https://doi.org/10.1016/j.watres.2017.04.059

Heath RJ, Rock CO (2000) Microbiology: a triclosan-resistant bacterial enzyme. Nature 406:145–146. https://doi.org/10.1038/35018162

Heath RJ, Li J, Roland GE, Rock CO (2000) Inhibition of the Staphylococcus aureusNADPH-dependent enoyl-acyl carrier protein reductase by triclosan and hexachlorophene. J Biol Chem 275:4654–4659. https://doi.org/10.1074/jbc.275.7.4654

Hu L, Flanders PM, Miller PL, Strathmann TJ (2007) Oxidation of sulfamethoxazole and related antimicrobial agents by TiO2 photocatalysis. Water Res 41:2612–2626. https://doi.org/10.1016/j.watres.2007.02.026

Hu Z, Shao Q, Huang Y, Yu L, Zhang D, Xu X, Lin J, Liu H, Guo Z (2018) Light triggered interfacial damage self-healing of poly(p-phenylene benzobisoxazole) fiber composites. Nanotechnology 29:185602. https://doi.org/10.1088/1361-6528/aab010

Huang X, Tu Y, Song C, Li T, Lin J, Wu Y, Liu J, Wu C (2016) Interactions between the antimicrobial agent triclosan and the bloom-forming cyanobacteria Microcystis aeruginosa. Aquat Toxicol 172:103–110. https://doi.org/10.1016/j.aquatox.2016.01.002

Huang M, Zhang Y, Zhou Y, Zhang C, Zhao S, Fang J, Gao Y, Sheng X (2017) Synthesis and characterization of hollow ZrO2–TiO2/Au spheres as a highly thermal stability nanocatalyst. J Colloid Interface Sci 497:23–32. https://doi.org/10.1016/j.jcis.2017.02.052

Ihara M, Tanaka K, Sakaki K, Honma I, Yamada K (1997) Enhancement of the absorption coefficient of cis-(NCS)2 Bis(2,2′-bipyridyl-4,4′-dicarboxylate)ruthenium(II) dye in dye-sensitized solar cells by a silver island film. J Phys Chem B 101:5153–5157. https://doi.org/10.1021/jp963931z

Jia Y, Wu C, Lee BW, Liu C, Kang S, Lee T, Park YC, Yoo R, Lee W (2017) Magnetically separable sulfur-doped SnFe2O4/graphene nanohybrids for effective photocatalytic purification of wastewater under visible light. J Hazard Mater 338:447–457. https://doi.org/10.1016/j.jhazmat.2017.05.057

Jones RD, Jampani HB, Newman JL, Lee AS (2000) Triclosan: a review of effectiveness and safety in health care settings. Am J Infect Control 28:184–196. https://doi.org/10.1067/mic.2000.102378

Kang AJ, Brown AK, Wong CS, Yuan Q (2018) Removal of antibiotic sulfamethoxazole by anoxic/anaerobic/oxic granular and suspended activated sludge processes. Bioresour Technol 251:151–157. https://doi.org/10.1016/j.biortech.2017.12.021

Karaolia P, Michael-Kordatou I, Hapeshi E, Drosou C, Bertakis Y, Christofilos D, Armatas GS, Sygellou L, Schwartz T, Xekoukoulotakis NP, Fatta-Kassinos D (2018) Removal of antibiotics, antibiotic-resistant bacteria and their associated genes by graphene-based TiO2 composite photocatalysts under solar radiation in urban wastewaters. Appl Catal B Environ 224:810–824. https://doi.org/10.1016/j.apcatb.2017.11.020

Kobayashi M, Kurosu S, Yamaguchi R, Kawase Y (2017) Removal of antibiotic sulfamethoxazole by zero-valent iron under oxic and anoxic conditions: removal mechanisms in acidic, neutral and alkaline solutions. J Environ Manag 200:88–96. https://doi.org/10.1016/j.jenvman.2017.05.065

Kolpin DW, Furlong ET, Meyer MT, Thurman EM, Zaugg SD, Barber LB, Buxton HT (2002a) Pharmaceuticals, hormones, and other organic wastewater contaminants in U.S. streams, 1999−2000: a national reconnaissance. Environ Sci Technol 36:1202–1211. https://doi.org/10.1021/es011055j

Kolpin DW, Furlong ET, Meyer MT, Thurman EM, Zaugg SD, Barber LB, Buxton HT (2002b) Response to comment on "Pharmaceuticals, hormones, and other organic wastewater contaminants in U.S. streams, 1999−2000: a national reconnaissance". Environ Sci Technol 36:4007–4008. https://doi.org/10.1021/es020136s

Kosera VS, Cruz TM, Chaves ES, Tiburtius ERL (2017) Triclosan degradation by heterogeneous photocatalysis using ZnO immobilized in biopolymer as catalyst. J Photochem Photobiol Chem 344:184–191. https://doi.org/10.1016/j.jphotochem.2017.05.014

Lalhriatpuia C, Tiwari D, Tiwari A, Lee SM (2015) Immobilized nanopillars-TiO2 in the efficient removal of micro-pollutants from aqueous solutions: physico-chemical studies. Chem Eng J 281:782–792. https://doi.org/10.1016/j.cej.2015.07.032

Leavey-Roback SL, Krasner SW, Suffet I(M)H (2016) Veterinary antibiotics used in animal agriculture as NDMA precursors. Chemosphere 164:330–338. https://doi.org/10.1016/j.chemosphere.2016.08.070

Li H, Zhang W, Zhang Z, Zhang X (2017) Sorption of triclosan to carbon nanotubes: the combined effects of sonication, functionalization and solution chemistry. Sci Total Environ 580:1318–1326. https://doi.org/10.1016/j.scitotenv.2016.12.095

Li Y, Zhou B, Zheng G, Liu X, Li T, Yan C, Cheng C, Dai K, Liu C, Shen C, Guo Z (2018) Continuously prepared highly conductive and stretchable SWNT/MWNT synergistically composited electrospun thermoplastic polyurethane yarns for wearable sensing. J Mater Chem C 6:2258–2269. https://doi.org/10.1039/C7TC04959E

Lin J, Chen X, Chen C, Hu JT, Zhou CL, Cai XF, Wang W, Zheng C, Zhang PP, Cheng J, Guo ZH, Liu H (2018) Durably antibacterial and bacterially antiadhesive cotton fabrics coated by cationic fluorinated polymers. ACS Appl Mater Interfaces 10:6124–6136. https://doi.org/10.1021/acsami.7b16235

Lindström A, Buerge IJ, Poiger T, Bergqvist PA, Müller MD, Buser HR (2002) Occurrence and environmental behavior of the bactericide triclosan and its methyl derivative in surface waters and in wastewater. Environ Sci Technol 36:2322–2329. https://doi.org/10.1021/es0114254

Liu H, Cao X, Liu G, Wang Y, Zhang N, Li T, Tough R (2013) Photoelectrocatalytic degradation of triclosan on TiO2 nanotube arrays and toxicity change. Chemosphere 93:160–165. https://doi.org/10.1016/j.chemosphere.2013.05.018

Liu H, Li Y, Dai K, Zheng G, Liu C, Shen C, Yan X, Guo J, Guo Z (2015) Electrically conductive thermoplastic elastomer nanocomposites at ultralow graphene loading levels for strain sensor applications. J Mater Chem C 4:157–166. https://doi.org/10.1039/C5TC02751A

Liu H, Dong M, Huang W, Gao J, Dai K, Guo J, Zheng G, Liu C, Shen C, Guo Z (2016) Lightweight conductive graphene/thermoplastic polyurethane foams with ultrahigh compressibility for piezoresistive sensing. J Mater Chem C 5:73–83. https://doi.org/10.1039/C6TC03713E

Liu Z, Liu X, Zheng G, Dai K, Liu C, Shen C, Yin R, Guo Z (2017) Mechanical enhancement of melt-stretched β-nucleated isotactic polypropylene: the role of lamellar branching of β-crystal. Polym Test 58:227–235. https://doi.org/10.1016/j.polymertesting.2017.01.002

Lou X, Lin C, Luo Q, Zhao J, Wang B, Li J, Shao Q, Guo X, Wang N, Guo Z (2017) Crystal structure modification enhanced FeNb11O29 anodes for lithium-ion batteries. ChemElectroChem 4:3171–3180. https://doi.org/10.1002/celc.201700816

Lucida H, Parkin JE, Sunderland VB (2000) Kinetic study of the reaction of sulfamethoxazole and glucose under acidic conditions: I. Effect of pH and temperature. Int J Pharm 202:47–62. https://doi.org/10.1016/S0378-5173(00)00413-0

Ma Y, Lv L, Guo Y, Fu Y, Shao Q, Wu T, Guo S, Sun K, Guo X, Wujcik EK, Guo Z (2017) Porous lignin based poly (acrylic acid)/organo-montmorillonite nanocomposites: swelling behaviors and rapid removal of Pb (II) ions. Polymer 128:12–23. https://doi.org/10.1016/j.polymer.2017.09.009

Martínez S, Morales-Mejía JC, Hernández PP, Santiago L, Almanza R (2014) Solar photocatalytic oxidation of triclosan with TiO2 immobilized on volcanic porous stones on a CPC pilot scale reactor. Energy Procedia 57:3014–3020. https://doi.org/10.1016/j.egypro.2014.10.337

Massé DI, Saady NMC, Gilbert Y (2014) Potential of biological processes to eliminate antibiotics in livestock manure: an overview. Animals 4:146–163. https://doi.org/10.3390/ani4020146

McFarland AD, Haynes CL, Mirkin CA et al (2004) Color my nanoworld. J Chem Educ 81:544A. https://doi.org/10.1021/ed081p544A

Mendioroz S, Pajares JA, Benito I, Pesquera C, Gonzalez F, Blanco C (1987) Texture evolution of montmorillonite under progressive acid treatment: change from H3 to H2 type of hysteresis. Langmuir 3:676–681. https://doi.org/10.1021/la00077a017

Mompelat S, Le Bot B, Thomas O (2009) Occurrence and fate of pharmaceutical products and by-products, from resource to drinking water. Environ Int 35:803–814. https://doi.org/10.1016/j.envint.2008.10.008

Munoz M, de Pedro ZM, Casas JA, Rodriguez JJ (2012) Triclosan breakdown by Fenton-like oxidation. Chem Eng J 198–199:275–281. https://doi.org/10.1016/j.cej.2012.05.097

Muzvidziwa T, Moyo M, Okonkwo O et al (2017) Electrodeposition of zinc oxide nanoparticles on multiwalled carbon nanotube-modified electrode for determination of caffeine in wastewater effluent. Int J Environ Anal Chem 97:1–14. https://doi.org/10.1080/03067319.2017.1337898

Nasseri S, Mahvi AH, Seyedsalehi M, Yaghmaeian K, Nabizadeh R, Alimohammadi M, Safari GH (2017) Degradation kinetics of tetracycline in aqueous solutions using peroxydisulfate activated by ultrasound irradiation: effect of radical scavenger and water matrix. J Mol Liq 241:704–714. https://doi.org/10.1016/j.molliq.2017.05.137

Nguyen LQ, Salim C, Hinode H (2008) Performance of nano-sized Au/TiO2 for selective catalytic reduction of NOx by propene. Appl Catal A Gen 347:94–99. https://doi.org/10.1016/j.apcata.2008.06.002

Noothongkaew S, Han JK, Lee YB, Thumthan O, An KS (2017) Au NPs decorated TiO2 nanotubes array candidate for UV photodetectors. Prog Nat Sci Mater Int 27:641–646. https://doi.org/10.1016/j.pnsc.2017.10.001

Pemberton RM, Hart JP (1999) Electrochemical behaviour of triclosan at a screen-printed carbon electrode and its voltammetric determination in toothpaste and mouthrinse products. Anal Chim Acta 390:107–115. https://doi.org/10.1016/S0003-2670(99)00194-4

Qinzhi H, Jing R, Haijun C et al (2018) Front cover: synergistic hematite-fullerene electron-extracting layers for improved efficiency and stability in perovskite solar cells (ChemElectroChem 5/2018). ChemElectroChem 5:722–722. https://doi.org/10.1002/celc.201800215

Rosu M-C, Coros M, Pogacean F, Magerusan L, Socaci C, Turza A, Pruneanu S (2017) Azo dyes degradation using TiO2-Pt/graphene oxide and TiO2-Pt/reduced graphene oxide photocatalysts under UV and natural sunlight irradiation. Solid State Sci 70:13–20. https://doi.org/10.1016/j.solidstatesciences.2017.05.013

Sanchez-Prado L, Llompart M, Lores M, García-Jares C, Bayona JM, Cela R (2006) Monitoring the photochemical degradation of triclosan in wastewater by UV light and sunlight using solid-phase microextraction. Chemosphere 65:1338–1347. https://doi.org/10.1016/j.chemosphere.2006.04.025

Seaton NA (1991) Determination of the connectivity of porous solids from nitrogen sorption measurements. Chem Eng Sci 46:1895–1909. https://doi.org/10.1016/0009-2509(91)80151-N

Seery MK, George R, Floris P, Pillai SC (2007) Silver doped titanium dioxide nanomaterials for enhanced visible light photocatalysis. J Photochem Photobiol Chem 189:258–263. https://doi.org/10.1016/j.jphotochem.2007.02.010

Shankar A, Salcedo E, Berndt A, Choi D, Ryu JE (2018) Pulsed light sintering of silver nanoparticles for large deformation of printed stretchable electronics. Adv Compos Hybrid Mater 1:193–198. https://doi.org/10.1007/s42114-017-0012-3

Shorke BS, Korake PV, Hankare PP, et al (2018) Synthesis and characterization of pure anatase TiO2 nanoparticles | SpringerLink. https://link.springer.com/article/10.1007%2Fs10854-010-0218-4. Accessed 22 Apr 2018

Singer H, Müller S, Tixier C, Pillonel L (2002) Triclosan: occurrence and fate of a widely used biocide in the aquatic environment: field measurements in wastewater treatment plants, surface waters, and lake sediments. Environ Sci Technol 36:4998–5004. https://doi.org/10.1021/es025750i

Sirés I, Oturan N, Oturan MA, Rodríguez RM, Garrido JA, Brillas E (2007) Electro-Fenton degradation of antimicrobials triclosan and triclocarban. Electrochim Acta 52:5493–5503. https://doi.org/10.1016/j.electacta.2007.03.011

Sivaraman S, Zwahlen J, Bell AF, Hedstrom L, Tonge PJ (2003) Structure−activity studies of the inhibition of FabI, the enoyl reductase from Escherichia coli, by Triclosan: kinetic analysis of mutant FabIs. Biochemistry (Mosc) 42:4406–4413. https://doi.org/10.1021/bi0300229

Son H-S, Ko G, Zoh K-D (2009) Kinetics and mechanism of photolysis and TiO2 photocatalysis of triclosan. J Hazard Mater 166:954–960. https://doi.org/10.1016/j.jhazmat.2008.11.107

Song Z, Wang N, Zhu L, Huang A, Zhao X, Tang H (2012) Efficient oxidative degradation of triclosan by using an enhanced Fenton-like process. Chem Eng J 198–199:379–387. https://doi.org/10.1016/j.cej.2012.05.067

Su T, Shao Q, Qin Z, Guo Z, Wu Z (2018) Role of interfaces in two-dimensional photocatalyst for water splitting. ACS Catal 8:2253–2276. https://doi.org/10.1021/acscatal.7b03437

Sun K, Xie P, Wang Z, Su T, Shao Q, Ryu JE, Zhang X, Guo J, Shankar A, Li J, Fan R, Cao D, Guo Z (2017a) Flexible polydimethylsiloxane/multi-walled carbon nanotubes membranous metacomposites with negative permittivity. Polymer 125:50–57. https://doi.org/10.1016/j.polymer.2017.07.083

Sun Z, Zhang L, Dang F, Liu Y, Fei Z, Shao Q, Lin H, Guo J, Xiang L, Yerra N, Guo Z (2017b) Experimental and simulation-based understanding of morphology controlled barium titanate nanoparticles under co-adsorption of surfactants. CrystEngComm 19:3288–3298. https://doi.org/10.1039/C7CE00279C

Sun K, Fan R, Zhang X, Zhang Z, Shi Z, Wang N, Xie P, Wang Z, Fan G, Liu H, Liu C, Li T, Yan C, Guo Z (2018) An overview of metamaterials and their achievements in wireless power transfer. J Mater Chem C 6:2925–2943. https://doi.org/10.1039/C7TC03384B

Thomaidi VS, Matsoukas C, Stasinakis AS (2017) Risk assessment of triclosan released from sewage treatment plants in European rivers using a combination of risk quotient methodology and Monte Carlo simulation. Sci Total Environ 603–604:487–494. https://doi.org/10.1016/j.scitotenv.2017.06.113

Tian Y, Gao B, Morales VL, Chen H, Wang Y, Li H (2013) Removal of sulfamethoxazole and sulfapyridine by carbon nanotubes in fixed-bed columns. Chemosphere 90:2597–2605. https://doi.org/10.1016/j.chemosphere.2012.11.010

Tiwari D, Lalhriatpuia C, Lalhmunsiama, Lalhriatpuia C, Lalhmunsiama, Lee SM, Kong SH (2015) Efficient application of nano-TiO2 thin films in the photocatalytic removal of Alizarin Yellow from aqueous solutions. Appl Surf Sci 353:275–283. https://doi.org/10.1016/j.apsusc.2015.06.131

Wan Z, Hu J, Wang J (2016) Removal of sulfamethazine antibiotics using CeFe-graphene nanocomposite as catalyst by Fenton-like process. J Environ Manag 182:284–291. https://doi.org/10.1016/j.jenvman.2016.07.088

Wang J, Wang S (2016) Removal of pharmaceuticals and personal care products (PPCPs) from wastewater: a review. J Environ Manag 182:620–640. https://doi.org/10.1016/j.jenvman.2016.07.049

Wang C, Zhao M, Li J, Yu J, Sun S, Ge S, Guo X, Xie F, Jiang B, Wujcik EK, Huang Y, Wang N, Guo Z (2017) Silver nanoparticles/graphene oxide decorated carbon fiber synergistic reinforcement in epoxy-based composites. Polymer 131:263–271. https://doi.org/10.1016/j.polymer.2017.10.049

Wang X, Liu X, Yuan H, Liu H, Liu C, Li T, Yan C, Yan X, Shen C, Guo Z (2018a) Non-covalently functionalized graphene strengthened poly(vinyl alcohol). Mater Des 139:372–379. https://doi.org/10.1016/j.matdes.2017.11.023

Wang Y, Fang Y, Lu W, Li N, Chen W (2018b) Oxidative removal of sulfa antibiotics by introduction of activated carbon fiber to enhance the catalytic activity of iron phthalocyanine. Microporous Mesoporous Mater 261:98–104. https://doi.org/10.1016/j.micromeso.2017.10.055

Wu Q, Shi H, Adams CD, Timmons T, Ma Y (2012) Oxidative removal of selected endocrine-disruptors and pharmaceuticals in drinking water treatment systems, and identification of degradation products of triclosan. Sci Total Environ 439:18–25. https://doi.org/10.1016/j.scitotenv.2012.08.090

Xu D, Liu K, Shi W et al (2015) Ag-decorated K2Ta2O6 nanocomposite photocatalysts with enhanced visible-light-driven degradation activities of tetracycline (TC). Ceram Int 3(Part B):4444–4451. https://doi.org/10.1016/j.ceramint.2014.11.136

Yang B, Ying G-G, Zhao J-L, Zhang LJ, Fang YX, Nghiem LD (2011) Oxidation of triclosan by ferrate: reaction kinetics, products identification and toxicity evaluation. J Hazard Mater 186:227–235. https://doi.org/10.1016/j.jhazmat.2010.10.106

Yang Y, Lu X, Jiang J, Ma J, Liu G, Cao Y, Liu W, Li J, Pang S, Kong X, Luo C (2017) Degradation of sulfamethoxazole by UV, UV/H2O2 and UV/persulfate (PDS): formation of oxidation products and effect of bicarbonate. Water Res 118:196–207. https://doi.org/10.1016/j.watres.2017.03.054

Yoon J-W, Baek M-H, Hong J-S, Lee CY, Suh JK (2012) Photocatalytic degradation of azo dye using TiO_2 supported on spherical activated carbon. Korean J Chem Eng 29:1722–1729. https://doi.org/10.1007/s11814-012-0076-2

Yu JC, Kwong TY, Luo Q, Cai Z (2006) Photocatalytic oxidation of triclosan. Chemosphere 65:390–399. https://doi.org/10.1016/j.chemosphere.2006.02.011

Yuval A, Eran F, Janin W, Oliver O, Yael D (2017) Photodegradation of micropollutants using V-UV/UV-C processes; Triclosan as a model compound. Sci Total Environ 601–602:397–404. https://doi.org/10.1016/j.scitotenv.2017.05.172

Zhang L, Qin M, Yu W, Zhang Q, Xie H, Sun Z, Shao Q, Guo X, Hao L, Zheng Y, Guo Z (2017a) Heterostructured TiO2/WO3

nanocomposites for photocatalytic degradation of toluene under visible light. J Electrochem Soc 164:H1086–H1090. https://doi.org/10.1149/2.0881714jes

Zhang L, Yu W, Han C, Guo J, Zhang Q, Xie H, Shao Q, Sun Z, Guo Z (2017b) Large scaled synthesis of heterostructured electrospun TiO2/SnO2 nanofibers with an enhanced photocatalytic activity. J Electrochem Soc 164:H651–H656. https://doi.org/10.1149/2.1531709jes

Zhao J, Wu L, Zhan C, Shao Q, Guo Z, Zhang L (2017) Overview of polymer nanocomposites: computer simulation understanding of physical properties. Polymer 133:272–287. https://doi.org/10.1016/j.polymer.2017.10.035